2009-12

Atlas of deep current observations for central California

Zamora, Ulysses D.

Monterey, California. Naval Postgraduate School

NAVAL POSTGRADUATE SCHOOL

MONTEREY, CALIFORNIA

THESIS

ATLAS OF DEEP CURRENT OBSERVATIONS FOR CENTRAL CALIFORNIA

by

Ulysses D. Zamora

December 2009

Thesis Advisor:	Curtis Collins
Second Reader:	Tetyana Margolina

Approved for public release; distribution is unlimited

THIS PAGE INTENTIONALLY LEFT BLANK

REPORT DOCUMENTATION PAGE			Form Approved OMB No. 0704-0188
Public reporting burden for this collection of information is estimated to average 1 hour per response, including the time for reviewing instruction, searching existing data sources, gathering and maintaining the data needed, and completing and reviewing the collection of information. Send comments regarding this burden estimate or any other aspect of this collection of information, including suggestions for reducing this burden, to Washington headquarters Services, Directorate for Information Operations and Reports, 1215 Jefferson Davis Highway, Suite 1204, Arlington, VA 22202-4302, and to the Office of Management and Budget, Paperwork Reduction Project (0704-0188) Washington DC 20503.			
1. AGENCY USE ONLY ***(Leave blank)***	**2. REPORT DATE** December 2009	**3. REPORT TYPE AND DATES COVERED** Master's Thesis	
4. TITLE AND SUBTITLE Atlas of Deep Current Observations for Central California			**5. FUNDING NUMBERS** N/A
6. AUTHOR LT Ulysses Zamora			
7. PERFORMING ORGANIZATION NAME(S) AND ADDRESS(ES) Naval Postgraduate School Monterey, CA 93943-5000			**8. PERFORMING ORGANIZATION REPORT NUMBER**
9. SPONSORING /MONITORING AGENCY NAME(S) AND ADDRESS(ES) N/A			**10. SPONSORING/MONITORING AGENCY REPORT NUMBER**
11. SUPPLEMENTARY NOTES The views expressed in this thesis are those of the author and do not reflect the official policy or position of the Department of Defense or the U.S. Government.			
12a. DISTRIBUTION / AVAILABILITY STATEMENT Approved for public release; distribution is unlimited			**12b. DISTRIBUTION CODE**

13. ABSTRACT (maximum 200 words)

Deep (~1000 m) currents were observed off California from August 1994 to September 2009 using current meters and RAFOS floats. Current meter data were collected at nine locations for time periods ranging from two months to 76 months. A total of 144 months of float data were collected. Analysis of current meter data included histograms, progressive vector diagrams, stick plots, kinetic energy and rotary spectra, stick plots, means and standard deviations. Float data were analyzed using trajectories and calculating means, standard deviations, and diffusivities.

For current meter data, semidiurnal tidal energy dominated the kinetic energy spectrum, anticyclonic rotary motion exceeded cyclonic motion, kinetic energy was typically an order of magnitude greater than for diurnal frequencies, and kinetic energy decreased about an order of magnitude as depth increased by 1000 m. Mean speed for current meter (float) data was 6.1 (4.0) cm/s and alongshore variability exceeded across shore variability. Two floats were entrained in mesoscale eddies, one cyclonic and the other anticyclonic; the eddies moved westward at a speed of about one cm/s. Seasonal variability along the continental slope was marked by late summer or early fall warming; eddy kinetic energy was minimum in February, 3 cm^2/s^2.

14. SUBJECT TERMS California Current, RAFOS floats, current meters, seasonal variability, mesoscale eddies, tides.			**15. NUMBER OF PAGES** 294
			16. PRICE CODE
17. SECURITY CLASSIFICATION OF REPORT Unclassified	**18. SECURITY CLASSIFICATION OF THIS PAGE** Unclassified	**19. SECURITY CLASSIFICATION OF ABSTRACT** Unclassified	**20. LIMITATION OF ABSTRACT** UU

NSN 7540-01-280-5500 Standard Form 298 (Rev. 2-89)
Prescribed by ANSI Std. 239-18

THIS PAGE INTENTIONALLY LEFT BLANK

Approved for public release; distribution is unlimited

ATLAS OF DEEP CURRENT OBSERVATIONS FOR CENTRAL CALIFORNIA

Ulysses D. Zamora
Lieutenant, United States Navy
B.A. University Studies, University of New Mexico, 2002

Submitted in partial fulfillment of the
requirements for the degree of

MASTER OF SCIENCE IN APPLIED SCIENCE
(PHYSICAL OCEANOGRAPHY)

from the

NAVAL POSTGRADUATE SCHOOL
December 2009

Author: Ulysses Zamora

Approved by: Curt Collins
Thesis Advisor

Tetyana Margolina
Second Reader

Commander Rebecca Stone, USN
Acting Chairman, Department of Oceanography

THIS PAGE INTENTIONALLY LEFT BLANK

ABSTRACT

Deep (~1000 m) currents were observed off California from August 1994 to September 2009 using current meters and RAFOS floats. Current meter data were collected at nine locations for time periods ranging from two months to 76 months. A total of 144 months of float data were collected. Analysis of current meter data included histograms, progressive vector diagrams, stick plots, kinetic energy and rotary spectra, stick plots, means and standard deviations. Float data were analyzed using trajectories and calculating means, standard deviations, and diffusivities.

For current meter data, semidiurnal tidal energy dominated the kinetic energy spectrum, anticyclonic rotary motion exceeded cyclonic motion, kinetic energy was typically an order of magnitude greater than for diurnal frequencies, and kinetic energy decreased about an order of magnitude as depth increased by 1000 m. Mean speed for current meter (float) data was 6.1 (4.0) cm/s and alongshore variability exceeded across shore variability. Two floats were entrained in mesoscale eddies, one cyclonic and the other anticyclonic; the eddies moved westward at a speed of about 1 cm/s. Seasonal variability along the continental slope was marked by late summer or early fall warming; eddy kinetic energy was minimum in February, 3 cm^2/s^2.

THIS PAGE INTENTIONALLY LEFT BLANK

TABLE OF CONTENTS

THIS PAGE INTENTIONALLY LEFT BLANK

LIST OF FIGURES

THIS PAGE INTENTIONALLY LEFT BLANK

LIST OF TABLES

THIS PAGE INTENTIONALLY LEFT BLANK

ACKNOWLEDGMENTS

This thesis would not have been accomplished without the aid and dedication of the following individuals. Thanks go to Dr. Curtis Collins for his untiring support and dedication to the completion of this thesis, I never would have made it without his support. I also want to give many thanks to Tetyana Margolina for her amazing and wizard-like skills in oceanography and MATLAB. Thanks go to Marla Stone for her technical support on current meters, seacats, and any other device under the water. And this paragraph would not be complete without mentioning Tarry Rago, whose support on everything from charts to editing proved to be decisive in the completion of this thesis.

I would also like to thank my parents for their love and support all these many years of my naval career, I certainly would not have made it this far in life without their support. And a very special thanks to all the friends that I have made at NPS and the San Juan Bautista Old Mission Church, it certainly made life more interesting. And finally, I would like to acknowledge and thank the two who have had the most influence in my life, without which I would not have my life and being, the Incarnate God and His Blessed Mother, whose blessings and protection have brought me here.

THIS PAGE INTENTIONALLY LEFT BLANK

I. INTRODUCTION

The purpose of this study is to analyze and describe deep (~1000 m or greater depth) currents in the California Current system using direct observations. The observations included both current meter and float observations. Time series of current meter data were collected at nine locations in Central and Southern California waters between 1997 and 2009. All but one current meter time series exceeded one year duration and a total of 322 months of data were studied. The float data spanned the period from 1994-2004 and totaled 144 months of data. The current meters typically sampled every half hour and resolved tidal processes while the float were sampled two or three times daily and only resolved mesoscale and longer period phenomena.

A. LITERATURE REVIEW

1. Deep Circulation of the California Current System

Previous observations of deep flow in the California Current system include both direct measurements with current meters as well as inferences about the deep flow made from temperature and salinity observations. Mantyla (1970) examined deep Nansen bottle casts for the region and showed it was possible to define the physical characteristics of the deep Northeast Pacific currents. His results indicated that 1) The California Current-Countercurrent system was confined to a zone from the ocean surface to a depth of 1 km; 2) The layer from 1 km to 4 km depth was characterized by a well developed temperature minimum throughout with monotonically increasing salinity and dissolved oxygen concentration with depth; a mean southward flow was inferred for this depth zone; 3) The layer from 4 km to 0.1 km above the bottom had the lowest potential temperature but the highest salinity and highest dissolved oxygen concentration. For this layer, an eastward flow into the southwest part of the region was inferred; 4) The layer less than 0.1 km above the bottom showed a steep decline in salinity, dissolved oxygen and silicate concentration.

The broader flow pattern for the mid-depths of the North Pacific Ocean was described by Reid and Mantyla (1978). They documented a zone of low oxygen near 30-40°N at the eastern boundary. They concluded that this was not compatible with a simple large scale subtropical anticyclonic flow at mid-depth. Using dynamic heights, they showed that the subtropical gyre had a very strong southward return flow to the east of the Kuroshio. This flow turned eastward near 20-25°N and extended eastward to at least as far as 160°E and, at greater depths, for example near 1000 m, it continued eastward across the entire Pacific.

There have been few direct measurements of deep currents in the California Current system, in part because the flows were thought to be too weak to measure. The largest such study was part of a study to investigate the circulation at a possible deep ocean storage site for nuclear waste (Stabeno and Smith, 1987). Currents were measured from 14 moorings to the south of the Mendocino Fracture Zone from 1979 to 1985. From 1979 to 1985 these moorings were in water depths greater than 3400 m. The duration of each record was from 5 to 13 months, and each of the moorings obtained measurements at different depths. The region offshore of the continental margin was found to be an area of low mean current even though it is within the California Current. The upper ocean currents were highly variable and had no significant meridional flow, but had a large root-mean-square amplitude of the order of 10 cm/s. The mean current was dominated by eddies, apparently influenced by the "squirts" and "cold filaments" that may originate in the vicinity of Point Arena and Cape Mendocino.

Currents and pressure at 3903 m depth on the lower continental margin were observed for 46 days in 1966 at a cabled geophysical observatory which was located 100 miles off the coast of northern California (Nowroozi *et al.*, 1968). The observatory was designated OBS III and was located at 38° 09.2′N and 124° 54.4′W on an abyssal plain in the eastern part of the Delgada fan. The current meter operated from 23 May 1966, 0900 UT, to 7 July 1966, 1800 UT. The data were dominated by tides, but gave no indication of a systematic pattern of subtidal flow. The trajectory indicated no inertial variability, but the mean drift was 0.622 cm/s in the direction of 273°T.

The near-bottom currents off the coast of Baja California were measured in 4 km depth by Isaacs *et al*. (1966) from 31 May 1965 to 10 October 1965. The length of record chosen for analysis was 24, 48, or 72 hours. These measurements were made 3 meters above the bottom at 3700 and 4300 m depth from 300 to 800 km west of the northern Baja California coast. Results showed a net flow of 2.2 cm/s toward the southeast and semidiurnal fluctuations of about 1.7 cm/s which rotated counterclockwise. The two measurements were mostly coherent over an area of 200 km^2, and the phase of the fluctuations was nearly constant with the tides at La Jolla, California, 400 to 800 km away.

B. THESIS ORGANIZATION

Data collected from RCM 8 current meters and RAFOS floats over the last 15 years have been analyzed. This analysis will provide characteristics of the deep ocean currents of the Central California Coast. Instruments utilized for data collection are discussed in Chapter II. Data analysis techniques are discussed in Chapter III and summary and conclusions with recommendation for future work is discussed in Chapter IV. There are 21 appendices that describe each data set. For clarity, each chapter begins with the body of text followed by figures and tables.

THIS PAGE INTENTIONALLY LEFT BLANK

II. DATA COLLECTION

Currents were observed with current meters and neutrally-buoyant floats. The current meters were fixed to moorings which were anchored to the sea bottom. Because these current meters are more or less fixed in space, their data are referred to as "Eulerian" measurements. The floats drifted freely in the ocean, carried by ocean currents, and are called "Lagrangian" measurements. Both current meters and floats measured temperature and pressure. On a few moorings, observations of temperature, conductivity, and pressure were made. The instruments are described below.

"Intermediate" type moorings were used as platforms for the current meters. "Intermediate" refers to the fact the main flotation for the mooring is submerged below the surface of the ocean so that it does not interact with surface gravity waves. Since the properties of the mooring affect the quality of the observations, moorings are also discussed below.

A. RCM 8

Almost all of the moored current observations were made by a recording current meter (model RCM8) developed in the 1970s for NATO and subsequently manufactured by Aanderaa (Operating Manual RCM 7&8, 1995). The RCM 8 was specifically designed for use in deep water with a depth capability of 6000 m, and measures current speed using a shielded paddle wheel and direction by means of a vane and a magnetic compass. The net weight of the RCM 8 is 15.2 kg in air and 10.9 kg in water. The current meter was designed to align itself with the current so that the paddle wheel is upstream and the vane downstream. The paddle wheel is mounted on top of an instrument canister measuring 520 x 128 mm. Speed and direction are sampled 50 times per sample interval (for example, every 36 seconds for a 30 minute sample interval). The RCM 8 resolves each measurement into north-south and east-west vector components, and records the average of these components at the end of the recording interval on a removable and reusable solid-state data storage unit. A built in quartz clock triggers the measuring cycle.

The RCM 8 also measured temperature and pressure (but not conductivity). Temperature was measured by a thermistor which had a resolution of 0.1% of the temperature range, an accuracy of ± 0.05°C, and a response time of 12 seconds. The temperature range was -2.46 to 21.48°C, so the resolution was 0.02°C. Pressure was measured by a silicon pressure sensor which had a range from 0 to 9000 psi and an accuracy of ± 0.5% of the range with a resolution of 0.1% of range.

The vane assembly was furnished with a spindle rod, which had a ball bearing housed in a pair of gimbals which permitted the spindle to deviate up to 27° from vertical in any direction. The vane assembly was 485 x 500 mm. The vane was also furnished with a pair of balance weights, ensuring static balance of the instrument. A pair of tail fins at the rear of the vane plate ensured dynamic balance of the meter.

The speed was measured with a rotor that has a magnetic coupling. The rotor will record speeds from 2 to 295 cm/s, and its accuracy was either +/- 1 cm/s or +/- 2% of actual speed, depending which is greater. The direction is determined by a magnetic compass with a needle clamped onto a potentiometer ring that has a resolution of 0.35° with an accuracy of ± 5° for speeds from 5 to 100 cm/s and ± 7.5° for current speeds 2.5 to 5 and 100 to 200 cm/s.

In practice, the Aanderaa current meters work well as long as they are not subjected to high frequency motions such as surface gravity waves or mooring vibration. Hamilton *et al.* (1997) discuss the latter effect and showed that speeds from the paddle wheel rotor were too small as a result of mooring vibration induced by vortex shedding from spherical in-line buoyancy. The vane response was too slow to keep the instruments aligned with flow speed relative to the current meter. This situation did not arise with the moorings used in this thesis where the mooring environment was similar to that in the Ulleung Basin where Teague et. al (2005) use similar Aanderaa current meters to resolve deep circulation patterns.

B. RAFOS FLOATS

Lagrangian measurements of flow at a nominal depth of 1500 m were made in the California Current System using isobaric RAFOS floats (Rossby *et al.*, 1986). The RAFOS float listened for regular 80 s broadcasts at 275 Hz from fixed sound sources and

recorded the time these signals arrived. The difference between the broadcast time and the time of arrival is converted to a range using the mean speed of sound in the local deep sound channel. With ranges from two or more sources, the path of the float can be reconstructed.

The RAFOS float hull was a glass cylinder 1.5 m long by 10 cm in diameter and weighing about 10-12 kg. They were easily handled and launched by hand from a ship. After launch, the float sank to the designated pressure surface and was carried passively by the ocean currents for a preset mission length, typically three or four years. In addition to recording the time of arrival of signals from the fixed sound sources, the float also recorded temperature and pressure. At the end of the mission, a weight was dropped, and the float surfaced. At the ocean surface, the float sent its data back to shore via radio broadcast to a satellite.

Isobaric RAFOS floats were used extensively to study the California Undercurrent by the Naval Postgraduate School at a pressure (depth) of about 300 dbar (300 m). Margolina *et al.* (2006) and Garfield *et al.* (1999) provide an overview of this program and describe preliminary results. Margolina *et al*. (2006) estimated the position error as 0.25 km at 200 km. The difference between the true and assumed mean sound speed was 1-4 m/s, which caused the position error. It is also important to note that these floats were quasi-isobaric. This is because the float density depended upon both the compressibility and the thermal expansion of the hull. As a result, when the temperature of ambient ocean water changed, the float was unable to stay at a fixed isobaric surface and moved slightly up (down) as the temperature decreased (increased). Goodman and Levine (1990) derived a "response ratio" to quantify whether a float followed either isobaric or isopycnal surfaces. Margolina *et al.* (2006) found that the response ratio for the NPS floats varied between 0.75 and 0.8. The mean standard deviation of the pressure along the float trajectory was 26 dbar for all mid-depth (300 dbar) floats.

Float density was also affected by seawater which leaked into the glass hull. According to Margolina *et al.* (2006), an increase in one gram of float mass translated to approximately a 40 dbar pressure change at intermediate depths. This was principally a problem for early floats, where the seal between the end plate and the glass tube

depended on the smoothness of the two surfaces. There were 58 floats of this particular design, and 14 leaked. Eventually, a new closure design eliminated the leakage problem.

C. SEACAT

Time series of electrical conductivity, temperature, and pressure were measured on moorings using instruments manufactured by Sea-Bird Electronics. Like the RCM 8, these instruments are self-powered and self-contained.

Three different models were used. The oldest was the SBE 16 SEACAT/Dual Mode (SEACAT SBE 16/Dual Mode Manual, 1987), which was used on Davidson Seamount. A somewhat newer SEACAT 19 (SEACAT SBE 19-01 Manual, 2004) was used on Pioneer Seamount, and an even newer SBE37-SM MicroCAT (SBE 37-SM MicroCAT Manual, 2004) was used on Hoke Seamount. Table 2-1 displays the characteristics of each instrument.

D. INTERMEDIATE MOORINGS

Although the mooring anchor is (hopefully) fixed, other elements of an intermediate mooring move horizontally and vertically in response to ambient currents. This movement affects measurements, not only by imparting additional motion to the current meters, but also by changing the depth of measurement (Fofonoff, 1966). The amount and distribution of buoyancy and mass of the mooring, as well as the strength and acceleration of the currents, affect current measurements. Although simplified measures of the mooring compliance or "softness" have been developed (Fofonoff, 1965), these have not been calculated. Instead a schematic diagram of the mooring, when available, is included with the data from each mooring site.

The fourth deployment at Pt. Sur SOSUS was located at 36° 18.876' N, 122° 23.465' W, where the water depth was 1396 m (Figure 1). Current meters were deployed on intermediate-type moorings, most of which were of short scope. A schematic diagram of the mooring used at the site of the Pt. Sur SOSUS array is shown in Figure 2. The principle flotation for the mooring was a 40-inch diameter syntactic foam buoy which was located at the top of the mooring, 28 m above the bottom. The current meter was

attached 2 m underneath this buoy. At greater depth, a hydrophone was connected to an autonomous acoustic recording package (HARP) attached to the mooring. The mooring was anchored using a 900 lb anchor wheel. Above the anchor was an acoustic release; immediately above the acoustic release, four glass balls provided supplementary flotation for the acoustic release in case the mooring were cut by trawling. The mooring was connected by means of 5/16" jacketed wire rope (JWR) with short sections of 3/8" chain at the top and bottom.

NAME	ACCURACY	RESOLUTION	MEMORY	MISSION
SEACAT SBE 16	Temperature: 0.01°C/6 months Conductivity: 0.001 S/m/month Pressure: 0.02% of full scale range	Temperature 0.001°C Conductivity: 0.0001 S/m Pressure: 0.0003% full scale range (moored)	CMOS static RAM, 64K or 256K byte: battery backed for minimum 2 years data retention.	Davidson Seamount
SEACAT SBE 19-01	Temperature: 0.01°C/6 months Conductivity: 0.001 S/m/month Pressure: 0.25% full scale range (50 to 1000 psia) 0.15% full scale range (3000 to 10,000 psia)	Temperature: 0.001°C Conductivity: 0.0001 S/m Pressure: 0.015% full scale range	CMOS static RAM, 128K or 512K or 1024K byte, battery backed for minimum of 2 years data retention.	Pioneer Seamount
SBE 37-SM MicroCAT	Temperature: 0.002°C(initial accuracy) Conductivity: 0.0003 S/m Pressure: 0.1% of full scale range	Temperature: 0.0001°C Conductivity: 0.00001 S/m Pressure: 0.002% full scale range	2048K byte non-volatile FLASH memory	Hoke Seamount

Table 2-1. Characteristics of moored conductivity-temperature-pressure measurement using instruments manufactured by Sea-Bird.

THIS PAGE INTENTIONALLY LEFT BLANK

III. DATA ANALYSIS TECHNIQUES

A. EULERIAN DATA

Statistical methods for describing Eulerian data are given below. Methods will be illustrated using data that were collected at the site of the former Pt. Sur SOSUS array at 36°-18'N, 122°-23.5'W at a depth of approximately 1368 m (Fig. 1). These data spanned a two year period, which consisted of four deployments ranging in length from four months to seven months (Table 2-2). The rotor failed after two months during the first deployment; so only the last three deployments were used for velocity time series statistics, although all four were used for temperature time series.

B. MEAN VELOCITY

Data are summarized using a statistical description of horizontal current measurements. Currents are a vector quantity, and most mechanical current meters measure speed S, direction, θ, as a function of time, t, using sensors such as described above for the RCM 8. The geographic direction, θ, is converted to mathematical (Cartesian) notation, φ; $\varphi = 90 - \theta$, i.e. an eastward current has a mathematical direction of zero degrees. Using the mathematical direction, the velocity is resolved into an east-west component, u(t), and a north-south component, v(t), $u(t) = S(t)\cos(\varphi(t)),\ v(t) = S(t)\sin(\varphi(t))$. To calculate the vector mean velocity, the u and v components were averaged:

$$\overline{u} = \frac{1}{n}\sum_{1}^{n} u(t),\ \overline{v} = \frac{1}{n}\sum_{1}^{n} v(t),$$

where the overbar refers to time averaging and n is the number of observations. The speed and direction of the vector mean is determined by $\vec{S} = \sqrt{\overline{u}^2 + \overline{v}^2}$, $\vec{\varphi} = \text{atan}(\overline{v} / \overline{u})$. Note that the speed of the vector mean is different that the mean speed, $\overline{S}$,

$$\overline{S} = \frac{1}{n}\sum_{1}^{n} S(t).$$

For Pt Sur data, the mean u (v) velocity component was -0.2 (1.1) cm/s. The mean speed was 11.02 cm/s. The speed (direction) of the vector mean was 1.1 cm/s (348.1°T).

C. PRINCIPAL COMPONENT ROTATION

The dispersion of the velocity components is characterized by the variance or standard deviation of the data. The first step in determining the variance is to remove the mean, $u'(t) = u(t) - \overline{u},\ v'(t) = v(t) - \overline{v}$. The variance, σ^2, is then calculated

$$\sigma_u^2 = \frac{1}{n-1}\sum_1^n u'(t)u'(t),\ \sigma_v^2 = \frac{1}{n-1}\sum_1^n v'(t)v'(t).$$

These variances are a function of the orientation of the coordinate system and, for current measurements, it is usual to tabulate only a maximum and minimum variance which results when the axes have been rotated so as to eliminate the cross variance. This rotation is called "principal component rotation." The orientation of the principal axis in mathematical coordinates, φ, is found as follows,

$$\phi = (1/2)\arctan\frac{2\langle u'(t)v'(t)\rangle}{\langle u'(t)^2\rangle - \langle v'(t)^2\rangle}$$

The dispersion of the horizontal current velocity is then uniquely defined by an ellipse whose major axis is oriented φ degrees (mathematical) from the horizontal axis and whose semi-major (semi-minor) axis is given by $\frac{1}{2}\sigma_{u_r}$ ($\frac{1}{2}\sigma_{v_r}$), where the subscript "r" indicates that the rotated coordinate system has been used. The eccentricity, ε, of this ellipse is given by $\varepsilon = \sqrt{1 - \sigma_{v_r}/\sigma_{u_r}}$. For the currents at Pt. Sur, the semi-major (semi-minor) axis magnitude was 9.6 cm/s (7.8 cm/s) with an orientation of 203.6°T. The eccentricity of the principal component ellipse was 0.43. An example of a variance ellipse is found in Figure 3.

D. HISTOGRAMS

Histograms show the distribution of the number of observations as a function of speed and direction and hence the underlying probability distribution function of the

horizontal current velocity. A specific problem in presenting these histograms for the RCM 8 was associated with the stalling of the speed sensor at 2 cm/s. This was dealt with by eliminating all samples for which the speed was 1 cm/s or less. The size of direction and speed bins used for the resulting histogram were determined by trial and error. The direction bin size was set at 10° and the speed bin size was 1 cm/s.

Figure 4 displays the histogram for the combined data set for moorings 2-4 deployed at the site of the former Pt. Sur SOSUS array. The histogram clearly shows two modes about 180 degrees apart. The largest mode corresponded to a speed of approximately 13 cm/s and a direction of 025°T. The second mode characteristics were a speed of 13 cm/s and a direction of 200°T. These directions are nearly reciprocal and correspond to the orientation of the local bathymetry.

E. STICK PLOTS

Stick plots were used to show the direction and magnitude of the sub-tidal flow as a function of time. The length of the stick represents the speed of the current. Each stick begins at the time of observation (abscissa) and zero north-south velocity (ordinate) so that its angle indicates the true direction of the current, with north directed toward the top of the page. To facilitate the visualization of seasonal effects, observations for a given year are presented on a single panel and sticks are drawn every other day.

Tides were removed by filtering using MATLAB® functions for a Butterworth filter and convolution of the filter with the data. The Butterworth filter was 4^{th} order and had a cutoff frequency of 0.14 cpd (corresponding to a period of one week). The function "filtfilt" was used for filtering the data, which results in no phase shift in the filtered data.

Figure 5 displays the stick plot and show the preponderance of the sticks indicating northward direction. One of the strongest current flows occurred in April 2007, when the current steadily increased in speed and moved in a northerly direction. In May 2007 and the summer and fall of 2007, flow was consistently northward with relatively strong flow, about 8 cm/s. In the first three months of 2007, the currents were moving in a southward direction but not going too fast. Sometimes the currents would change direction, but the speed was less than 4 cm/s. In the early half of 2008 until May there is no strong flow in either direction, with the speed normally less than 4 cm/s but

the current going either north or south. In May 2008 the current has a strong northerly flow, with some speeds approaching 8 cm/s. In June 2007 and July 2008 there is a strong southerly current with a speed that approaches 8 cm/s. Later in July 2008 the current shifts to northerly, moving at a speed of approximately 4 cm/s.

F. PROGRESSIVE VECTOR DIAGRAMS (PVD)

While current accelerations are easy to view on a stick plot, it is more difficult to see longer term trends. For this reason, progressive vector diagrams were generated for each deployment. These show the cumulative displacement as calculated by summing the velocity from the start of the current data:

$$x(t) = \sum_{0}^{t} u(t)\Delta t,\ y(t) = \sum_{0}^{t} v(t)\Delta t,$$

The progressive vector diagram resembles a float trajectory, and shows how the water parcel would have moved if the water were accelerated at the same rate everywhere in the measurement domain. Disadvantages of the progressive vector diagram are that it is difficult to see accelerations that occur only for a short period of time and it is also difficult to keep track of time and date. To remedy the latter, the start of the year was labeled clearly and the seasons were represented by a series of colors: winter (December through February) was blue, spring (March through May) was magenta, summer (June through August) was green, and fall (September through November) was red. In Figure 6, the PVD for the Pt Sur current measurements shows the speed and direction and the time and season for the data. For most of the deployment, the current was northward. At the beginning of the first deployment, the current was southward before reversing direction and moving to the north. When there is a change in season, for example the March-May and June-August time frames, the current goes in random directions and speeds; but once the seasonal change is effected, then the current resumes its leisurely northerly movement.

G. KINETIC ENERGY SPECTRUM

Kinetic energy is the amount of work needed to accelerate a body of a given mass from rest to its current velocity. For ocean currents, it is usual to assume a unit mass, so the kinetic energy per unit mass is given by

$$KE(t) = 0.5(u^2(t) + v^2(t))$$

Spectra of kinetic energy were used to determine how the kinetic energy is distributed as a function of frequency. For a finite time series of east-west components of velocity, u_n, of duration $T=N\Delta t$, where N is the total number of samples and Δt is the sampling interval, the energy spectral density, $S_u(f_k)$, as a function of frequency f_k is estimated as the discrete Fourier transform of u_n, e.g.

$$S_u(f_k) = |U_k|^2,\ U_k = \Delta t \sum_{n=1}^{N} u_n e^{-i2\pi kn/N},\ f_k = k/N\Delta t,\ \text{k=0,...,N}.$$

The energy spectral density of the north south component, $S_v(f_k)$, is calculated in a similar manner, and the kinetic energy spectrum is then

$$S_{ke}(f_k) = 0.5(S_u(f_k) + S_v(f_k))$$

The above is the equation for a one-sided power spectral density for the positive frequency interval only.

A summary of different methods to estimate spectral density is given by Emery and Thomson (1997). Here kinetic energy spectra were calculated using the Welch method (the pwelch.m program in MATLAB®). The mean and the trend of the time series were first removed. The following variables were specified: (1) the window length was set to 1024 samples; (2) the length of the overlap was 512 samples; (3) the length of the fast Fourier transform was 1024, and (4) the Nyquist frequency for half hour sampling rate was one sample per hour or 24 samples per day. The resulting spectral resolution for this Nyquist frequency was 1/1024 cph or about 0.001 cph.

Spectral estimates can be equated to variances. The ratio of the product of the number of degrees of freedom, ν, and the estimated variance, $s^2(f)$, to the true value of the variance, $\sigma^2(f)$, is distributed as a chi-square variable with ν degrees of freedom, e.g.

$$\frac{\nu s^2(f)}{\sigma^2(f)} = \chi^2_\nu .$$

Then the confidence interval, (1-α)100%, is

$$\frac{(\nu-1)s^2(f)}{\chi^2_{1-\alpha/2,\nu}} < \sigma^2(f) < \frac{(\nu-1)s^2(f)}{\chi^2_{\alpha/2,\nu}}$$

and spectral peaks which fall outside of this confidence level are considered "real", i.e. they cannot have occurred by chance. Confidence limits are determined by the number of degrees of freedom using a chi-squared table; but here they were provided by the pwelch.m function.

Plots of spectra involve the choice of linear vs. logarithmic axes. The choice is determined by the analyst, depending upon what features are felt to be important. Here kinetic energy spectra will be presented as variance preserving semi-log axes. The true signal variance within frequency band Δf is:

$$\sigma^2(f_c) = \int_{f_c-\Delta f/2}^{f_c+\Delta f/2} f S_{ke}(f)\, d\left[\log(f)\right] = \int_{f_c-\Delta f/2}^{f_c+\Delta f/2} S_{ke}(f) df .$$

If the power spectral density $S_{ke}(f) \approx S_c$ is nearly constant over the frequency increment Δf, then $\sigma^2(f_c) = S_c \Delta f$ is the signal variance in band Δf centered at the frequency f_c.

Figure 7 displays the kinetic energy spectrum for the current measurements at the site of the Pt. Sur SOSUS array. There is a large peak at the semi-diurnal frequency 0.08 cph (cycles per hour) and a smaller peak at the diurnal frequency 0.041 cph, with a series of smaller peaks at 0.12, 0.13, and 0.16 cph. The local inertial frequency is 0.049 cph, but there is not a corresponding peak at that frequency, suggesting the local inertial frequency is insignificant in this frequency band.

H. ROTARY SPECTRUM

Instead of considering spectra for u and v velocity components, greater insight into the physical character of the velocity field can often be gained by considering the flow at a given frequency to consist of clockwise and counterclockwise rotating components. The rotary spectrum decomposes a vector signal into clockwise (A_k^+) and

anticlockwise (A_k^-) rotary spectral amplitude components as a function of frequency (Gonella, 1972, Mooers, 1973 , Emery and Thomson, 1997),

$$S(f_k^+) = \frac{(A(f_k^+))^2}{N\Delta t},\ S(f_k^-) = \frac{(A(f_k^-))^2}{N\Delta t},\ f_k = 0,...,1/(2\Delta t)$$

Note that at a given frequency, the currents can be represented as an ellipse with semi-major axis length of $L_M = (A_k^+ + A_k^-)$ and semi-minor length $L_m = \left|A_k^+ + A_k^-\right|$. Rotary spectra are plotted as a function of positive frequency only, and the polarization of the flow is determined by the larger of the two spectral components.

Rotary spectra have been plotted using log-log plots. The log-log scale uses the logarithm of $S_{yy}(f)$ as the ordinate and the logarithm of frequency as the abcissa, i.e. $\log[S_{yy}(f)]$ versus log(*f*). Log-log plots are typically used to describe the cascade of energy from low to high frequencies.

A rotary coefficient, r(f_k), is defined as

$$r(f_k) = \frac{S(f_k^+) - S(f_k^-)}{S(f_k^+) + S(f_k^-)}.$$

The rotary coefficient ranges from +1 for counterclockwise circular motion to -1 for clockwise circular motion. The flow is unidirectional or rectilinear when the rotary coefficient is zero. Graphs of the rotary coefficient will be presented below the rotary spectra.

Phase angles $\varepsilon_k^+,\ \varepsilon_k^-$, corresponding to amplitude coefficients, can also be derived from rotary spectral analysis. These phase angles determine the tilt of the current ellipse as well as the time that the current vector is oriented along the major axis of the ellipse. This information is not presented in this atlas.

Figure 8 displays rotary current spectra for the current meter data collected at the site of the Pt. Sur SOSUS array. The rotary spectra show the clockwise (CW) and counterclockwise (CCW) components of the current meter data. In the power spectral density it is seen that the peaks correspond with the frequencies noted in the kinetic energy spectrum diagram. At the lower frequencies the currents were more rectilinear, meaning that both the CW and CCW were roughly the same value. At the frequency of

0.08 cph the CW component dominates and the rotary coefficient confirms the clockwise direction of the power spectral density, thus indicating the current at the semi-diurnal frequency is anti-cyclonic.

I. TIDAL ANALYSIS

For the moored current meter observations, it is clear that diurnal and semidiurnal tidal energy dominated the variability. To the degree that this reflects the barotropic tide, the characteristics of the tidal currents can be determined and hence accurately predicted in the future. Tidal signals can be removed by high- or band-pass filtering; however, the classical harmonic method of analysis can make it possible to remove tidal signals from the data and retain information on non-tidal currents at tidal frequencies.

Techniques for harmonic analysis of oceanographic time series have been developed by Godin (1972), Foreman (1977), and Foreman (1978), and subsequently have been adapted to MATLAB® by Pawlowicz *et al.* (2002). These programs make it easy to determine the magnitude and phase of the tidal currents associated with various tidal harmonics and were applied to the four sets of RCM 8 data at the site of the Pt. Sur SOSUS array. Neither phase nor amplitude appeared to be consistent from deployment to deployment. This suggested baroclinic tidal influences and means that harmonic coefficients are of limited use. As a consequence, harmonic constants were not included in this atlas.

J. LAGRANGIAN DATA

Since the RAFOS floats collected data every eight or 12 hours, all the statistics described above for current meters could be used. Since position (latitude, longitude, pressure) are measured by the float, means, variances and spectra could be added for these quantities. Note that the Nyquist frequency for 12 hour samples would be one cycle per day, so semidiurnal and inertial period motions could not be resolved.

Two characteristics of Lagrangian data are unique: the path and dispersion. These characteristics are important for naval operations, as path describes where a particle will move and when it will get there, and dispersion describes how quickly a conservative chemical agent will become diluted. Path and dispersion can be reproduced from

Eulerian measurements only under special circumstances. Davis (1991) and Freeland et. al (1975) provide examples and guidance for analysis of float data.

An example of a path is given by the trajectory of NPS float 74 (Fig. 9). The mean speed for the entire trajectory was 7.53 cm/s and the vector mean speed (direction) was 0.77 cm/s (294.6°T). The float was entrained in an anticyclonic mesoscale eddy as indicated by successive loops from November 30, 1999, to September 18, 2000. The float t mean (standard deviation) pressure was 1542 dbar (37 dbar) and mean (standard deviation) temperature was 2.71°C (0.07°C). The pressure and temperature stayed within the mean plus or minus one standard deviation until the last two months of the mission (Fig. 10, upper). Note that pressure and temperature increased or decreased together (*in situ* temperature decreases with increasing pressure at these depths in the Northeastern Pacific) which indicated correct functioning of the isobaric float (Fig. 10, lower).

The dispersion was determined from the Lagrangian auto-correlation functions $R_{UU}(\tau), R_{VV}(\tau)$, which are defined as follows (Collins *et al.*, 2004):

$$R_{UU}(\tau) = \frac{1}{V_0}\langle U(x_0,t)U(x_0,t+\tau)\rangle = \frac{1}{V_0^2}\lim_{T\to\infty}\frac{1}{T}\int_{t_0}^{t_0+T} U(x_0,t)U(x_0,t+\tau)dt,$$

$$R_{VV}(\tau) = \frac{1}{V_0}\langle V(x_0,t)V(x_0,t+\tau)\rangle = \frac{1}{V_0^2}\lim_{T\to\infty}\frac{1}{T}\int_{t_0}^{t_0+T} V(x_0,t)V(x_0,t+\tau)dt,$$

where the $\langle ... \rangle$ means averaging over a Lagrangian trajectory, τ is the time lag and T is the reference period. The reference period was 120 days as it was necessary to reduce the noise that would affect the integration over the longer trajectories. The cross-shore and alongshore diffusivities are then calculated from the auto-correlation functions as follows (Collins *et al*., 2004):

$$K_{UU} = V_0^2\int_0^\infty R_{UU}(\tau)d\tau, \quad K_{VV} = V_0^2\int_0^\infty R_{VV}(\tau)d\tau\,.$$

Figure 11 displays the original and de-trended (linear trend removed) trajectory in Cartesian coordinates rotated 30° clockwise and the cross-shore and alongshore diffusivities.

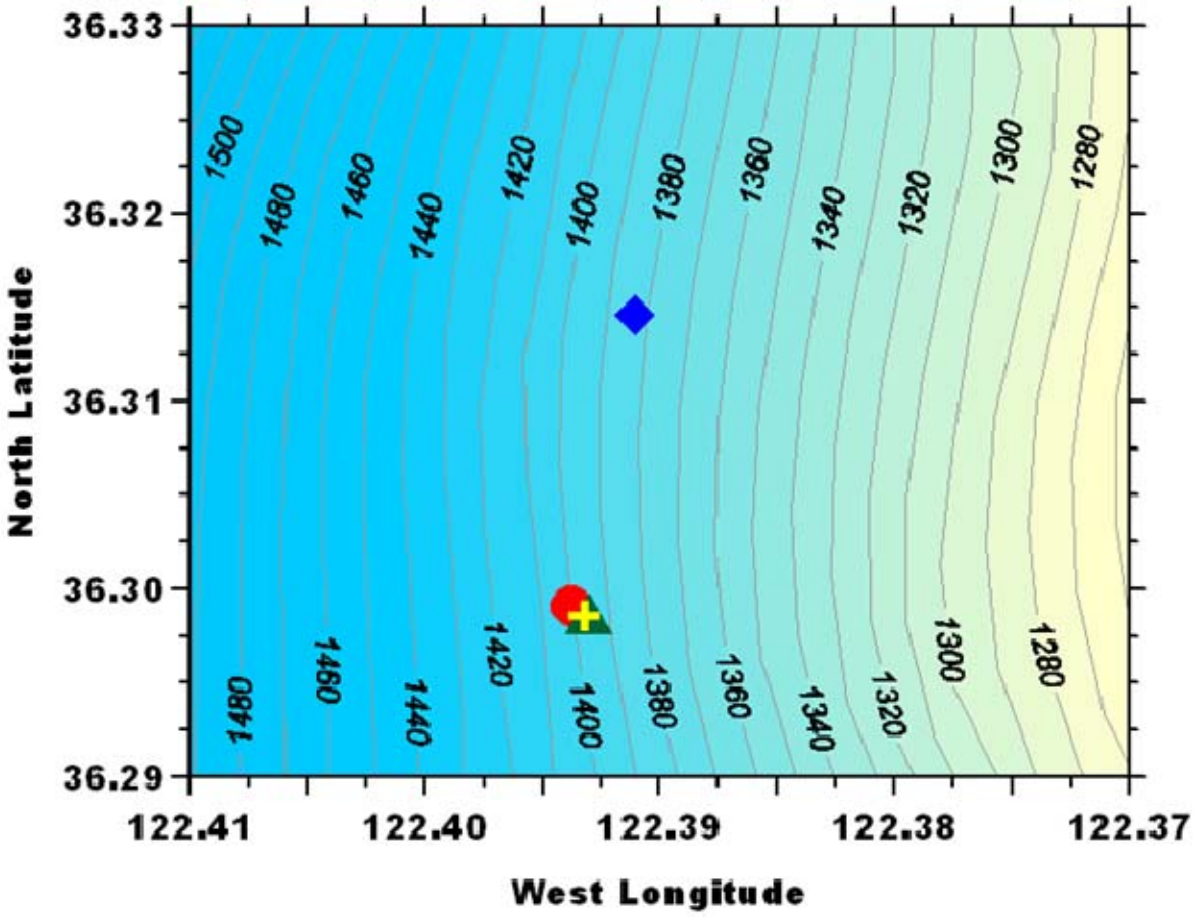

Figure 1. Mooring locations for the four deployments at the site of the Pt Sur SOSUS array. Deployment 1 is denoted by the red dot, 2 by the plus sign, 3 by the green triangle and 4 by the blue square. Soundings are in meters and the contour interval is 10 m.

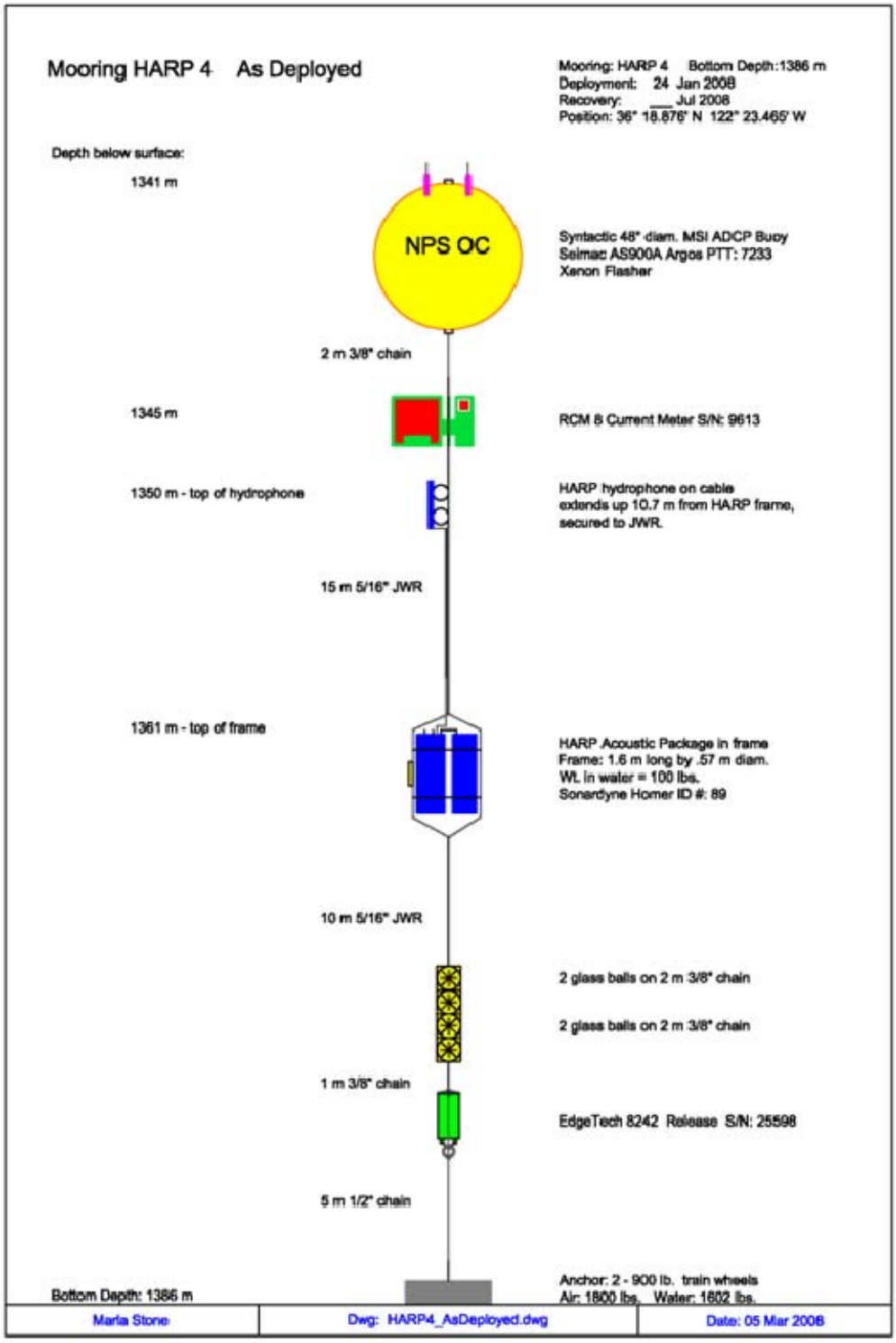

Figure 2. Schematic diagram for mooring used for measurements at Pt. Sur SOSUS array.

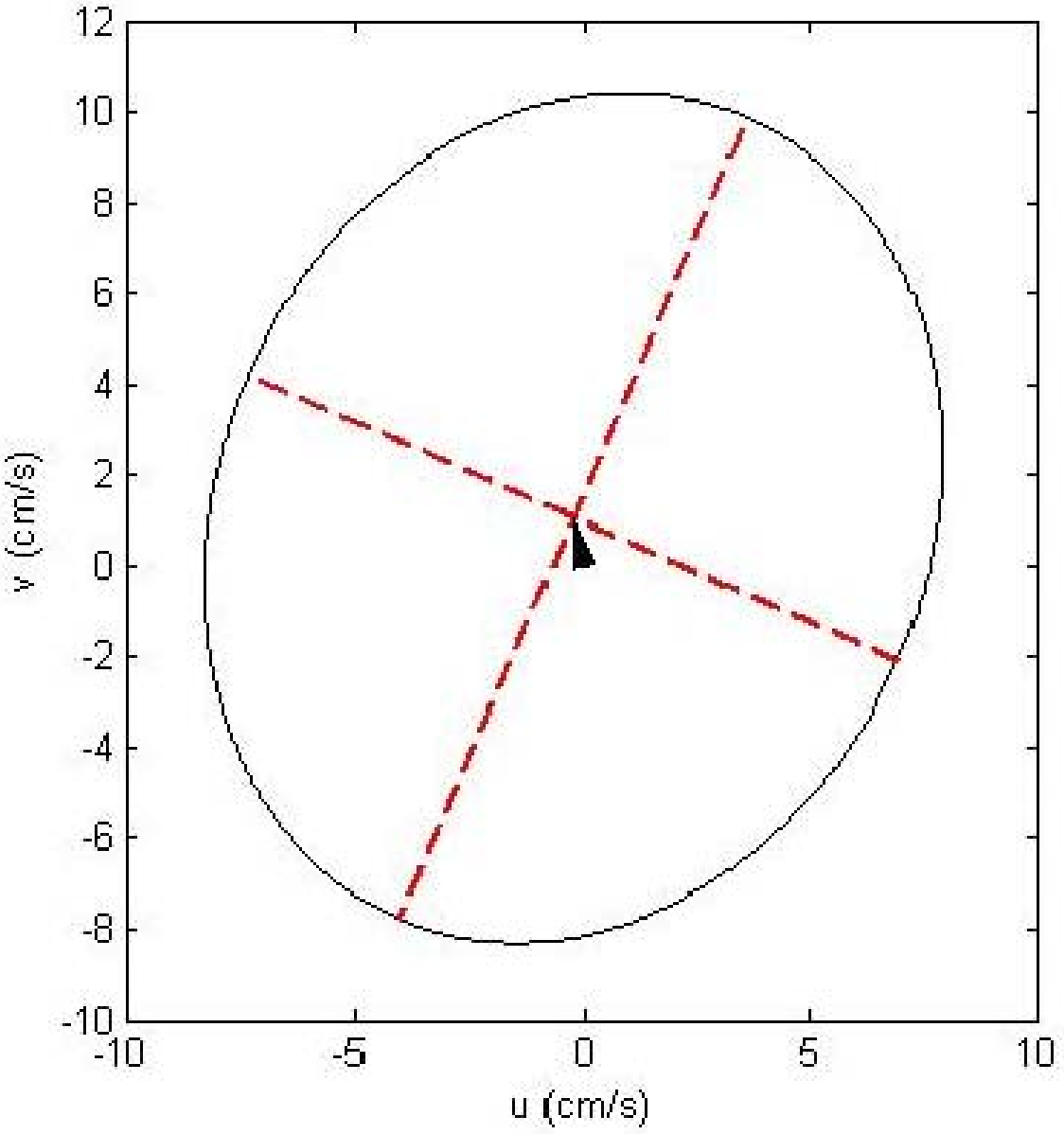

Figure 3. **Mean and standard deviation of currents at the site of the Pt. Sur SOSUS array. Mean speed (direction) of the mean vector flow was 1.1 cm/s (348.1°T) as shown by arrowhead at center. The semi-major (semi-minor) axis was 9.6 cm/s (7.8 cm/s) and was oriented along 203.6-023.6°T.**

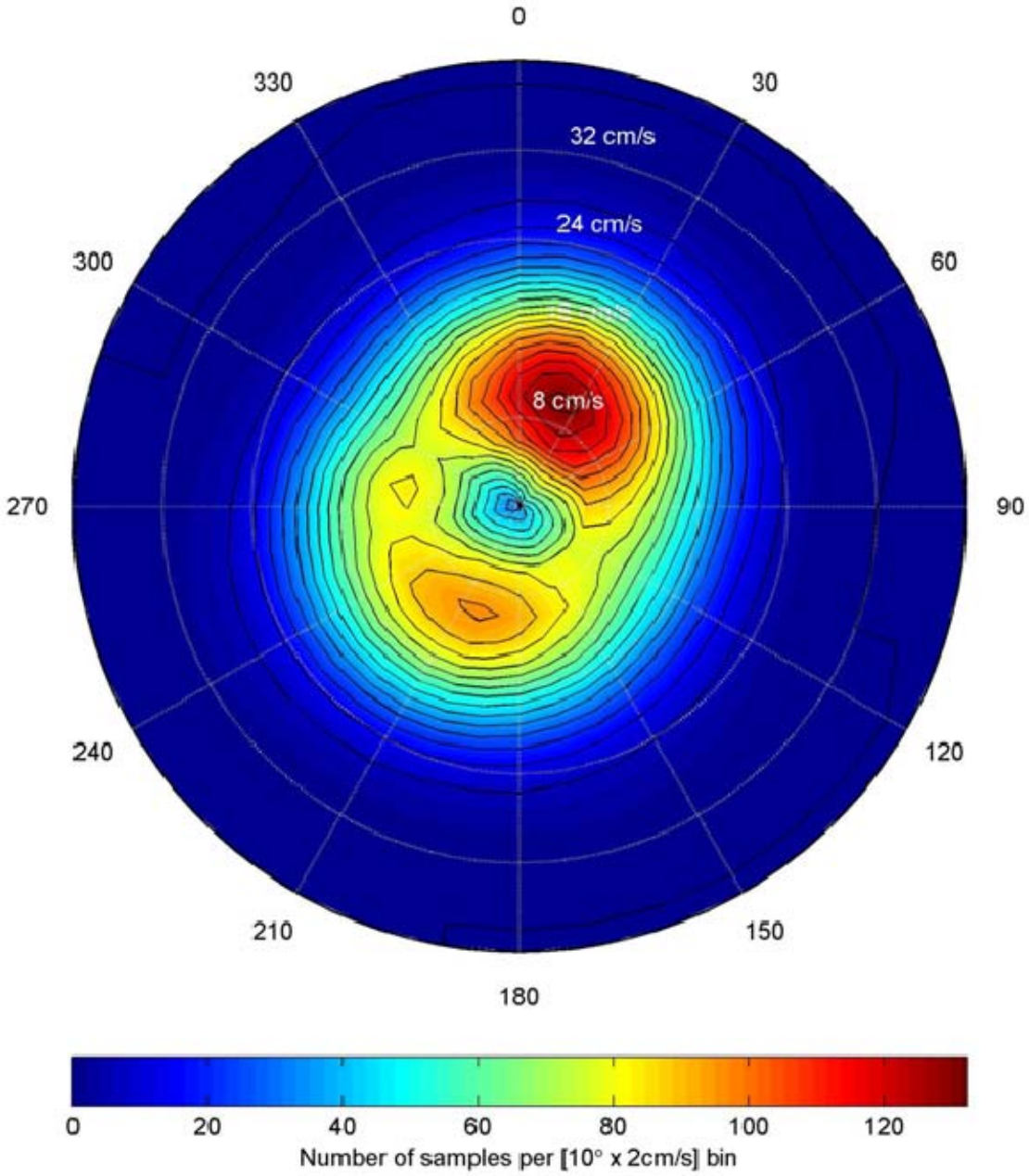

Figure 4. Histogram of velocity observations at the Pt. Sur SOSUS deployments (1-4). The total number of observations is 29,741. 898 observations with a speed less than 1 cm/s were omitted. Total number of bins is 777.

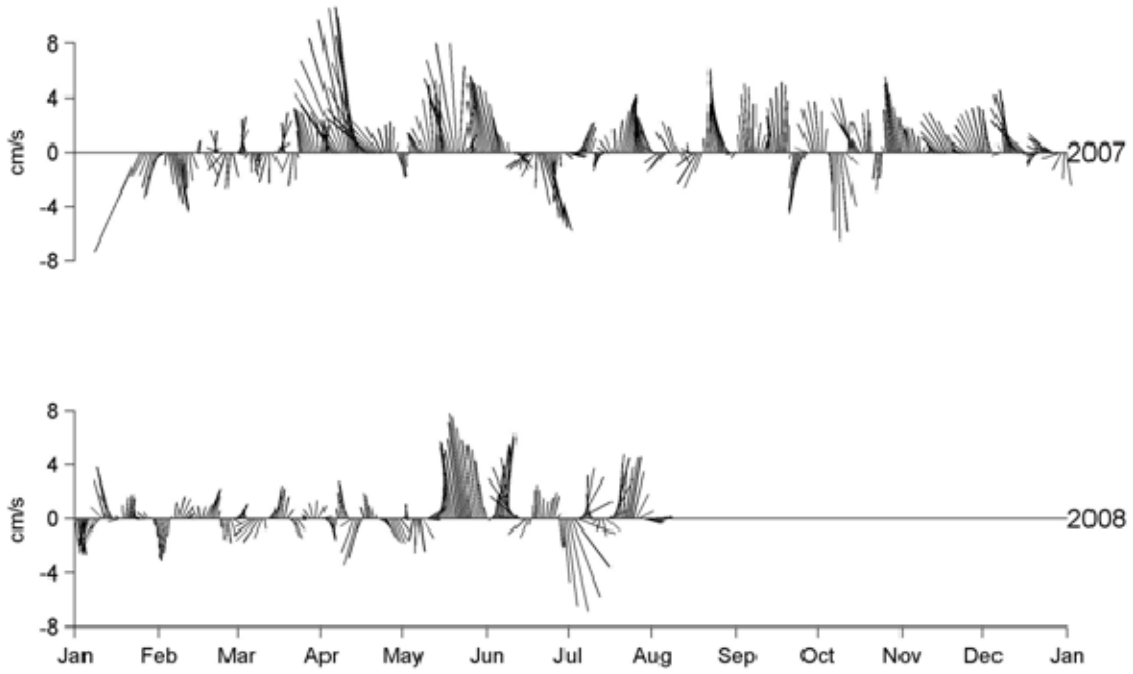

Figure 5. Currents with tides removed at the site of the Pt. Sur SOSUS as a function of time, 2007-2008. Currents were smoothed using a Butterworth filter with a cut off period of one week.

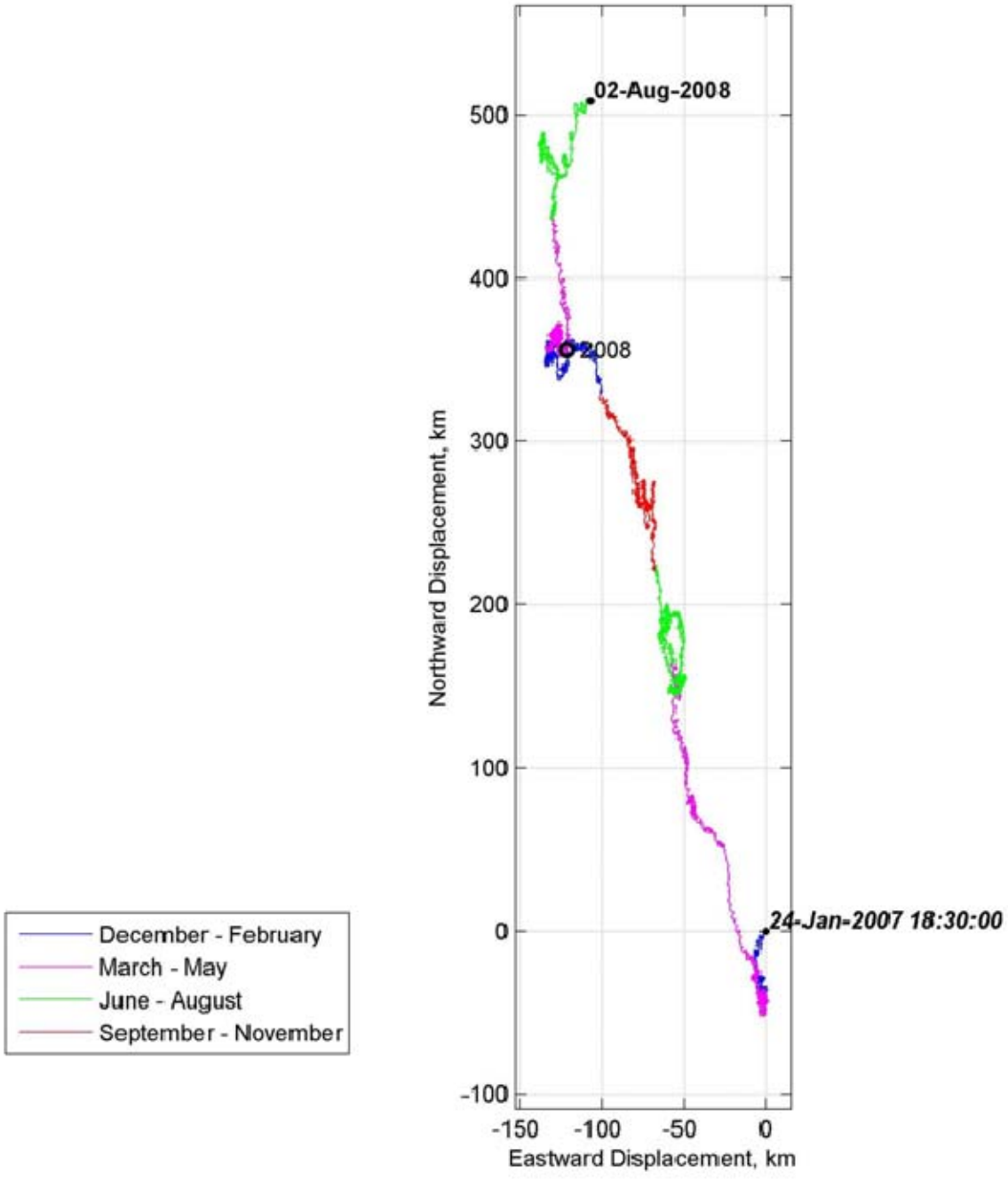

Figure 6. Progressive vector diagram for currents measured at the location of Pt. Sur SOSUS array on moorings 2-4.

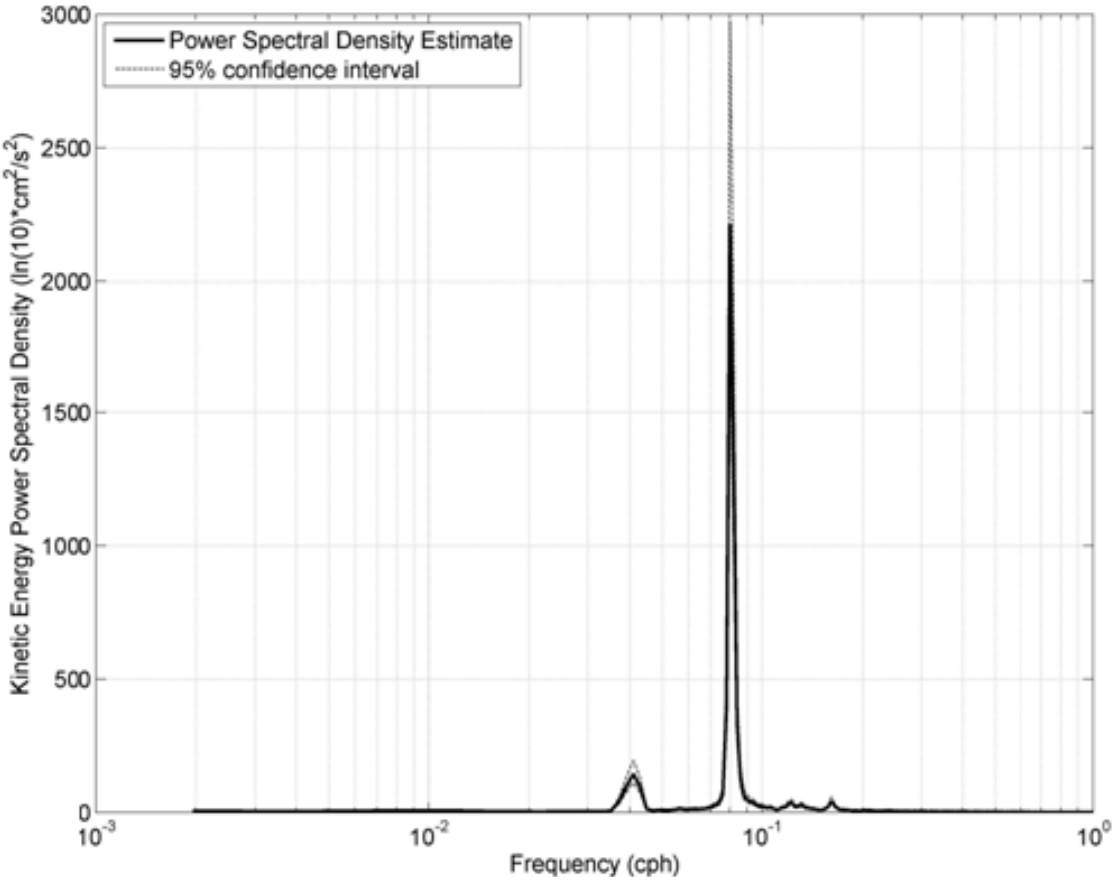

Figure 7. Kinetic energy spectrum for currents at Pt. Sur SOSUS array using moorings 2-4. Diurnal peak at 0.041 cph, semi-diurnal at 0.08 cph.

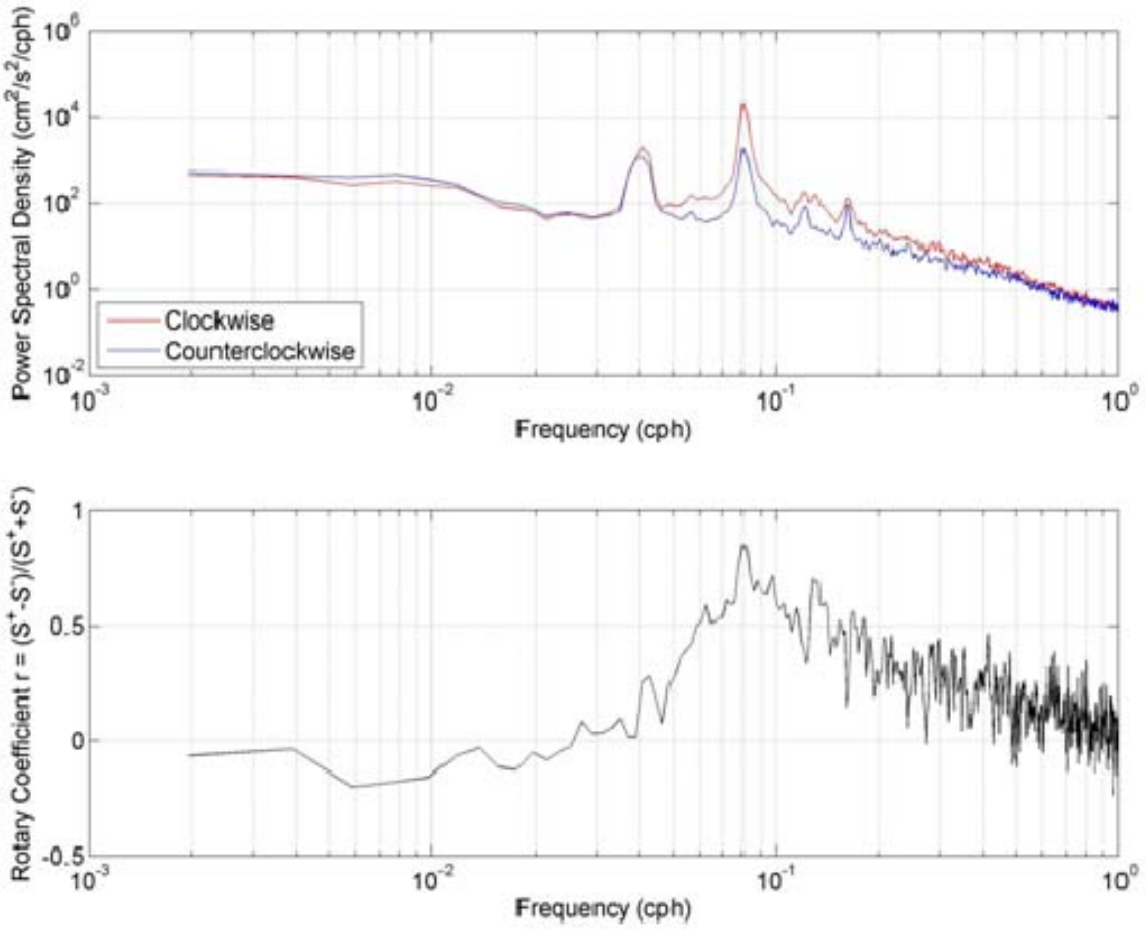

Figure 8. **(upper) Rotary spectra for currents measured at the location of the Pt. Sur SOSUS array, moorings 2-4. (lower) Rotary coefficient.**

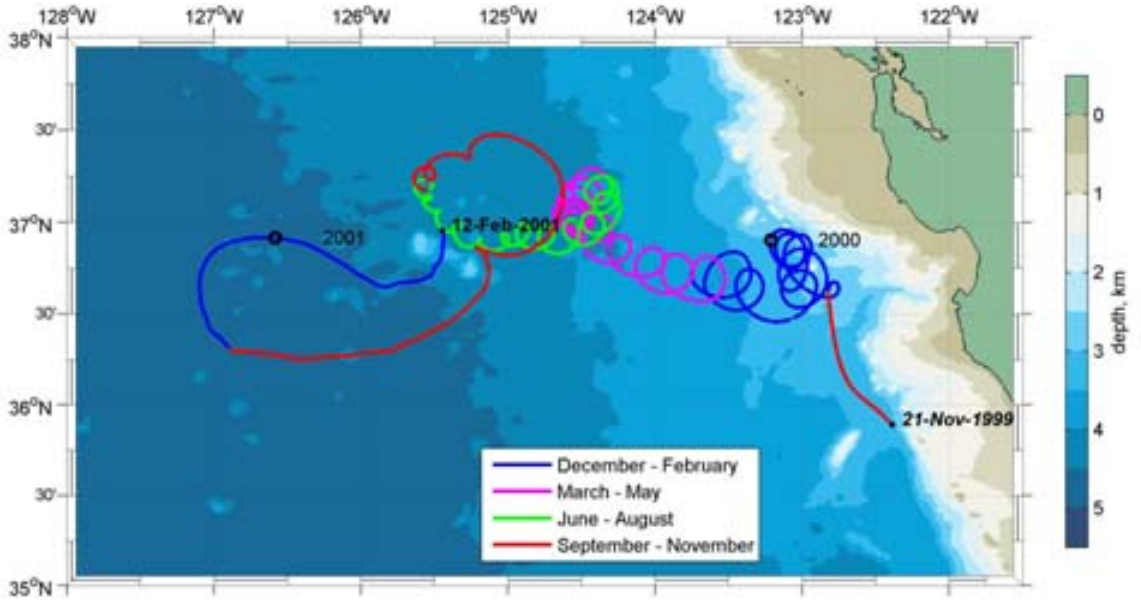

Figure 9. **The trajectory for RAFOS 74. Trajectory color indicates season. The color bar to the right gives the depth of water.**

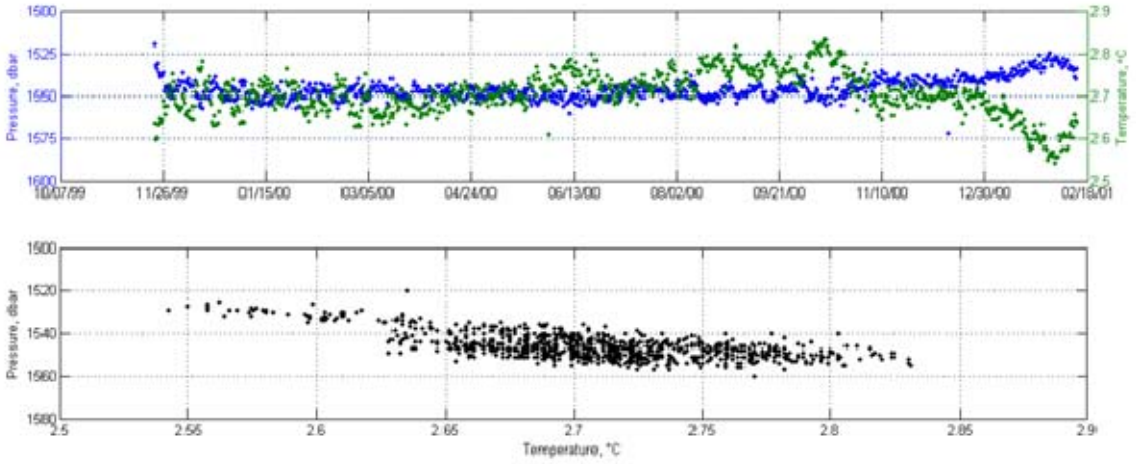

Figure 10. **Temperature and Pressure for RAFOS 74. (upper) Time series. (lower) Temperature versus pressure.**

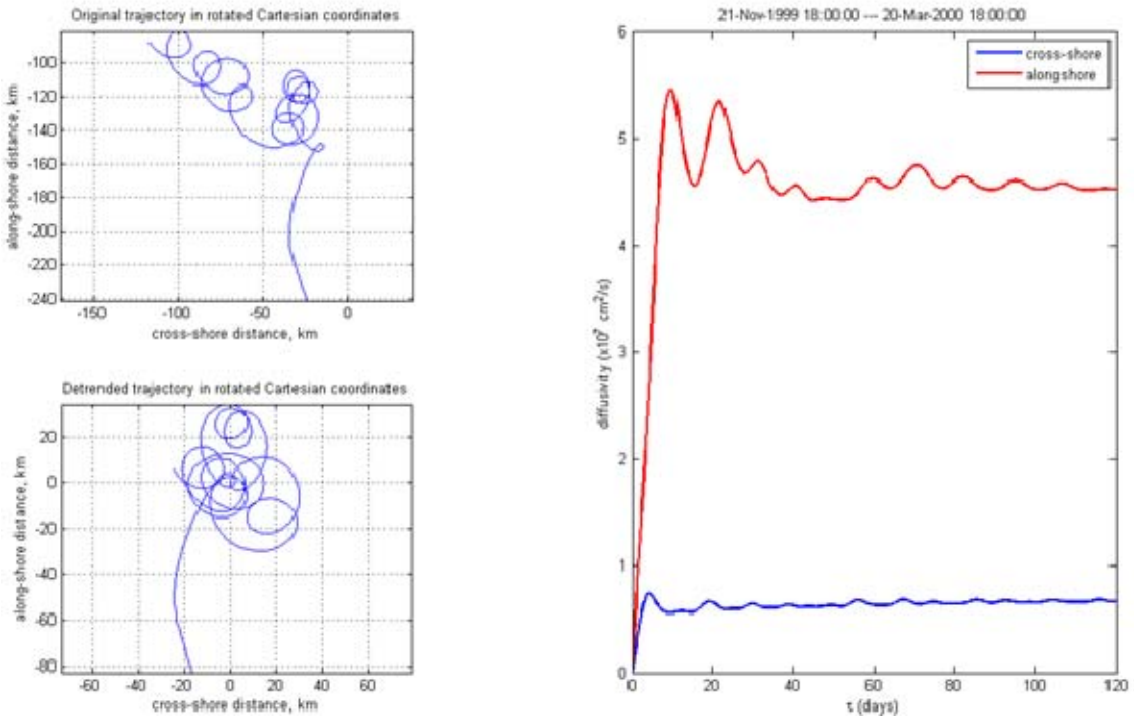

Figure 11. Diffusivity estimate for the RAFOS 74 drift. (upper left) Original trajectory in Cartesian coordinates. (lower left) Detrended trajectory in a coordinate system rotated by 030°. (right) Diffusivity, cm^2/s.

Deployment Number	Deployment Time (GMT) & Date	Latitude, N	Longitude, W	Instrument Depth (m)	Bottom Depth (m)	Sample Rate (minutes)	Compass Correction (E)	Timing Error	Instrument Type
1	03 Oct. 2006 - 24 Jan. 2007	36° 17.946’	122° 23.623’	1378	1400	30	0’	2’ 38”	RCM 8
2	24 Jan. 2007 – 17 July 2007	36° 17.924’	122° 23.583’	1376	1400	30	0’	2’ 15”	RCM 8
3	18 July. 2007 - 24 Jan. 2008	36° 17.918’	122° 23.595’	1372	1396	30	0’	1’ 30”	RCM 8
4	24 Jan. 2008 – 02 Aug. 2008	36° 18.876’	122° 23.465’	1345	1386	30	0’	4’ 40”	RCM 8

Table 3-1. Moorings at the site of the former Pt Sur SOSUS Array.

IV. SUMMARY, RESULTS, AND CONCLUSIONS

This chapter has two sections. The first section is a summary of the physical characteristics of deep currents off Central California. This section summarizes results from current meter and float measurements which are described in the appendices and tabulated in tables 4-1 and 4-2. The deep circulation features that are discussed include the mean flow, seasonal variability, mesoscale eddies, and tidal-inertial period variability. The second section presents conclusions.

A. SUMMARY OF CHARACTERISTICS OF DEEP CURRENTS IN CENTRAL CALIFORNIA

1. Mean Flow

Although the progressive vector diagrams for multiyear moorings and trajectories of multiyear floats described in the appendices indicated a complex non-stationary behavior for frequencies and spatial scales that should be in geostrophic or quasi-geostrophic equilibrium, it is useful to compare the mean values of the velocity measurements to those derived from geostrophic estimates based upon the distribution of mass in deeper waters of the Eastern North Pacific. Reid and Mantyla (1978) have charted the dynamic topography of the 1000 dbar surface relative to the 3500 dbar surface for the North Pacific Ocean and show the region of central and southern California to correspond to a maximum of dynamic height (>1.32 dyn m) relative to waters off Washington or central Baja California. In the central gyre, charts of dissolved oxygen confirm the direction of flow implied by this ridge, e.g. toward California to the north and toward Hawaii to the south of the ridge. Within about 500 km of the coast, Reid and Mantyla (ibid) indicated that the 1.31 dyn m isostere was parallel to the coast, which implied northward geostrophic flow along the coast to the north and south of the dynamic ridge. Reid and Mantyla (1976) also charted the dynamic topography along the west coast of North America for the surface relative to 500, 1000, 2000 and 4000 dbars; this chart contains data every 300-500 km and showed variability in the thickness

between the deeper isobars although a minimum occurred at 38°N. Since coastal flows are constrained by topography, the alongshore gradient of geopotential inferred poleward (equatorward) surface flow along Central California to the south (north) of 38°N.

To update the Reid and Mantyla (1976, 1978) results described above, the 2005 World Ocean data base (http://www.nodc.noaa.gov/OC5/WOD05/pr_wod05.html) was used to determine the regional pattern of the dynamic height of the 1000 dbar surface relative to 3000 dbar. Results were superimposed on the dissolved oxygen distribution (in ml/l) at 1000 m and are shown in Figure 4-1. A ridge (>1.11 dyn. m) was oriented to the southwest off California and was bounded by troughs (<1.105 dyn. m) to the north and south, similar to Reid and Mantyla (1978). Largest dynamic heights (> 1.12 dyn. m) were found at the 3000 m isobaths off San Francisco and the entrance to the Gulf of California. Contours of dissolved oxygen at 1000 dbar indicated a local maximum, 0.65 ml/l, centered under the offshore peak of dynamic height. Dissolved oxygen decreased to the north and south of this maximum with lines of constant dissolved intersecting the coast at nearly right angles.

The pattern of geostrophic flow at 1000 dbar relative to 3000 dbar is shown in Figure 4-2. The mean speed was 0.24 cm/s, the maximum was 0.98 cm/s, and the standard deviation 0.13 cm/s. Along the coast of California, geostrophic flow was directed poleward but farther from the coast, the geostrophic flow was more complex with northward flow to the west of the ridge in dynamic height and southward flow inshore.

Figure 4-3 and 4-4 display the vector mean flow and variance ellipses for all RCM 8 moorings except Hoke Seamount. With the exception of S2, the flow for all slope moorings was directed poleward, e.g. northward or westward. Moorings D1 and D2 had vector mean flow to the northwest with vector mean speeds 0.2 and 0.1 for D1 at 2000 m and 2400 m respectively and 1.4 for D2. R1 had westward mean flow with a low vector mean speed of 0.6 cm/s. S3 had a westward flow at a speed of 0.7 cm/s. Pt. Sur SOSUS had a nearly northwestward direction with a speed of 1.1 cm/s. The Santa Rosa Gap flow was westward but had the largest speed, 16.9 cm/s. Flow at S2 (Davidson Seamount) was directed to the southeast (southwest) with a 1.0 (2.0) cm/s speed. A

possible cause for the reversal of currents at S2 is deep mixing in Monterey Submarine Canyon (the mixing would reduce stratification in the Canyon with respect to offshore waters which would result in an up-Canyon directed horizontal pressure gradient). The vector mean flow at Hoke Seamount was 0.2 cm/s toward 073.7°T which is in agreement with the geostrophic flow shown in Fig. 4-2.

RAFOS float data were averaged by placing data into a northern and southern bin (see Figure 4-5). The vector mean flow for the northern (southern) bin was 0.46 (0.16) cm/s directed toward 282.5 (140.2)°T. The northern bin contained RAFOS 15, 16, 44, 74 and 79 trajectories and the bottom bin contained only data from the RAFOS 86 trajectory. Results for the northern bin agree with geostrophic estimates (Fig. 4-5) but the southward flow in the southern bin does not.

Variance ellipses for the binned RAFOS data are shown in Fig. 4-5 and had major axes of 3.67 cm/s (2.88 cm/s) for the northern (southern) bin; the minor axis was 3.15 (2.46) cm/s for the northern (southern) bin and the corresponding eccentricities were 1.11 (1.48). The axes for the variance ellipses of slope moorings decreased with depth and the major axes were parallel to the local isobaths (Table 4.1). The variance ellipses for the Davidson and Hoke seamount moorings were oriented parallel to the California coastline as were the ellipses for the float measurements.

2. Seasonal Variability

Seasonal variability for long term (~ 5 years) current measurements at 350 m depth in 800 m of water off Pt. Sur has been described by Collins *et al.* (1996). Morales (2003) described seasonal variability of currents at 300 m and 1200 m at S2. And seasonal variability of shallow (300-400 m) float measurements have been described by Collins et al. (2004). At 300 m level these results showed that coastal flow was poleward and accelerated from March through June. Temperatures, which were coolest in late winter, rose as poleward flow accelerated and were warmest in August as isopycnals (isotherms) adjusted geostrophically to increased poleward flow. Maximum variability of the alongshore flow occurred in fall when temperatures were slightly less than their maximum value.

Seasonal variability was assessed in the appendices by examining stick plots and temperature time series by year day. The most easily discerned seasonal feature was the temperature maximum that occurred in slope moorings during summer or fall (Table 4-3). Figure 4-6 shows smoothed velocity and temperature time series at S2 that have been averaged by year day and is similar to Figure III-10 from Aguilar (2003) except that results described here include an additional 16 months of data. The temperature data have somewhat more of a semiannual character than those at 300 m with temperature minimums, 3.42°C, in mid-April and mid-October, and a maximum, 3.55°C, in mid July. The temperature minima were associated with periods of weak poleward or no flow but the summer flow was directed equatorward at about 5 cm/s, opposite to those described at shallower depth. Note that the coincidence of equatorward flow and temperature maximum is consistent with geostrophic equilibrium only when the level of no motion is above the depth of the current measurement. While this is clearly the case at S2 (the 300 m currents were directed poleward during this season), these results do bring into question the assumption that 3000 dbar is a better level of no motion than 1000 dbar everywhere in the Northeast Pacific.

3. Mesoscale Variability

RAFOS float 74 (79) was entrapped in an anticyclonic (cyclonic) mesoscale eddy for 294 (181) days at a pressure of 1541 (1152.6) dbar. The period of the anticyclonic (cyclonic) eddy was 8.6 (15.1) days and the diameter 22.7 (37.4) km. The swirl velocities and eddy kinetic energies were similar for each float, 9.5 cm/s and 45.6 cm^2/s^2 for the anticyclonic eddy and 9.0 cm/s and 40.6 cm^2/s^2 for the cyclonic eddy. The anticyclonic (cyclonic) eddy moved toward 291 (277) ºT at 1.0 (1.5) cm/s. The ratio of intertial to Coriolis force for these eddies is given by the Rossby number, $Ro = U/Lf$, where U is the swirl velocity, L is the eddy diameter, and f is the Coriolis parameter; for the anticyclonic (cyclonic) eddy the Rossby number was 0.1 (0.05).

Another feature that was noted in the float appendices were four figure “8” shaped trajectory segments. The first two were noted in the northward movement of

RAFOS 15 as it was sinking in Gorda Basin. RAFOS 16 during winter 1995 also circumscribed a figure "8" during winter 1995-6 over the slope to the west of Pt. Reyes. Finally, RAFOS79 shortly after launch in fall 2000, followed a figure "8" pattern over the upper slope to the west of Monterey Bay. These features could be caused by flow around a pair of cyclonic and anticyclonic eddies. In Gorda Basin, they might be associated with Kelvin waves propagating around the Basin.

When tides were strong, progressive vector diagrams exhibited a regular series of loops, e.g. Fig. H5 for Sur Ridge. A similar series of loops associated with mesoscale variability was rare. But most stick diagrams show a series of weekly to monthly variations in the strength and sometimes the direction of the flow which on occasion manifest themselves as loops in the progressive vector diagram, e.g. 1999-2003 at S2 (Fig. F5). To further investigate the character of these low frequency current variations at S2, the eddy kinetic energy (EKE) was calculated as specified by Schmitz et. al, (1987) using data that had been rotated to principal axes, smoothed to remove tidal variability, and averaged by month. The EKE can also be decomposed into three terms,

$$EKE = \frac{1}{2}(u_r^{'} + v_r^{'})^2 = \frac{1}{2}u_r^{'2} + u_r^{'}v_r^{'} + \frac{1}{2}v_r^{'2}$$

Results are shown in Fig. 4-7 (see also Figure III-18 in Aguilar, 2003). EKE was minimum in February, 3 cm^2/s^2, and exceeded 10 cm^2/s^2 in April, June and July. Larger values were associated with larger alongshore variability but the Reynolds stress terms, <u'v'>, did not appear to be a factor as they had magnitude less than 2 cm^2/s^2 in each month. At 300 m depth, float data show maximum EKE in August (Collins et. al, 2004).

4. Tidal and Inertial Period Variability

Tidal variability was not a focus of this study although tidal and inertial-period variability dominated the kinetic energy spectrum of each current meter. Within this frequency band, the semidiurnal tide was dominant (Table 4-1), typically an order of magnitude greater energy than that associated with diurnal tides. For diurnal tides, the M_2 component of the semidiurnal tide is largest along the California coast. The M_2 tide propagates poleward as a combination of a Kelvin (which has greatest influence) and

Poincaré waves as well as a wave forced by tide generating forces (Munk et. al, 1970). As distance from the coast increases, these three waves combine to produce a tidal amphidrone near 26°N, 135°W (Irish et. al, 1971). The semidiurnal currents described in the appendices were consistent with a poleward propagating Kelvin wave as they were anticyclonic. Figure 4-8 (left) shows the variation of the semidiurnal kinetic energy as a function of depth. On average, the semidiurnal kinetic energy is an order of magnitude greater at shallow depths compared to deeper depths.

For California tides, the K1 component dominates diurnal tides and can be described as the sum of the same three waves as the diurnal tide although the Kelvin wave component is not nearly as large (Munk et. al, 1970). At only one location, the bottom of the northern gap in the ridge between Santa Rosa Island and Cortez Bank, was the diurnal kinetic energy the same order of magnitude as the semidiurnal kinetic energy. As noted above, the diurnal kinetic energy was more typically an order of magnitude less than that of the diurnal kinetic energy and was less than 100 cm^2/s^2 for all depths except for Sur Ridge and Santa Rosa Gap. Note too that no diurnal kinetic energy was observed for Hoke Seamount as it was subsumed by a broad inertial-period peak. Figure 4-8 (center) shows that the magnitude of the diurnal kinetic energy was a function of depth---the diurnal kinetic energy at depth was only a tenth of that for shallower depths. Rotary coefficients for diurnal tides were typically positive although two of the four current meters to the west of San Francisco had negative coefficients.

The kinetic energy at inertial periods were typically not significantly greater than noise at about half the mooring sites and spectral peaks of kinetic energy were observed only at D1 (2000 m), R1, S2, S3, Davidson and Hoke Seamounts. The greatest inertial period kinetic energy, 60 cm^2/s^2, was observed at Hoke Seamount where the inertial period was close to that of the diurnal tide. Inertial period kinetic energy was 49 cm^2/s^2 (41 cm^2/s^2) at R1 (Davidson Seamount). Where inertial kinetic energy peaks were observed, the rotary coefficient was close to one and the kinetic energy at depth was an order of magnitude less than at shallower depths (Figure 4-8, right).

B. CONCLUSIONS AND RECOMMENDATIONS FOR FUTURE WORK

Eulerian current meter data from nine locations along and offshore the California Coast have been analyzed in this thesis. These data covered a period of 12 years from 1997 to the summer of 2009. Measurement locations extended from 37.64°N to 32.12°N and 123.36°W to 126.91°W. Instrument depths ranged from 724 m to 2400 m and the duration of the time series was about one year or longer. An exception is a short two month data set from the northern gap in the ridge that connects Santa Rosa Island and Cortez bank which was a relatively shallow 337 m. The total duration of current meter data analyzed was 320 months.

Currents were observed with Aanderaa RCM 8 current meters. Although these meters are now about twenty five years old, they are still a reliable means of collecting data. Failures were rare: during the 321 months of data collection, only eight months of data were lost due to rotor failures. A greater difficulty was due to the stall speed of the paddle wheel. For example, there were a total of 127,774 half hour observations at a depth of 1180 m at S2 of which 20,960 observations (16% of the total) had a recorded speed less than 1 cm/s. At deeper depths, this percentage increased. These missing low speed data don't affect the results presented here but they could distort vector averages, standard deviations, etc. for observations where the mean or median speed approaches the stall speed.

Tidal energy dominated the kinetic energy spectra for the current meter data. And the semi-diurnal spectral density dominated the tidal kinetic energy except for the current meter data from the northern gap in the ridge between Santa Rosa Island and Cortez Bank. At semidiurnal frequencies, anticyclonic rotary motion exceeded cyclonic motion and the kinetic energy was typically an order of magnitude greater than for diurnal frequencies. At both diurnal and semidiurnal frequencies, the kinetic energy decreased about an order of magnitude as depth increased by 1000 m.

Deep RAFOS floats were also used to observe lower frequency currents. Nine floats were deployed off the California and Oregon Coasts over a period of 10 years from 1994 to 2004 at pressures ranging from 1152 dbar to 2205 dbar. The float trajectories

covered a region from 32°N to 40°N and from the coast to a distance of about 300 km offshore. The deep float trajectories indicated the weak, (mean speed 4.0 cm/s) meandering and dispersive character of the deep flow. The mean speed of the current meter data was 6.1 cm/s.

Historical hydrographic data showed that the currents should have an overall poleward movement near 1000 dbars at the coast. Both the RCM8 and the northern RAFOS datasets tend to confirm this observation. One exception was a mooring just north of Monterey Submarine Canyon where the currents at 1180 m were persistently southward. Long term mean currents at Sur Ridge and Davidson Seamount were also southward as was the mean displacement of a float off Southern California. Bathymetry affected the variance of the currents: alongshore variability exceeded cross-shore variability.

For eighteen of the 144 months of float measurements, two floats were trapped within mesoscale eddies, one cyclonic and the other anticyclonic. The eddies moved westward with a speed of about one cm/s while the floats swirled around the eddies at a speed of about nine cm/s. The period of the anticyclonic (cyclonic) eddy was 8.6 (15.1) days and the diameter 22.7 (37.4) km. When 350 dbar floats were trapped in eddies, the shallow eddies were clearly delineated by sea level anomalies; there appear to be no correlation between sea level anomalies and the two deep eddies (Chelton, personal communication). This suggests that these deep eddies were baroclinic features.

Only one current meter record was sufficiently long to study the eddy kinetic energy as a function of month. This record, near Monterey Bay, showed little EKE in February, ~3 cm^2/s^2; maximum eddy kinetic energy, greater than 10 cm^2/s^2, occurred in April, June and July.

Seasonal variability along the continental slope was marked by late winter to fall temperature fluctuations. Temperature maxima were observed summer or fall and coincided with strong alongshore flow. Temperature minima occurred in late winter and fall when currents were not as strong.

A large number of the current measurements were made on moorings of opportunity, e.g. moorings that were principally deployed to collect acoustic or sediment trap data. The current data reported here are sufficiently interesting that additional current measurements on moorings of opportunity are warranted, especially as these are likely to be deployed near the depth of the deep sound channel where the paddle wheel should function well. Features observed at two sites are also worthy of additional data collection. At the bottom of the gap connecting Santa Rosa basin to the Pacific Ocean, diurnal currents were nearly as strong as semidiurnal currents and during the period of strongest eastward tidal flow, warmest temperatures occurred. At Hoke Seamount, the inertial period is 22.5 hours, and the kinetic energy at this frequency was 60 cm^2/s^2, larger than that observed at other mooring locations.

Name of Deployment	Mean Speed (cm/s)	Vector Mean Flow °T (speed cm/s)	Mean t °C (std °C)	Semi-major cm/s (semi-minor cm/s)	Semi-major axis orientation°T	Semi-diurnal spectral density cm^2/s^2 (rotary coefficient)	Diurnal spectra density cm^2/s^2 (rotary coefficient)	Inertial spectral density cm^2/s^2 (rotary coefficient)	Spectral density ratio (diurnal/semi-diurnal)	Instrument Depth (m) RCM8	Bottom Depth (m)	Length of deployment (days)
Mooring D1 2000m	3.63	354.9 (0.2)	2.06 (2.07)	3.5 (2.8)	294.0	214.6 (-0.19)	55.34 (0.4)	12.09 (0.9)	0.26	2000	2450	357
Mooring D1 2400m	4.28	348.9 (0.1)	1.82 (1.82)	4.8 (2.5)	253.9	464.5 (0.009)	21.11 (-0.03)	N/A	0.045	2400	2450	357
Mooring D2	7.39	327.8 (1.4)	3.443 (3.447)	6.8 (4.9)	355.1	1033 (0.163)	82.19 (-0.164)	N/A	0.08	1142	1200	357
Mooring R1	8.89	266.5 (0.6)	4.41 (4.4)	9.3 (4.3)	351.5	779.5 (0.47)	59.66 (0.16)	49.18 (0.97)	0.077	793	1400	358
Pioneer Seamount	N/A	N/A	4.52 (4.56)	N/A	N/A	N/A	N/A	N/A	N/A	766	841	670
S2	5.37	162 (1)	3.48 (3.48)	4.9 (3.9)	349.0	89.11 (0.27)	16.84 (0.43)	29.93 (0.96)	0.19	1180	1798	2297
S3	2.74	263.4 (0.7)	1.83 (1.82)	4.6 (2.7)	335.1	148.1 (0.34)	8.202 (0.13)	6.874 (0.91)	0.055	2348	2995	850
Sur Ridge	11.48	162.4 (0.3)	4.58 (4.57)	11.8 (6.5)	306.5	1503 (0.65)	359.6 (0.62)	N/A	0.24	789	834	417
Pt. Sur SOSUS	11.02	348.4 (1.1)	3.05 (3.04)	9.6 (7.8)	203.6	2215 (0.84)	144.5 (0.25)	N/A	0.065	1368	1396	669
Davidson Seamount	8.2	196.4 (2.0)	3.22 (3.21)	8.2 (5.4)	323	807.7 (0.85)	20.84 (0.75)	40.53 (0.89)	0.026	1235	1290	556
Santa Rosa Gap	24.9	250.4 (16.9)	7.73 (7.76)	20.9 (6.1)	250.1	1271 (-0.5)	834.4 (0.15)	N/A	0.66	337	359	54
Hoke Seamount	5.19	073.7 (0.2)	5.43/4.624 (5.42/4.62)	4.6 (4.1)	337.3	146.9 (0.2)	N/A	59.91 (0.96)	N/A	724	774	2708

Table 4-1. RCM 8 current meter results.

RAFOS Number	Vector mean flow direction °T (speed cm/s)	Mean Pressure (dbars)	Mean Temperature (°C)	Mean Diffusivity Ratio	Mean speed (cm/s)	Length of Deployment (days)
15	002(1.2)	1586	2.8	0.559	3.5	550
16	197.5(0.039)	1657	2.63	0.924	3.2	925
37	339.1(0.2)	2204.9	2.1	0.357	4.3	55
38	024.2(0.21)	2202.5	2.04	1.05	1.5	125
44	319.1(3.62)	1852	2.33	0.421	5.3	56
58	250.4(0.5)	2023	2	0.099	3.6	350
74	294.6(0.77)	1541.6	2.7	1.27	7.5	449
79	284.5(0.75)	1152.6	3.48	1.71	5.4	665
86	114.7(0.08)	1567.7	2.71	0.519	3.0	1146

Table 4-2. RAFOS float results

Name of mooring location	Maximum Temperature (°C)	Date of Maximum temperature
Mooring D1 2000M	2.268	11 June 1998
Mooring D1 2400M	1.954	3 June 1998
Mooring D2	3.815	24 December 1997
Mooring R1	3.39	27 November 1997
Pioneer Seamount	5.0043	29 June 2000
S2	3.933	2 July 2000
S3	1.932	18 January 2000
Sur Ridge	14.732	30 April 2009
Pt. Sur SOSUS	3.34	28 June 2008
Davidson Seamount	3.591	25 September 1999
Hoke Seamount	5.936	05 July 2000

Table 4-3. Maximum temperatures and date of observations for data collected from RCM8 current meters.

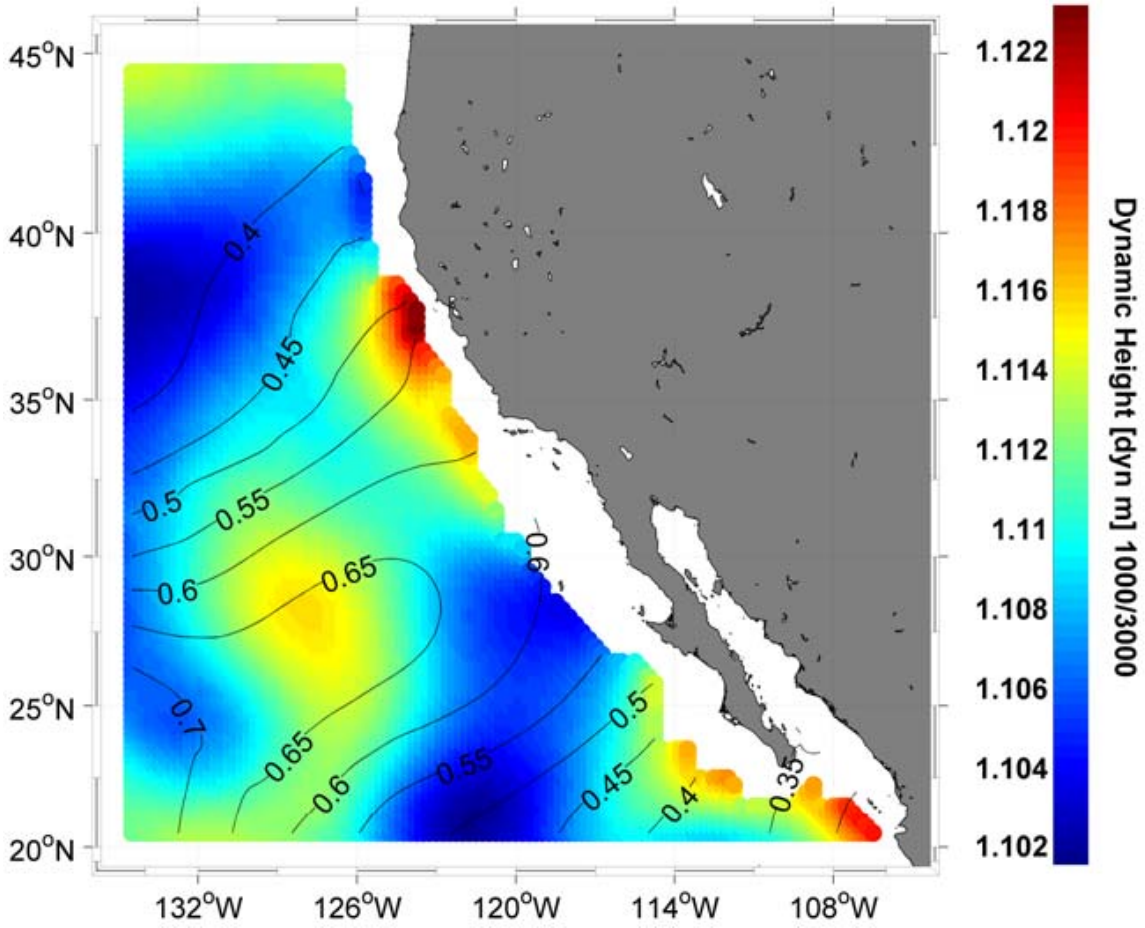

Figure 4-1. Dynamic topography of 1000 dbar relative to 3000 dbar in dynamic meters superimposed by the distribution of dissolved oxygen at 1000 dbar. The scale for dynamic height is given at the right. Dissolved oxygen units are ml/l and the contour interval is 0.05 ml/l. Data are from the 2005 World Ocean Data base.

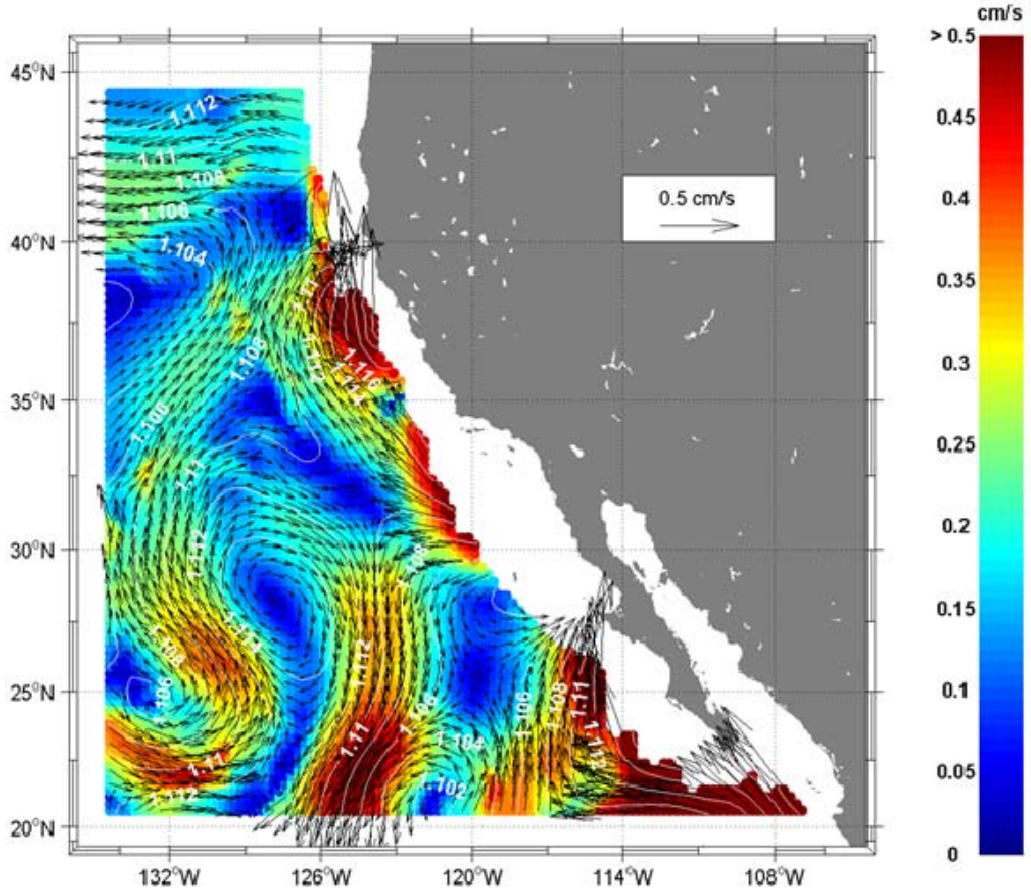

Figure 4-2. Geostrophic flow at 1000 dbar relative to 3000 dbar. The color bar on the right shows the speed in cm/s. White numbers and lines represent the dynamic thickness between 1000 and 3000 dbar in dyn. m (also shown in Fig. 4-2) and black arrows represent the geostrophic flow.

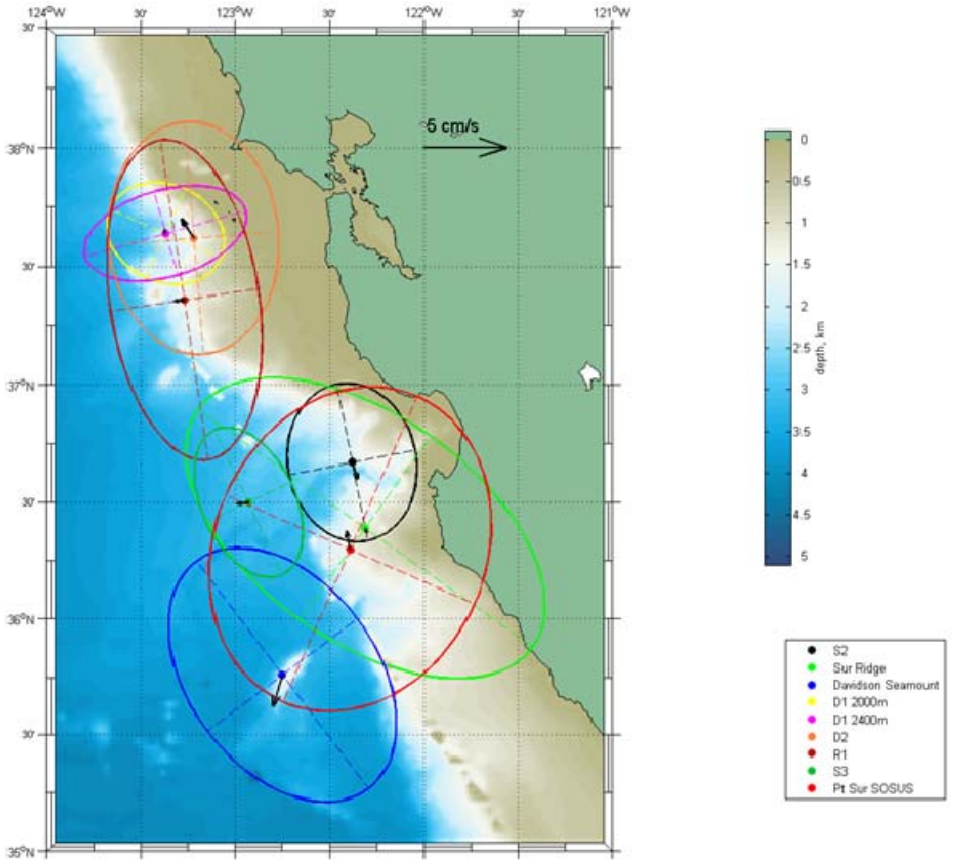

Figure 4-3. Vector mean velocity and variance ellipses for current meter deployments excluding Hoke Seamount and Santa Rosa Gap. The color bar to the right indicates the water depth in kilometers and the legend below the color bar gives the location of each current meter.

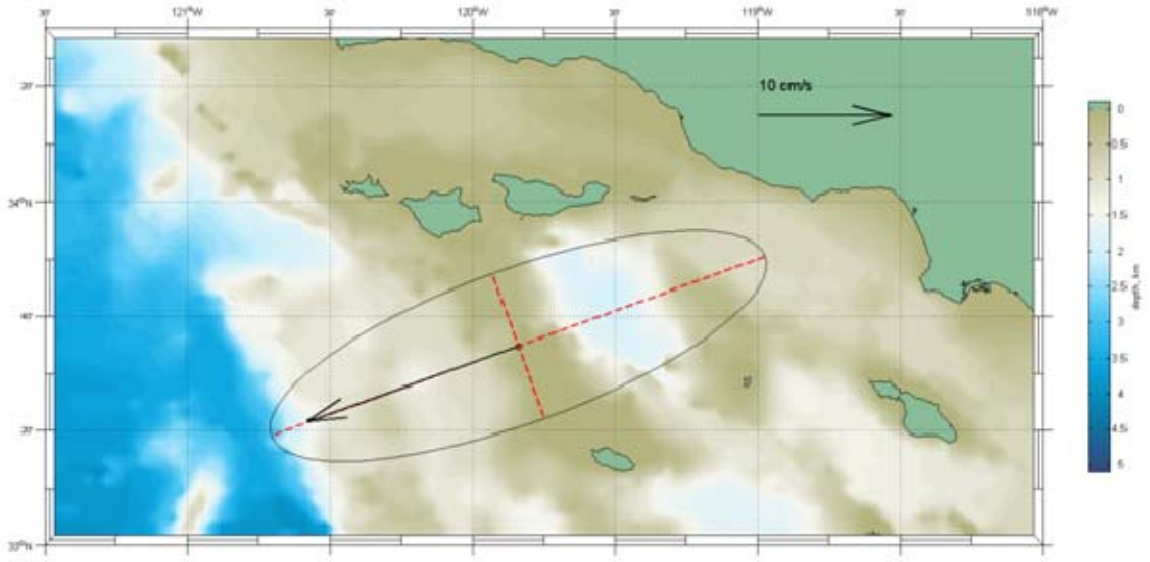

Figure 4-4. Vector mean ve locity and variance ellipse for current meter measurements near the bottom of the northern gap (referred to as Santa Rosa gap) in the ridge between Santa Rosa Island and Cortez Bank.

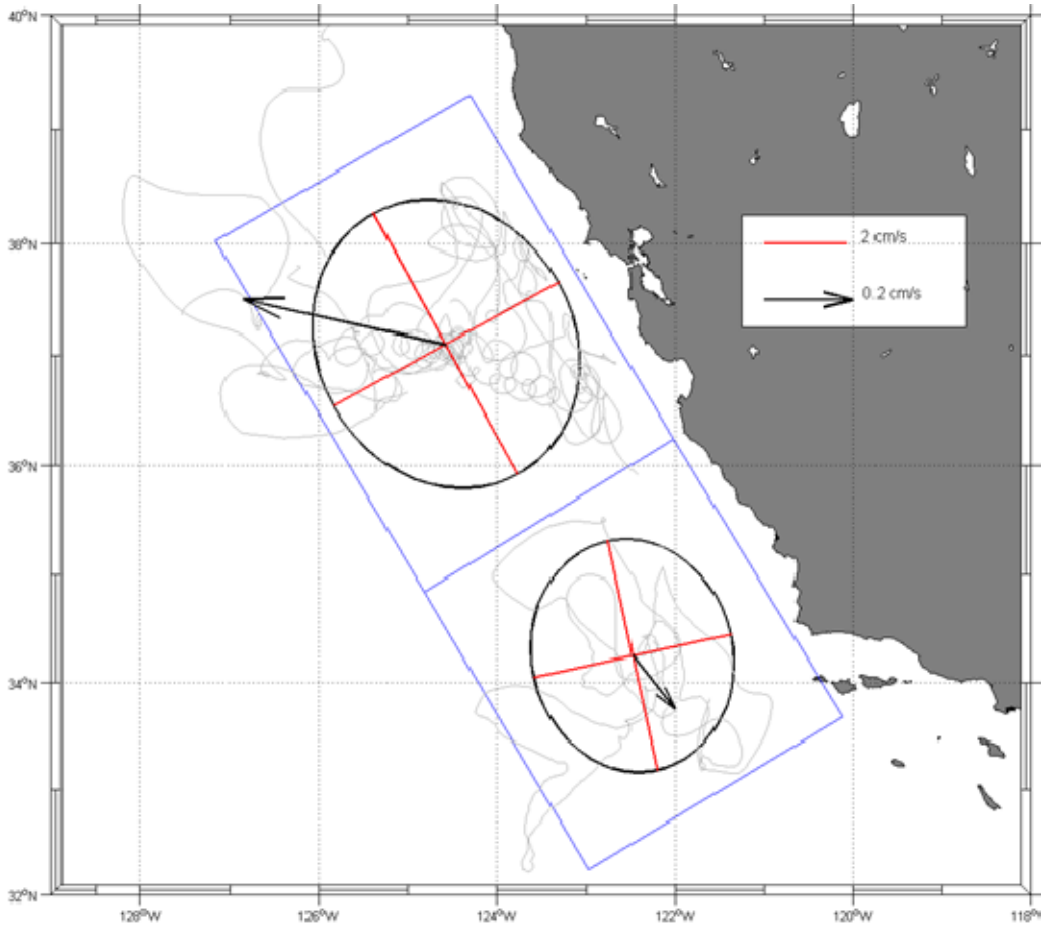

Figure 4-5. Mean and standard deviation of velocities from RAFOS floats. Data were binned in the geographical areas outlined in blue. The northern bin contains data from trajectories for RAFOS 15, 16, 44, 74, and 79. The bottom bin contains data from RAFOS 86. Note that different scales are used for the mean velocity and the variance ellipse.

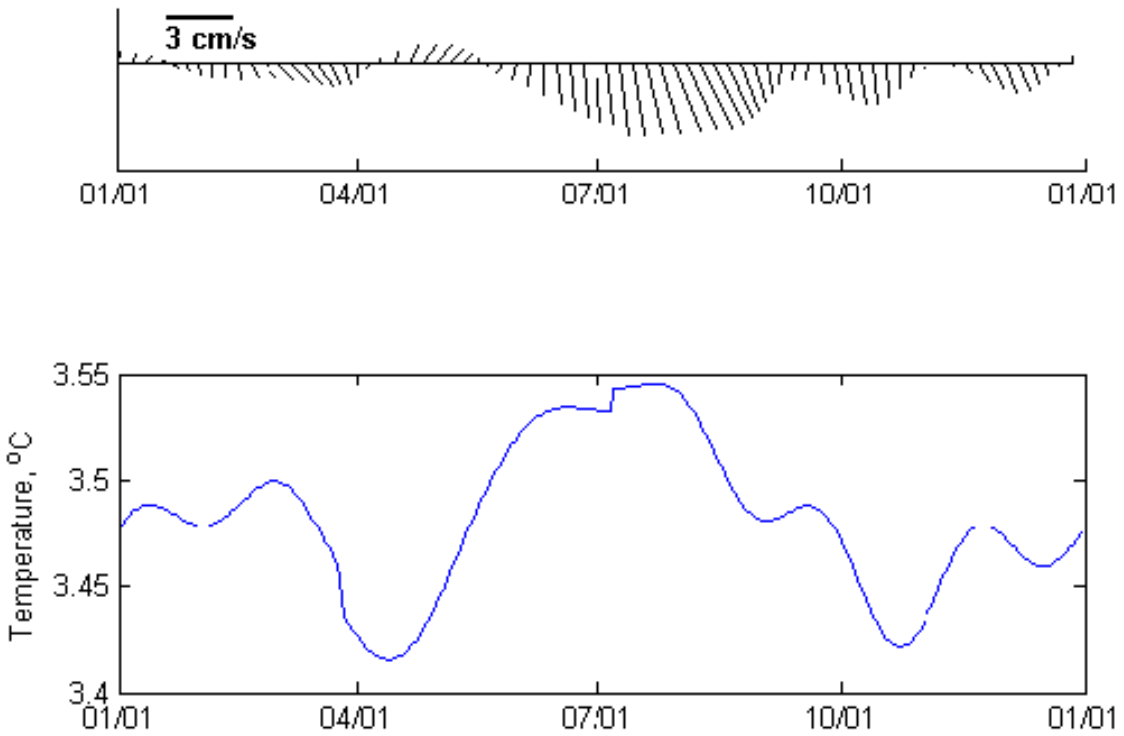

Figure 4-6. S2 seasonal variability. This location is immediately to the north of Monterey Submarine Canyon. Observations are for a depth of 1180 m. (upper) Velocity, cm/s. (lower) Temperature, °C.

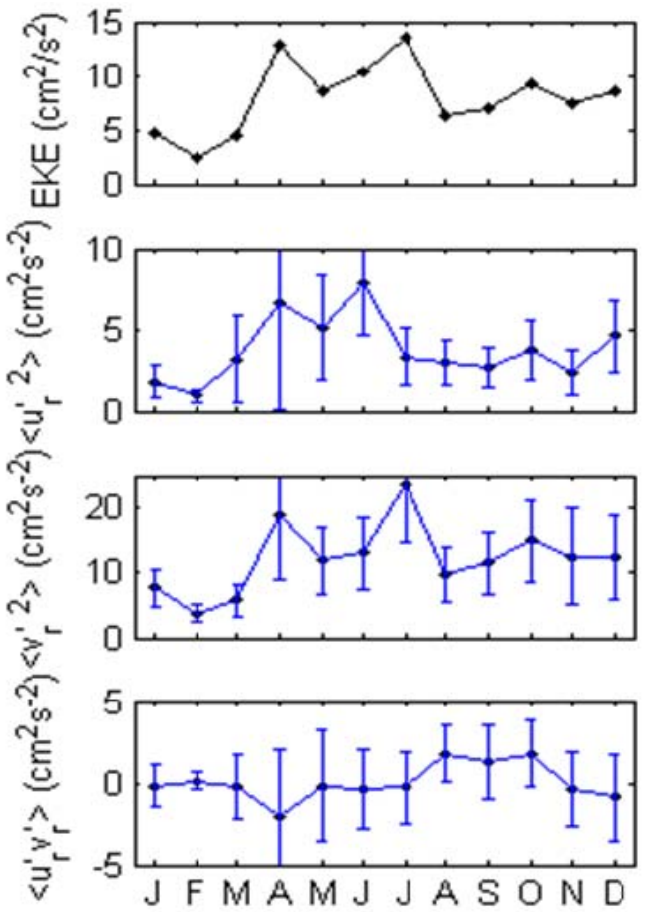

Figure 4-7. Monthly variability of eddy kinetic energy at S2. This location is immediately to the north of Monterey Submarine Canyon. Observations are for a depth of 1180 m. (top) Eddy kinetic energy. (upper middle) Onshore component. (lower middle) Alongshore component. (bottom) Reynolds stress.

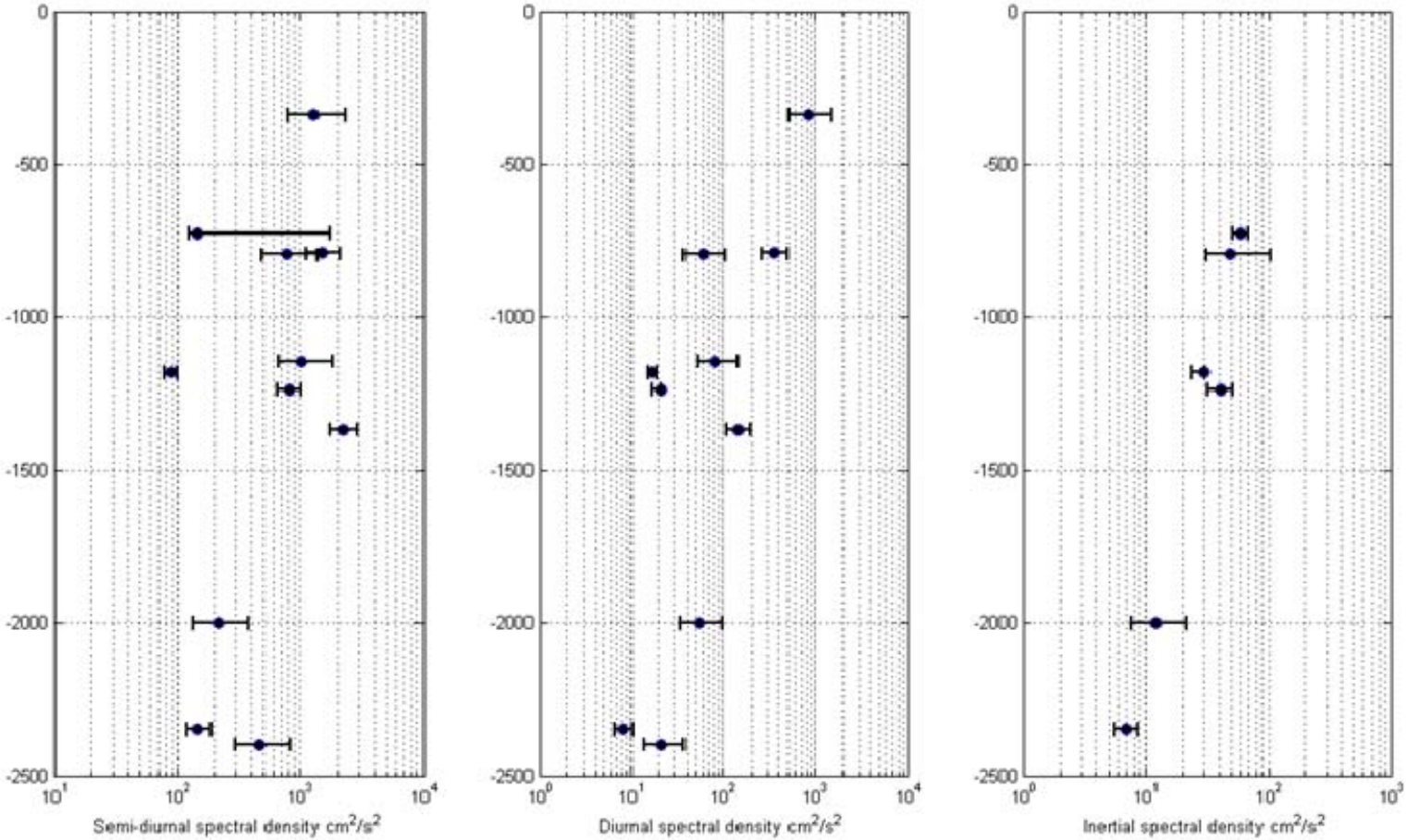

Figure 4-8. Plot of depth versus spectral density estimates of kinetic energy for semi-diurnal, diurnal, inertial periods. Horizontal bars indicate the 95% confidence limits.

APPENDIX A MOORING D1 2000M

This appendix covers the RCM 8 current measurements at a depth of 2000 m at mooring D1 (Fig. A1) deployed from 12 November 1997 to 04 November 1998. The mooring was set near the axis of a submarine valley on the 2450 isobath. The mooring extended upward to a depth of 100 m, and included a number of current meters at shallower depths as well as one at 2400 m (see appendix B). Table A1 contains specific information about the D1 mooring deployment. The sampling rate for the RCM 8 current meter was one sample per hour. The collection of these data was sponsored by the Environmental Protection Agency and managed by Dr. Marlene Noble of the United States Geological Survey.

Northward flow was most common at 2000 m. The mean speed was 3.63 cm/s. Direction (speed) of the vector mean flow was 354.9°T (0.2 cm/s) (Fig. A2). The semi-major (minor) axis magnitude was 3.5 cm/s (2.8 cm/s) and the eccentricity of the variance ellipse was 0.45. The semi-major axis was directed along 294°T to 114°T.

The velocity histogram (Fig. A3) showed the principal mode contained 37 observations at 315°T and a speed of 5 cm/s. There was a smaller mode (nearly reciprocal) with a heading of 105°T at a speed of 5 cm/s with 35 observations.

The PVD (Fig. A4) confirmed the northward flow tendencies. In winter, spring and fall flow was northward, with a weak eastward set in winter and a weak westward set in spring and fall. Summer currents were mostly south-southeast, although a period of westward flow was observed in early August. Due to the large scale of Fig. A4 and the relative strength of the tidal currents, tidal excursions were clearly visible. Longer period eddy-like features, e.g. April-May 1998, also occurred. The stick plot (Fig. A5) used an ordinate with maximum velocity of 2 cm/s (instead of 8 cm/s, used in other appendices): clearly currents at 2000 m were weaker than those at shallower depths. The maximum speed, 15.68 cm/s, was observed on 12 March 1998 (not displayed).

The kinetic energy spectrum (Fig. A6) shows the semi-diurnal frequency completely dominating the variance as well as a smaller but significant peak for the diurnal tides. The local inertial frequency is 0.051 cph with a period of 19.6 hours, but it

is difficult to determine if the energy at this frequency is statistically greater than zero. Similarly, smaller peaks occur at tidal harmonics greater than 0.1 cph.

The rotary spectra (Fig. A7) showed the clockwise component was greater than the counterclockwise component at most frequencies. The largest rotary coefficient, >0.9, corresponded to inertial period flow. At diurnal (semi-diurnal) frequencies the rotary coefficient was ~0.4 (-0.1911).

The temperature histogram (Fig. A8) used a bin size of 0.03°C. The median temperature was 2.07°C and the mean temperature was 2.06°C. The smoothed temperature time series (Fig. A9) showed strong semi-annual character with maximum (minimum) temperatures >2.15°C (<2°C) in mid June and late November (February and mid-October).

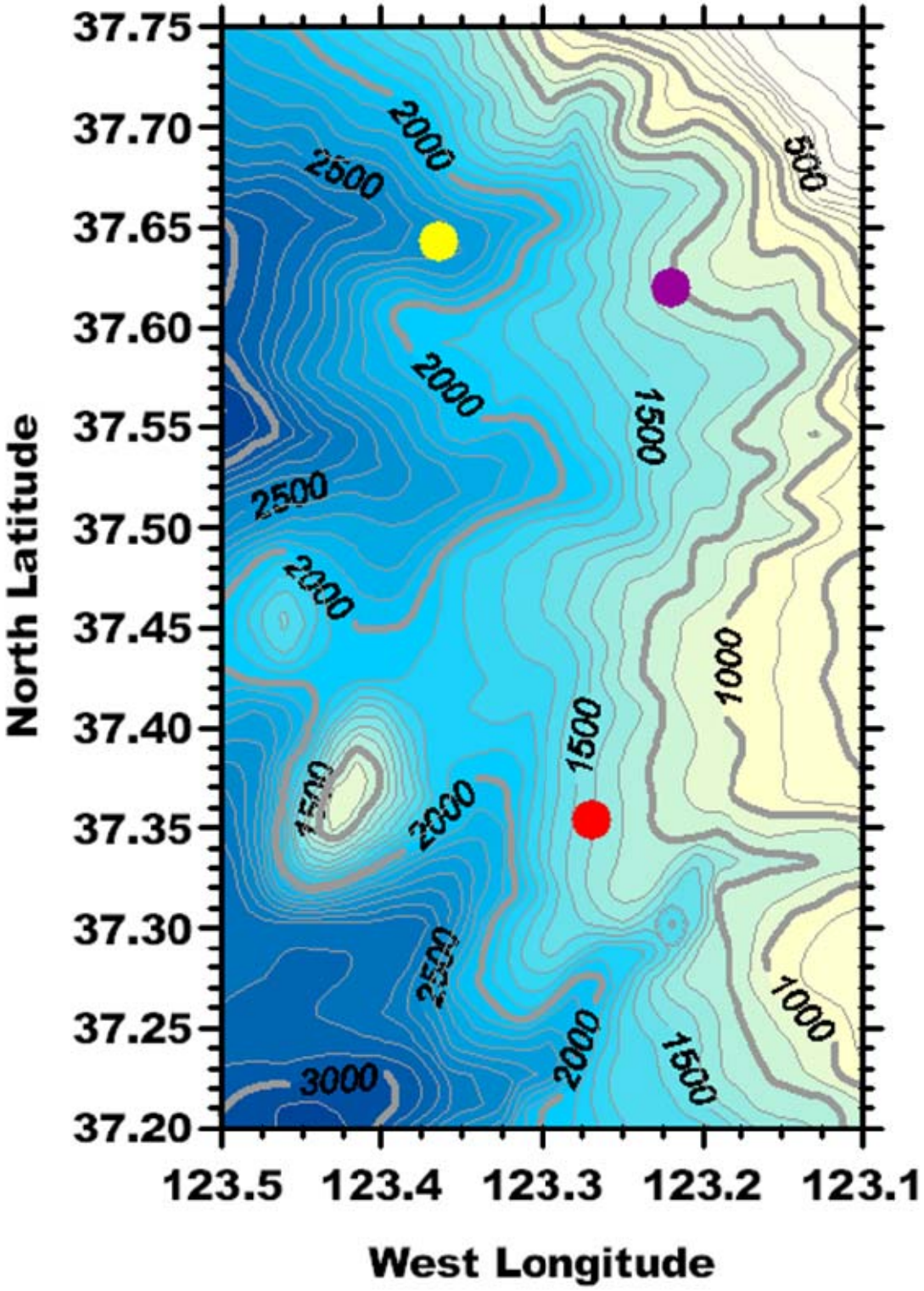

Figure A1. The yellow dot indicates the location of the D1 mooring. Soundings are in meters and the contour interval is 100 m. Pioneer (37.4N, 123.4W) and Gumdrop (37.45N, 123.45W) Seamounts are shown along the western margin of the

chart.

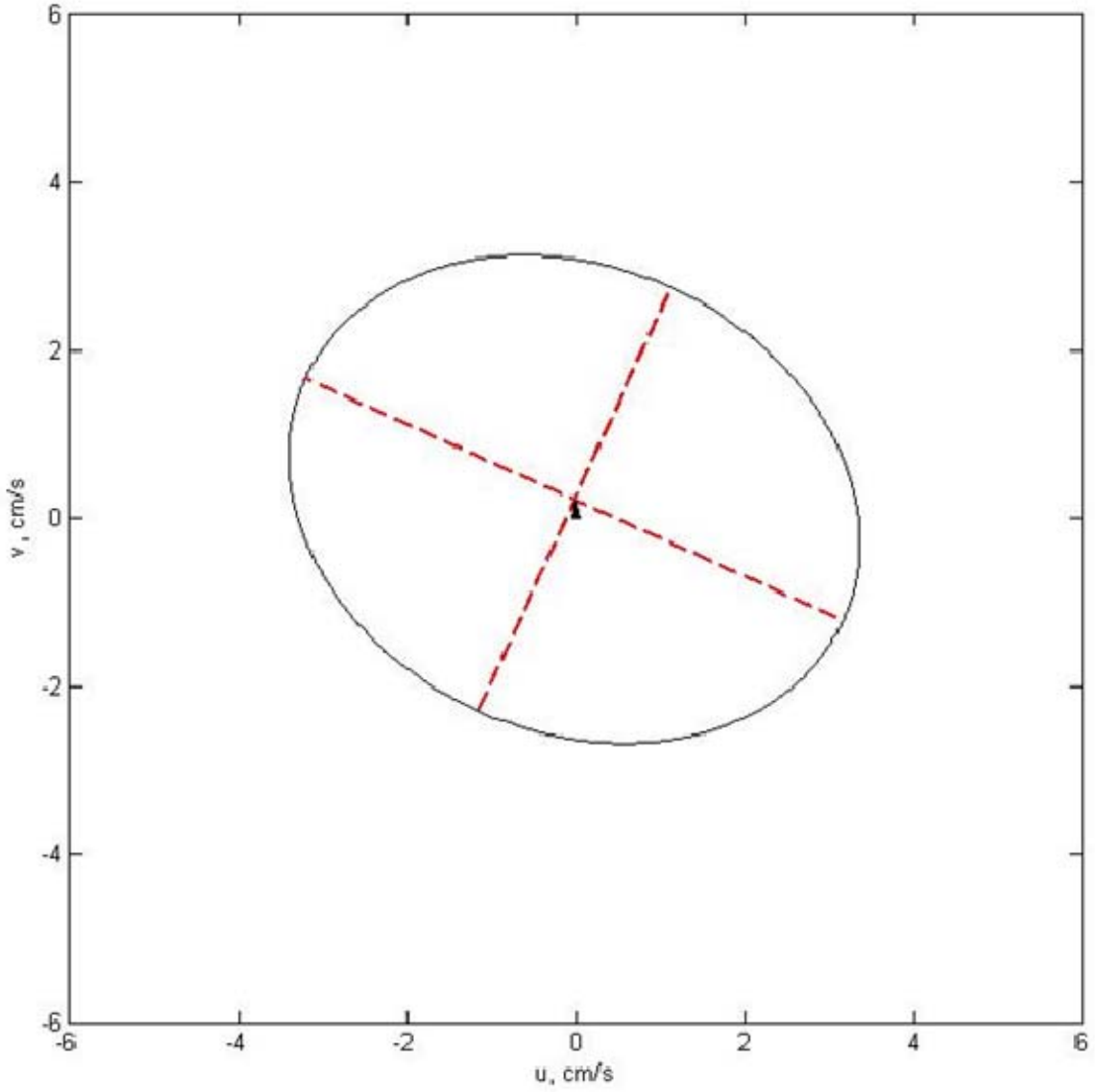

Figure A2. Mean and standard deviation of currents measured at a depth of 2000 m at the D1 mooring. Speed (direction) of the mean vector flow was 0.2 cm/s (354.9°T). The semi-major (semi-minor) axis was 3.5 cm/s (2.8 cm/s) and was oriented along 294°-114°T.

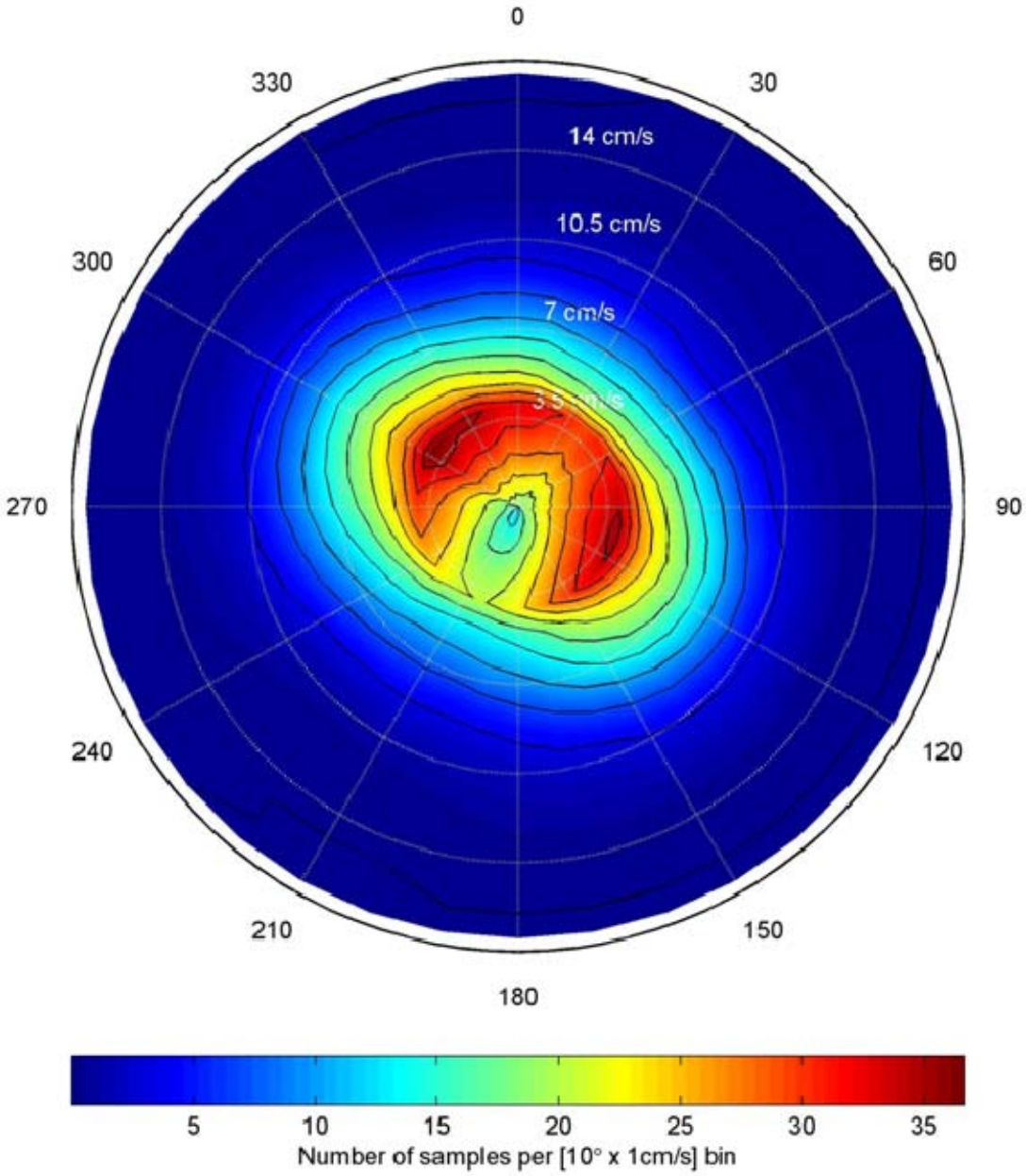

Figure A3. Histogram of velocity observations at 2000 m at mooring D1. The total number of observations is 8,757. 1,238 observations with a speed less than 1 cm/s were omitted. Total number of bins is 666.

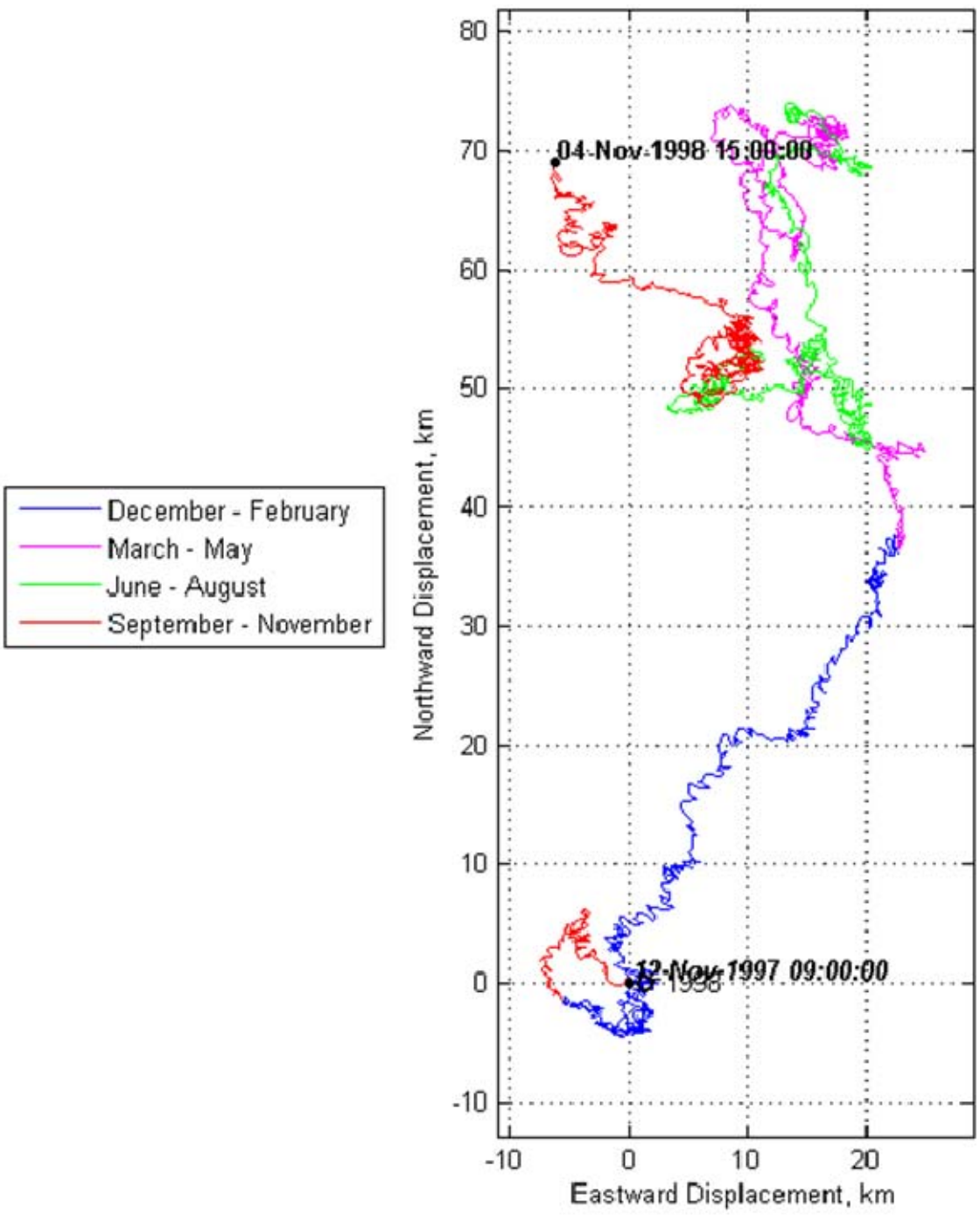

Figure A4. Progressive vector diagram for currents at 2000 m at mooring D1.

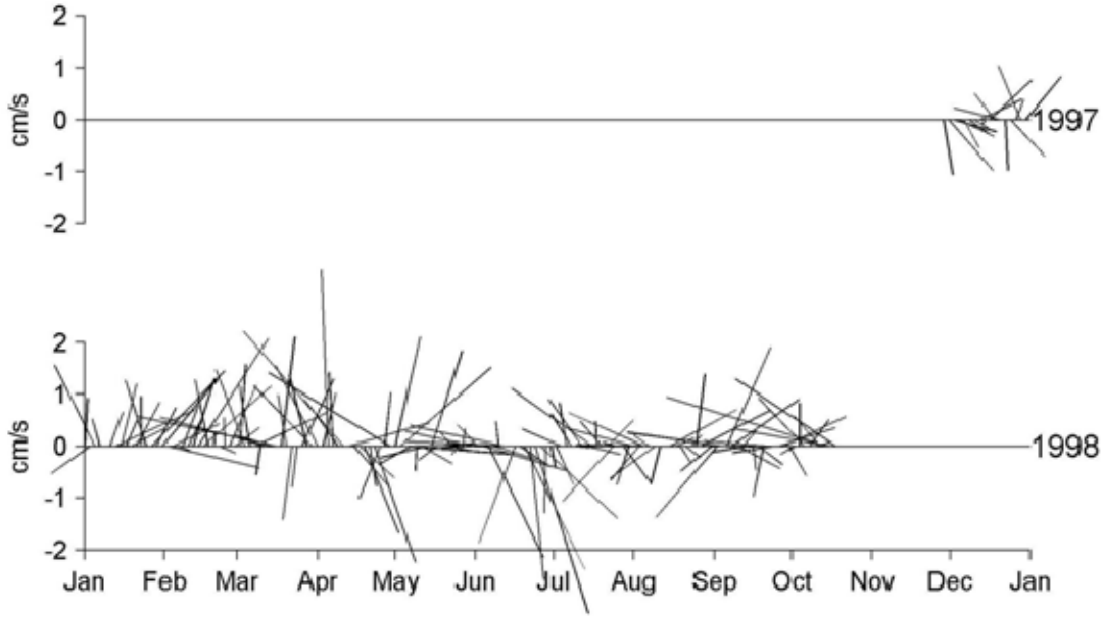

Figure A5. Current velocity at 2000 m at mooring D1 as a function of time. Currents were smoothed using a Butterworth filter with a cutoff period of one week.

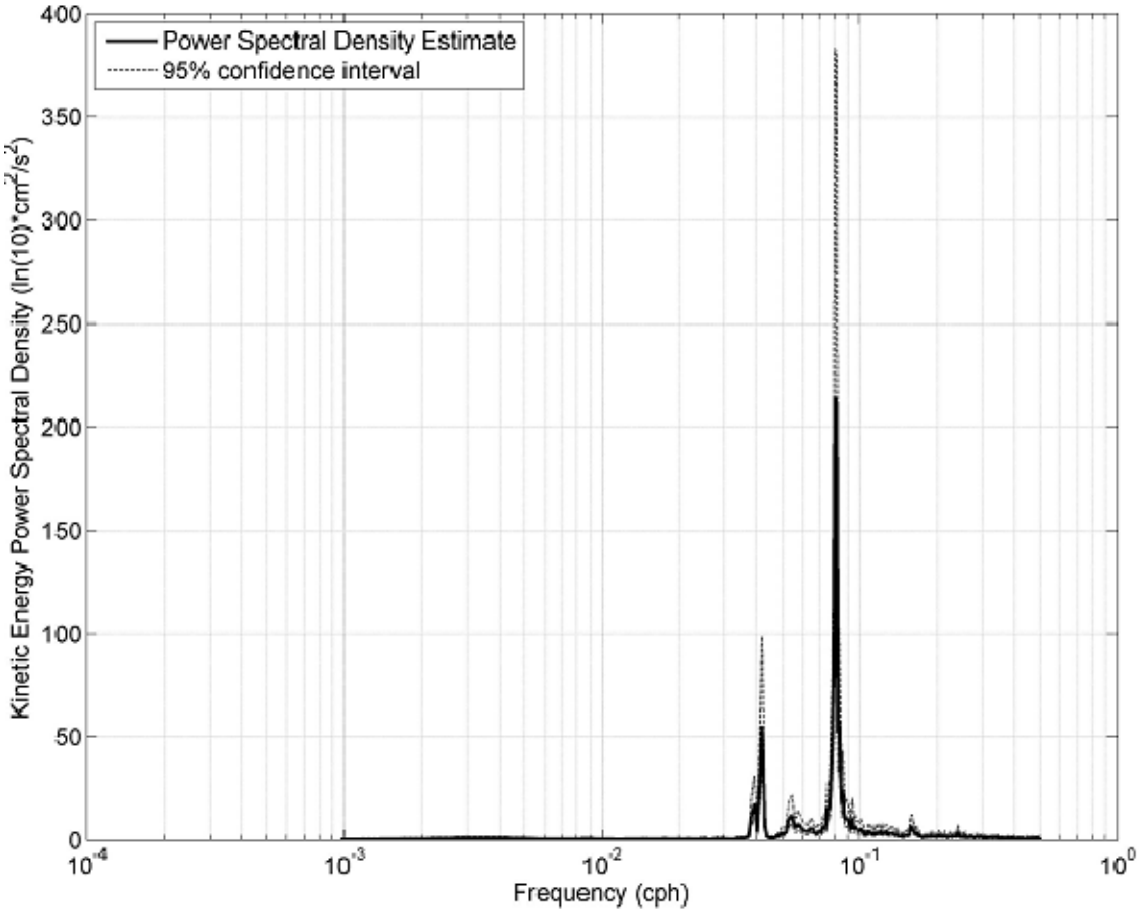

Figure A6. Kinetic energy spectrum for currents at 2000 m at mooring D1. Semi-diurnal peak at 0.08 cph with peaks at 0.039, 0.042, and 0.055 cph.

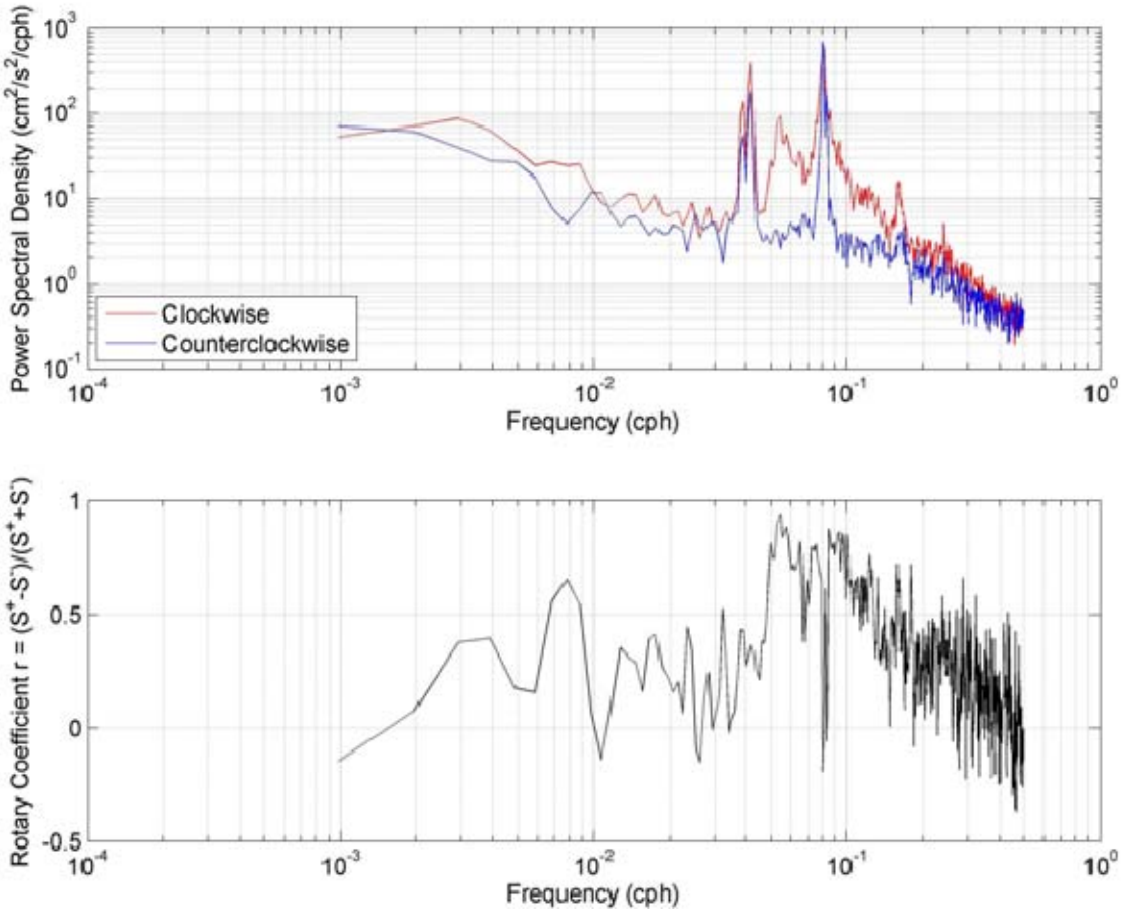

Figure A7. (upper) Rotary spectra for 2000 m currents at mooring D1. (lower) Rotary coefficient.

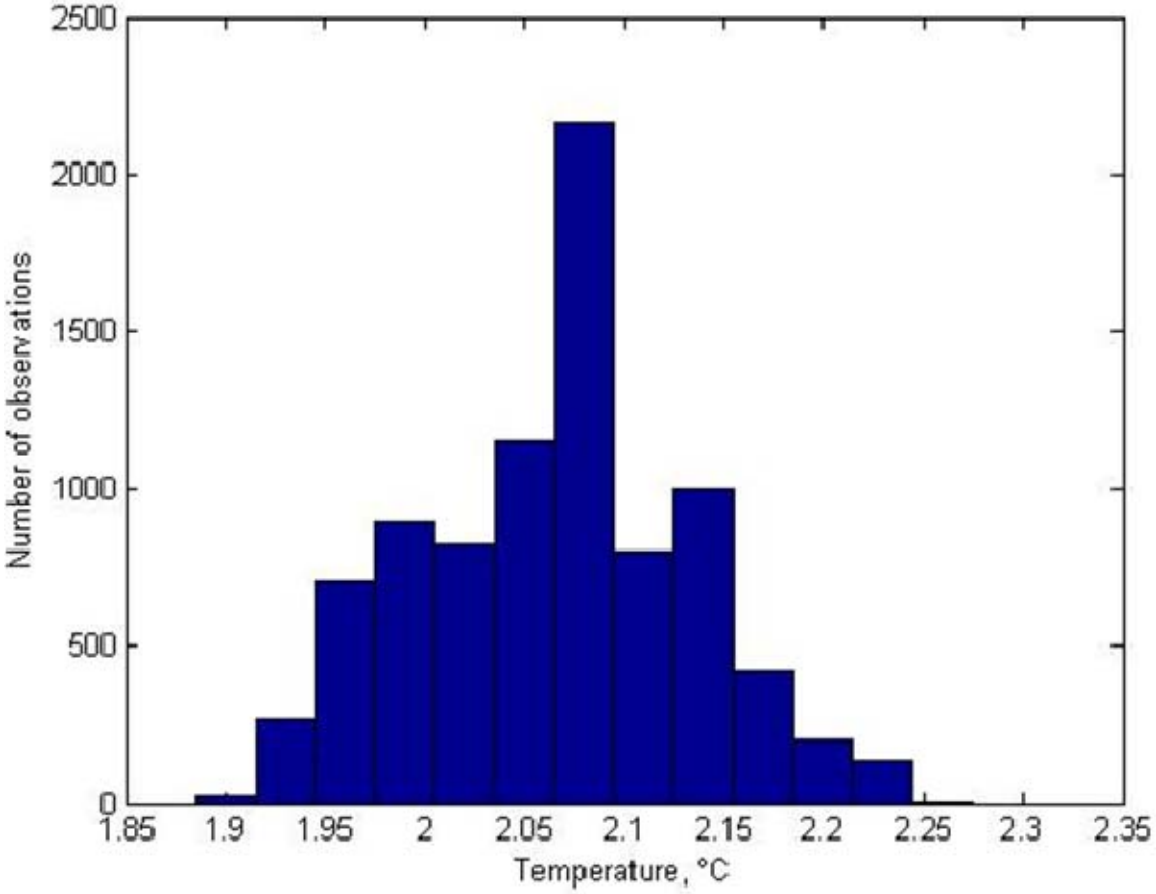

Figure A8. Temperature histogram at 2000 m at mooring D1 using a bin size of 0.03°C.

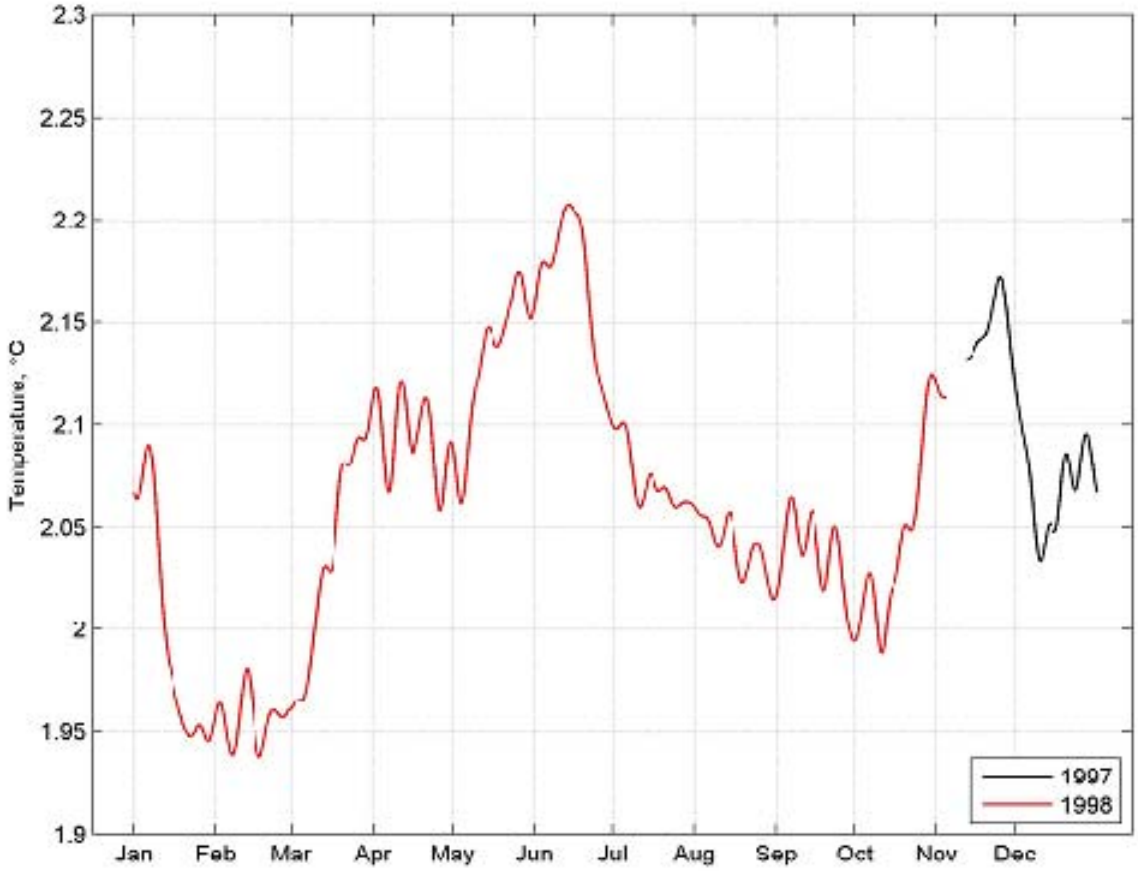

Figure A9. Temperature time series at 2000 m at mooring D1. Temperatures were smoothed using a Butterworth filter that cut off periods less than one week.

Deployment Name	Date of Deployment	Latitude	Longitude	Instrument Depth (m)	Bottom Depth (m)	Compass Correction (E)	Timing Error
D1 Mooring	12 November 1997- 4 November 1998	37° 38.568'N	123° 21.884'W	2000	2450	8’	5’

Table A1. D1 Mooring Deployment Data at 2000 m. The RCM 8 current meter collected one sample per hour.

THIS PAGE INTENTIONALLY LEFT BLANK

APPENDIX B MOORING D1 2400M

This appendix covers the RCM 8 current measurements which were made 50 m above the bottom (current meter depth 2400 m) at mooring D1 (Fig. B1) deployed from 12 November 1997 to 04 November 1998. The data for this current meter suggest the existence of bathymetric flow constraints when compared to the 2000 m current meter described in the previous appendix. The mooring was set near the axis of a submarine valley on the 2450 m isobath. The mooring extended upward to a depth of 100 m, and included a number of current meters at shallower depths. Table B1 contains specific information about the D1 mooring deployment. The sampling rate for the RCM 8 current meter was one sample per hour. The collection of these data was sponsored by the Environmental Protection Agency and managed by Dr. Marlene Noble of the United States Geological Survey.

The mean speed was 4.28 cm/s. Direction and speed of vector mean flow was 348.9°T and 0.1 cm/s, respectively (Fig. B2). The semi-major (minor) axis magnitude was 4.8 cm/s (2.5 cm/s) and the eccentricity of the variance ellipse was 0.69. The semi-major axis was directed along 253.9°T to 073.9°T.

The velocity histogram (Fig. B3) showed the principal mode contained 38 observations at 075°T and a median speed of 5 cm/s. There was a smaller mode with a heading of 265°T at a speed of 5 cm/s with 35 observations.

The PVD (Fig. B4) showed a ~20 km anticyclonic loop from deployment on 12 November 1997 through May 1998. Subsequently flow was westward in summer 1998 and eastward in September and October 2008. Starting on 12 November 1997 the current moves in a southerly direction briefly before shifting north, south, and west during the winter of 1997-1998. For the remainder of 1998 the current is moving in a broadly northerly and westerly heading before ending on a northeasterly heading. Due to the large scale of Fig. B4 and the relative strength of the tidal currents, tidal excursions were clearly visible. Longer period eddy-like features, e.g. April-May 1998, also occurred. The stick plot (Fig. B5) used an ordinate with maximum velocity of 2 cm/s (instead of 8 cm/s, used in other appendices): clearly currents at 2400 m were weaker than those at

shallower depths. The maximum speed, 21.34 cm/s, was observed on 27 February 1998 (not displayed).

The kinetic energy spectrum (Fig. B6) showed the semi-diurnal frequency completely dominating the variance with about twice the energy density observed at 2000 m. The local inertial frequency is 0.051 cph with a period of 19.6 hours. Although small blips occur at diurnal and tidal harmonics >0.1 cph, they were not statistically significant, and the absence of a well defined diurnal peak contrasts with results at 2000 m. The rotary spectra at 2400 m (Fig. B7) showed less dominance of the counterclockwise component than at 2000 m (Fig. A7) with generally smaller rotary coefficients. At the diurnal frequencies, the rotary coefficient was ~-0.2 and at semi-diurnal frequency the rotary coefficient was 0.009; the latter indicated rectilinear flow.

The temperature histogram (Fig. B8) used 0.03°C temperature bins. The median and mean temperatures were 1.82°C. The smoothed temperature time series (Fig. B9) showed strong semi-annual character with maximum (minimum) temperatures >1.88°C (<1.78°C) in May-June and late November (February and early-October).

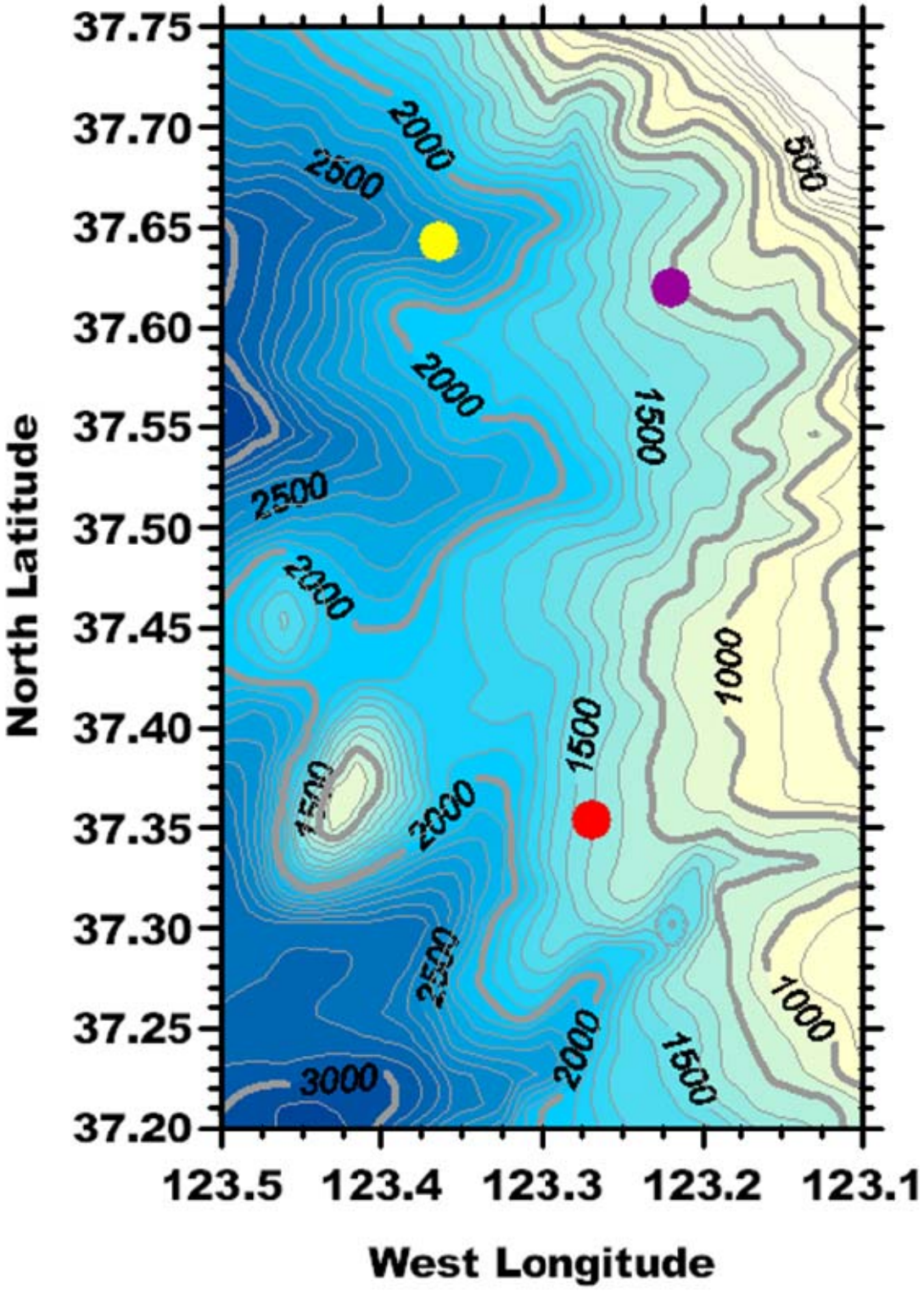

Figure B1. The yellow dot marks the location of mooring. Soundings are in meters and the contour interval is 100 m. Pioneer (37.4N, 123.4W) and Gumdrop (37.45N, 123.45W) Seamounts are shown along the western margin of the chart.

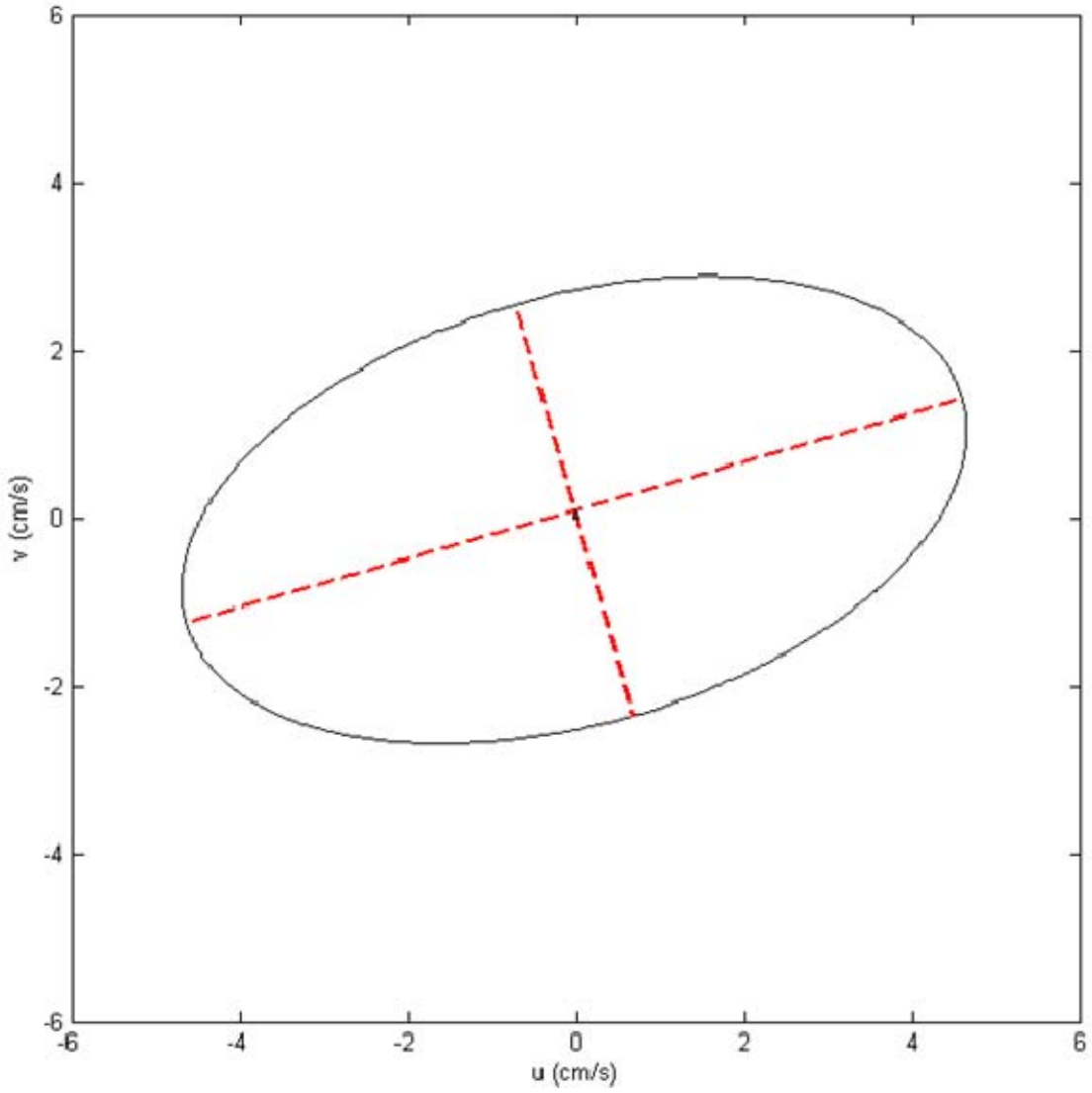

Figure B2. Mean and standard deviation of currents measured at 2400 m at mooring D1. Mean speed (direction) of the mean vector flow was 0.1 cm/s (348.9°T). The semi-major (semi-minor) axis was 4.8 cm/s (2.5 cm/s) and was oriented along 253.9°-073.9°T.

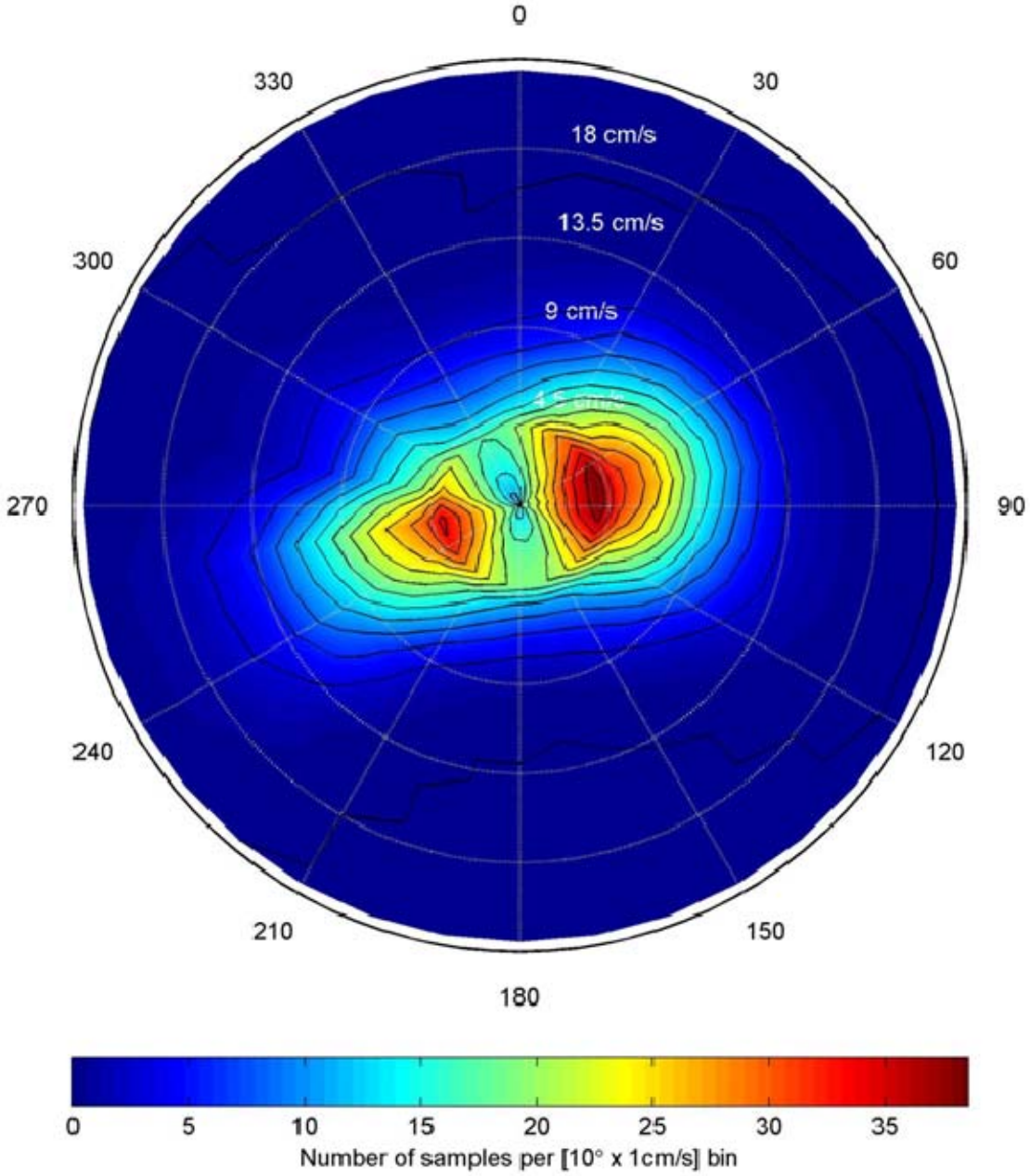

Figure B3. Histogram of velocity observations at 2400 m at mooring D1. The total number of observations is 8,575. 1,253 observations with a speed less than 1 cm/s were omitted. Total number of bins is 851.

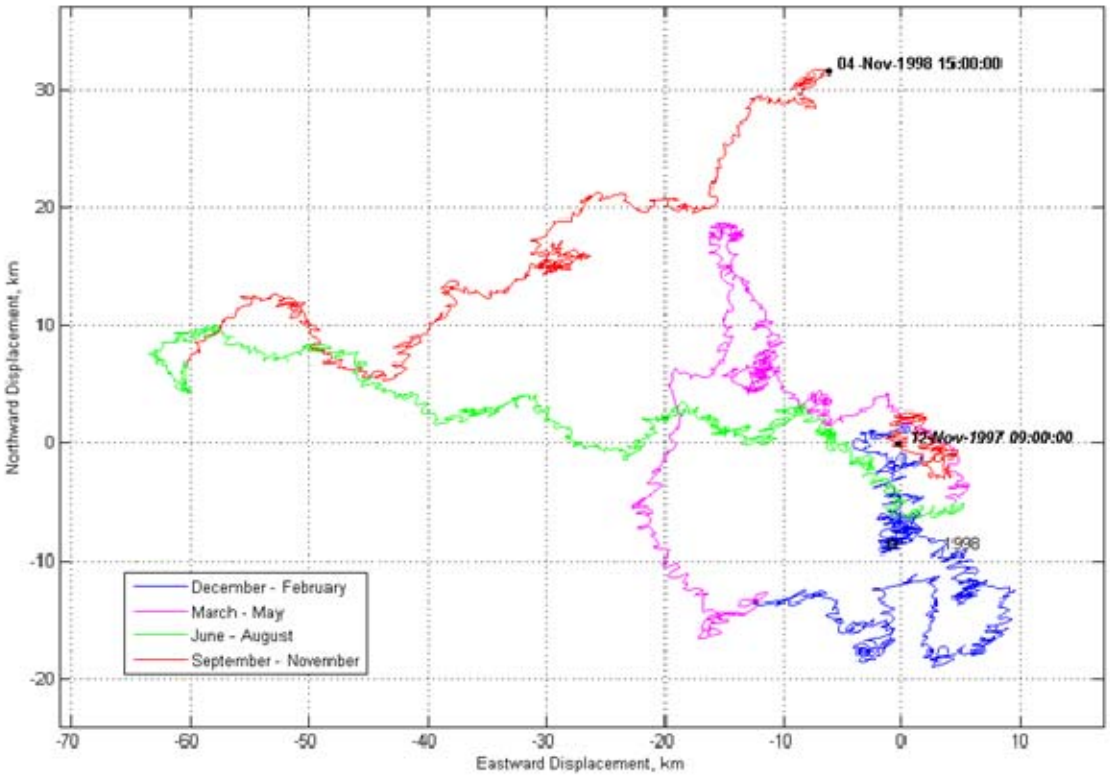

Figure B4. Progressive vector diagram for currents at 2400 m at mooring D1.

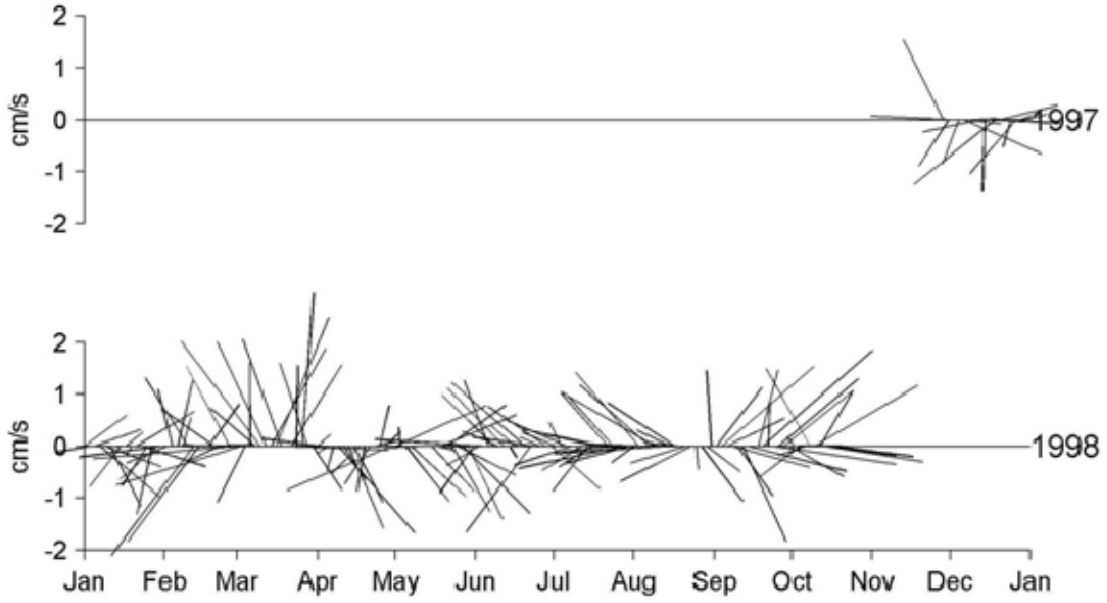

Figure B5. Current velocity at 2400 m at mooring D1 as a function of time. Currents were smoothed using a Butterworth filter with a cutoff period of one week.

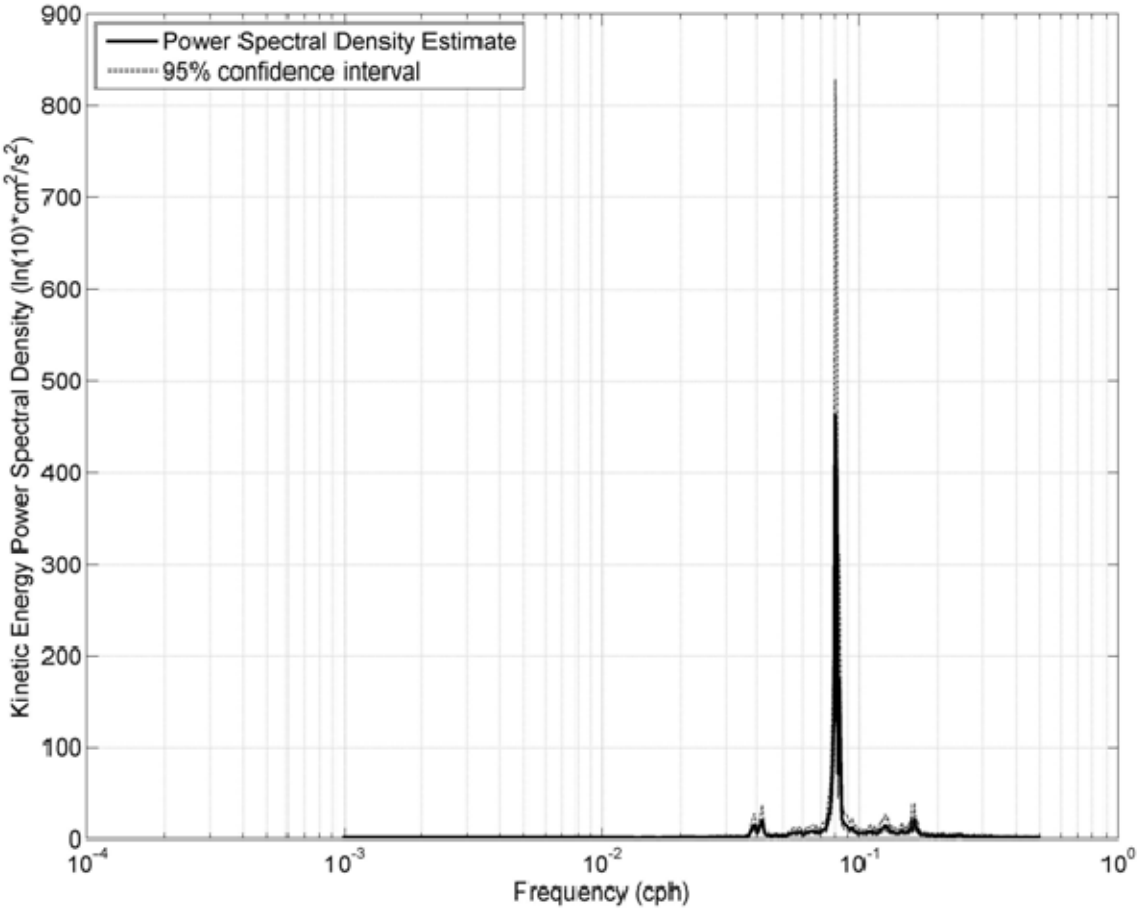

Figure B6. Kinetic energy spectrum for currents at 2400 m at mooring D1. The semi-diurnal peak is 0.08 cph.

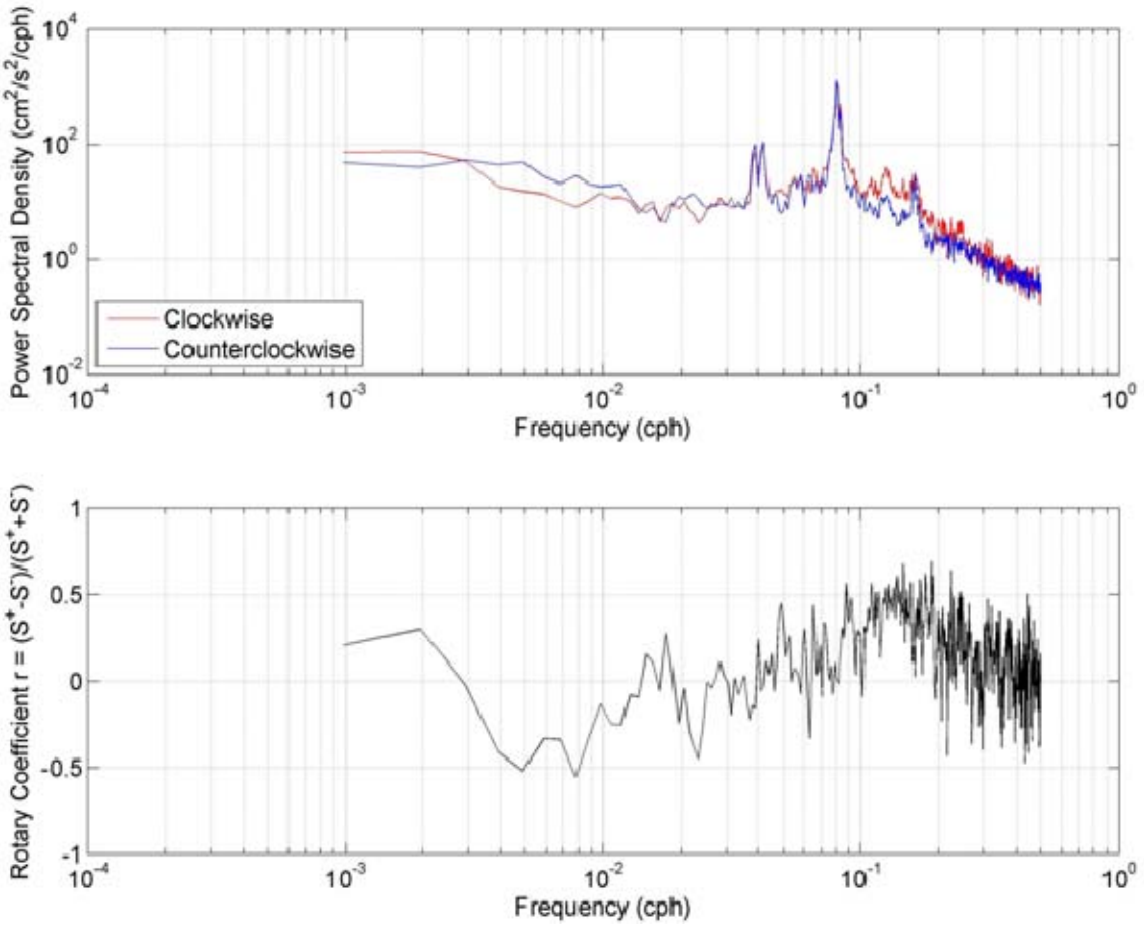

Figure B7. (upper) Rotary spectra for currents at 2400 m at mooring D1. (lower) Rotary coefficient.

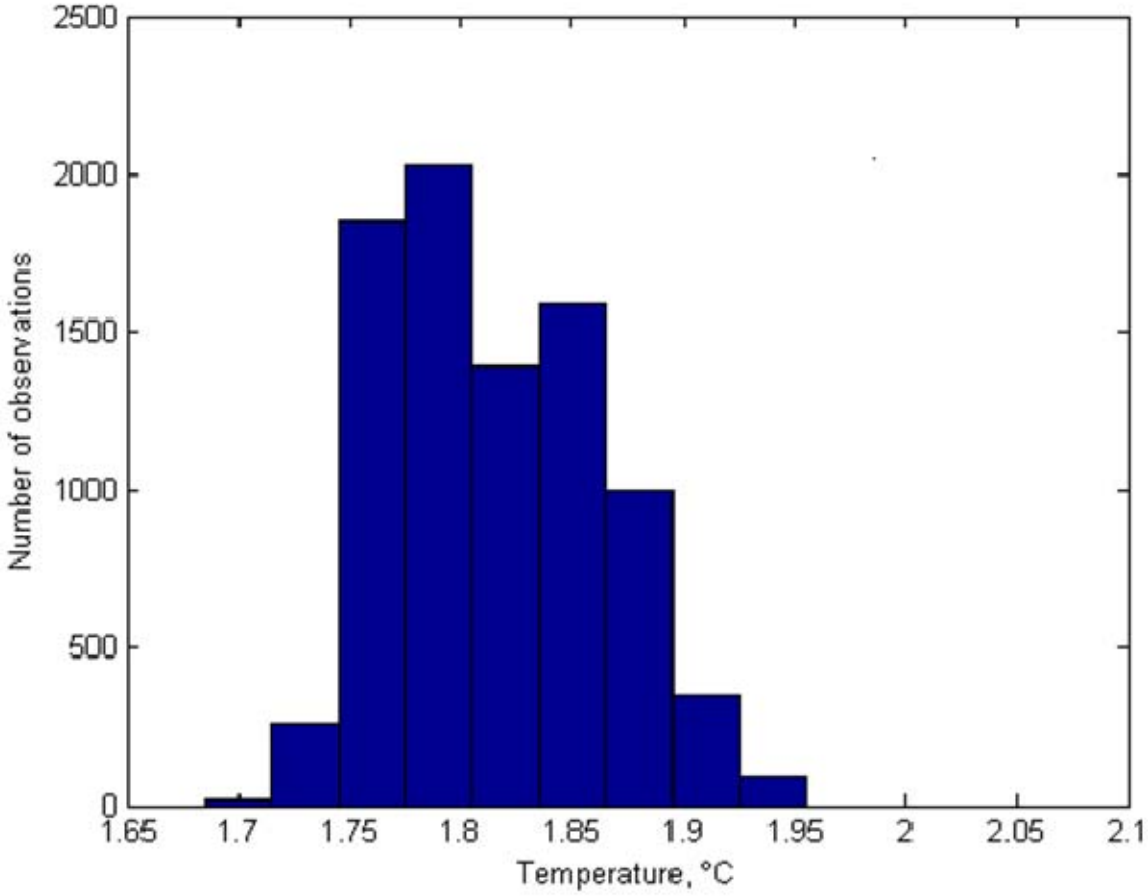

Figure B8. Temperature histogram at 2400 m at mooring D1 using a bin size of 0.03°C.

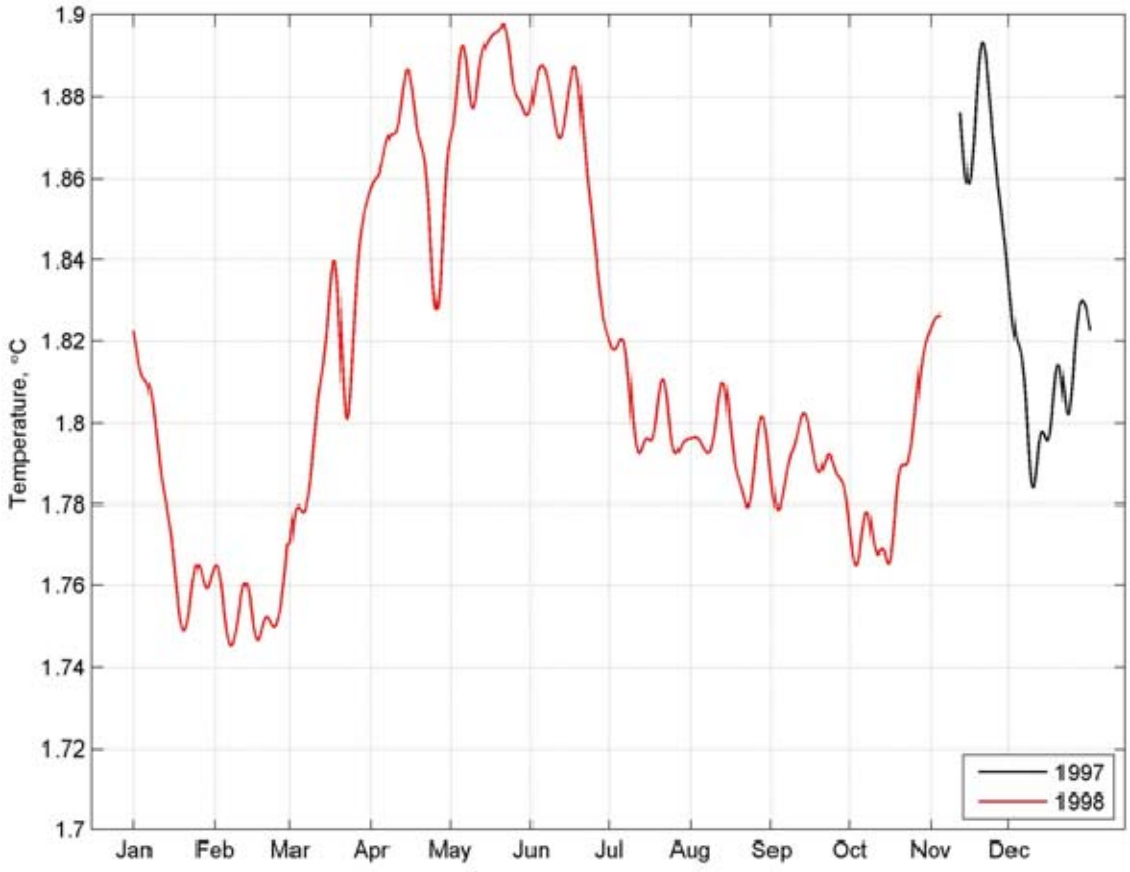

Figure B9. Temperature time series at 2400 m at mooring D1. Temperatures were smoothed using a Butterworth filter that cut off periods less than one week.

Deployment Name	Date of Deployment	Latitude	Longitude	Instrument Depth (m)	Bottom Depth (m)	Compass Correction (E)	Timing Error
D1 Mooring	12 November 1997- 4 November 1998	37° 38.568'N	123° 21.884'W	2400	2450	8’	5’

Table B1. D1 Mooring Deployment Data. The RCM 8 current meter collected one sample per hour.

THIS PAGE INTENTIONALLY LEFT BLANK

APPENDIX C MOORING D2

This appendix covers the deployment at mooring D2 (denoted by purple in Fig. C1) from 12 November 1997 to 04 November 1998 at a depth of 1142 m. The mooring utilized the RCM 8 for oceanographic measurements. Table C1 contains specific information about this deployment. The sampling rate for the RCM 8 device was one hour.

The mean speed was 7.39 cm/s. Direction and speed of vector mean flow was 327.8°T and 1.4 cm/s, respectively (Fig. C2). The semi-major (minor) axis magnitude was 6.8 cm/s (4.9 cm/s) and the eccentricity of the variance ellipse was 0.53. The semi-major axis was directed along 355.1°T to 175.1°T.

The velocity histogram (Fig. C3) showed the principal mode contained 31 observations per bin at 000°T and a median speed of 8 cm/s. There is a smaller mode with a heading of 190°T at a speed of 8 cm/s with 21 observations per bin.

The PVD (Figure C4) shows predominantly a northeastward flow. Starting on 12 November 1997 the current moves in a northeasterly direction until near the end of its deployment, when the current shifts to a southwesterly direction.

The stick plot (Figure C5) displays fast moving currents moving primarily in a northeasterly pattern, confirming the observation from the PVD. The maximum speed was 24.77 cm/s observed on 25 January 1998 and the minimum speed was 0.1128 cm/s observed on 21 September 1998. The maximum speed is not observable from the stick plot due to smoothing of data, but is calculable from the raw data.

The kinetic energy spectrum (Figure C6) shows the semi-diurnal frequency completely dominating the variance. The calculated local inertial frequency is 0.051 cph with a period of 19.7 hours; but at that frequency it is difficult to make out a peak, suggesting that in these currents it is inconsequential. There are two distinct diurnal peaks at frequencies of 0.039 and 0.042 cph with periods of 25.6 hours and 23.8 hours, respectively.

The rotary spectra (Figure C7) display the counterclockwise component dominating the clockwise component during the diurnal frequencies, but changing

dominance during the higher frequencies. At the diurnal peaks the rotary coefficient is -0.16 and -0.007. At the semi-diurnal peak the rotary coefficient is 0.163, and the spectra display shows the counterclockwise component and the clockwise component almost equivalent. The current at the semi-diurnal frequency was nearly rectilinear, while the diurnal frequencies were cyclonic. At other frequencies the current was anti-cyclonic.

The temperature histogram (Fig. C8) used 0.05°C and the median temperature was 3.447°C with a mean temperature of 3.443°C. The time series (Fig. C9) displays the temperature over time. The highest peak was observed on 22 December 1997 at a temperature of 3.68°C, while the minimum was observed on 28 Feb. 1998 at a temperature of 3.12°C.

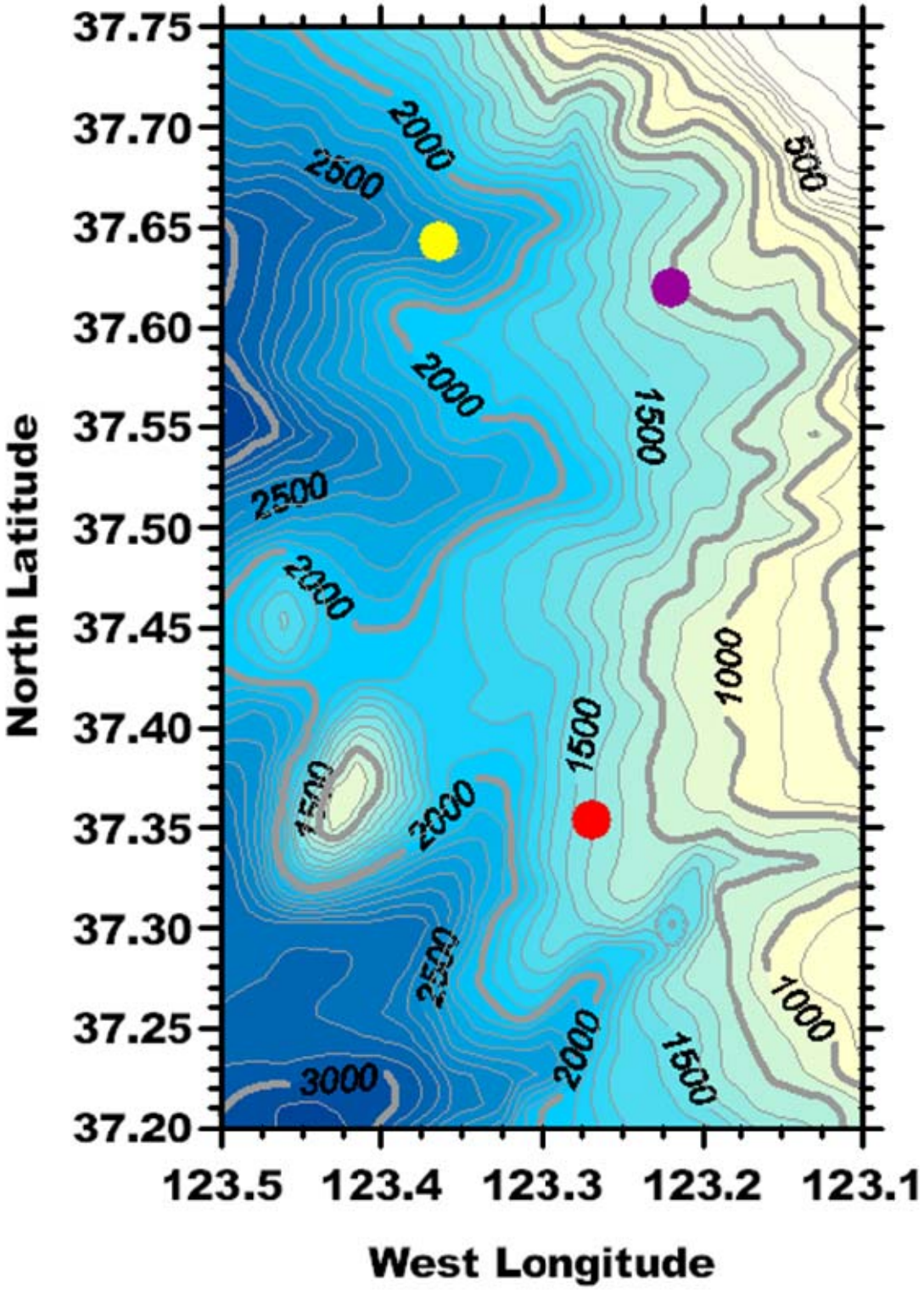

Figure C1. D2 mooring location is designated in purple. Soundings are in meters and the contour interval is 100 m.

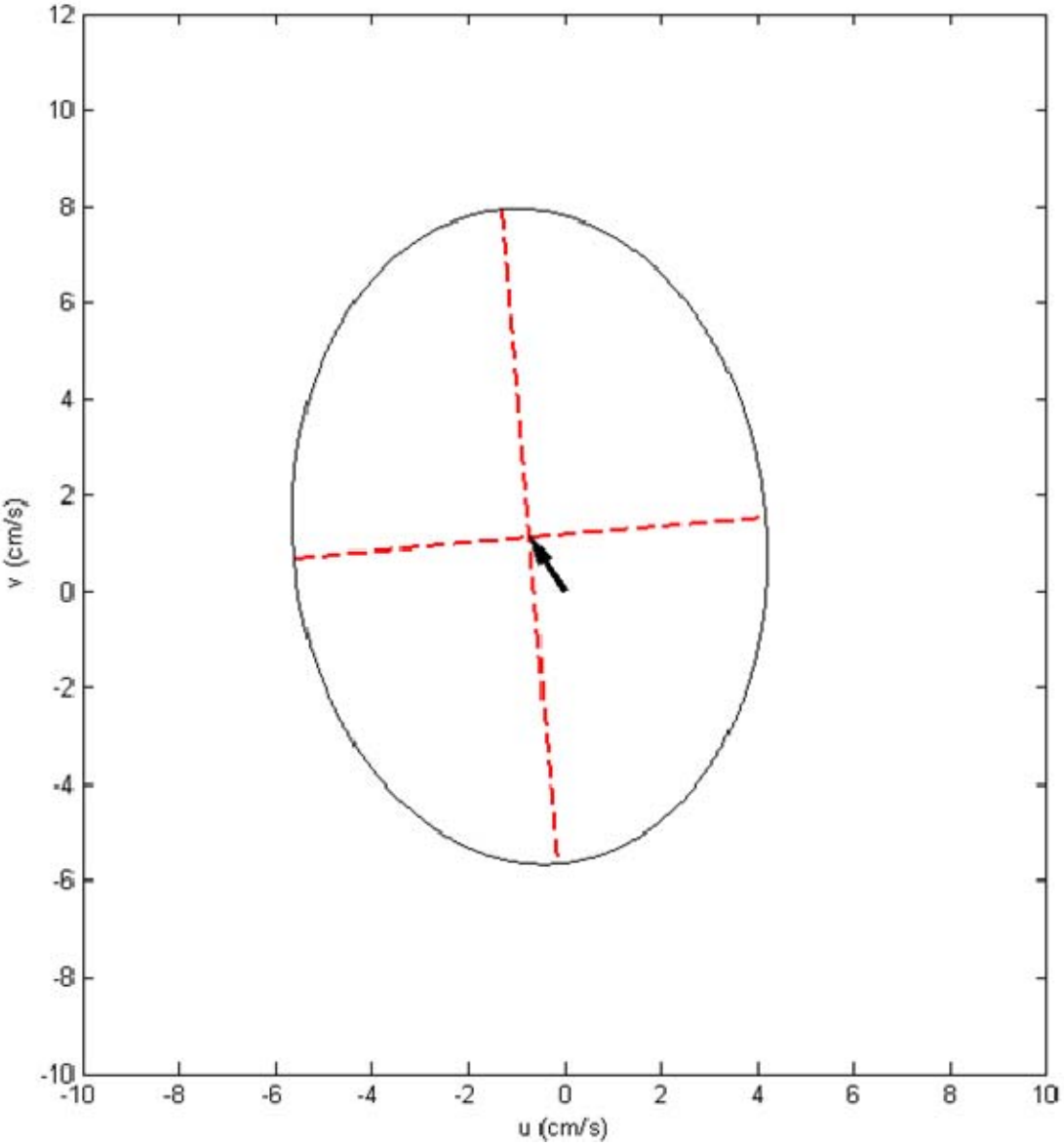

Figure C2. Mean and standard deviation of currents measured at the D2 mooring. Mean speed (direction) of the mean vector flow was 1.4 cm/s (327.8°T). The semi-major (semi-minor) axis was 6.8 cm/s (4.9 cm/s) and was oriented along 355.1°-175.1°T.

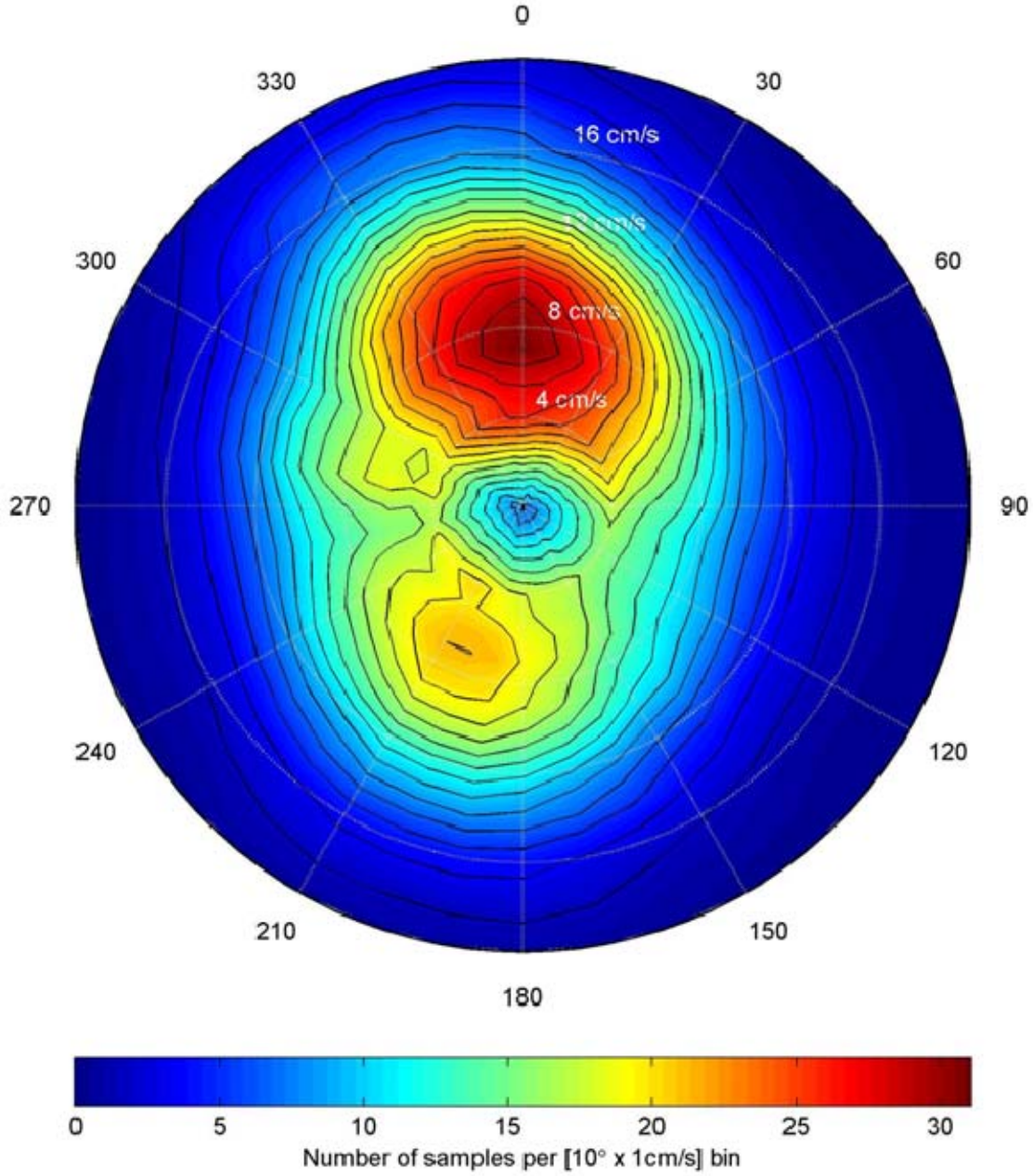

Figure C3. Histogram of velocity observations at mooring D2. The total number of observations is 8,571. 240 observations with a speed less than 1 cm/s were omitted. Total number of bins is 777.

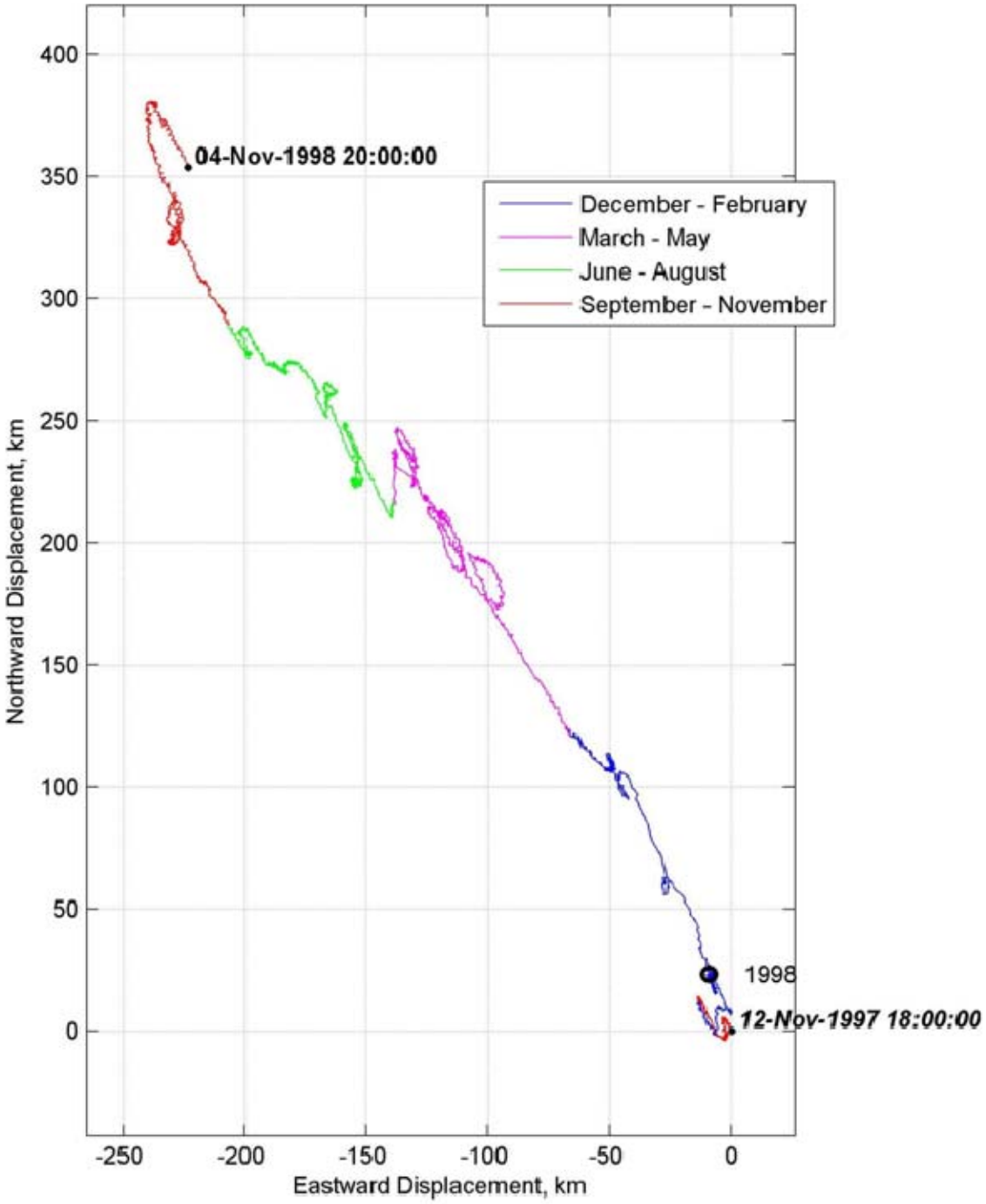

Figure C4. Progressive vector diagram for currents at D2.

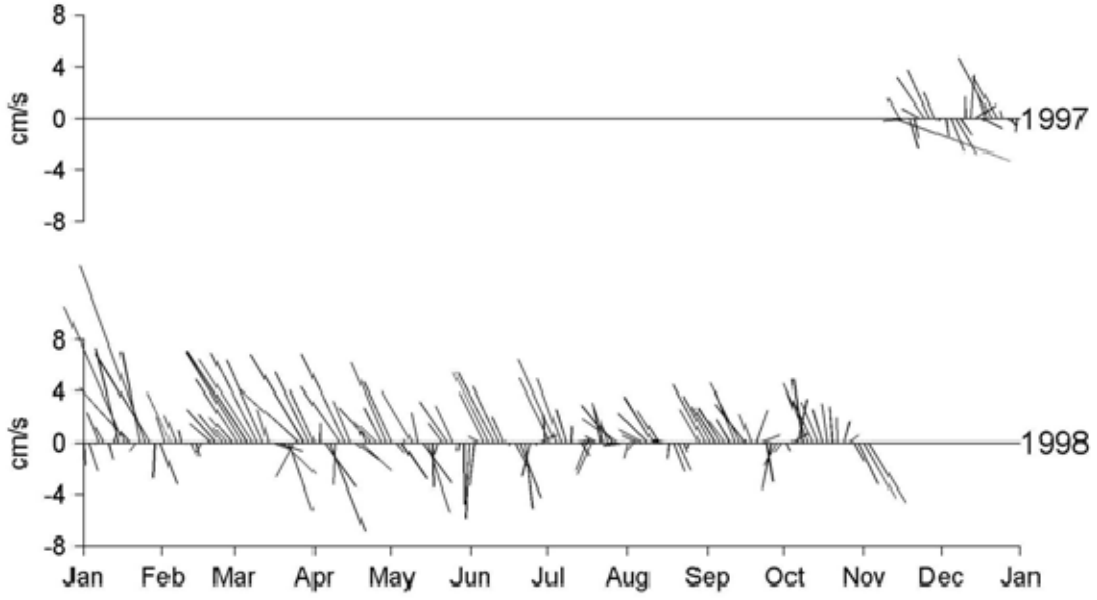

Figure C5. Current velocity at mooring D2 as a function of time. Currents were smoothed using a Butterworth filter with a cutoff period of one week.

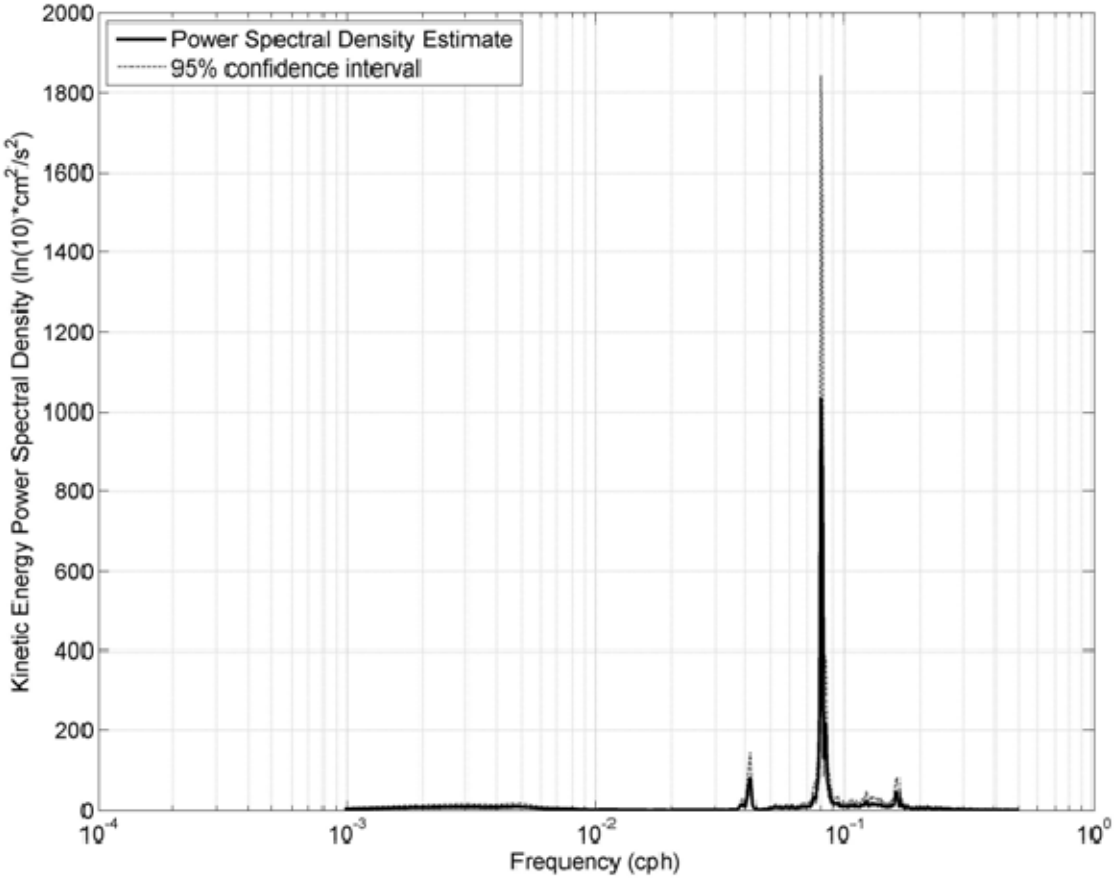

Figure C6. Kinetic energy spectrum for currents at mooring D2. Semi-diurnal peak at 0.08 cph with diurnal peaks at 0.039 and 0.042 cph.

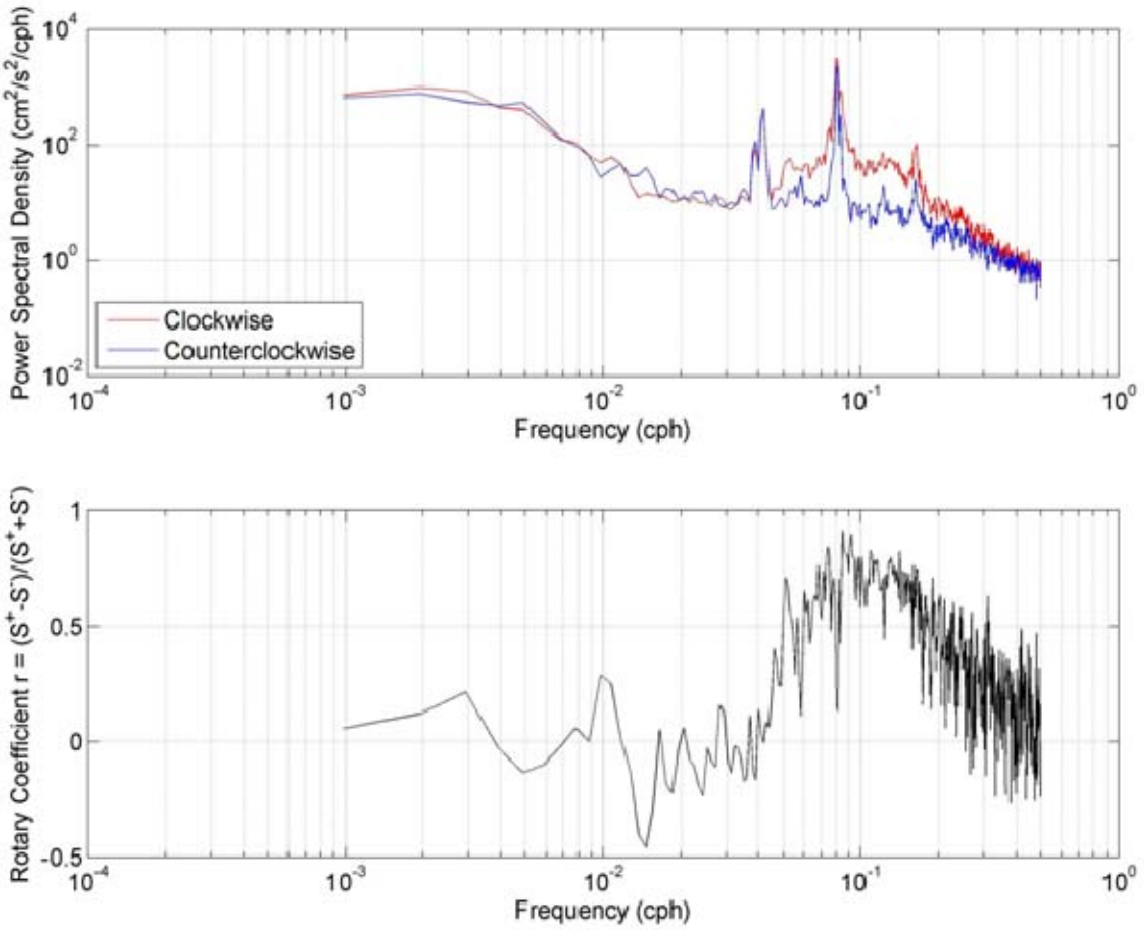

Figure C7. (upper) Rotary spectra for mooring D2. (lower) Rotary coefficient for mooring D2.

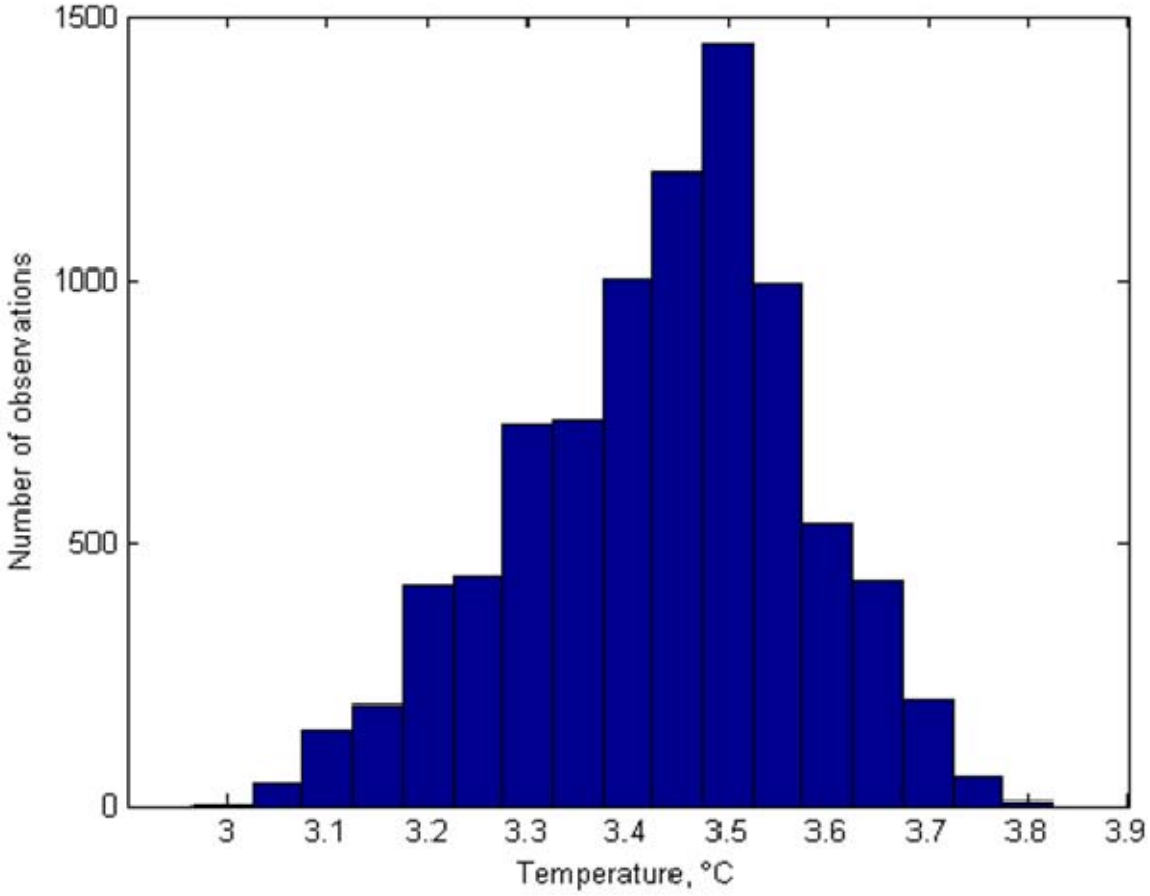

Figure C8. Temperature histogram of currents at mooring D2 using a bin size of 0.05°C.

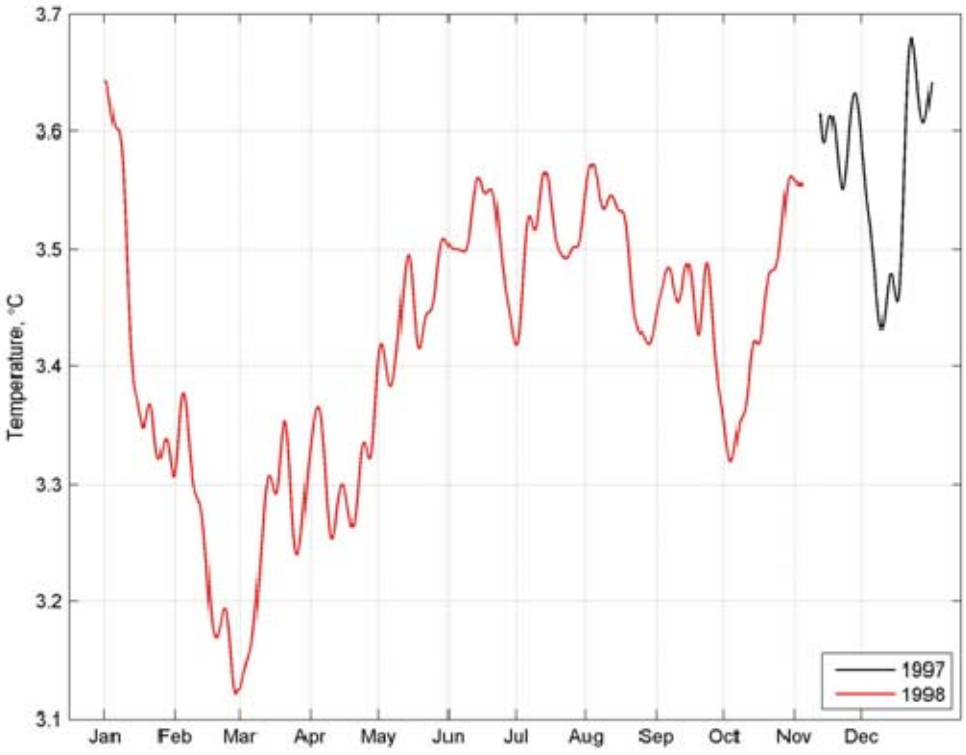

Figure C9. Temperature time series of currents at mooring D2. Temperatures were smoothed using a Butterworth filter that cut off periods less than one week.

Deployment Name	Date of Deployment	Latitude	Longitude	Instrument Depth (m)	Bottom Depth (m)	Compass Correction (E)	Timing Error
D2 Mooring	12 November 1997- 4 November 1998	37° 37.20'N	123° 13.16'W	1142	1200	30’	7’

Table C1. D2 mooring deployment data. The sampling rate for the RCM 8 device was one hour.

THIS PAGE INTENTIONALLY LEFT BLANK

APPENDIX D MOORING R1

This appendix summarizes the current meter data at 800 m at mooring R1 (Fig. D1), which was set on the 1400 m isobath on the continental slope to the west of the Gulf of the Farallones. The mooring was set on 12 November 1997 and recovered on 5 November 1998. Table D1 contains specific information about this deployment. The sampling rate for the RCM 8 current meter was one sample per hour. These data were collected as part of a project sponsored by the Environmental Protection Agency and managed by Marlene Noble of the United States Geological Survey.

The mean speed was 8.89 cm/s. Direction and speed of vector mean flow were 266.5°T and 0.6 cm/s, respectively (Fig. D2). The semi-major (minor) axis magnitude was 9.3 cm/s (4.3 cm/s) and the eccentricity of the variance ellipse was 0.73. The semi-major axis was directed nearly north-south, along 351.5°T to 171.5°T.

The velocity histogram (Fig. D3) displayed two prominent modes of motion. The northward mode had a median heading of 350°T at a speed of 7 cm/s with 30 observations. The southward mode had a median heading of 180°T at a speed of 10 cm/s with 27 observations. The PVD (Fig. D4) displays an initial northward trajectory for November; but during the following winter the flow was southward for a total displacement of more than 700 km. In spring, the flow reversed (northward) and slowed to about half the speed of winter. Summer 1998 flow was to the northwest, with short periods of southerly or southeasterly flow in late June and late August. In September 1998 currents were weak, but strong northward flow returned in October. The period of strong sustained southward flow in winter 1998 also stands out on the stick plot (Fig. D5). During other periods, unidirectional currents persist for no more than three weeks and are interrupted by relaxation and flow reversals. The maximum speed, 31.9 cm/s, was observed on 14 November 1997 (not displayed).

Only the spectral peak associated with semi-diurnal tides was clearly significant in the kinetic energy spectrum (Fig. D6). Much smaller blips were observed at the diurnal frequency (0.042 cph) and the local inertial frequency (0.052 cph or a period of 19.2 hours). The rotary spectra (Fig. D7) indicated that the clockwise component

dominated tidal and inertial band with corresponding positive rotary coefficients. For the diurnal frequency the rotary coefficient was 0.16, and at the local inertial frequency the rotary coefficient was maximum, 0.97.

The temperature histogram (Fig. D8) used a bin size of 0.05°C. The median temperature was 4.40°C and the mean temperature was 4.41°C. The smoothed time series (Fig. D9) indicated a seasonal cycle similar to that observed at 350 m off Point Sur (Collins *et al.*, 1996): the temperatures cooled from a maximum of 4.8°C on 10 January 1998 to a minimum temperature of 4.07°C on 18 March 1998, then and subsequently warmed to 4.56°C on 19 August 1998. During the remainder of 1998, temperatures cooled to 4.25°C in mid October.

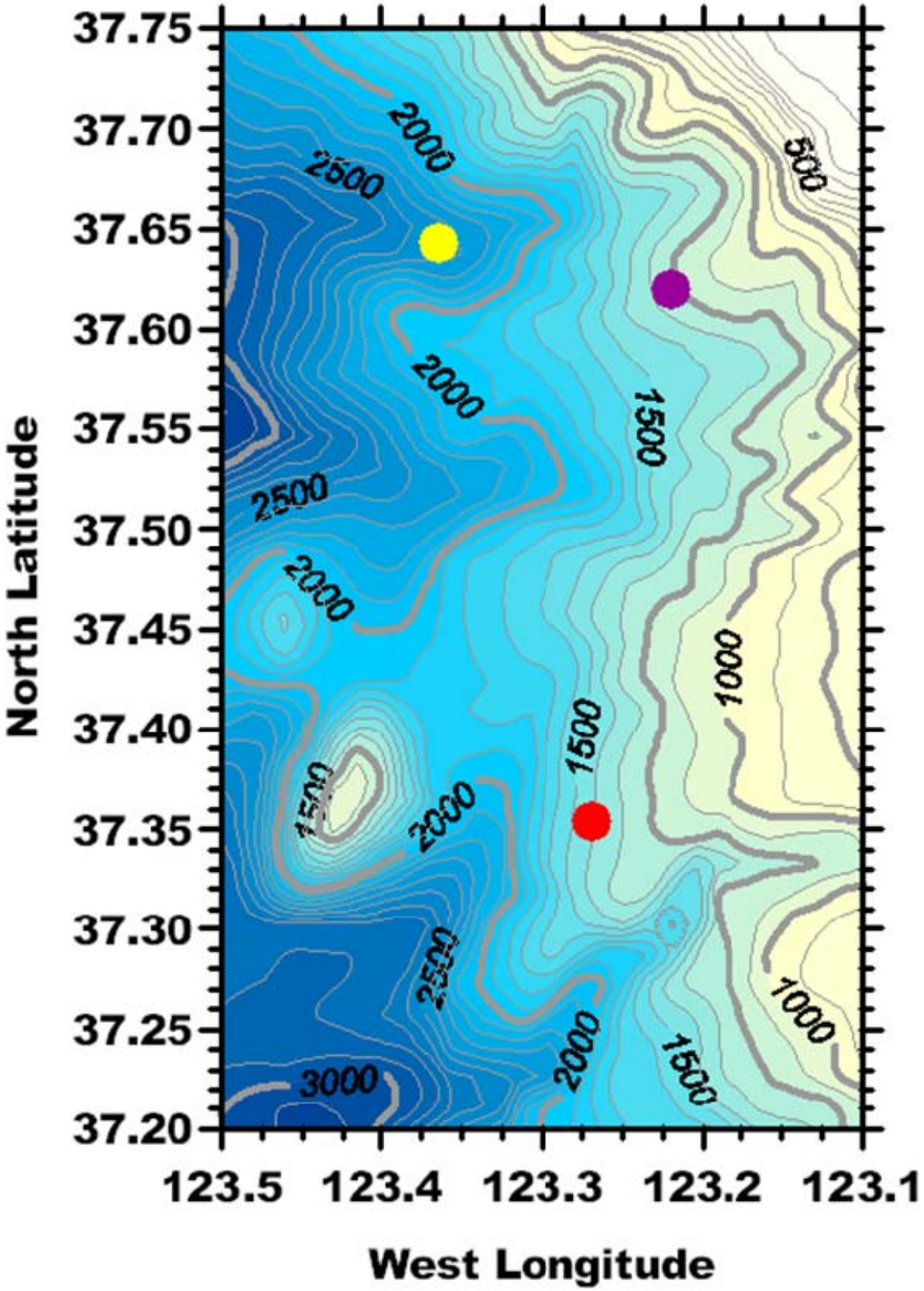

Figure D1. Location of mooring R1 is designated by the red dot. Soundings are in meters and the contour interval is 100 m. Pioneer (37.4N, 123.4W) and Gumdrop (37.45N, 123.45W) Seamounts are shown along the western margin of the chart.

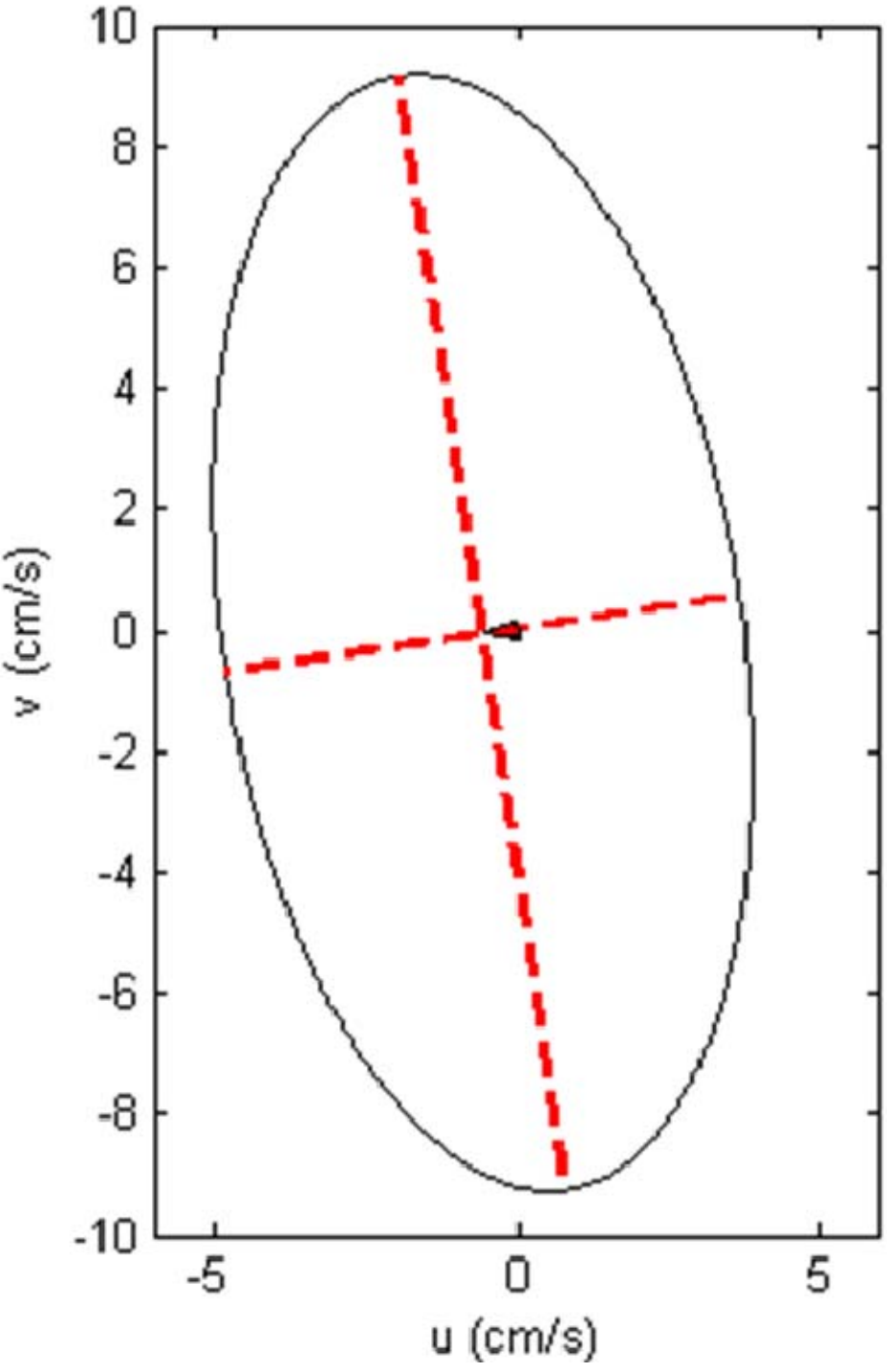

Figure D2. Mean and standard deviation of currents measured at 800 m at the R1 mooring. Mean speed (direction) of the mean vector flow was 0.6 cm/s (266.5°T). The semi-major (semi-minor) axis was 9.3 cm/s (4.3 cm/s) and was oriented along 351.5°-171.5°T.

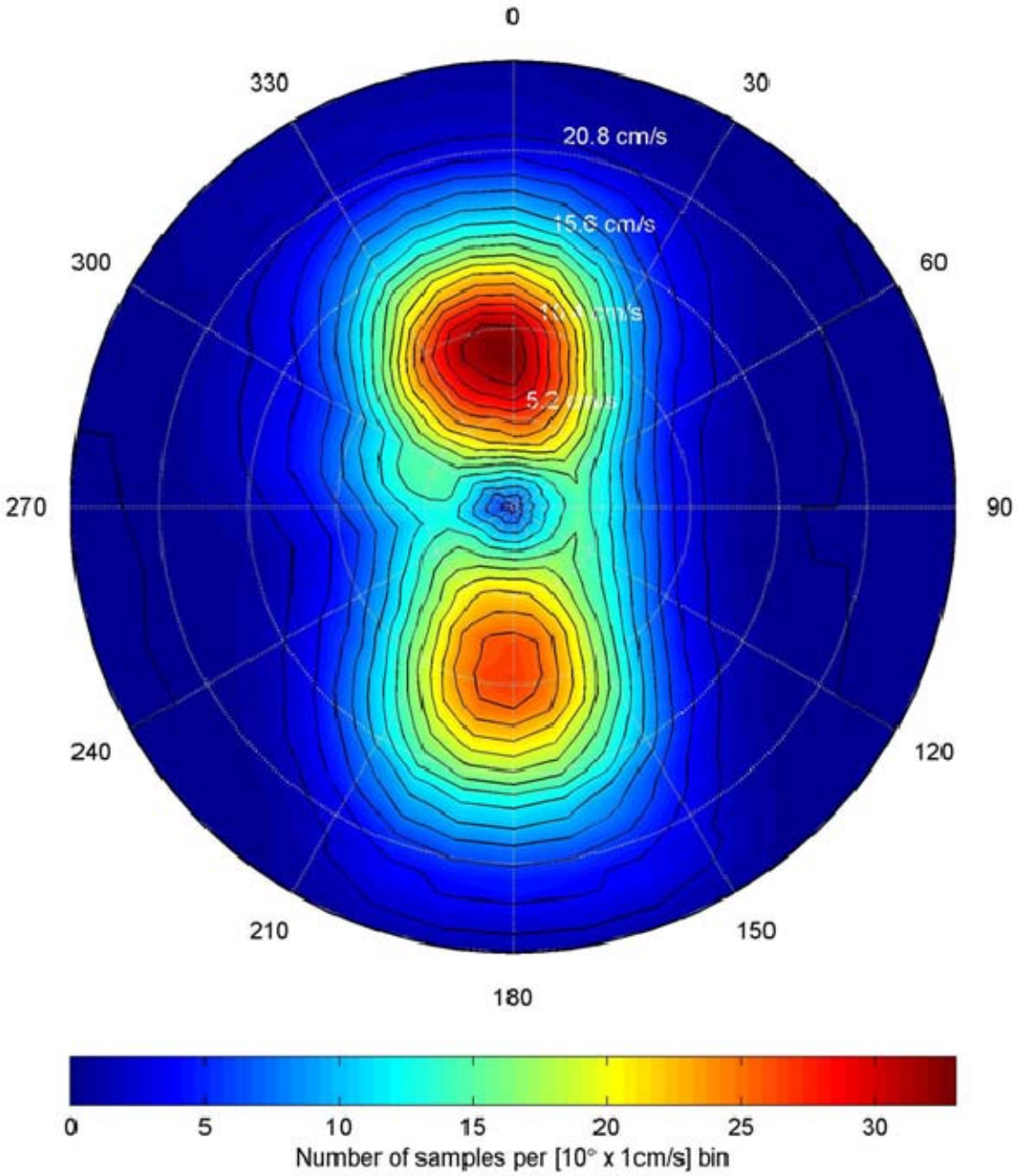

Figure D3. Histogram of velocity observations at 800 m at mooring R1. The total number of observations is 8,584. 65 observations with a speed less than 1 cm/s were omitted. Total number of bins is 999.

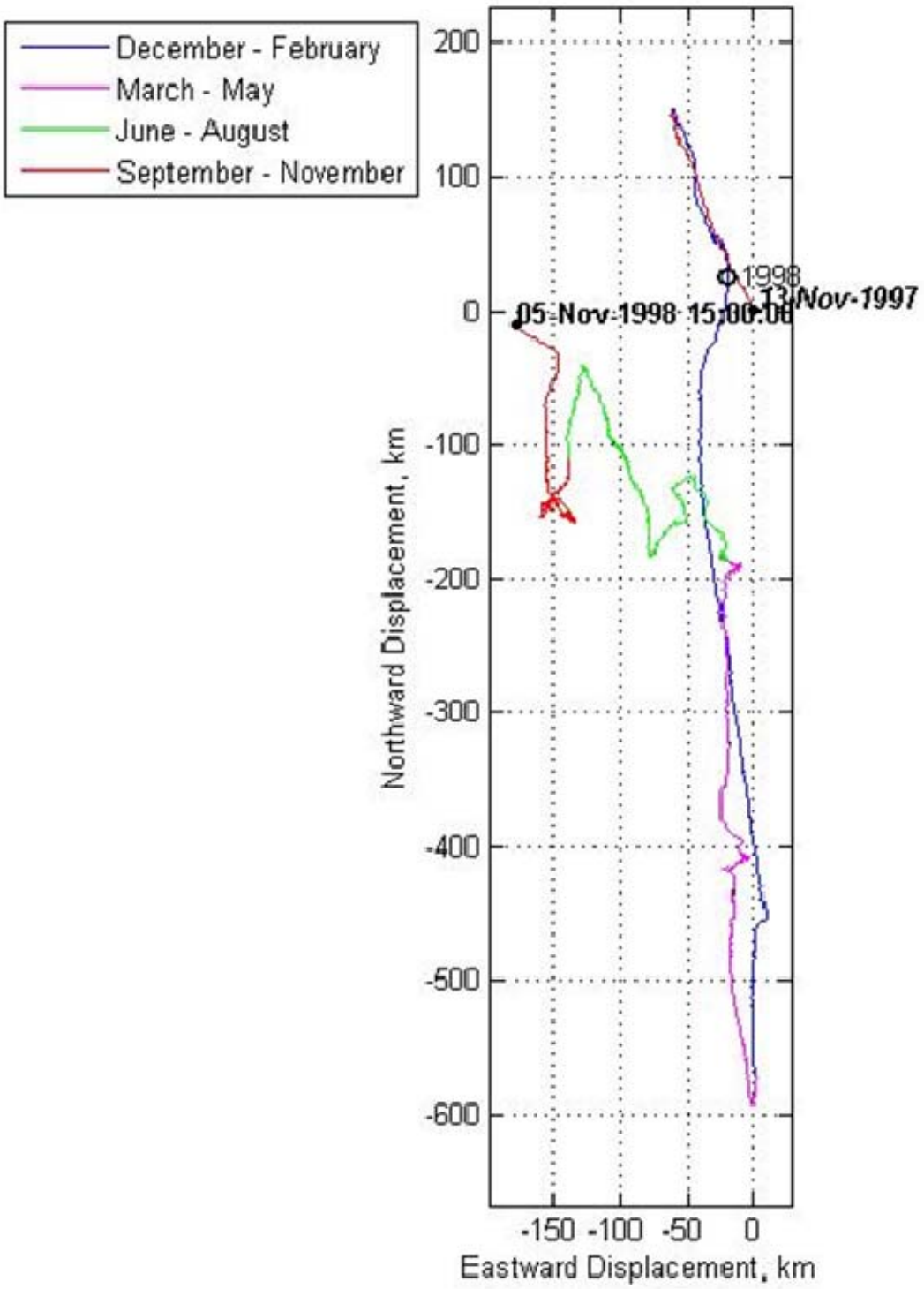

Figure D4. Progressive vector diagram for currents at 800 m at mooring R1.

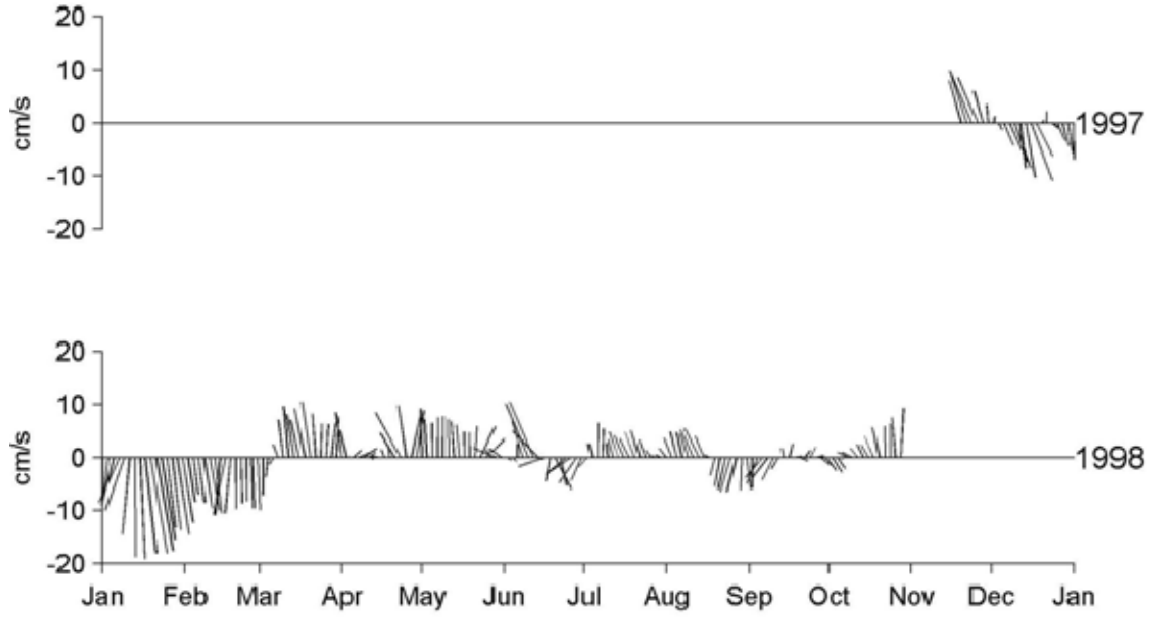

Figure D5. Current velocity at 800 m at mooring R1 as a function of time. Currents were smoothed using a Butterworth filter with a cutoff period of one week.

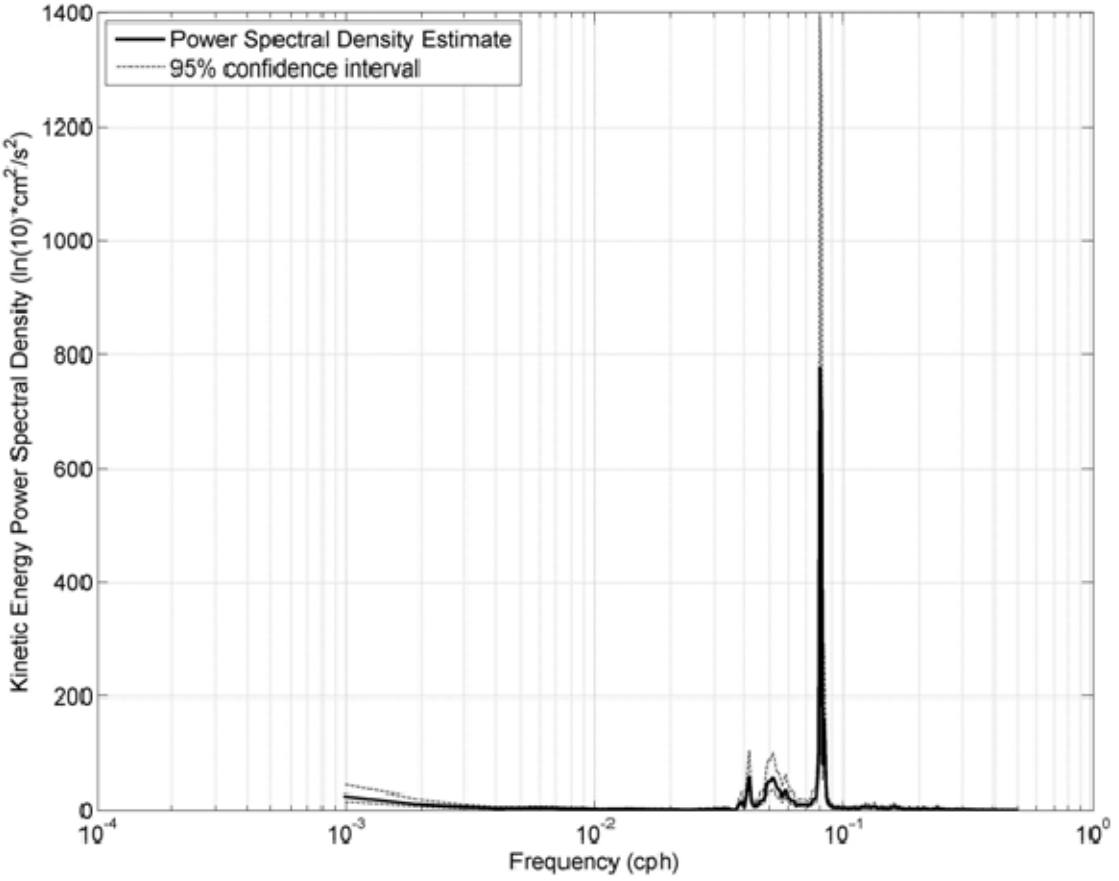

Figure D6. Kinetic energy spectrum for currents at 800 m at mooring R1. Semi-diurnal peak at 0.08 cph with diurnal peak at 0.042 and local inertial frequency at 0.052 cph.

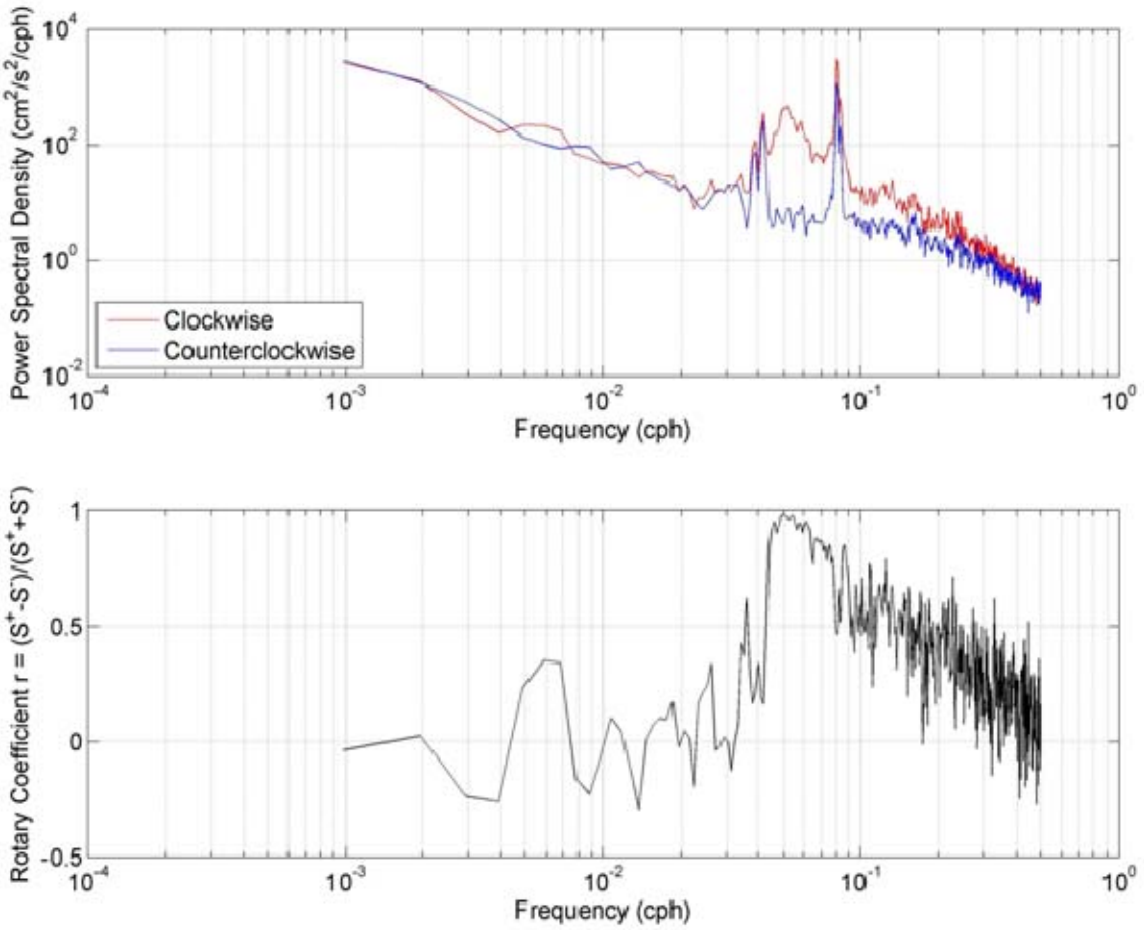

Figure D7. (upper) Rotary spectra for currents at 800 m at mooring R1. (lower) Rotary coefficient.

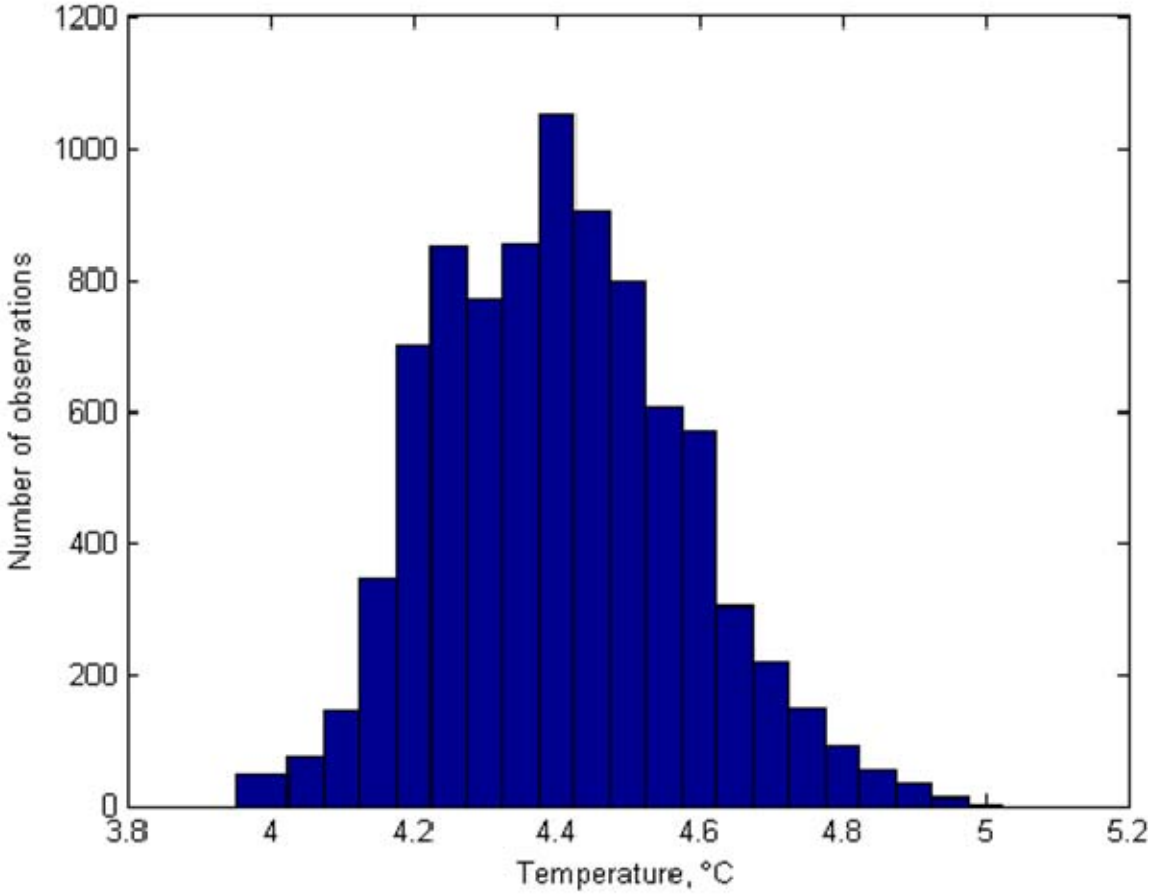

Figure D8. Temperature histogram at 800 m at mooring R1 using a bin size of 0.05°C.

Figure D9. Temperature time series at 800 m at mooring R1. Temperatures were smoothed using a Butterworth filter that cut off periods less than one week.

Deployment Name	Date of Deployment	Latitude	Longitude	Instrument Depth (m)	Bottom Depth (m)	Compass Correction (E)	Timing Error
R1 mooring	12 November 1997- 5 November 1998	37° 21.23'N	123° 16.1'W	793	1400	25’	4’ 4”

Table D1. R1 mooring deployment data. The RCM 8 current meter sampled once per hour.

THIS PAGE INTENTIONALLY LEFT BLANK

APPENDIX E PIONEER SEAMOUNT

A single mooring was set on Pioneer seamount deployed from 28 January 1999 to 28 November 2000 (Fig. E1). The mooring included an acoustic tomography transponder, an RCM 8 current meter and a SEACAT 19 (Fig. E2). The RCM 8 was lost, probably scraped off the mooring by a trawl, so only the SEACAT data were available. The mean depth of the SEACAT was 766 m, 68 m above the bottom (Table E1). The mean temperature (salinity) at this depth was 4.52°C (34.32) and the standard deviation of temperature (salinity) was 0.19°C (0.03). Histograms of temperature (Figure E6), salinity (Figure E4), and a bivariate histogram of temperature and salinity (Figure E7) illustrate bimodal character.

The time series of temperature (Figure E5) and salinity (Figure E3) had seasonal minima in September. This suggested increased influence of subarctic intermediate waters during this month. For temperature, the September transition was rapid. In 1999, temperatures were near 4.6°C before the September transition and 4.3°C after the transition (the minimum temperature was 4.13°C on 27 September 1999). In 2000, temperature warmed from January to July (maximum was 4.99°C on 30 June) and then cooled to 4.7°C by September. The stability of the temperature before and after the September transition (especially in 1999) resulted in the bimodal character of the temperature distribution shown in Figure E5.

The common seasonal feature in the salinity time series was the minimum salinity, 34.26, which occurred on 10 September 2000 (Fig. E3). In 1999, maximum salinity (34.37) occurred on 02 April, subsequently decreasing to a September minimum. Salinities subsequently increased to 34.32 in October and remained near this value in 2000 except for the September period.

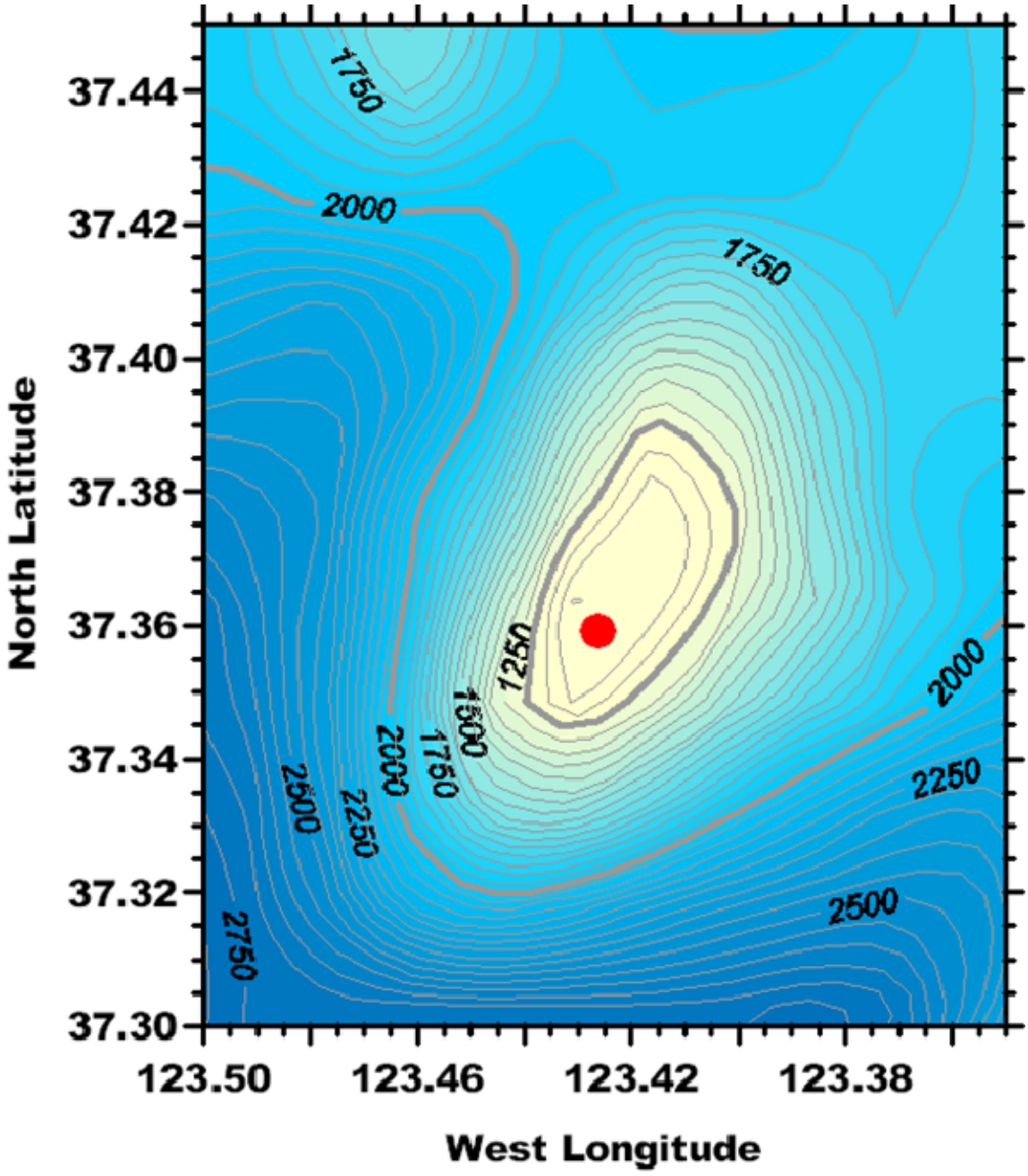

Figure E1. Mooring location at Pioneer Seamount. Soundings are in meters and the contour interval is 50 m.

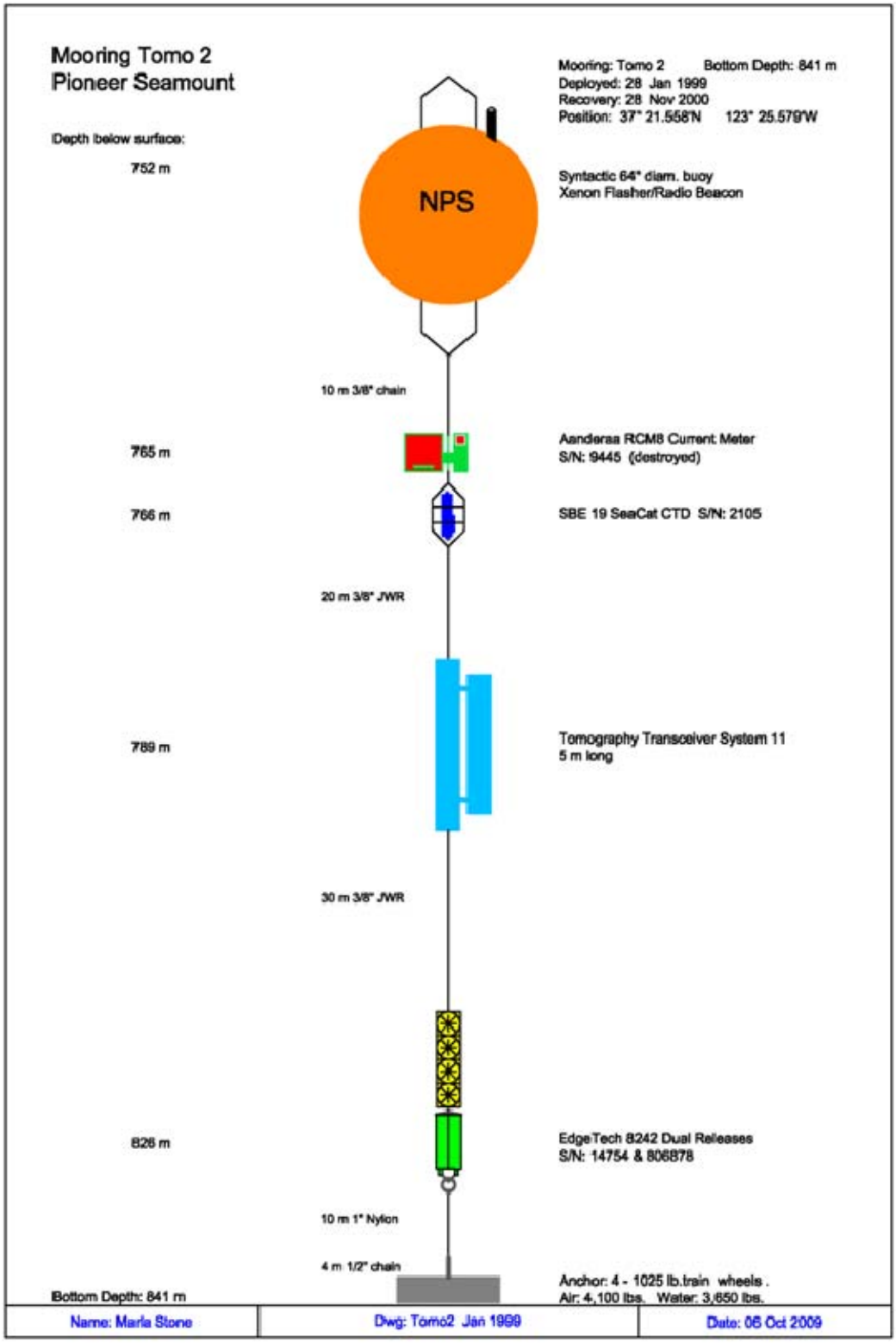

Figure E2. Intermediate mooring design for Pioneer Seamount.

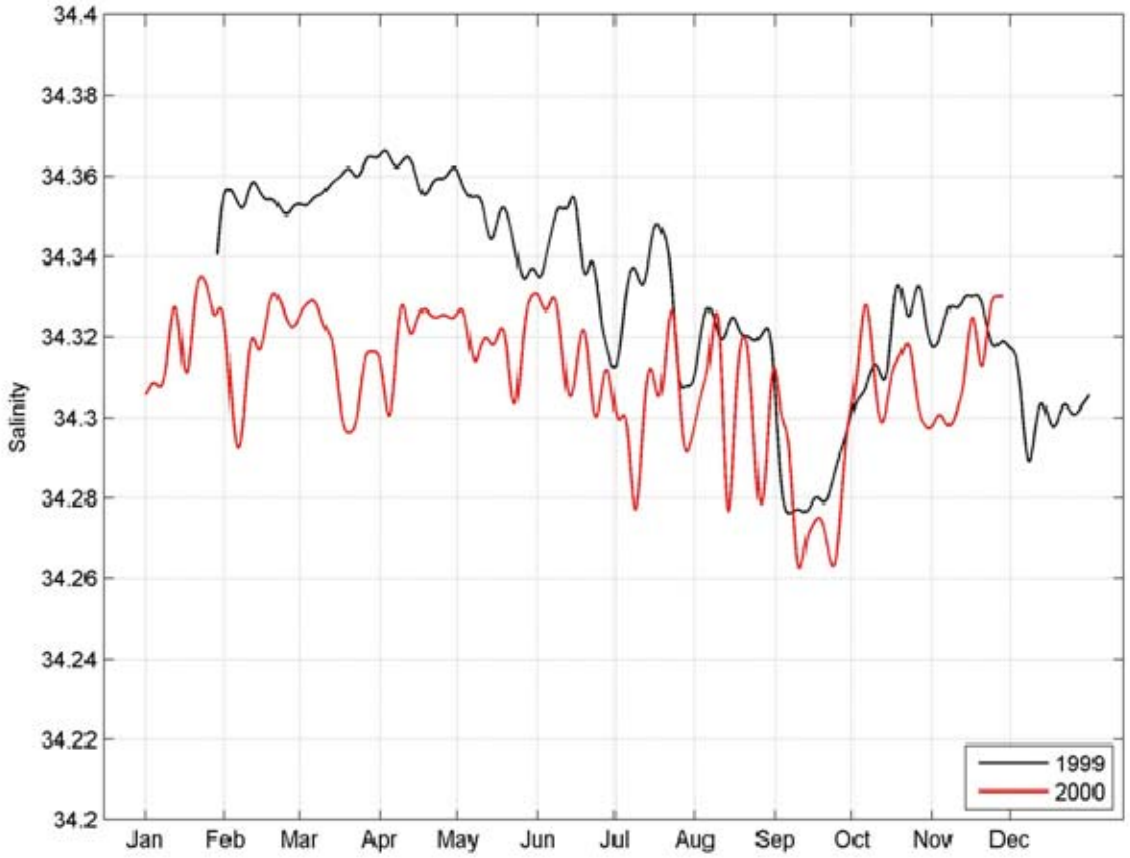

Figure E3. Salinity time series of Pioneer Seamount deployment with Microcat device. Salinity was smoothed using a Butterworth filter that cut off periods less than one week.

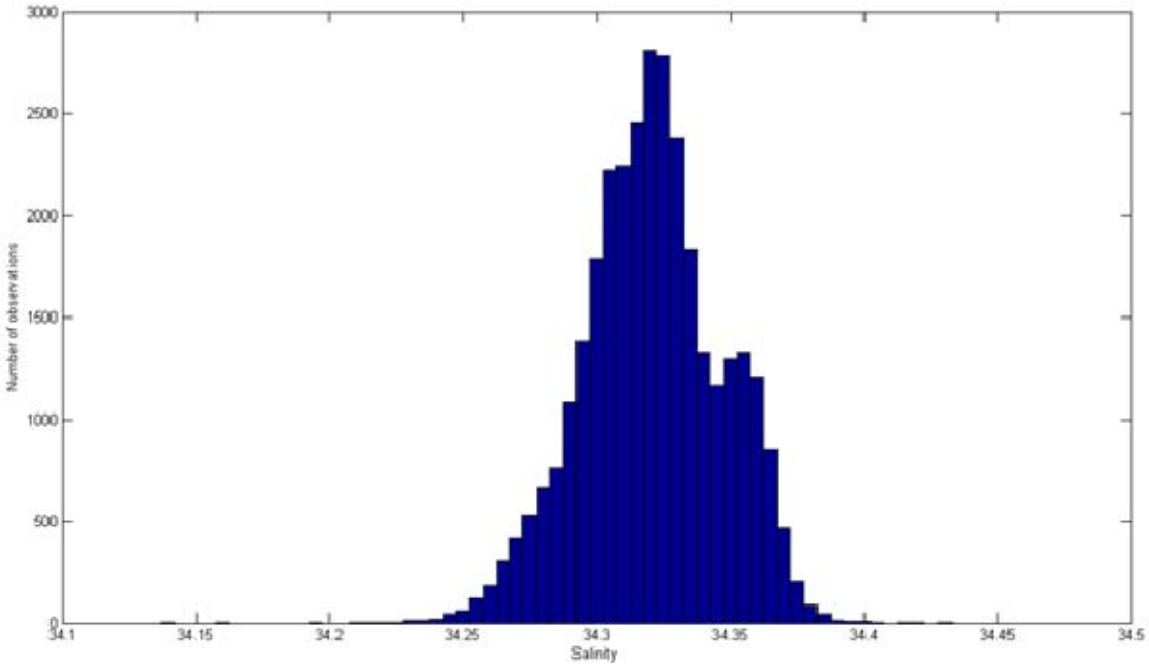

Figure E4. Salinity Histogram of Pioneer Seamount deployment using a bin size of 0.005.

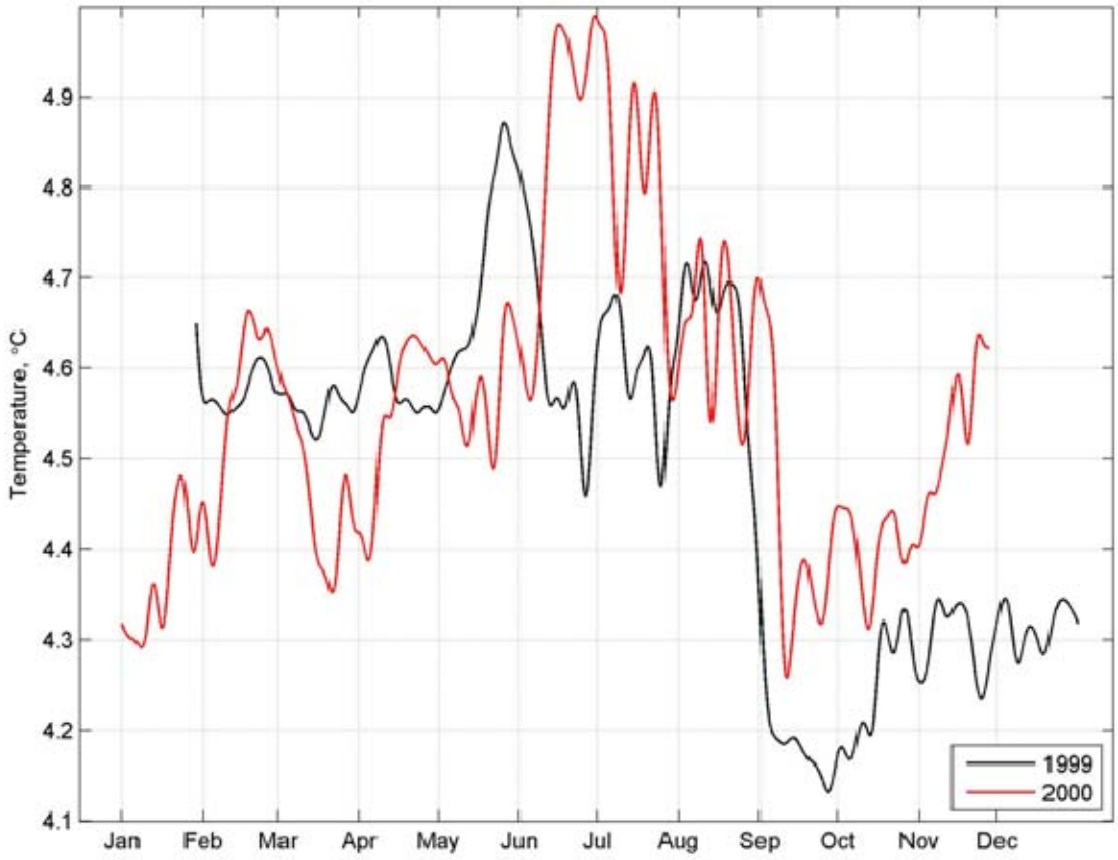

Figure E5. Temperature time series of Pioneer Seamount deployment with Microcat device. Temperature was smoothed using a Butterworth filter that cut off periods less than one week.

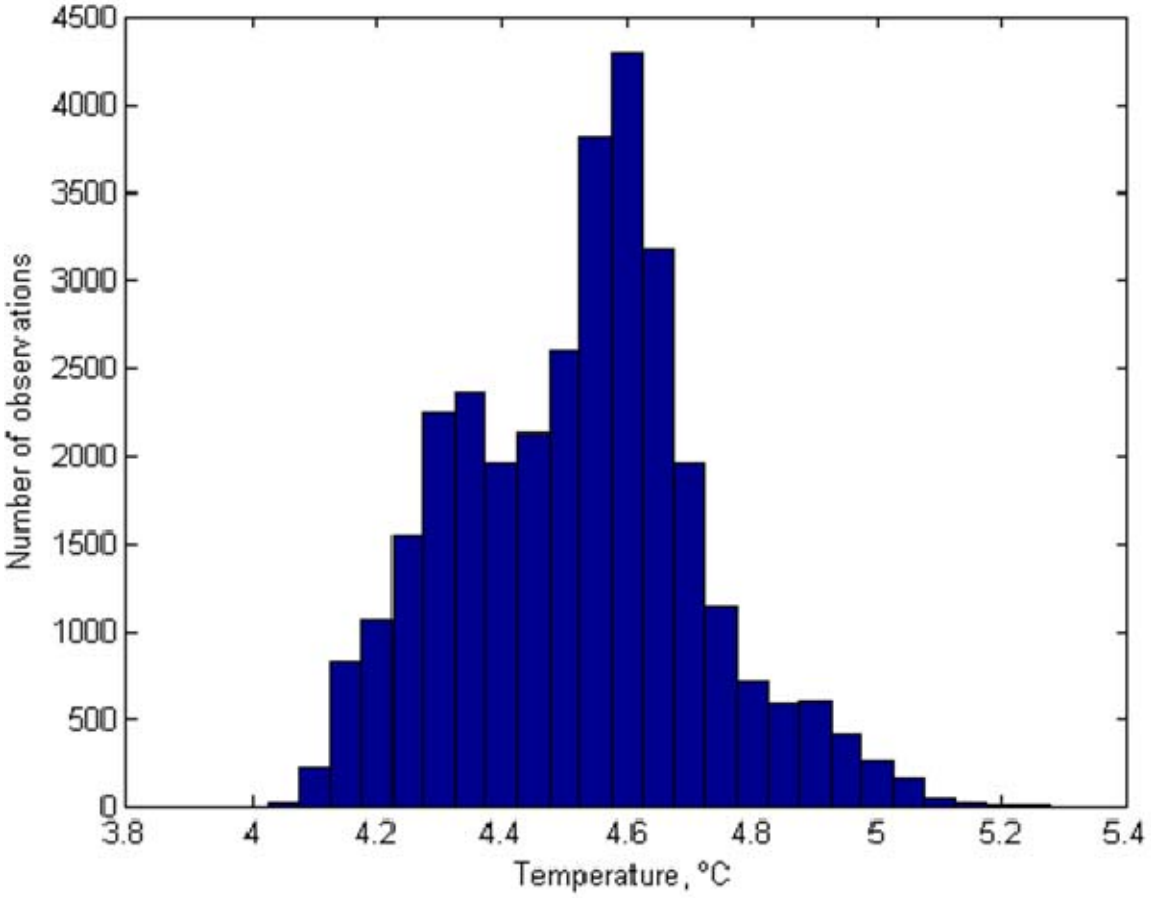

Figure E6. Temperature histogram of Pioneer Seamount deployment using a bin size of 0.05°C.

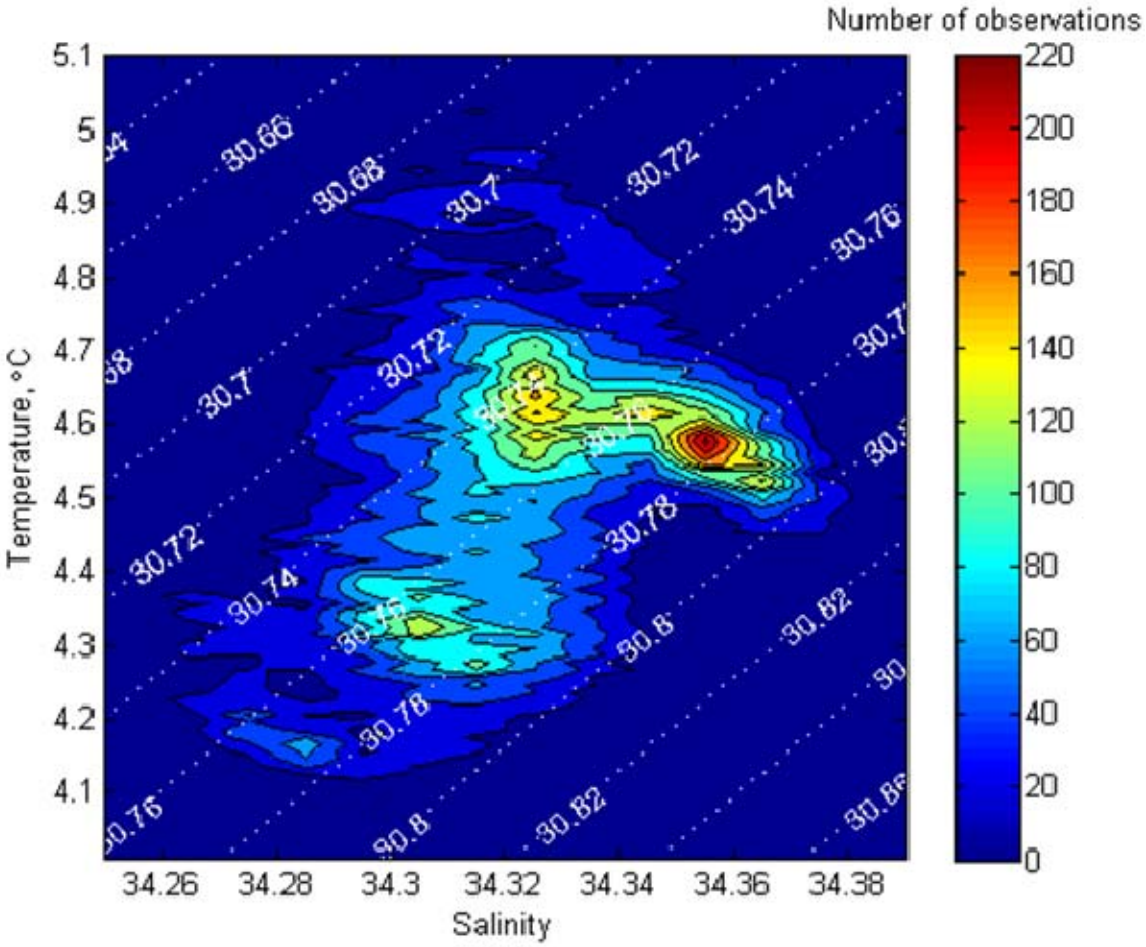

Figure E7. Bi-variate histogram which shows the salinity and temperature at Pioneer Seamount. The white dotted lines denote density.

Deployment Name	Dates of Deployment	Latitude	Longitude	Instrument Depth (m)	Bottom Depth (m)	Compass Correction (E)	Timing Error
Pioneer Seamount	28 Jan 99-28 Nov 00	37° 21.558'N	123° 25.579'W	766	841	N/A	11' 20"

Table E1. Pioneer Seamount SEACAT 19 Data.

APPENDIX F S2

The deep RCM 8 measurements at S2 were long term, spanning 7 years (March 1998 to July 2005) at a mean depth of 1200 meters, and co-located with a sediment trap. The mooring was located in water which was approximately 1800 m deep. Table F1 contains specific details for each of the fourteen deployments. These measurements were made just to the north of Monterey Submarine Canyon (Fig. F1) from an intermediate mooring that extended upwards to 300 m below the water surface (Fig. F2). The sampling rate was half-hourly except for the last deployment, which was sampled hourly; the data from the last deployment were interpolated to half hour samples to provide consistency with previous deployments. Results of both deep and shallow (300 m) current measurements at S2 were summarized by Morales (2003).

Southward flow dominated the S2 currents. The mean speed over the seven years was 5.37 cm/s. Direction and speed of vector mean flow was 162°T and 1 cm/s, respectively (Fig. F3). The variance ellipse displays the standard deviation along the principal axis of variation. The semi-major (minor) axis magnitude was 4.9 cm/s (3.9 cm/s) and the eccentricity of the variance ellipse was 0.07. The semi-major axis was directed along 349°T to 169°T.

The velocity histogram (Fig. F4) showed the principal mode contained 526 observations at a speed of 4 cm/s and a direction of 165°T. A secondary mode associated with northward flow events contained 330 observations at a speed of 4 cm/s and a direction of 010°T with a total of 300 samples per bin. This direction was 25° from the reciprocal of the principal mode and reflects the upstream bathymetry. The maximum speed, 24.42 cm/s, was observed for southward flow on 30 November 2002.

The progressive vector diagram (Fig. F5) showed net southward displacement for each year of measurement except for the half year of 2005 data. During 1999, 2000, and 2001 the mean flow had about the same velocity (Fig. F5), i.e. the net displacements were about the same. The mean flows in 2002 and 2003 were about twice as large and had a distinct eastward component. The mean flow in 2005 appeared to double again. Figure

F5 also illustrates seasonal variability during each year. Summer (June through August) currents had net southward flow each year and winter currents (December through February) showed little net displacement each year. Currents in spring and fall had greater variability from year to year.

Stick plots for S2 are shown in Figures F6a and F6b. The most striking features of these figures are the strong (>4 cm/s) bursts of southward velocity that occurred during summer and late fall of most years. These southward flows exceeded 8 cm/s in July 2000, October and December 2002, June 2003, and April and July 2004. There are also instances of strong (>8 cm/s) northward flow in April 2003 and 2005. The periods of northward flow rotated anticyclonically, while the southward flows had a persistent direction.

The semi-diurnal tides dominated the variance of the kinetic energy spectrum (Fig. F7); distinct peaks also occurred at diurnal, quarter-diurnal, and the local inertial (0.05) frequencies. The rotary spectra (Fig. F8) show that clockwise (anticyclonic) motion occurred for motions with periods ranging from 2 to 30 hours; the rotary coefficient was largest, 0.95, for inertial-period motion.

The temperature histogram (Fig. F9) used 0.05°C bins and the median temperature was 3.48°C. The mean temperature (standard deviation) was 3.48°C (0.1°C). The maximum (minimum) temperature was 3.93°C (3.10°C).

The smoothed temperature time series is shown in Fig. F10. The maximum (minimum) temperature occurred on 26 June 2000 (27 March 2003). For each year, minimum temperatures, in April or May, were followed by maximum temperatures in June or July, and the associated temperature change was about 0.4°C. But the temperatures also exhibited a high degree of month-to-month variability with corresponding temperature changes of 0.2°C.

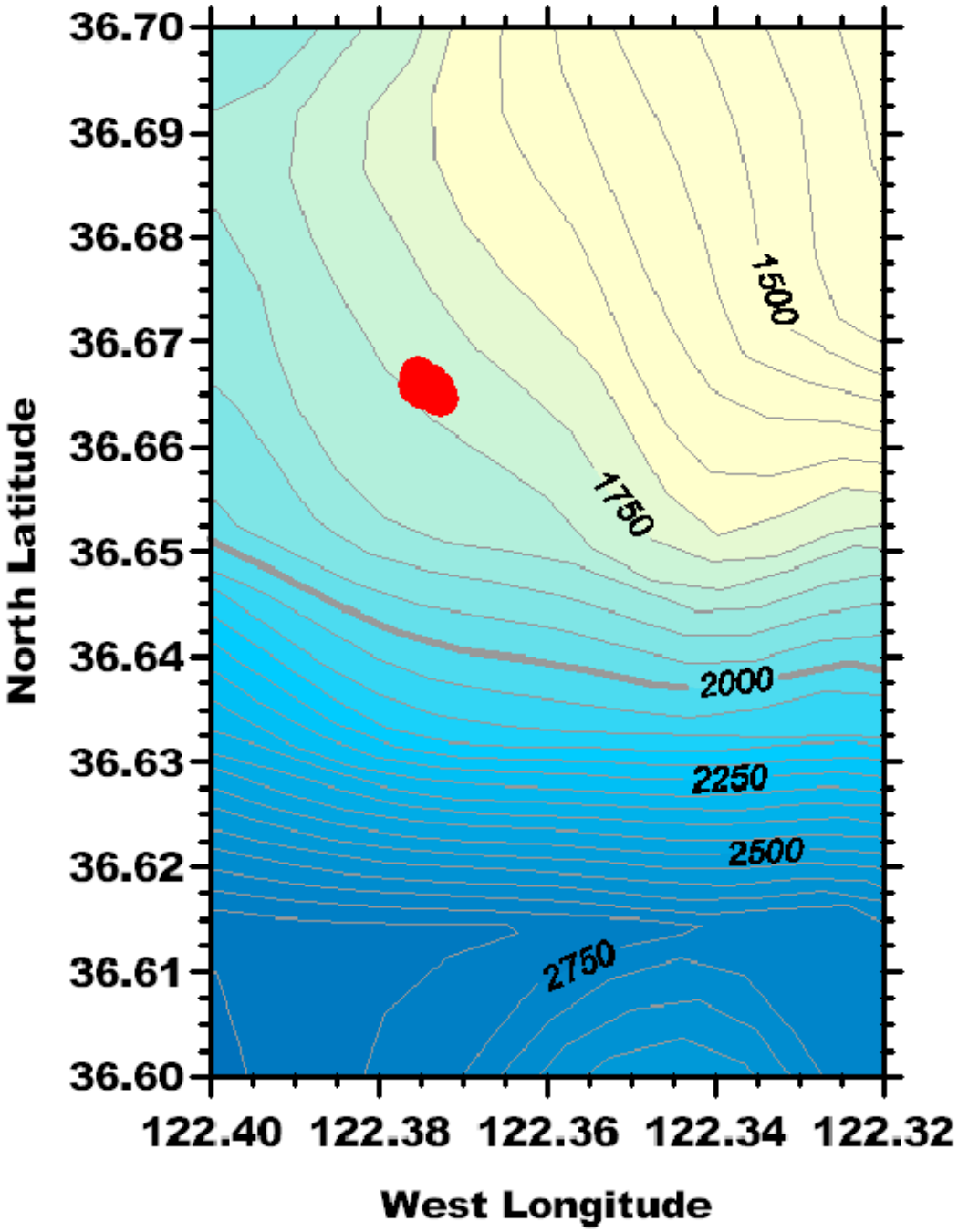

Figure F1. S2 mooring locations. The trench along the southern boundary of the figure is Monterey Submarine Canyon. Soundings are in meters and the contour interval is 100 m.

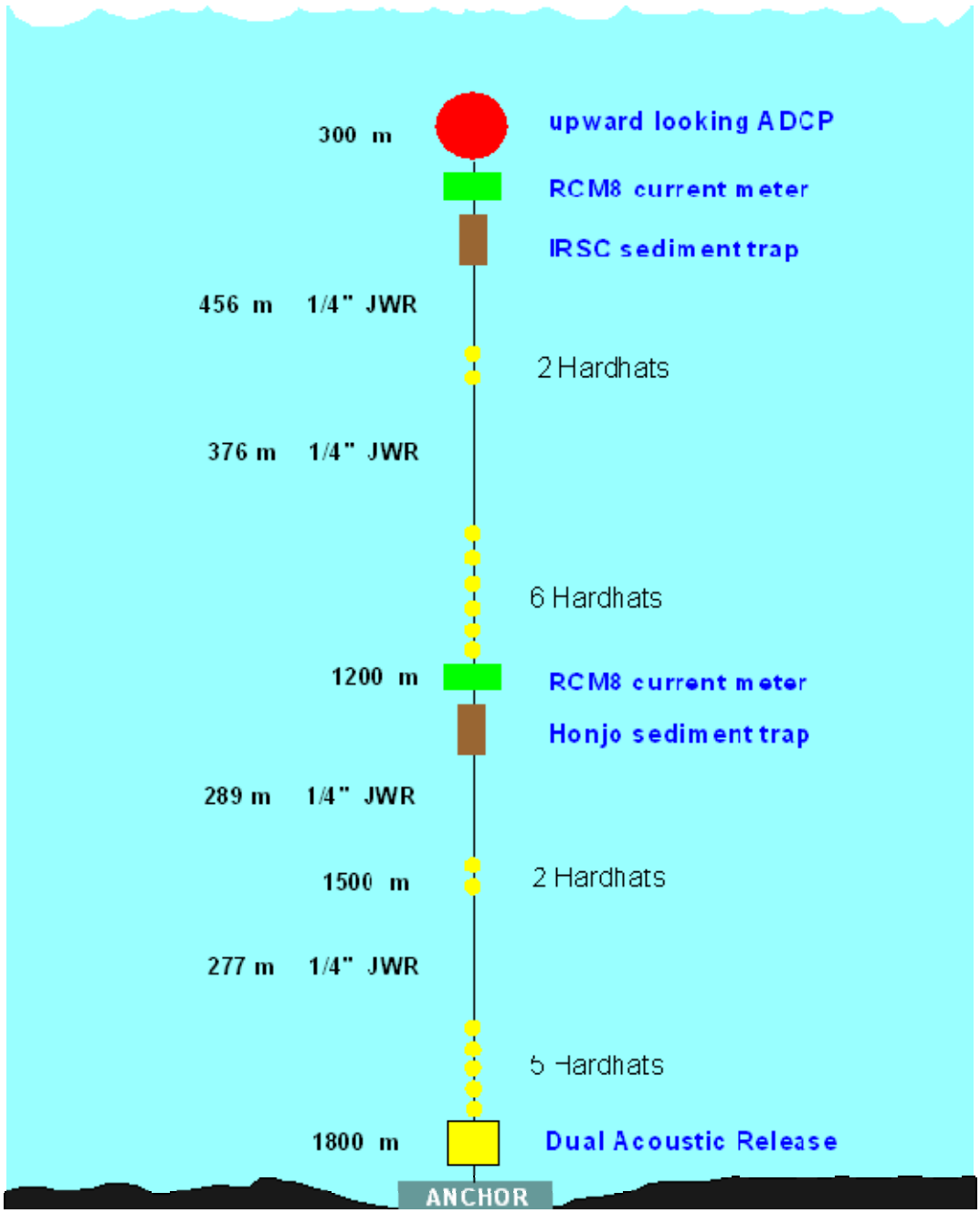

Figure F2. Schematic diagram of mooring S2. Jacketed wire rope (JWR) is torque balanced and designed for oceanographic applications; 1/4" (3/16") diameter was used in the upper (lower) portion of the array. Hardhats are enclosures that hold glass flotation spheres. A total of 13 hardhats were used in the array.

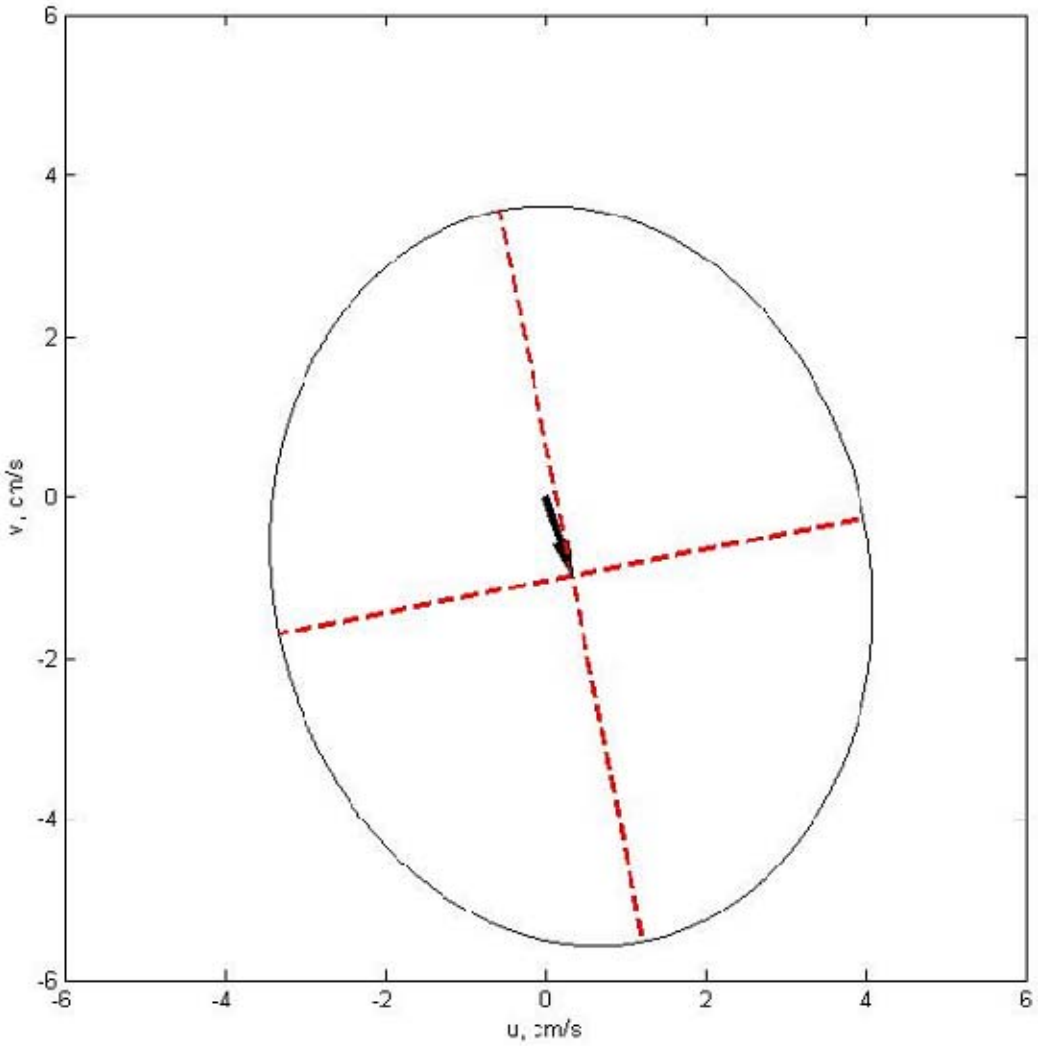

Figure F3. Mean and standard deviation of 1200 m currents at S2. Mean speed (direction) of the mean vector flow was 1.0 cm/s (162°T). The semi-major (semi-minor) axis was 4.9 cm/s (3.9 cm/s) and was oriented along 349-169°T.

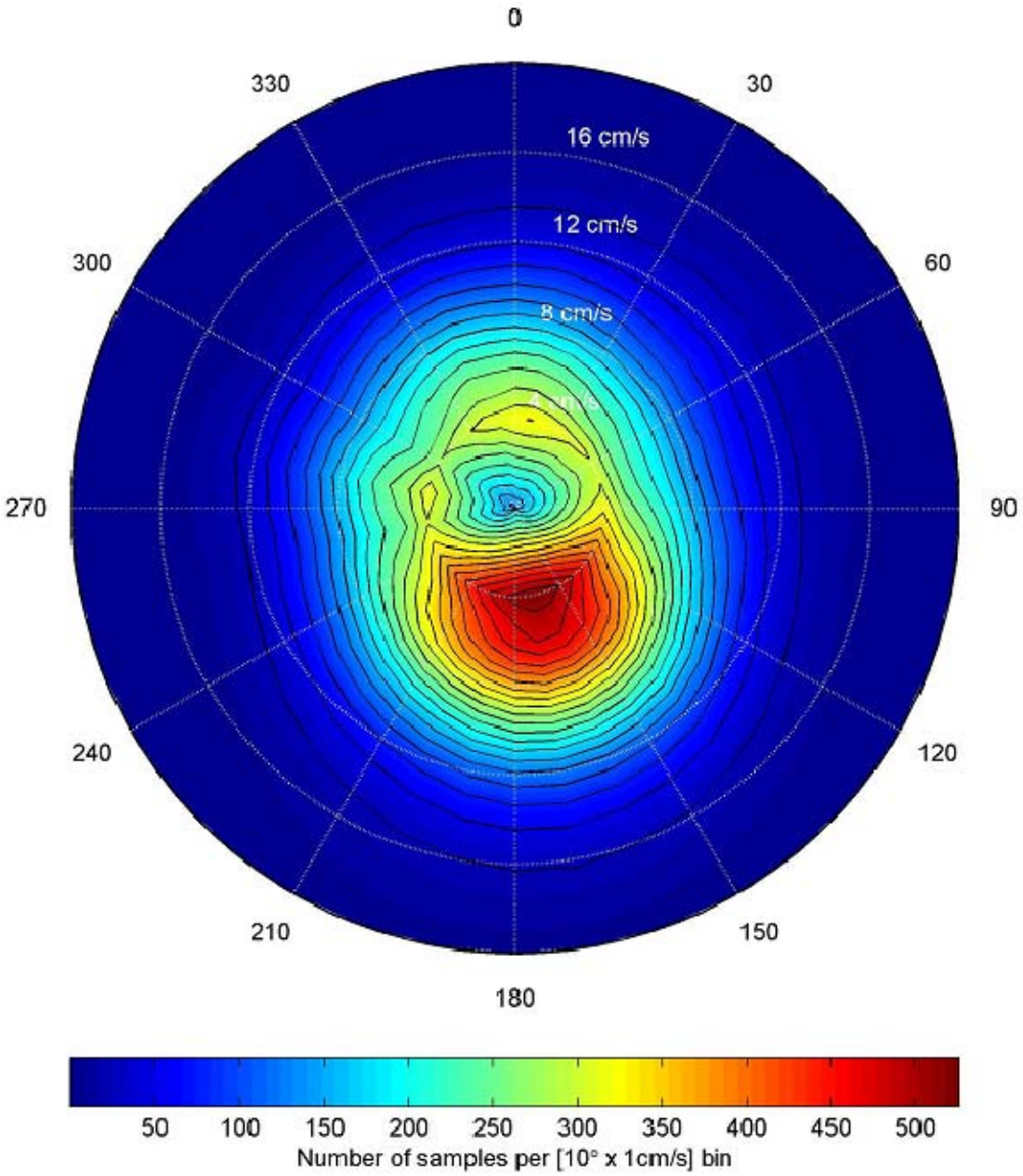

Figure F4. Histogram of 1200 m velocity observations at S2. The total number of half hour observations for this histogram is 127,774. 20,960 observations with a speed less than 1 cm/s were omitted.

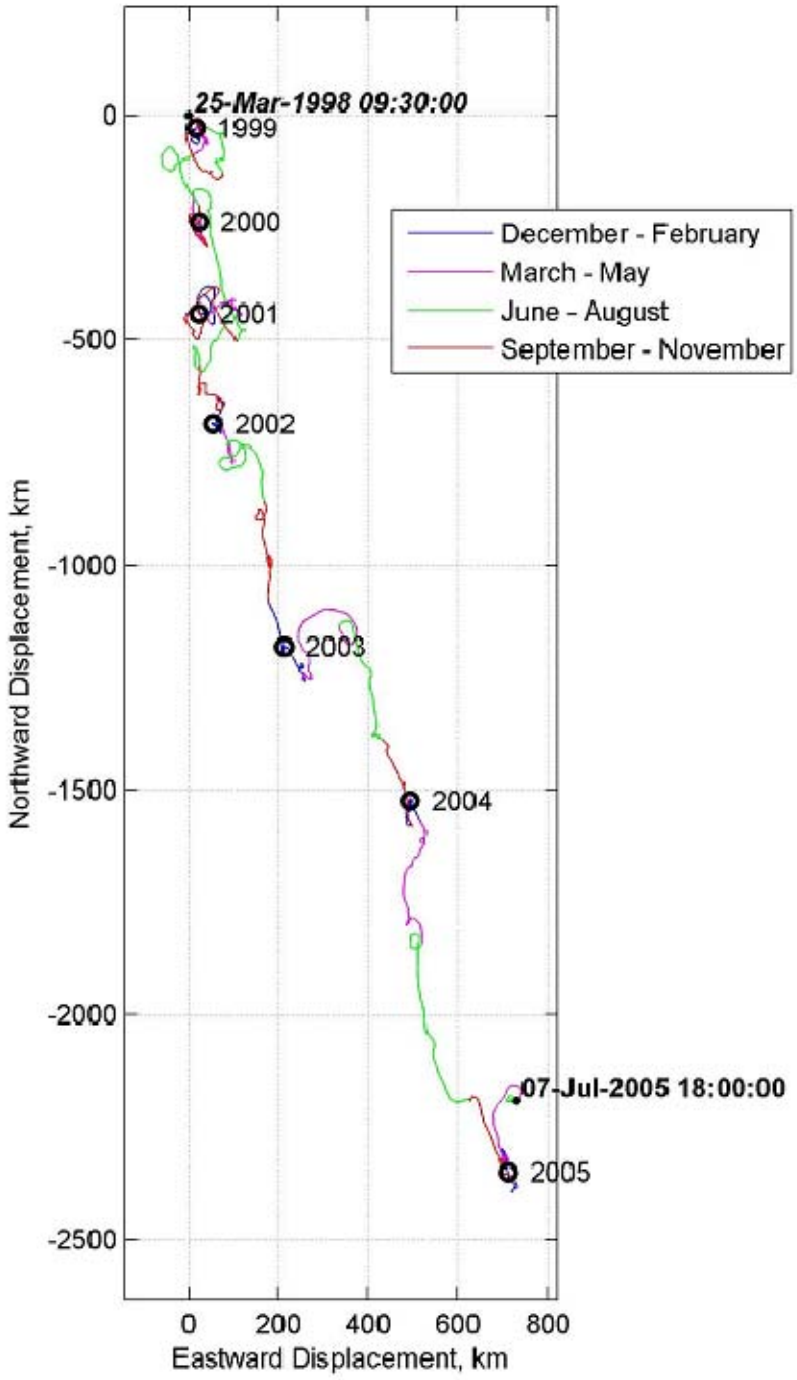

Figure F5. Progressive vector diagram for 1200 m currents at S2.

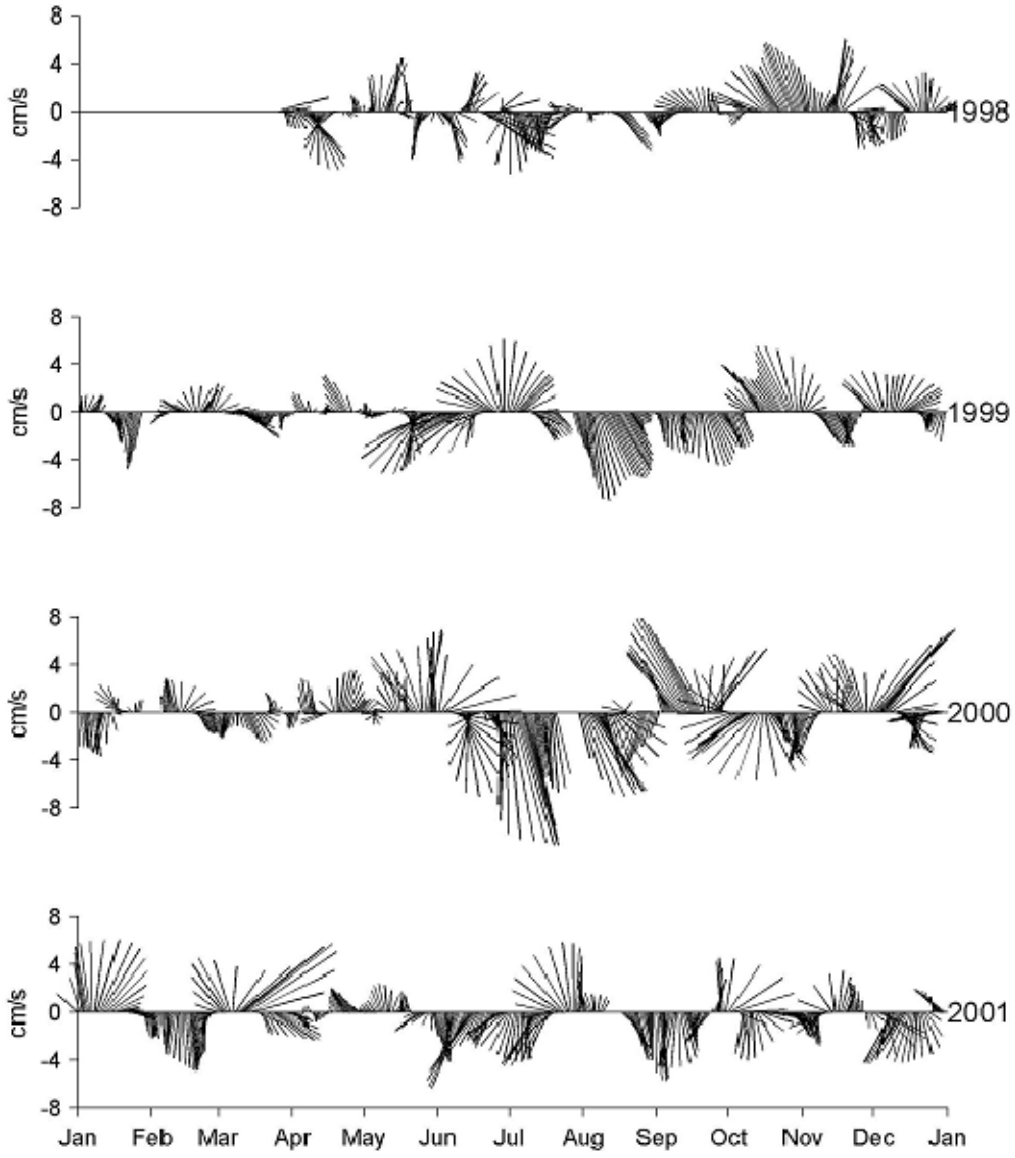

Figure F6 (a). 1200 m velocity at S2 as a function of time, 1998-2001. Currents were smoothed using a Butterworth filter with a cutoff period of one week.

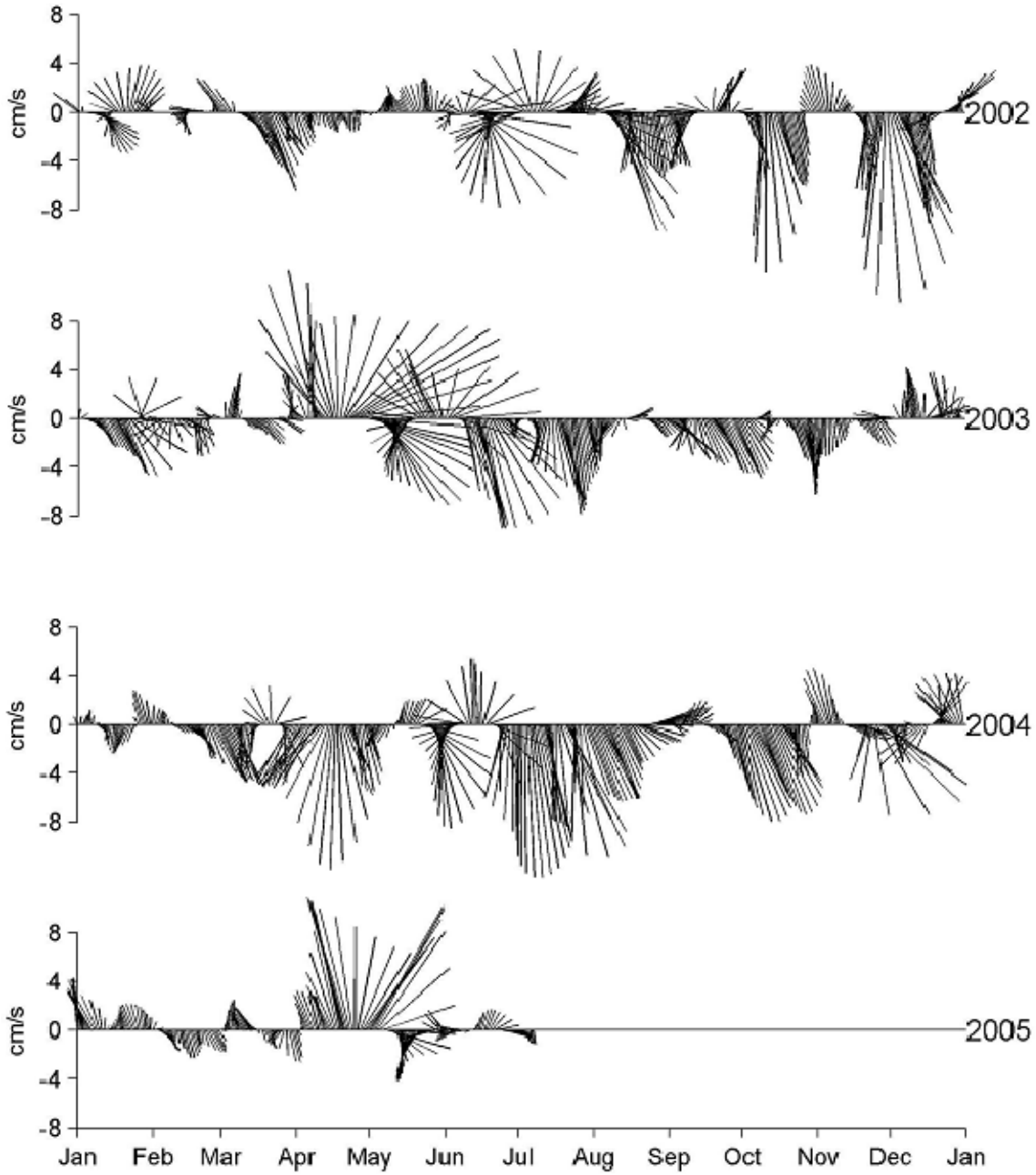

Figure F6 (b). 1200 m velocity at S2 as a function of time, 2002-2005. Currents were smoothed using a Butterworth filter with a cutoff period of one week.

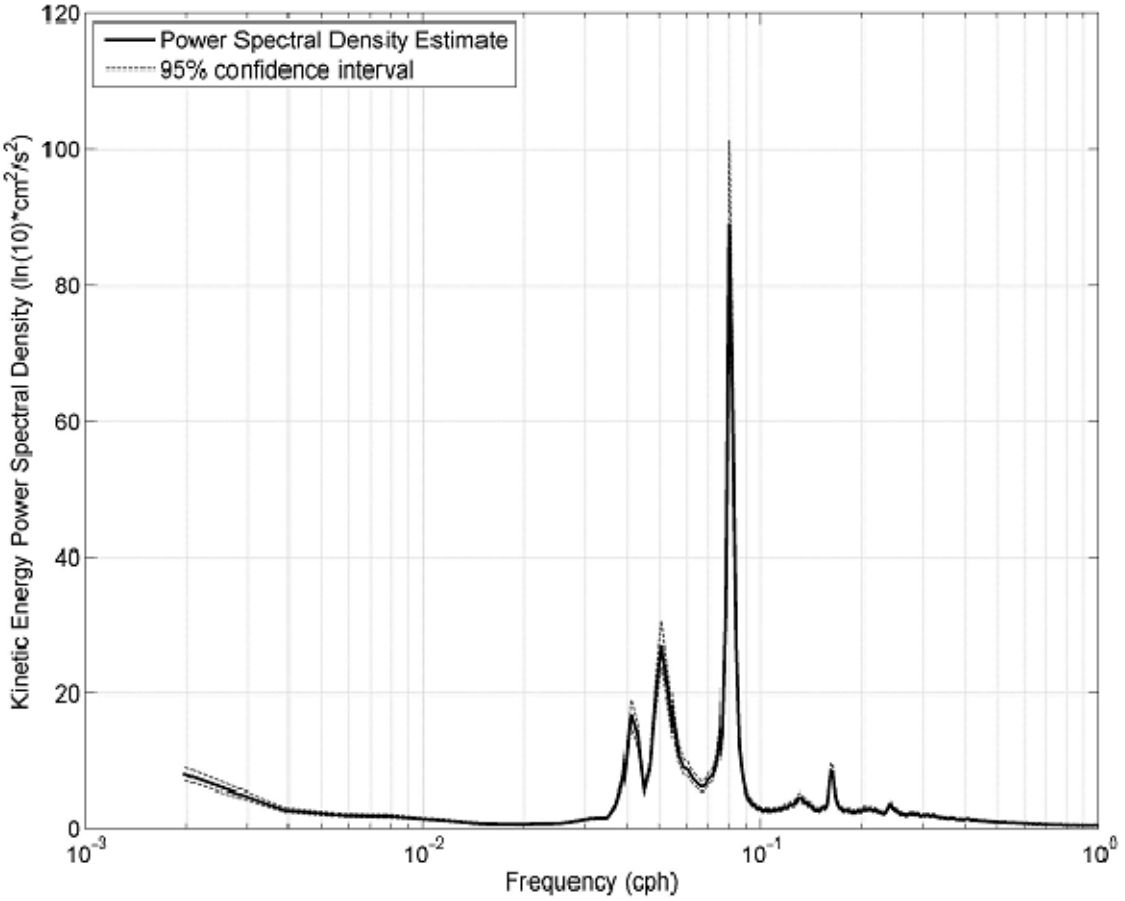

Figure F7. Kinetic energy spectrum for 1200 m currents at S2. Diurnal peak at 0.041 cph, inertial at 0.051 cph, semi-diurnal at 0.08 cph with smaller peaks at 0.1309 cph and 0.1602 cph.

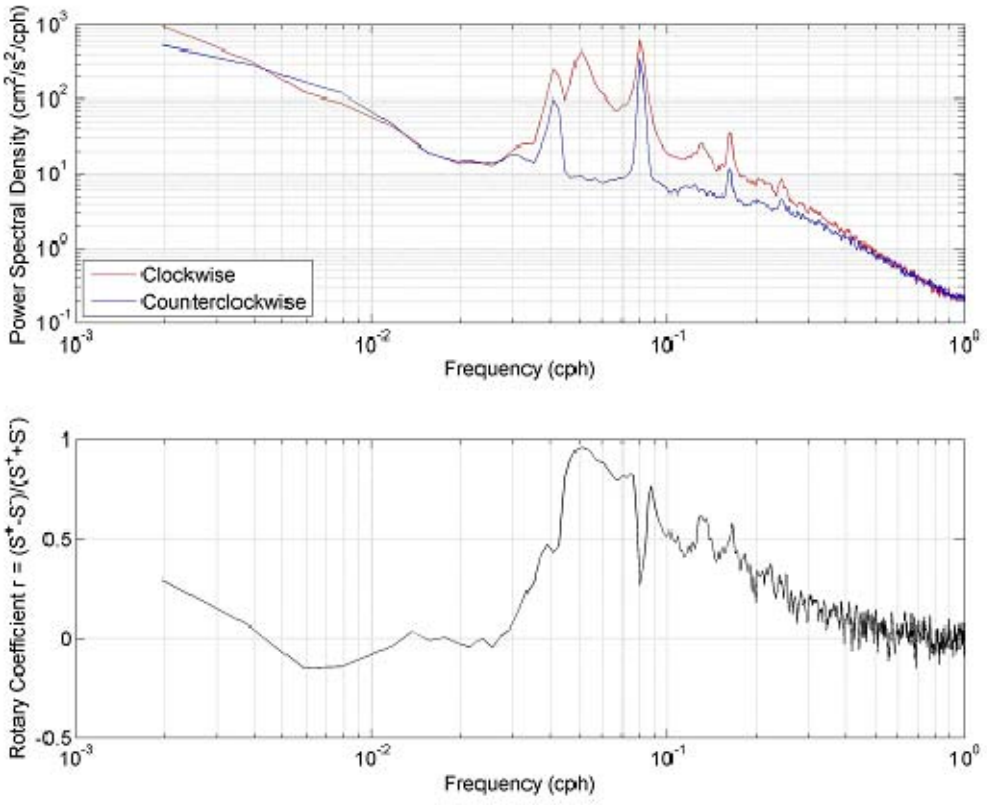

Figure F8. (upper) Rotary spectra for 1200 m currents at S2. (lower) Rotary coefficient for 1200 m currents.

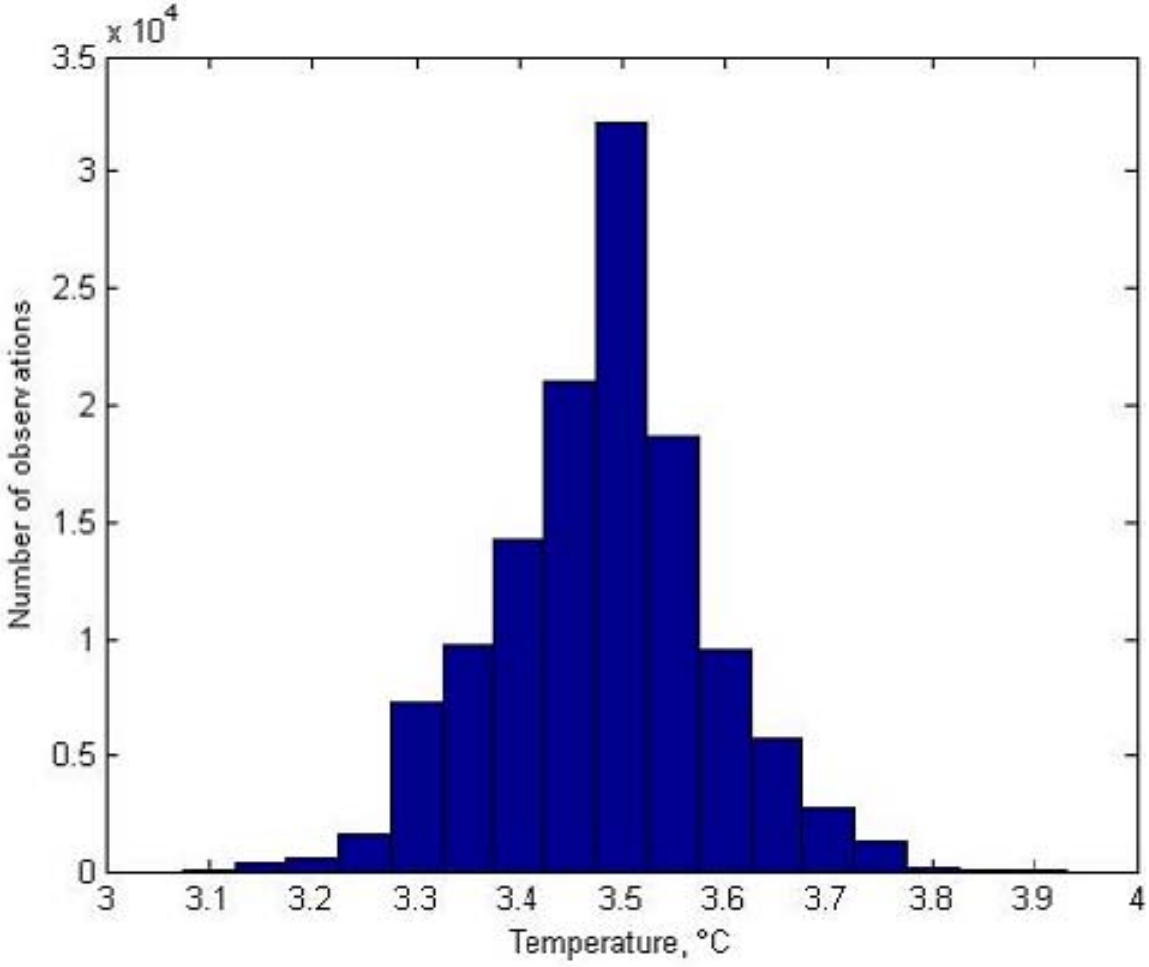

Figure F9. Histogram of 1200 m temperatures at S2 using a bin size of 0.05°C.

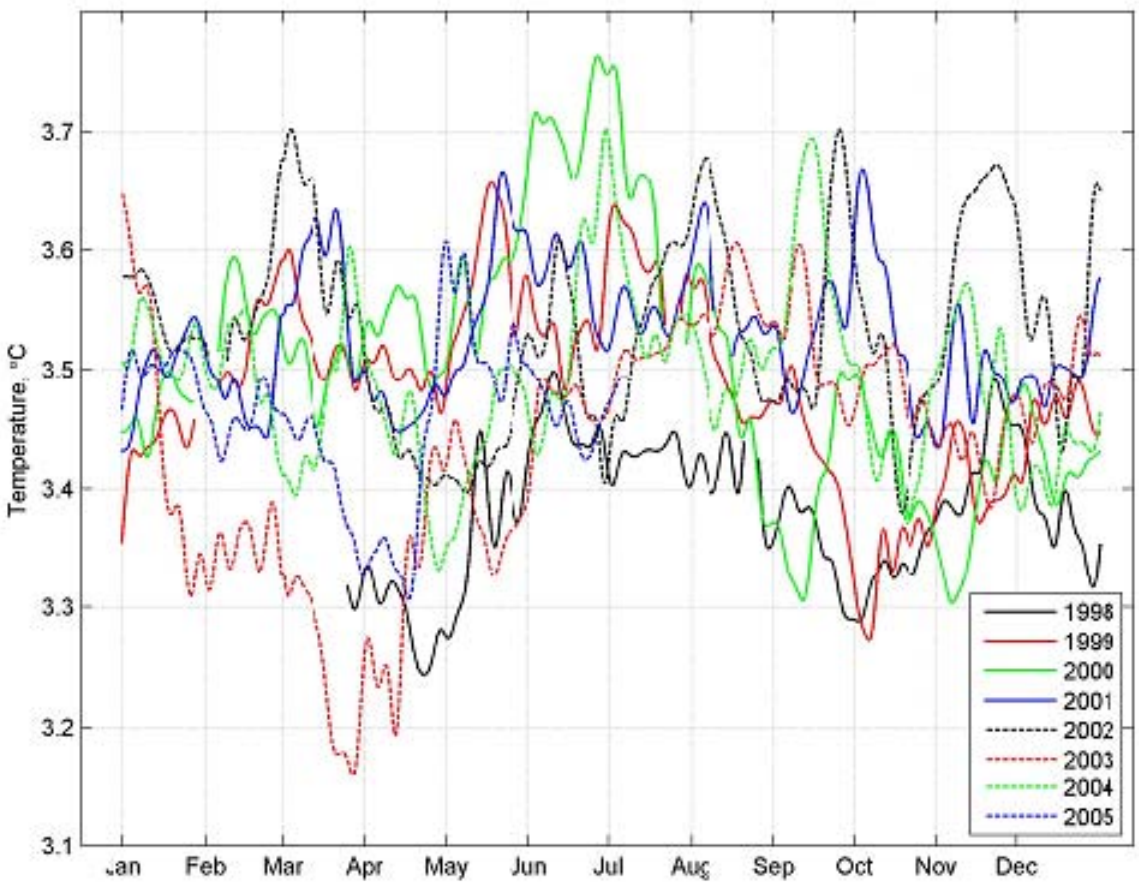

Figure F10. Time series of 1200 m temperature measurements at S2. Temperatures were smoothed using a Butterworth filter that cut off periods less than one week.

Deployment Number	Date of Deployment	Latitude	Longitude	Mooring Depth (m)	Bottom Depth (m)	Compass Correction (E)	Timing Error
1	24 MAR 98-20 AUG 98	36° 40.016'N	122° 22.523'W	1194	1800	6'	3' 03"
2	26 AUG 98-27 JAN 99	36° 39.953'N	122° 22.536'W	1199	1800	6'	11' 04"
3	04 FEB 99- 21 JUL 99	36° 39.920'N	122° 22.482'W	1185	1790	6'	2' 10"
4	27 JUL 99- 27 JAN 00	36° 39.920'N	122° 22.448'W	1172	1809	3'	2' 25"
5	05 FEB 00- 20 JUL 00	36° 39.925'N	122° 22.448'W	1173	1801	5'	2' 07"
6	29 JUL 00- 25 JAN 01	36° 39.884'N	122° 22.374'W	1176	1792	5'	2' 22"
7	25 JAN 01- 09 AUG 01	36° 39.932'N	122° 22.399'W	1175	1797	6'	4' 09"
8	16 AUG 01-01 FEB 01	36° 39.929'N	122° 22.381'W	1177	1785	6'	5' 55"
9	08 FEB 02- 28 AUG 02	36° 39.971'N	122° 22.463'W	1175	1802	5'	4' 13"
10	28 AUG 02-11 MAR 03	36° 39.971'N	122° 22.449'W	1177	1792	5'	2' 33"
11	11 MAR 03-07 SEP 03	36° 39.949'N	122° 22.454'W	1180	1802	5'	2'40''
12	07 SEP 03- 16 MAR 04	36° 39.953'N	122° 22.462'W	1173	1800	5'	2'15"
13	16 MAR 04-02 SEP 04	36° 39.940'N	122° 22.426'W	1176	1802	5'	2'20"
14	02 SEP 04- 07 JUL 05	36° 39.937'N	122° 22.436'W	1185	1800	6'	3'56"

Table F1. S2 RCM 8 Deployment Data. The sampling rate was 30 minutes with exception of deployment #14, which was sampled once per hour.

APPENDIX G S3

This appendix covers a series of deployments at site S3 (Fig. G1). The deployments were between 24 March 1998 and 21 July 2000 at a mean depth of 2348 m. Table G1 contains details of these deployments. The sampling rate for the RCM 8 current meter for all five deployments was 30 minutes. During the third deployment the RCM 8 failed to collect any velocity data.

The mean speed was 2.74 cm/s. Direction and speed of vector mean flow were 263.4°T and 0.7 cm/s, respectively (Fig. G2). The semi-major (minor) axis magnitude was 4.6 cm/s (2.7 cm/s) and the eccentricity of the variance ellipse was 0.64. The semi-major axis was directed along 335.1°T to 155.1°T, reflecting the trend of the local bathymetry (Fig. G1).

The velocity histogram (Fig. G3) showed the principal mode at a median direction of 340°T and a median speed of 4 cm/s containing 141 observations per bin. A secondary mode had a median direction of 180°T with a median speed of 5 cm/s and 100 observations per bin.

The PVD (Fig. G4) was constructed by omitting the third deployment. Thus the second deployment joined the fourth deployment where the trajectory changed from blue to green near -200 km eastward displacement and 100 km northward displacement. In 1998 and 1999, the spring and early summer flow was directed to the north-northwest. The current direction changed in late summer to flow southwest and west-southwest, and appeared to revert back to north-northwest in November (1999) or December (1998). In winter 2000, the seasonal flow pattern changed and was directed to the southwest in both spring and early summer.

The stick plot (Fig. G5) also has a gap which corresponds to the third deployment. The two 30 km diameter loops on the PVD (Fig. G4) in May 1998 and February 2000 had a clear eddy-like stick structure. The periods of sustained northward or southward flow were interspersed with monthly or bi-monthly acceleration. The sticks in early 1998 displayed a northward direction at a higher speed than would be seen later in the year. The sticks then changed direction to a south-westerly heading at reduced speeds. The

period of strongest flow, almost 8 cm/s, occurred shortly after the first mooring was set in spring 1998.

The kinetic energy spectrum (Fig. G6) showed the semi-diurnal tides dominating the variance. At lower frequencies, small diurnal (0.041 cph) and inertial (0.05) peaks were observed. At frequencies higher than the semidiurnal tides, only one small peak was significant at 0.16 cph, corresponding to a period of 6.2 hours.

The rotary spectra (Fig. G7) showed that the clockwise (anticyclonic) component was larger than the counterclockwise component at low frequencies (<0.008 cph) and through the tidal and inertial frequency bands. The rotary coefficient was 0.34 at the semi-diurnal frequency, 0.13 at the diurnal frequency, and largest, 0.91, for inertial motions. Lowest values of the rotary coefficient were observed near 0.01 cph and 0.7 cph.

The temperature histogram (Fig. G8) used 0.02°C for the bin size. The median temperature was 1.82°C and mean temperature 1.83°C. The smoothed time series (Fig. G9) indicated a semiannual pattern. Temperatures were warm in winter (1.84°C in March 1989 and 1.88°C in January 2000), subsequently cooled (1.76°C in April 1998, 1.82°C in May 1999, and 1.82°C in June 2000), then warmed (1.88°C in August 1988, 1.86°C in September 1999). Thereafter, waters cooled relatively rapidly, reaching a minimum of 1.76°C (1.78°C) in December 1998 (November 1999).

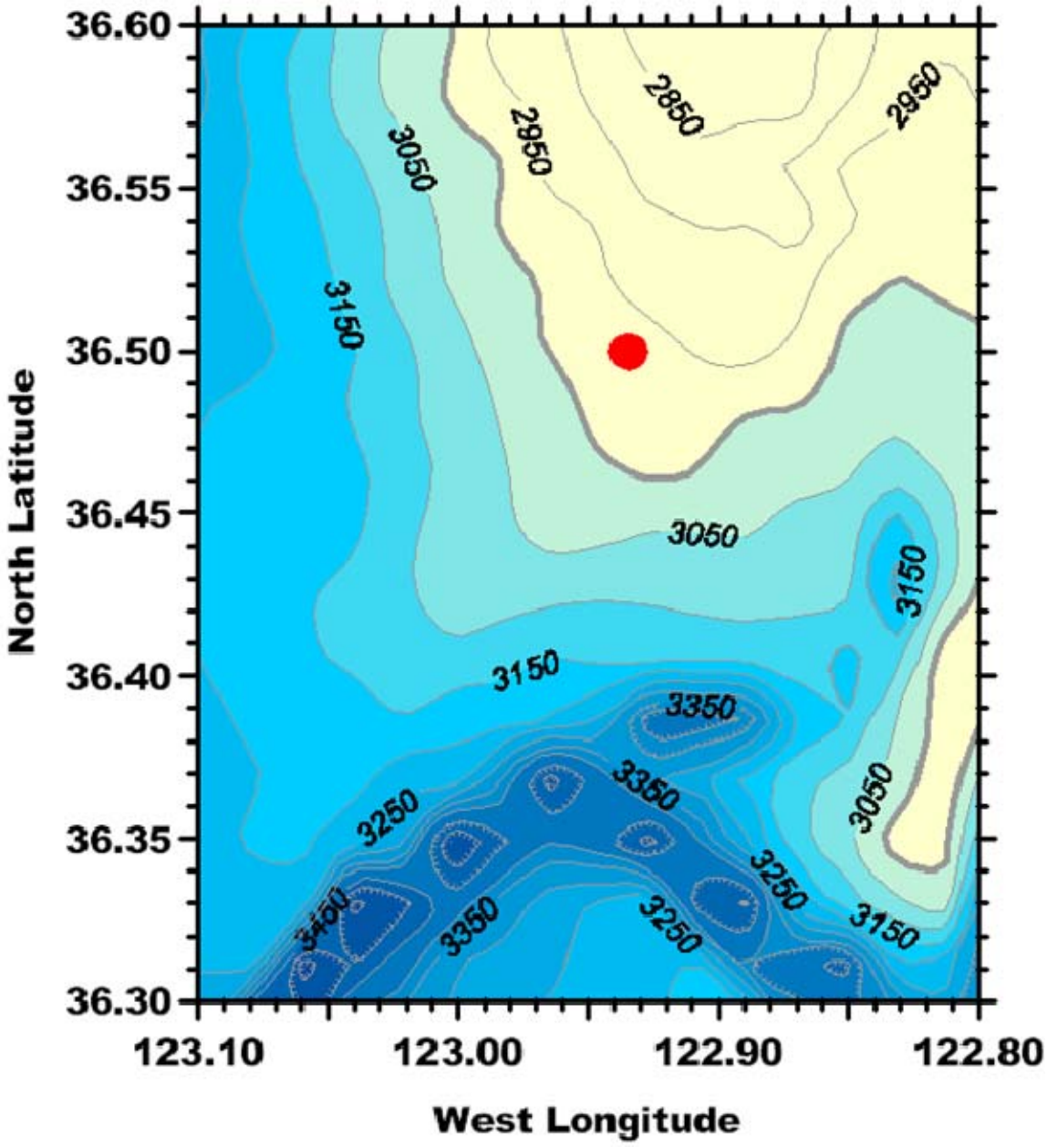

Figure G1. Mooring locations for S3 deployments. Soundings are in meters and the contour interval is 100 m. A portion of Monterey Submarine Canyon is shown in the lower portion of the chart.

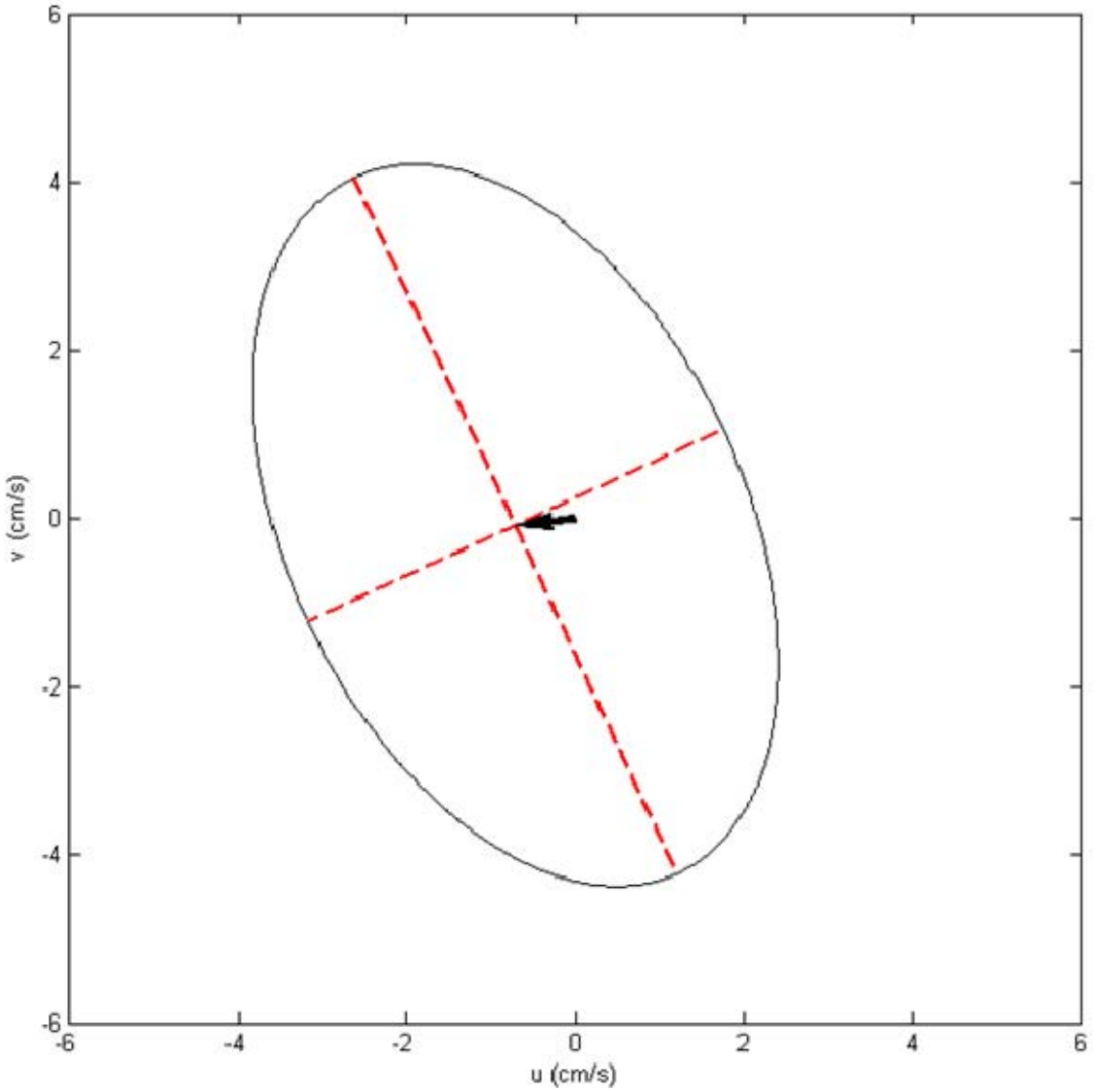

Figure G2. Mean and standard deviation of currents measured at 2348 m at S3. Mean speed (direction) of the vector mean flow was 0.7 cm/s (263.4°T). The semi-major (semi-minor) axis was 4.6 cm/s (2.7 cm/s) and was oriented along 335.1°-155.1°T.

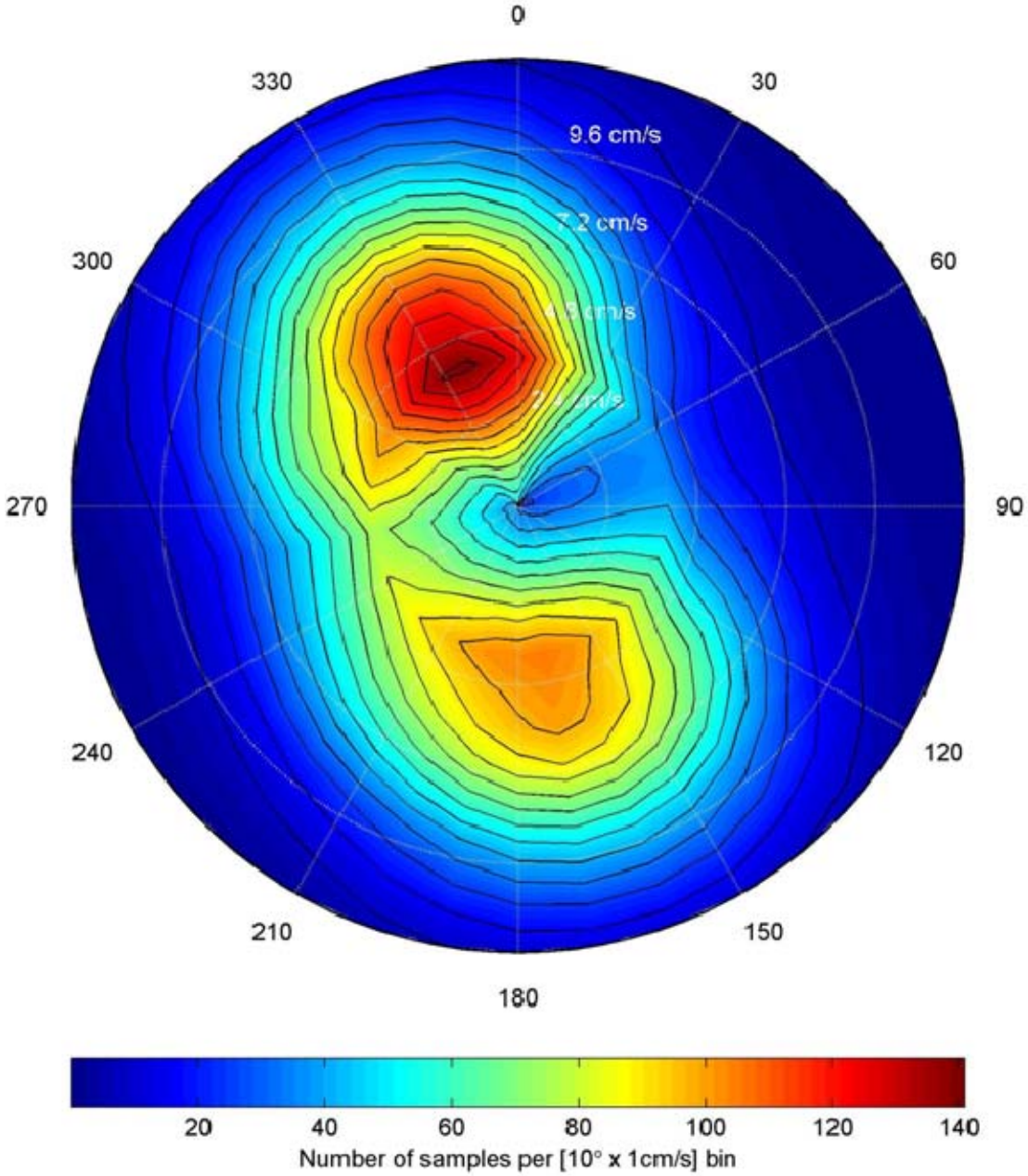

Figure G3. Histogram of velocity observations at 2348 m at S3. The total number of observations is 24,222. 1,961 observations with a speed less than 1 cm/s were omitted. Total number of bins is 481.

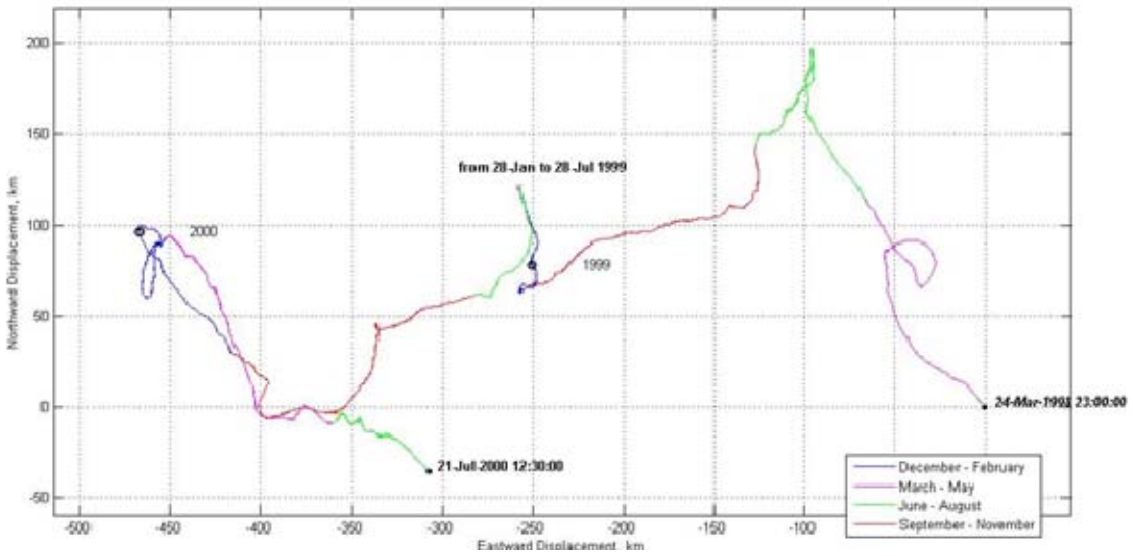

Figure G4. Progressive vector diagram for currents at 2348 m at S3. No current measurements were available for the third deployment; so the second and fourth deployments are joined where the blue changes to green near -250 km east and 100 km north, as noted on the figure.

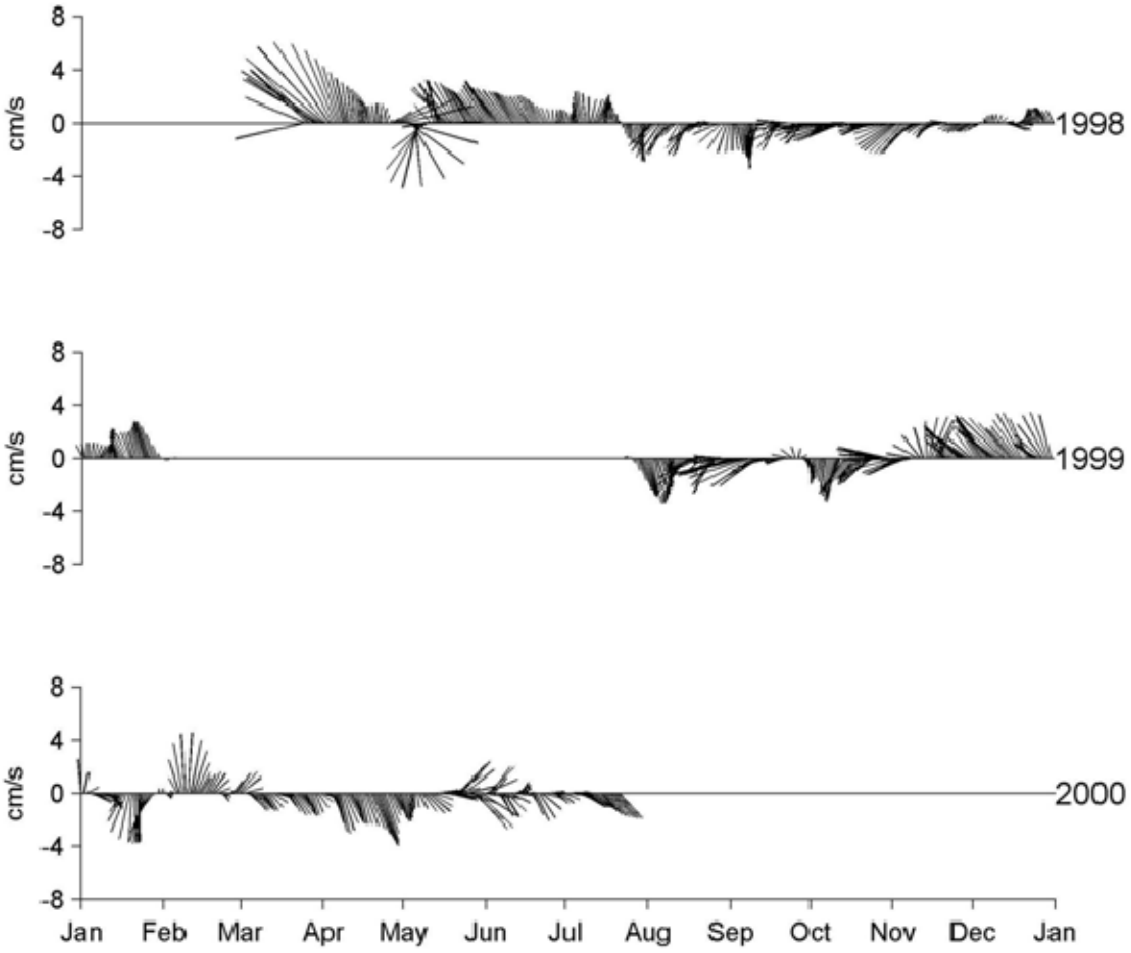

Figure G5. Current velocity at 2348 m at S3 as a function of time. Currents were smoothed using a Butterworth filter with a cutoff period of one week.

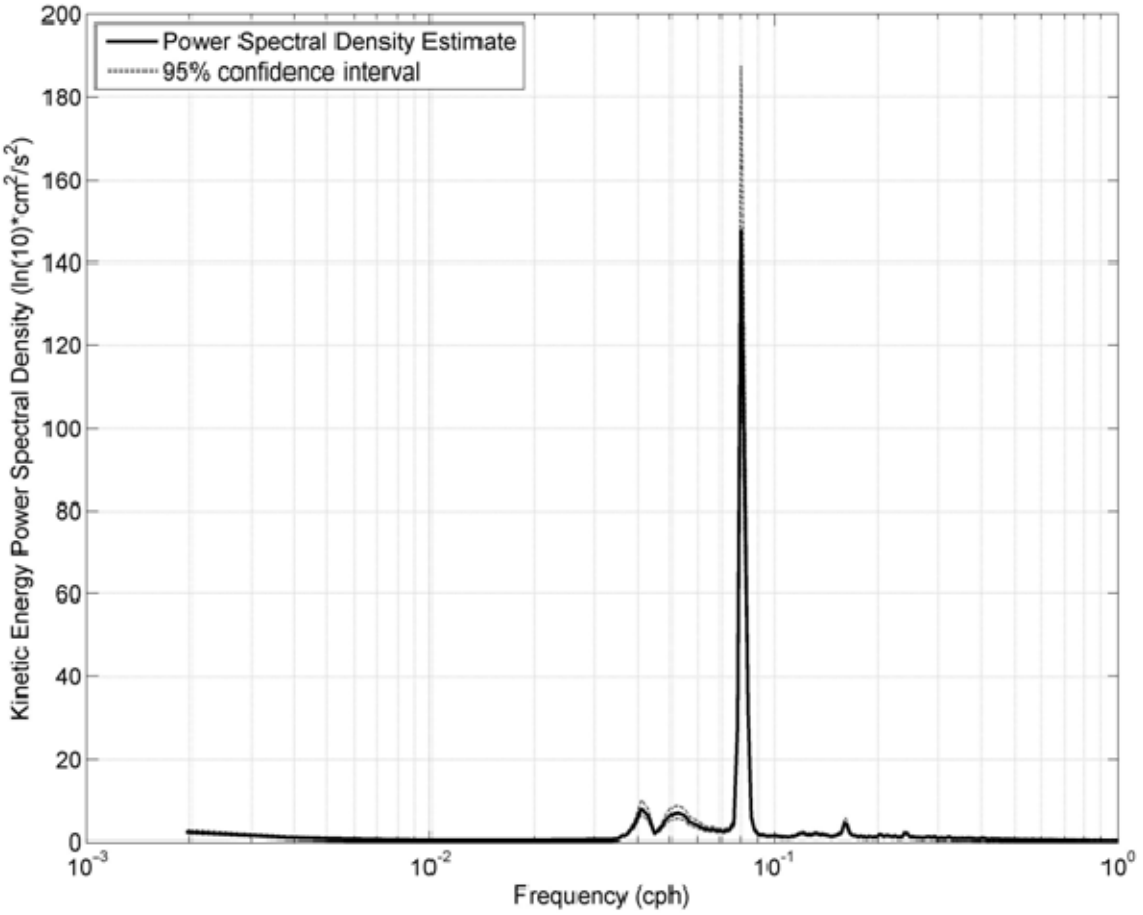

Figure G6. Kinetic energy spectra for currents at 2348 m at S3. Semi-diurnal peak at 0.08 cph, diurnal peak at 0.041 cph, and local inertial frequency at 0.05 cph.

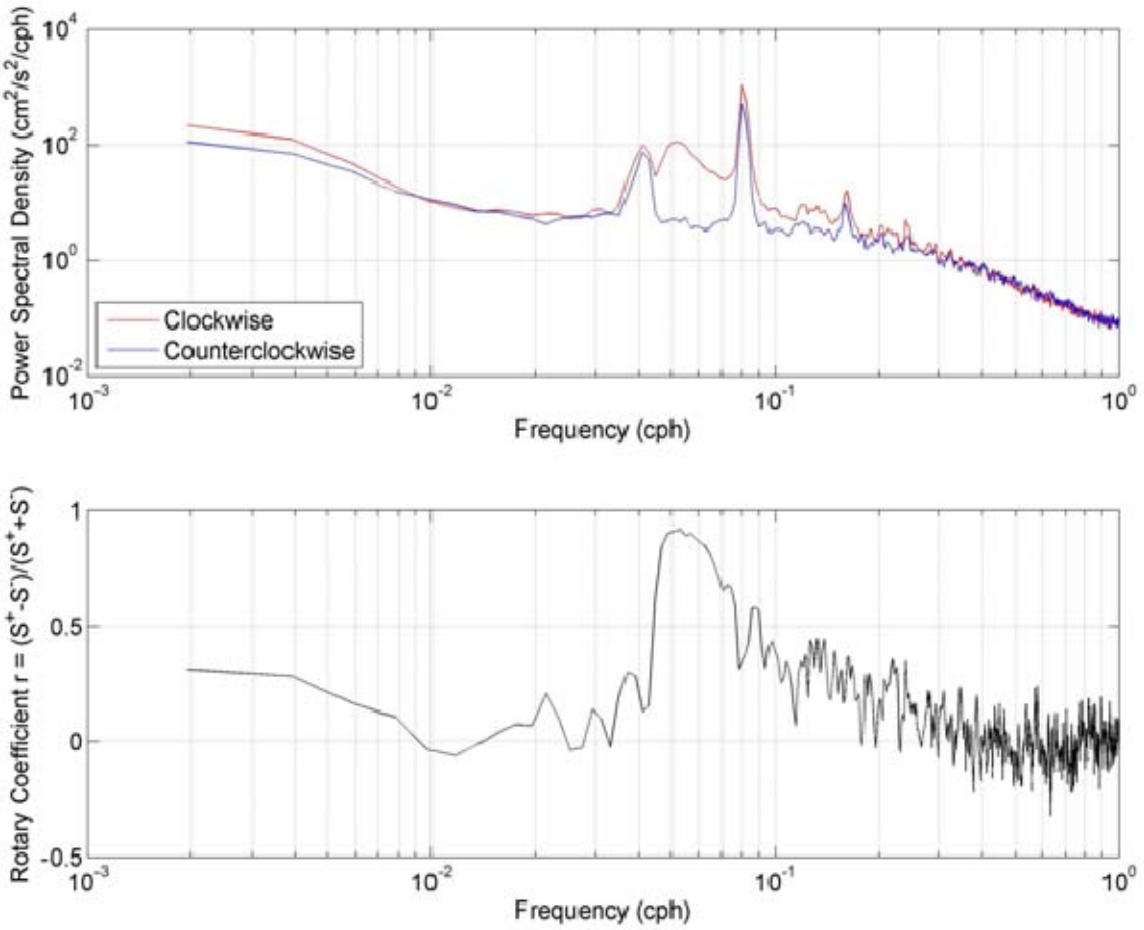

Figure G7. (upper) Rotary spectrum at 2348 m for S3 currents. (lower) Rotary coefficient for S3 currents.

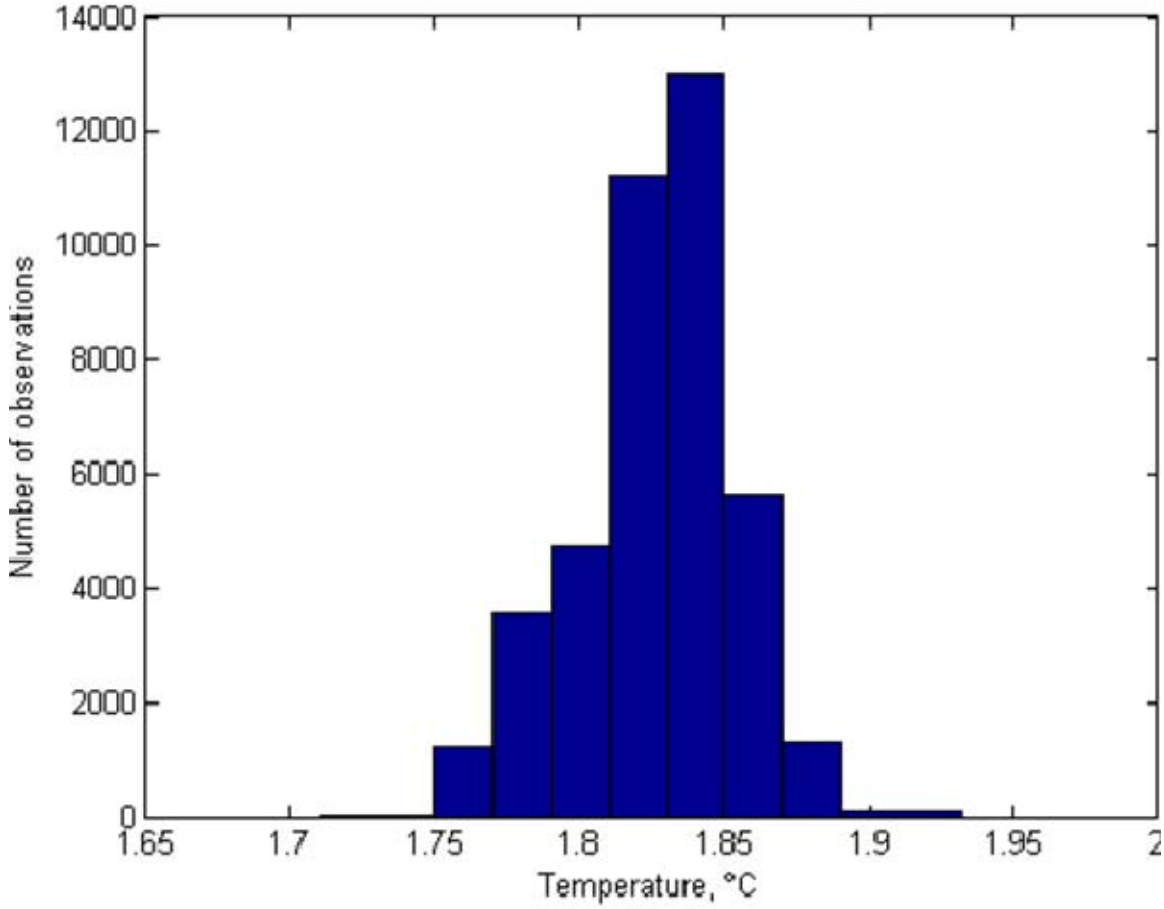

Figure G8. Temperature histogram at about 2348 m at S3 using a bin size of 0.02°C.

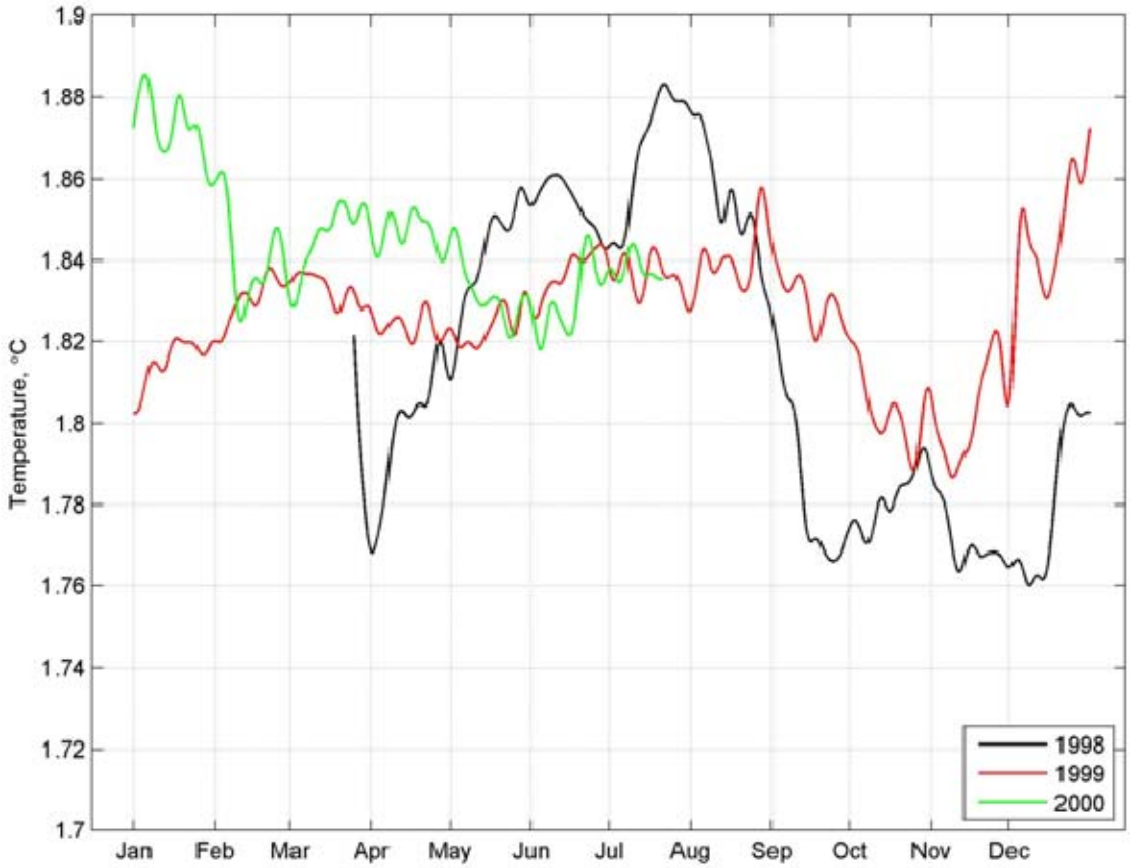

Figure G9. Temperature time series at about 2348 m at S3. Temperatures were smoothed using a Butterworth filter that cut off periods less than one week.

Deployment Number	Date of Deployment	Latitude	Longitude	Instrument Depth (m)	Bottom Depth (m)	Compass Correction (E)	Timing Error
1	24 March 1998 – 21 August 1998	36° 29.990'N	122° 56.008'W	2355	3000	7’	2'
2	25 August 1998 – 28 January 1999	36° 29.996'N	122° 56.005'W	2350	3000	7’	3' 47”
3	05 February 1999 – 21 July 1999	36° 29.972'N	122° 56.050'W	2345	2997	7’	2' 50”
4	28 July 1999 – 26 January 2000	36° 29.978'N	122° 56.067'W	2342	2998	7’	3'
5	06 February 2000 – 21 July 2000	36° 29.995'N	122° 56.155'W	2347	2980	7’	2' 50”

Table G1. S3 mooring deployment data. The sampling rate for the RCM 8 device for all deployments was 30 minutes.

APPENDIX H SUR RIDGE

This appendix describes results of a series of current meter deployments on the top of Sur Ridge. The main purpose of these moorings was to collect acoustic recordings near the former Navy SOSUS array to the west of Point Sur, California. Table H1 contains specific details for the deployment. The bottom depths varied with deployment from 828 to 837 m (Table H1) and the current meter depth varied from 41 m to 51 m above the bottom. Figure H2 shows a schematic diagram of the mooring that was used. All RCM 8 current meters collected data every thirty minutes.

The currents on top of Sur Ridge had a mean speed of 11.48 cm/s. Direction and speed of vector mean flow was 162.4°T and 0.3 cm/s, respectively (Fig. H3). The semi-major (minor) axis magnitude was 11.8 cm/s (6.5 cm/s) and the eccentricity of the variance ellipse was 0.67. The semi-major axis was directed along 306.5°T to 126.5°T.

The velocity histogram (Fig. H4) showed three distinct modes. The principal mode had a heading (speed) of 310°T (10 cm/s) and contained 85 observations. A secondary westward mode had a heading (speed) of 260°T (6 cm/s) and contained 82 observations. A southward third mode had at a heading (speed) of 130°T (12 cm/s) and contained 72 observations. The total number of bins used in the velocity histogram was 592.

The progressive vector diagram (Fig. H5) showed a figure "8" pattern with north south displacements twice those of the east-west displacement. The flow appeared to be somewhat seasonal, with south-southwestward flow in spring and summer of 2008, north-northwestward flow in spring 2009, and eastward flow in winter and July-August 2009. Daily tidal excursions were clearly visible, as were occasional longer period current reversals, e.g. January and February 2009. Stick plots show the relative strength of these flow patterns (typically 8 cm/s) and confirm the seasonal tendencies. Month-long periods of unidirectional flow occurred in September 2008 (southward) and March 2009 (northward) but otherwise the flow seems to relax or rotate, either clockwise or counterclockwise, bi-weekly.

The stick plot (Fig. H6) displays the current velocities for the deployments at Sur Ridge. The most striking feature of these figures are the amazingly strong (>8 cm/s) bursts of southward velocity during the first part of the deployment in 2008. During the summer months of 2008 we see the velocity magnitudes as high as 8 cm/s or greater, and at other times greater than 4 cm/s. During the fall of 2008 heading into 2009 the current loses its dramatic speed from earlier months, and the current shifts to a northward direction at the end of 2008 and into the beginning of 2009. During the remainder of 2009 the current remains in a northern heading until the summer months, when the current shows a strong southern bias with the exception of a few sticks that burst north.

Semi-diurnal tides dominated the variance of the kinetic energy spectrum (Fig. H7) with a distinct peak at the diurnal frequency (0.041 cph). The only other spectral peak that was clearly significant was for the diurnal tide. The rotary spectra (Fig. H8) showed that clockwise (anticyclonic) motion dominated for motions through the diurnal and semidiurnal tidal bands for periods ranging from 28 hours to 3 hours. The largest rotary coefficients in this band were about 0.7.

The temperature histogram (Fig. H9) used 0.05°C bins and was bivariate with peaks at 4.45°C and 4.7°C. The mean temperature (standard deviation) was 4.58°C (0.20°C). The maximum (minimum) temperature was 5.42°C (4.09°C). The smoothed temperature time series is shown in Figure H10 and, reflecting the bivariate character of the histogram, indicated two seasons: a winter from October through April with smoothed temperatures between 4.4°C and 4.5°C, and a summer from May through September with temperatures from 4.7°C to 4.9°C.

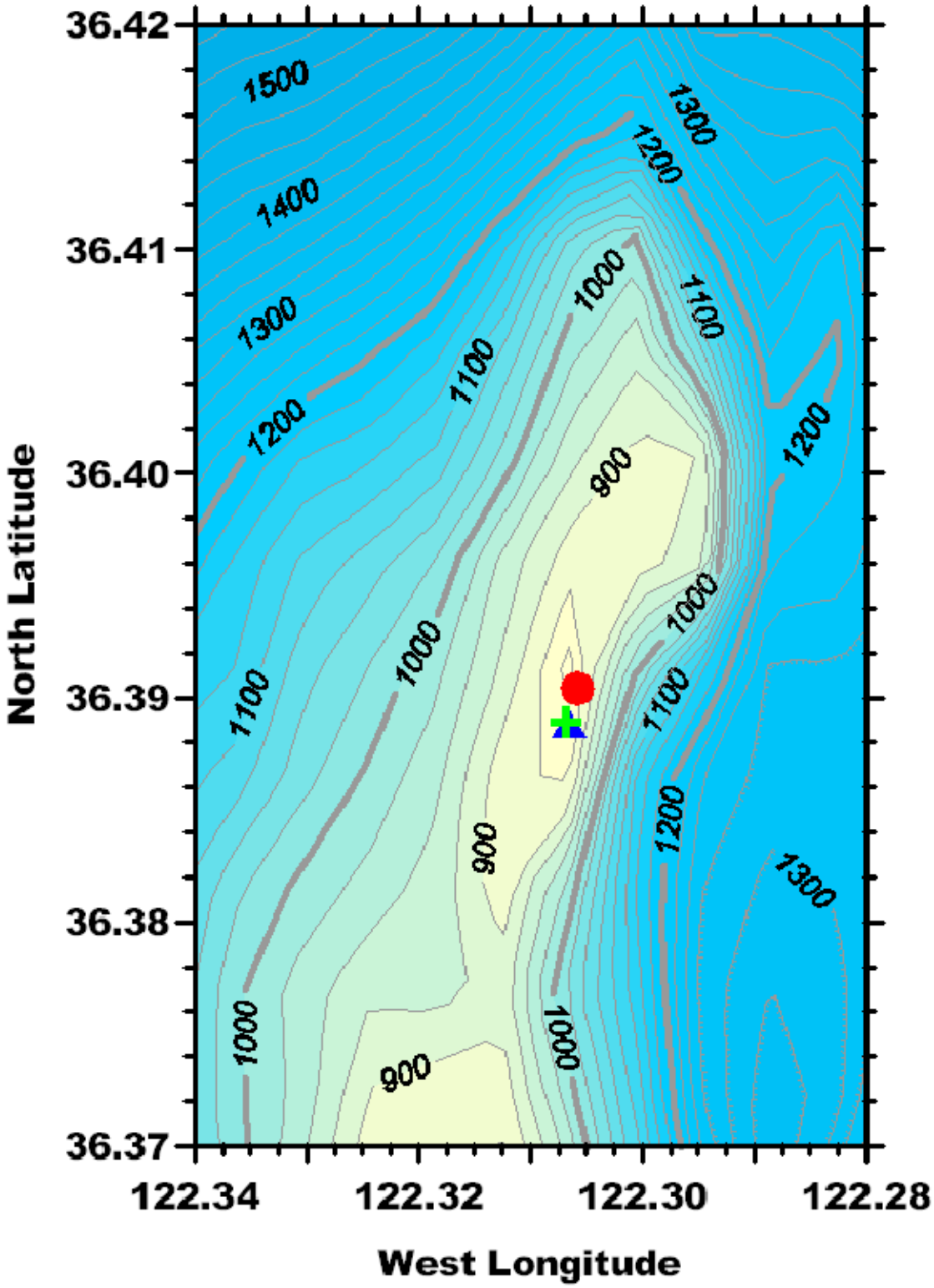

Figure H1. Mooring locations on the northern tip of Sur Ridge. Soundings are in meters and the contour interval is 25 m.

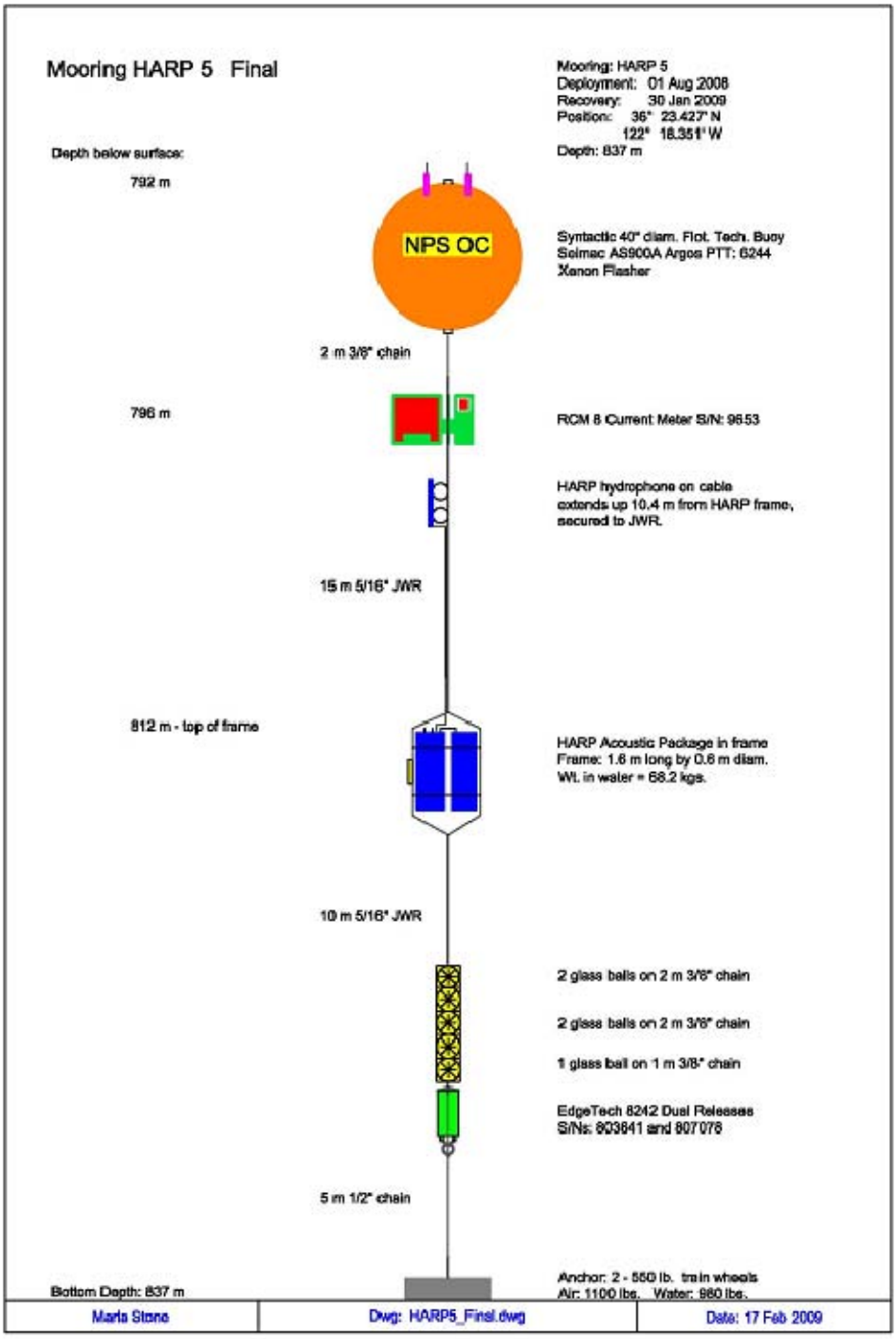

Figure H2. Schematic diagram of the mooring used on Sur Ridge from 1 August 2008 to 30 January 2009. Later mooring deployments used a similar mooring. Jacketed wire rope (JWR) was torque balanced and designed for oceanographic applications.

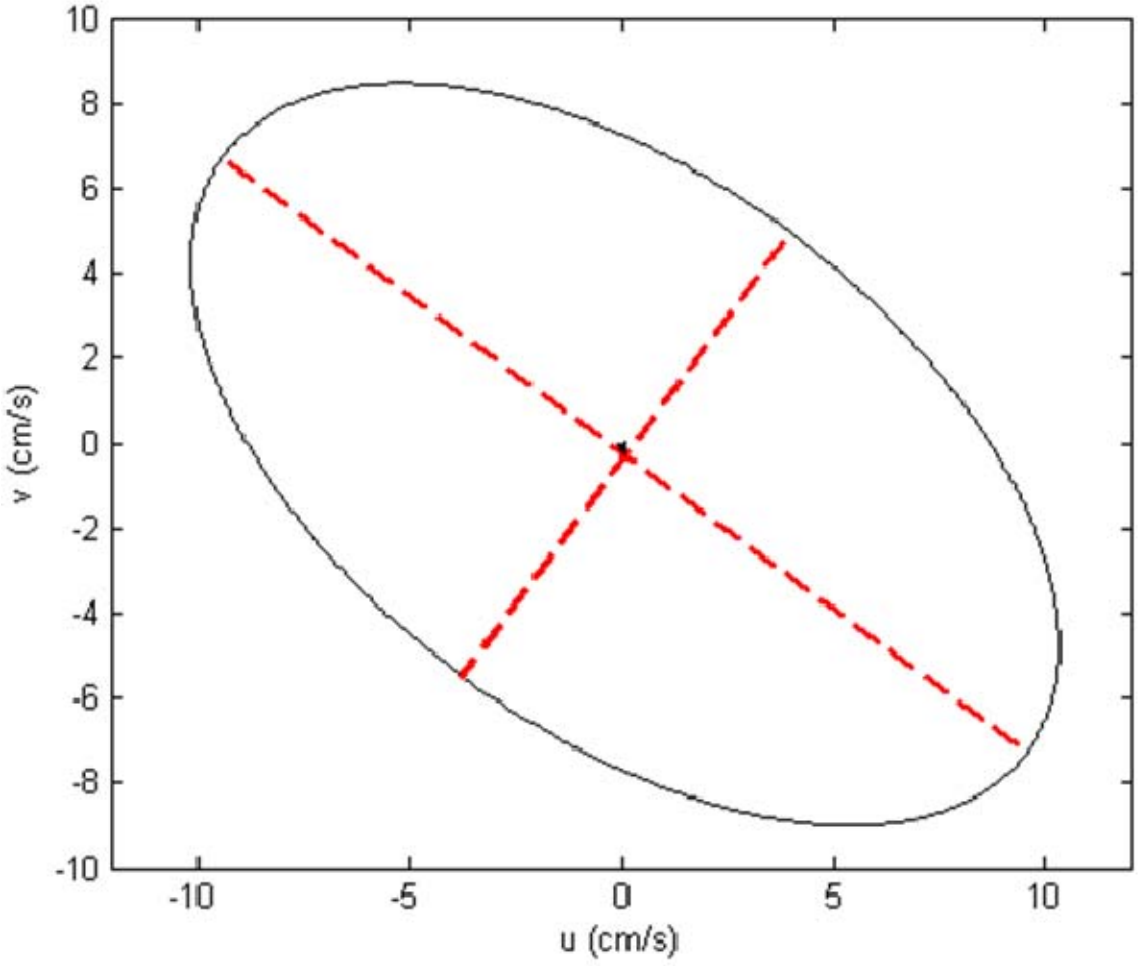

Figure H3. Mean and standard deviation of currents at 796 m on Sur Ridge. Mean speed (direction) of the mean vector flow was 0.3 cm/s (162.4°T). The semi-major (semi-minor) axis was 11.8 cm/s (6.5 cm/s) and was oriented along 306.5-126.5°T.

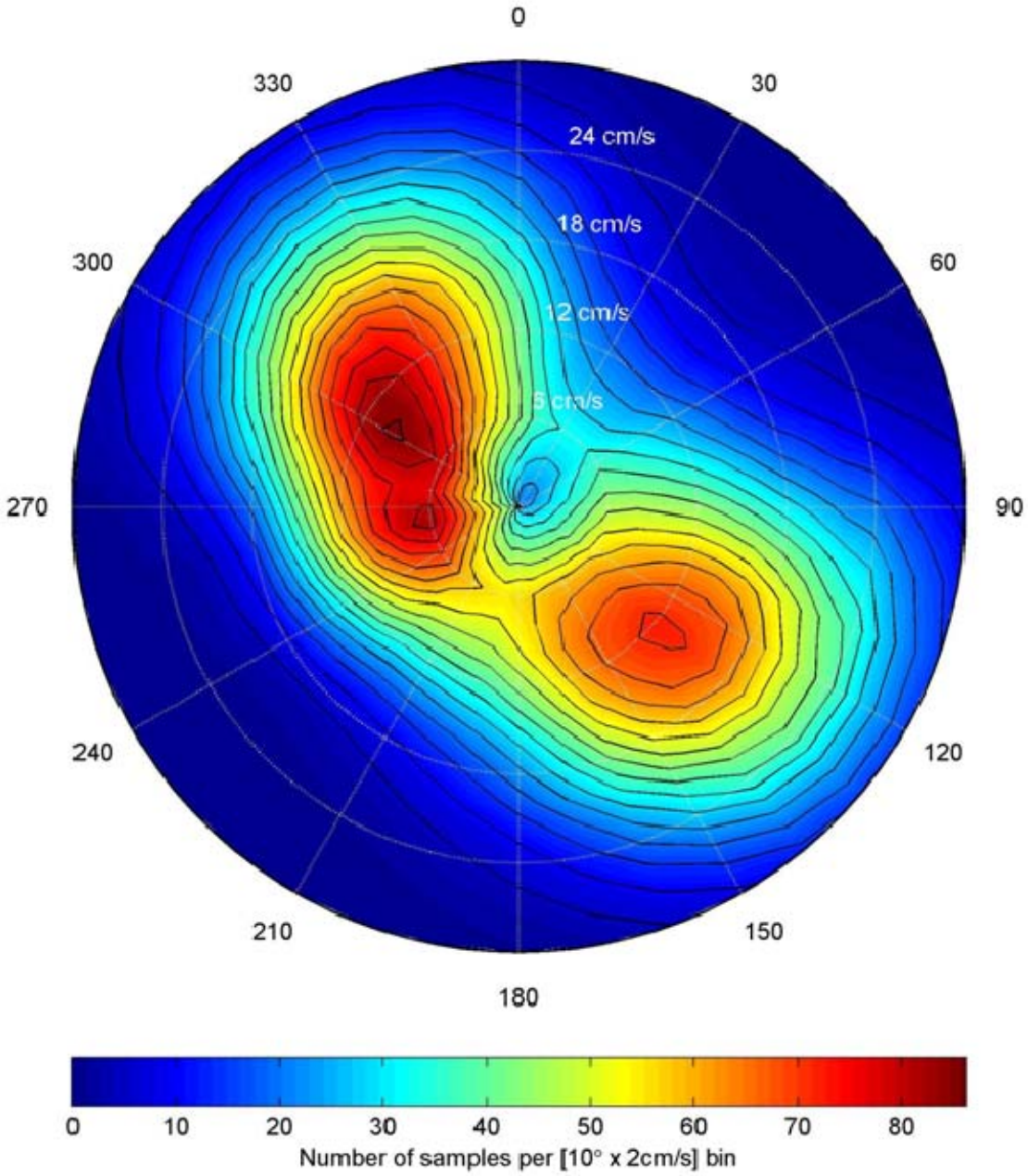

Figure H4. Velocity histogram of currents at 796 m on Sur Ridge. The total number of half hour observations for this histogram is 20,006. 345 observations with a speed less than 1 cm/s were omitted. Total number of bins is 592.

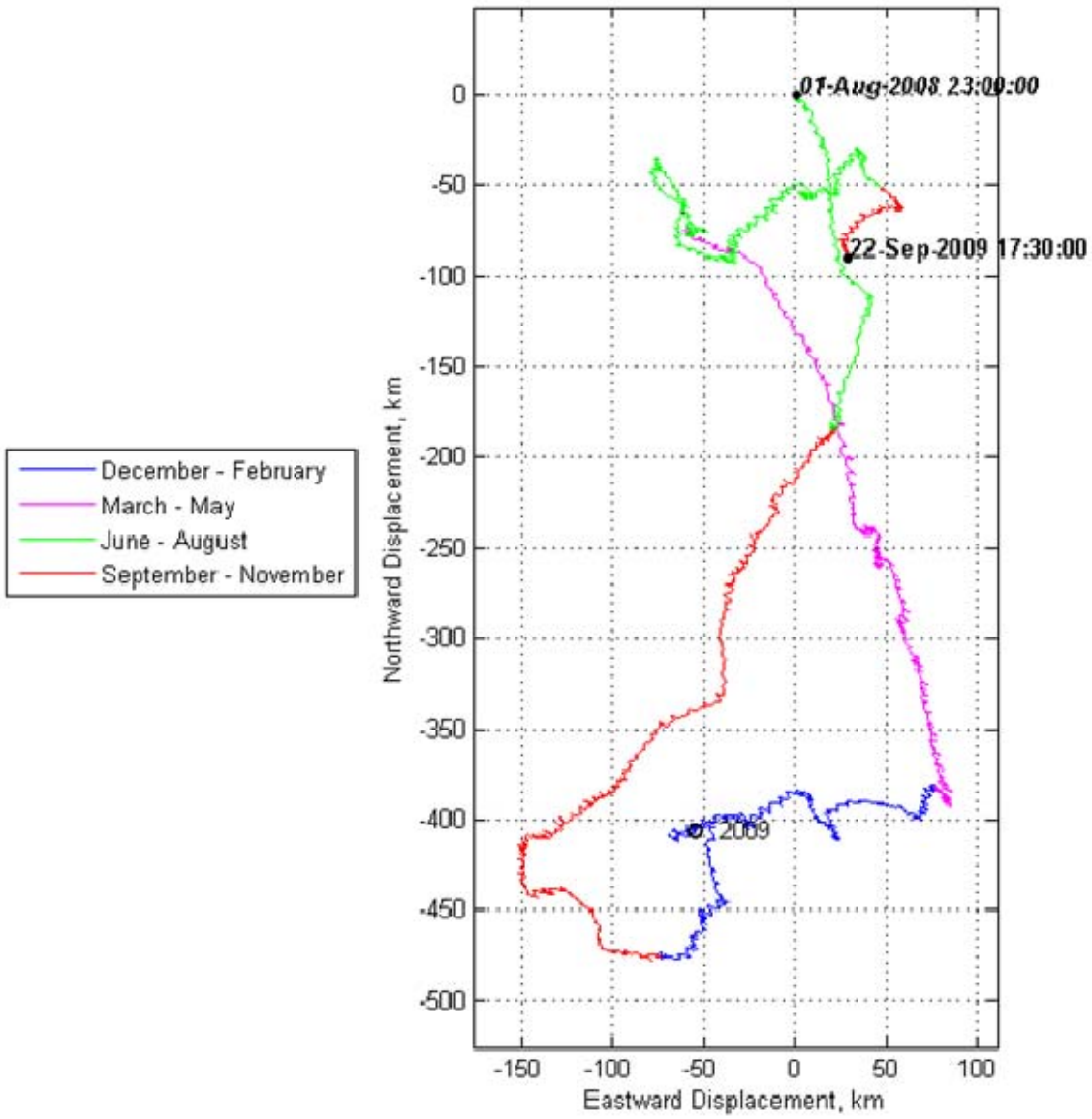

Figure H5. Progressive vector diagram for currents at 796 m on Sur Ridge.

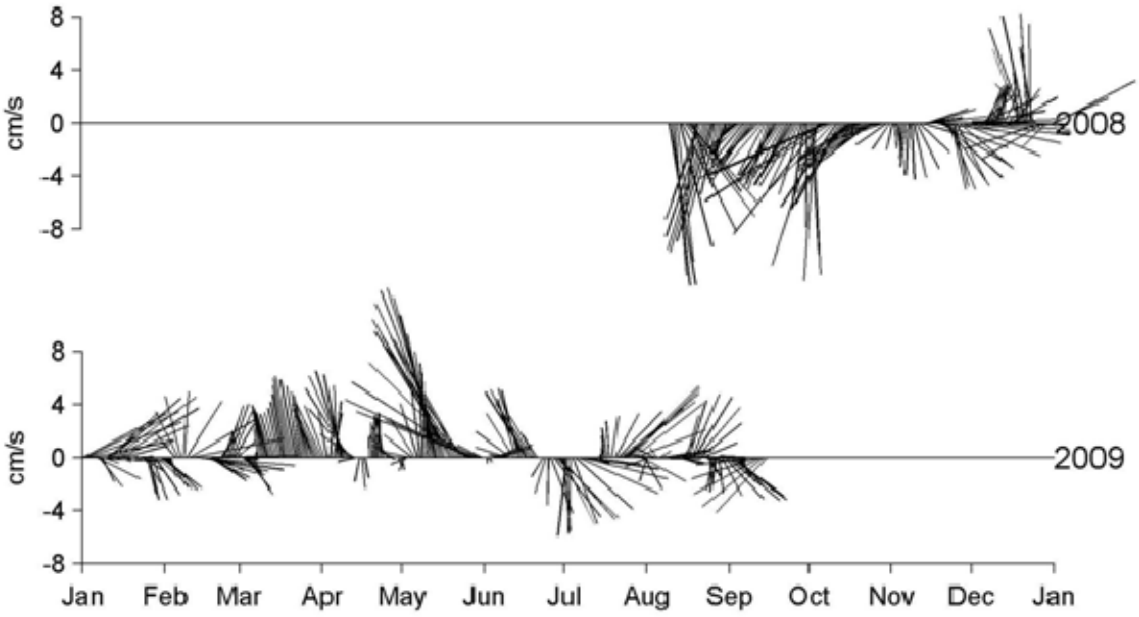

Figure H6. Current velocities at 796 m at Sur Ridge as a function of time, 2008-2009. Currents were smoothed using a Butterworth filter with a cutoff period of one week.

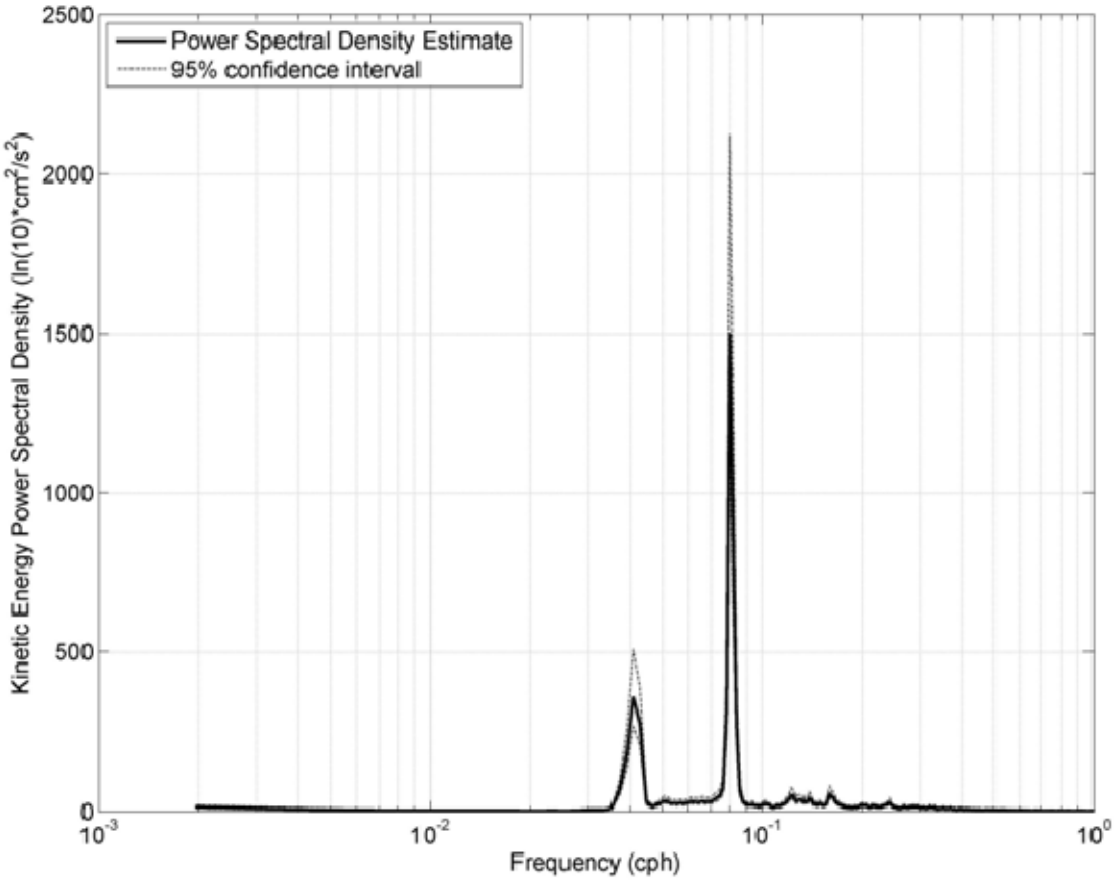

Figure H7. Kinetic energy spectrum for currents at 796 m at Sur Ridge. Diurnal peak at 0.041 cph, semi-diurnal at 0.08 cph, with smaller peaks at 0.123, 0.139, and 0.16 cph.

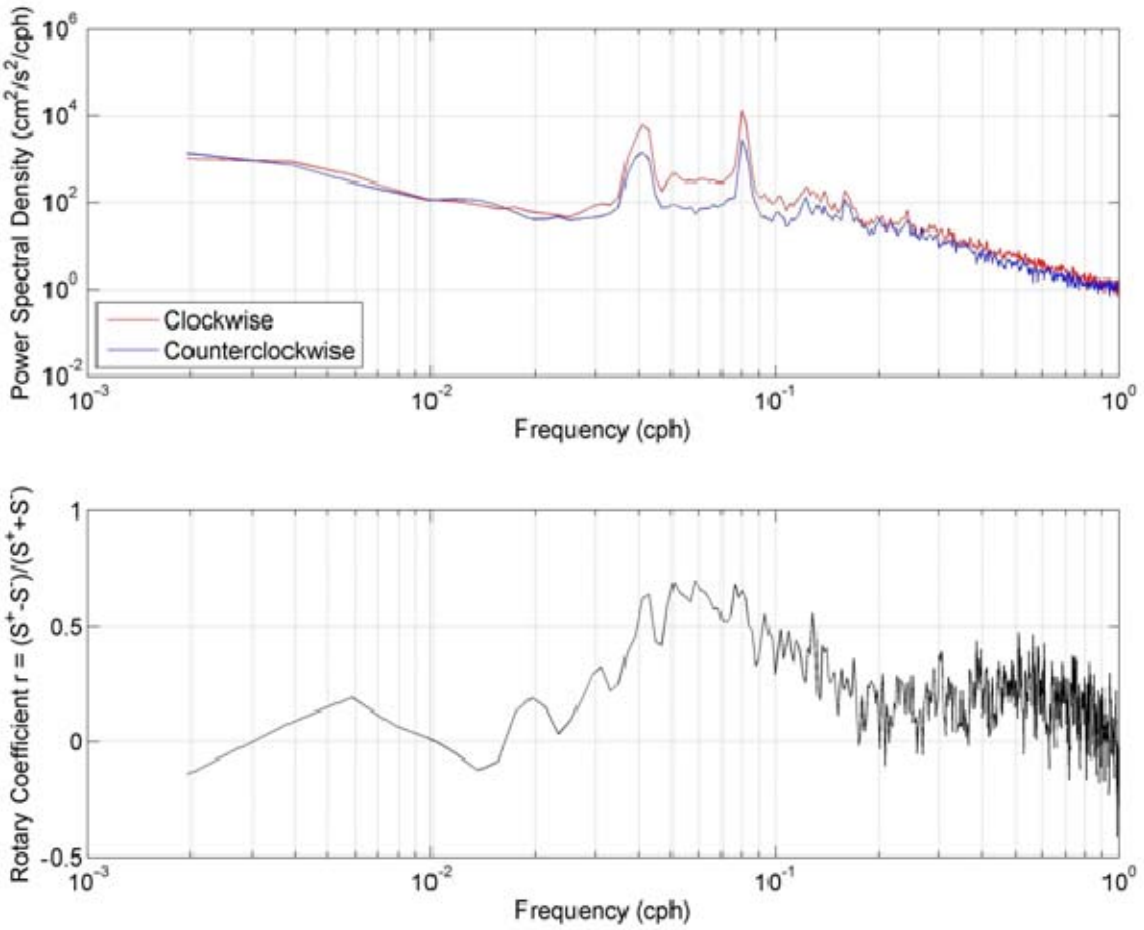

Figure H8. (upper) Rotary spectra for currents at 796 m at Sur Ridge. (lower) Rotary coefficient.

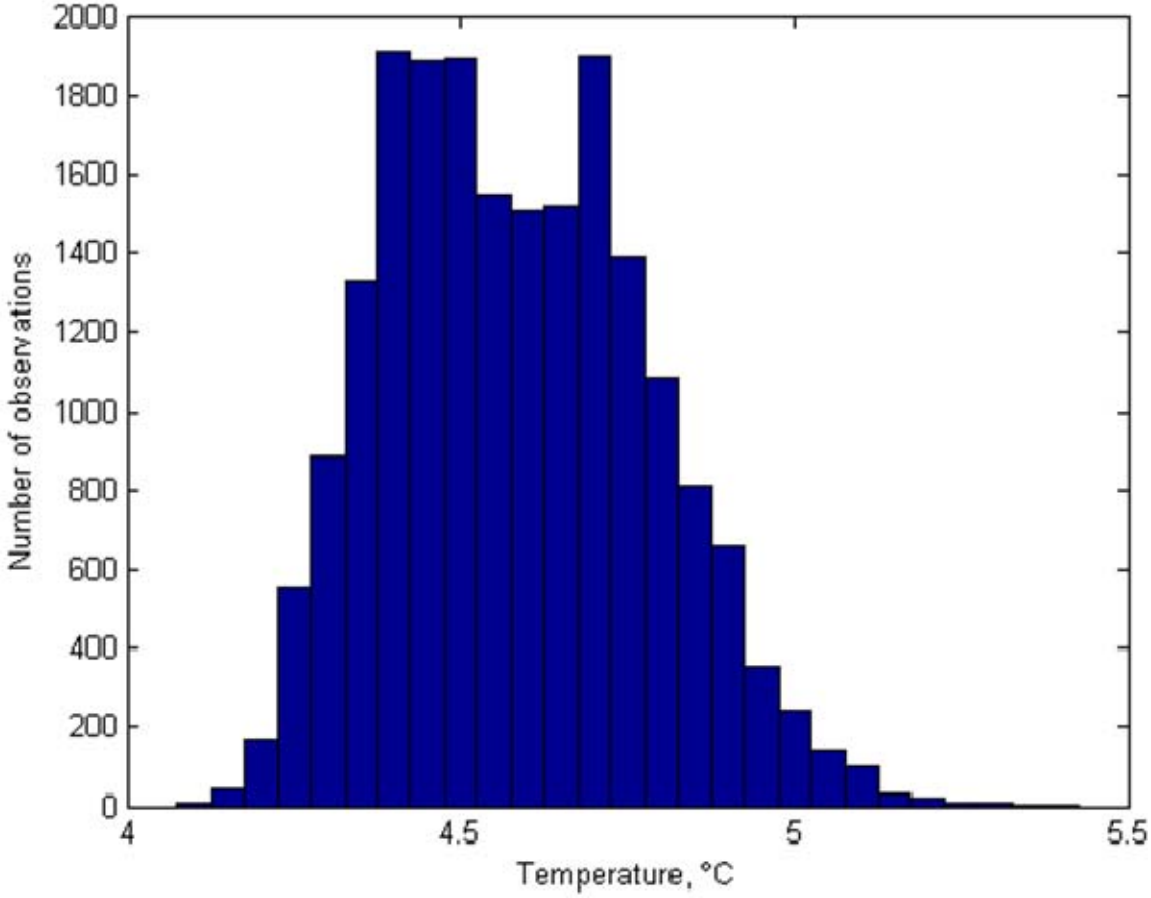

Figure H9. Histogram of temperatures at 796 m at Sur Ridge using a bin size of 0.05°C.

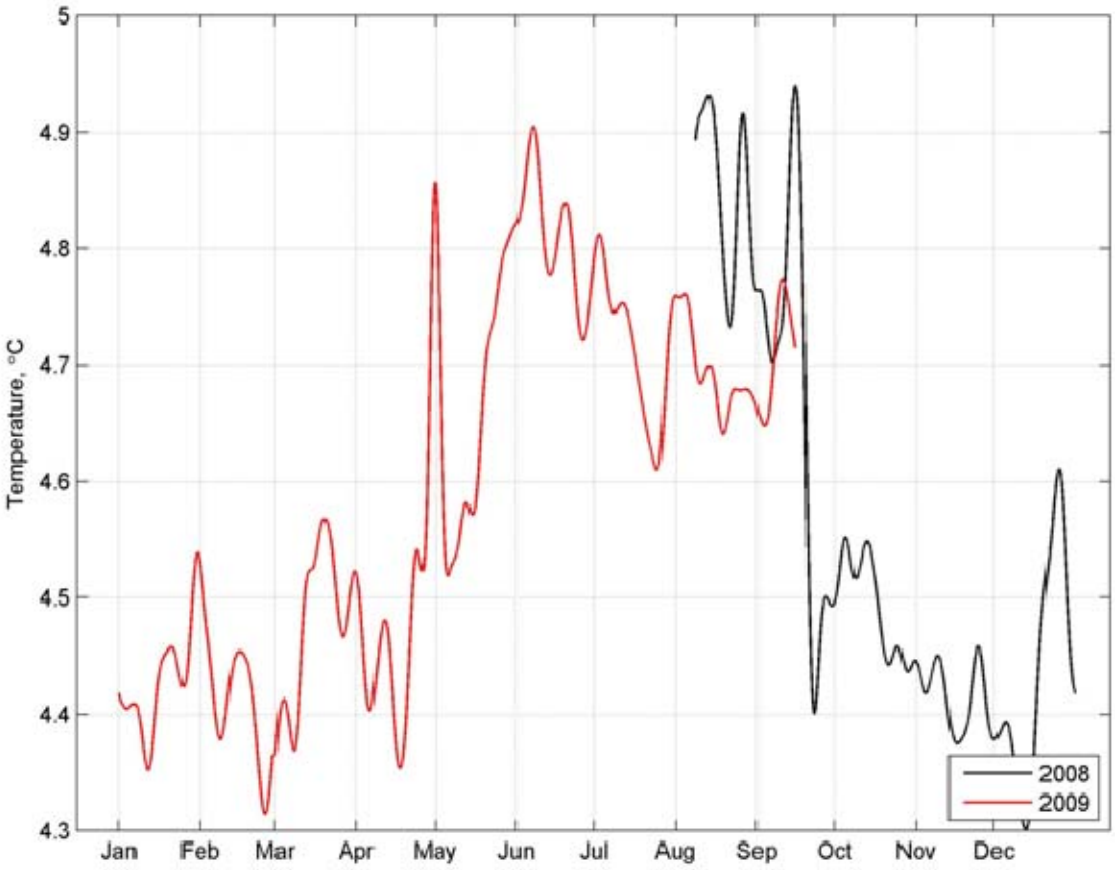

Figure H10. Time series of temperature measurements at 796 m at Sur Ridge. Temperatures were smoothed using a Butterworth filter that cut off periods less than one week.

Deployment Name	Date of Deployment	Latitude	Longitude	Current Meter Depth (m)	Bottom Depth (m)	Compass Correction (E)	Timing Error
Sur Ridge Harp 5	01 Aug 08-30 Jan 09	36° 23.427'N	122° 18.351'W	786	837	1'	2' 25"
Harp 6	30 January 2009 – 30 April 2009	36° 23.332'N	122° 18.396'W	793	836	0'	0' 14"
Harp 7	30 April 2009 – 22 September 2009	36° 23.336'N	122° 18.409'W	787	828	1'	1' 50"

Table H1. Sur Ridge RCM 8 Deployment Data. The sampling rate was 30 minutes for all three deployments.

APPENDIX I PT SUR SOSUS

This appendix covers the series of deployments at Pt. Sur SOSUS (Fig. I1) deployed from 03 October 2006 to 02 August 2008 at a mean depth of 1368 m. Table I1 contains specific information about this deployment. The sampling rate for the RCM 8 device for all four deployments was 30 minutes. For the first deployment the RCM 8 failed to collect any data after 07 December 2006.

The mean speed was 11.02 cm/s. Direction and speed of vector mean flow was 348.4°T and 1.1 cm/s, respectively (Fig. I2). The semi-major (minor) axis magnitude was 9.6 cm/s (7.8 cm/s) and the eccentricity of the variance ellipse was 0.43. The semi-major axis was directed along 203.6°T to 023.6°T.

The velocity histogram (Fig. I3, contains information from deployments 1-4) shows one strong mode heading in a direction of 030°T at an approximate speed of 7 cm/s. This mode contained 107 observations per bin. In the opposite heading (210°T) is another mode with 89 observations per bin at a speed of 6 cm/s. At heading 280°T is another small mode with 77 observations per bin at 6 cm/s.

The PVD (Fig. I4) contains information from deployments 2-4. For most of the deployments the current maintains a northwesterly current with few exceptions. This would appear to be at variance with the histogram (Fig. I3), which has the largest mode moving in a northeasterly direction. However, the extra deployment contained in Fig. I3 could explain this discrepancy.

The stick plot (Fig. I5) contains information from deployments 2-4. For most of the deployment the majority of sticks are pointed in a northward direction. The maximum speed was 39.88 cm/s observed on 18 July 2007 and the minimum speed was 0.05 cm/s observed on 20 October 2007 (not displayed).

The kinetic energy spectrum (Fig. I6) shows the semi-diurnal frequency dominating the variance. There is a diurnal peak at frequency 0.041 cph with a period of 24.4 hours, and the semi-diurnal peak is at a frequency of 0.08 cph with a period of 12.5 hours.

The rotary spectra (Fig. I7) display the clockwise component dominating the counterclockwise component during the diurnal and semi-diurnal frequencies. The rotary coefficient is 0.84 at the semi-diurnal frequency, the highest peak for the rotary coefficient, and at the diurnal peak the rotary coefficient is 0.25. All this demonstrates the anti-cyclonic nature of the currents at the Pt. Sur SOSUS.

The temperature histogram (Fig. I8) used 0.05°C and the median temperature was 3.04°C with a mean temperature of 3.05°C. The time series displays the temperature over time. The highest peak was observed on 28 June 2008 at a temperature of 3.34°C, while the minimum observed was on 27 March 2007 at a temperature of 2.8°C.

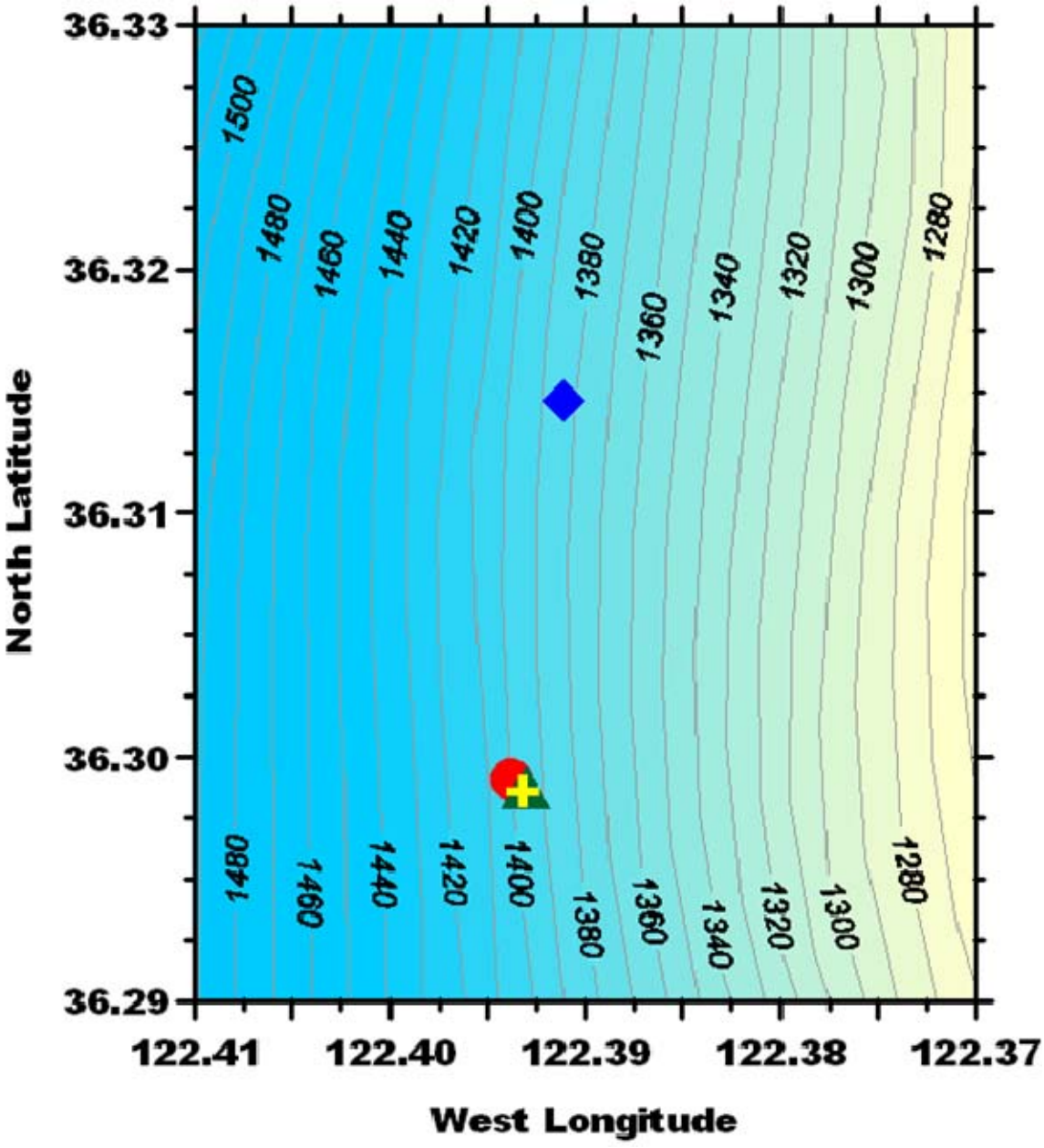

Figure I1. Mooring locations for Pt. Sur SOSUS deployments. Soundings are in meters and the contour interval is 10 m.

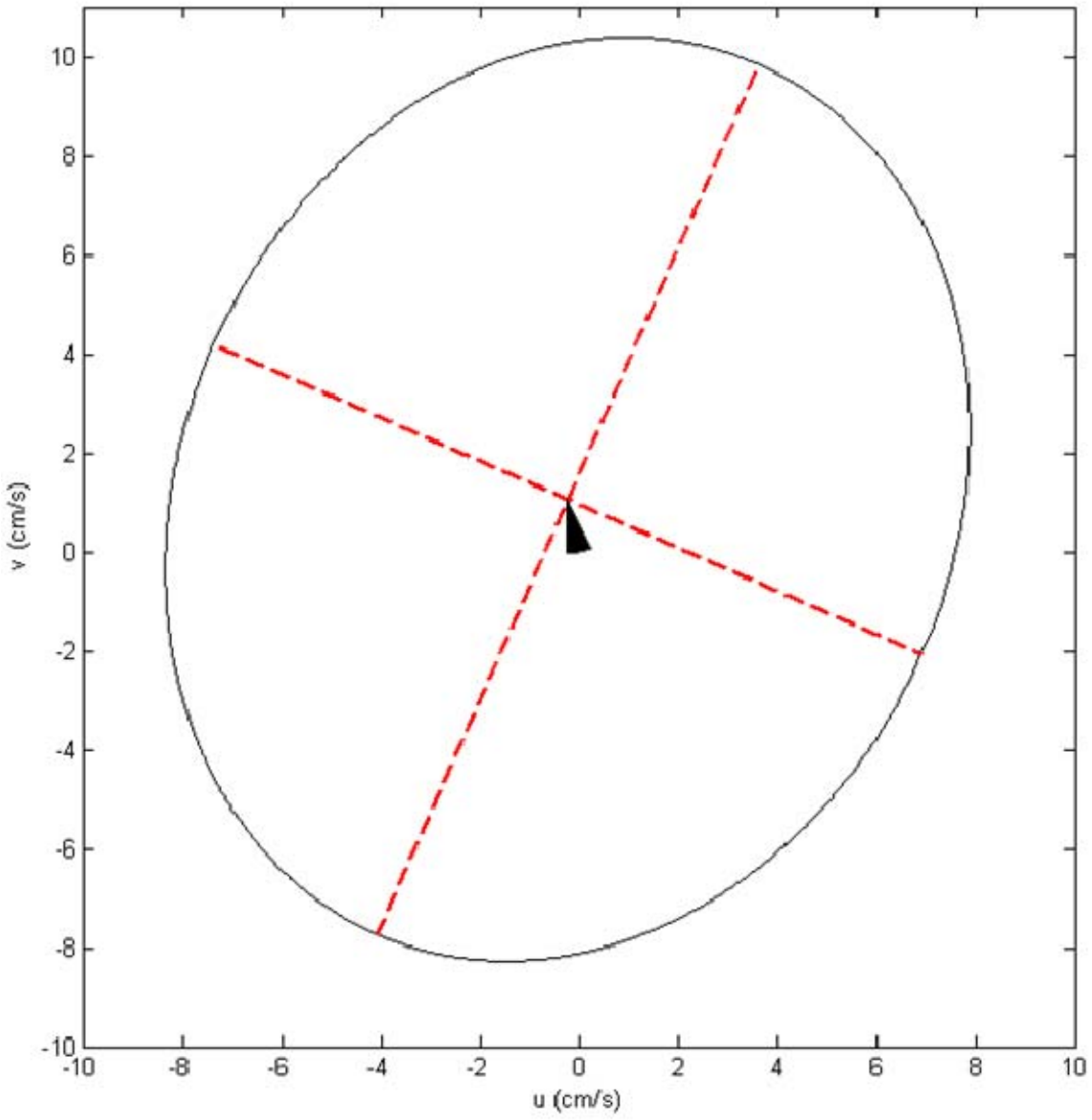

Figure I2. Mean and standard deviation of currents measured over all four Pt. Sur SOSUS deployments. Mean speed (direction) of the mean vector flow was 1.1 cm/s (348.1°T). The semi-major (semi-minor) axis was 9.6 cm/s (7.8 cm/s) and was oriented along 203.6°-023.6°T.

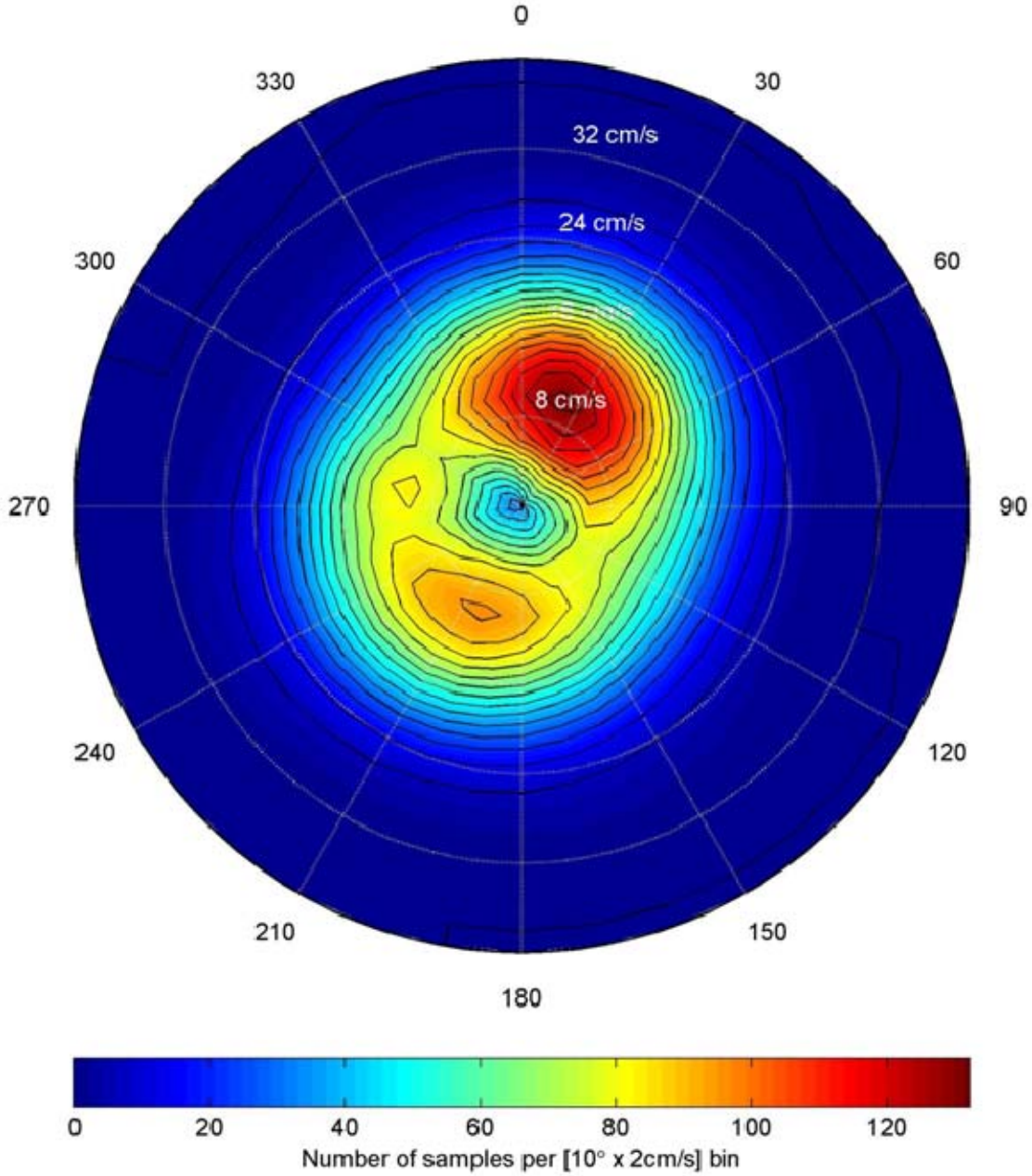

Figure I3. Histogram of velocity observations at the Pt. Sur SOSUS deployments (1-4). The total number of observations is 29,741. 898 observations with a speed less than 1 cm/s were omitted. Total number of bins is 777.

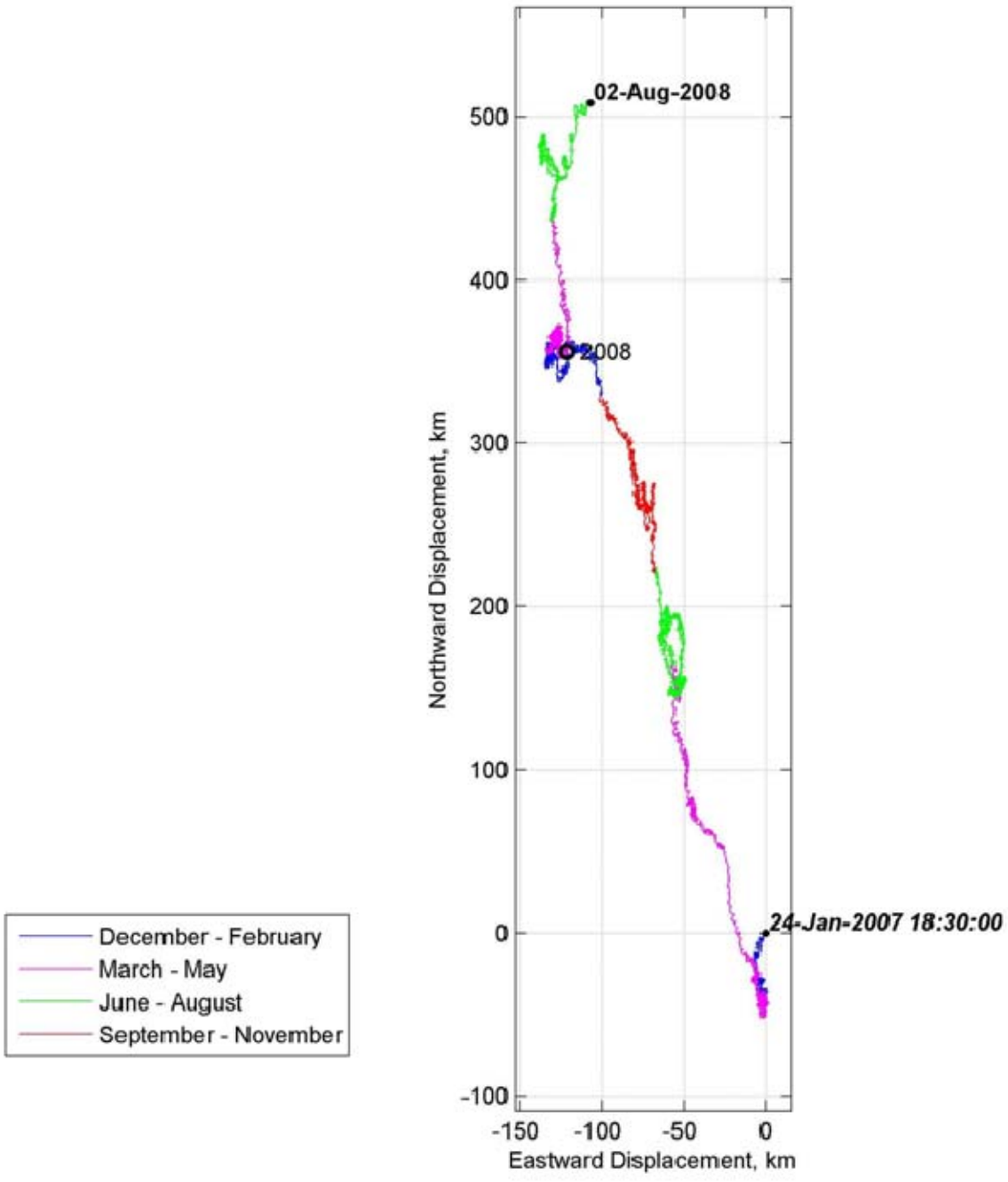

Figure I4. Progressive vector diagram for currents at the Pt. Sur SOSUS (2-4).

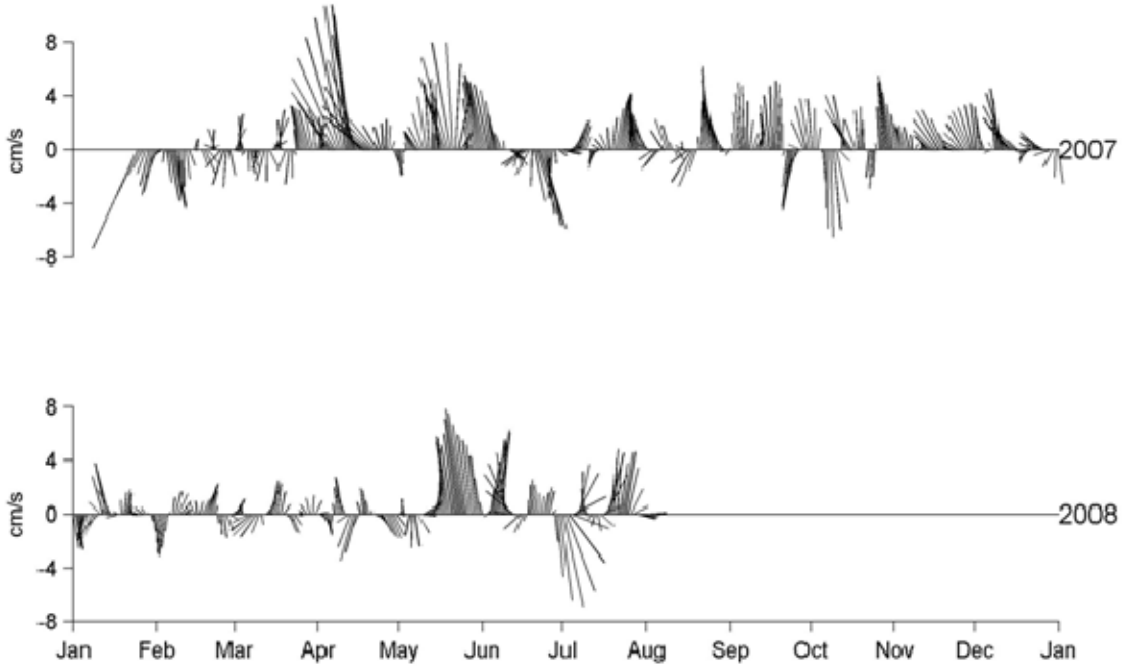

Figure I5. Current velocity at Pt. Sur SOSUS as a function of time. Currents were smoothed using a Butterworth filter with a cutoff period of one week.

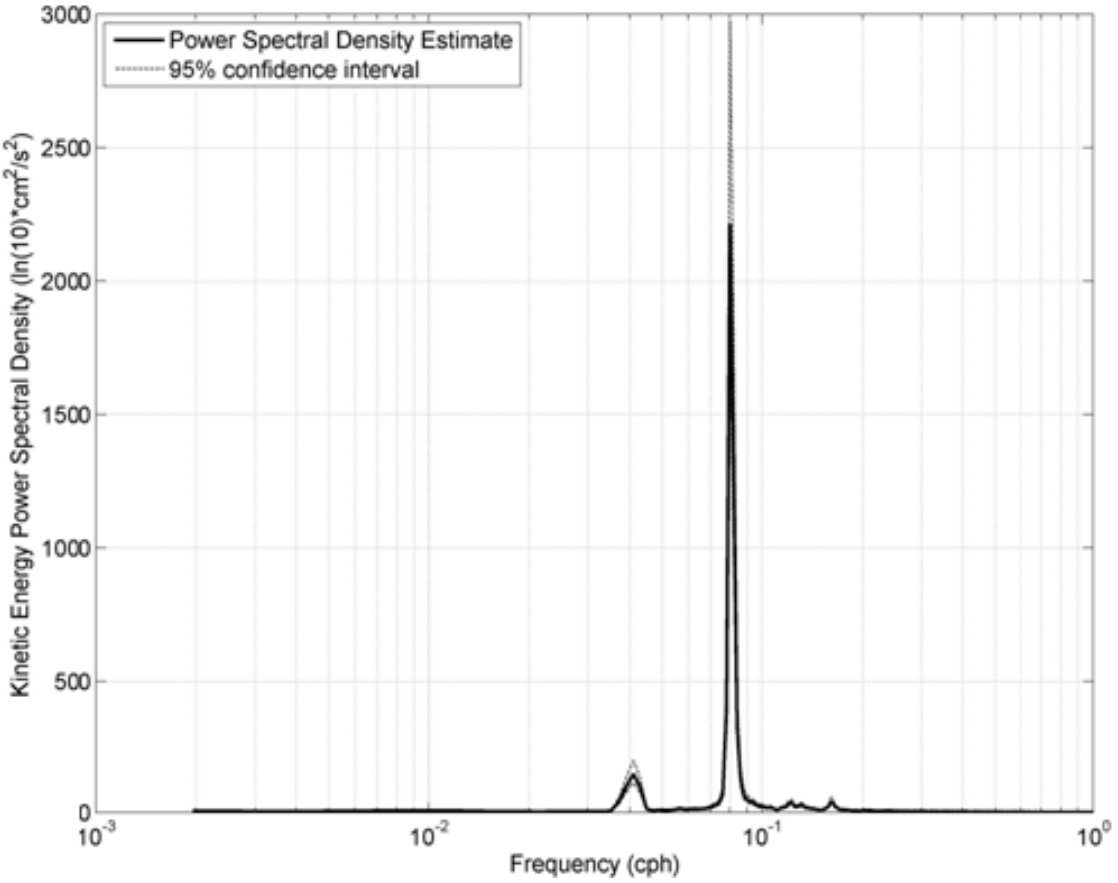

Figure I6. Kinetic energy spectrum for currents at Pt. Sur SOSUS (deployments 2-4). Semi-diurnal peak at 0.08 cph with diurnal peak at 0.041 cph.

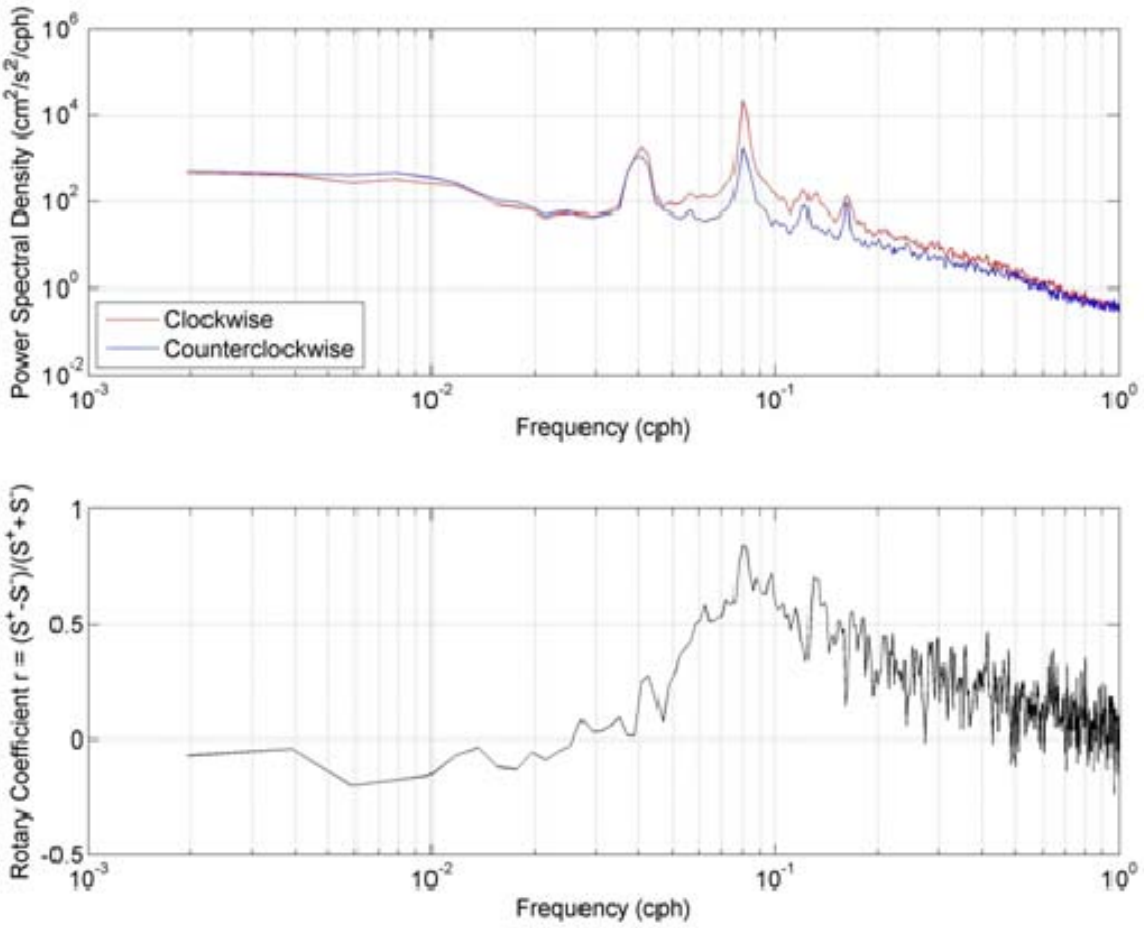

Figure I7. (upper) Rotary spectra for Pt. Sur SOSUS deployments 2-4. (lower) Rotary coefficient for Pt. Sur SOSUS deployment 2-4.

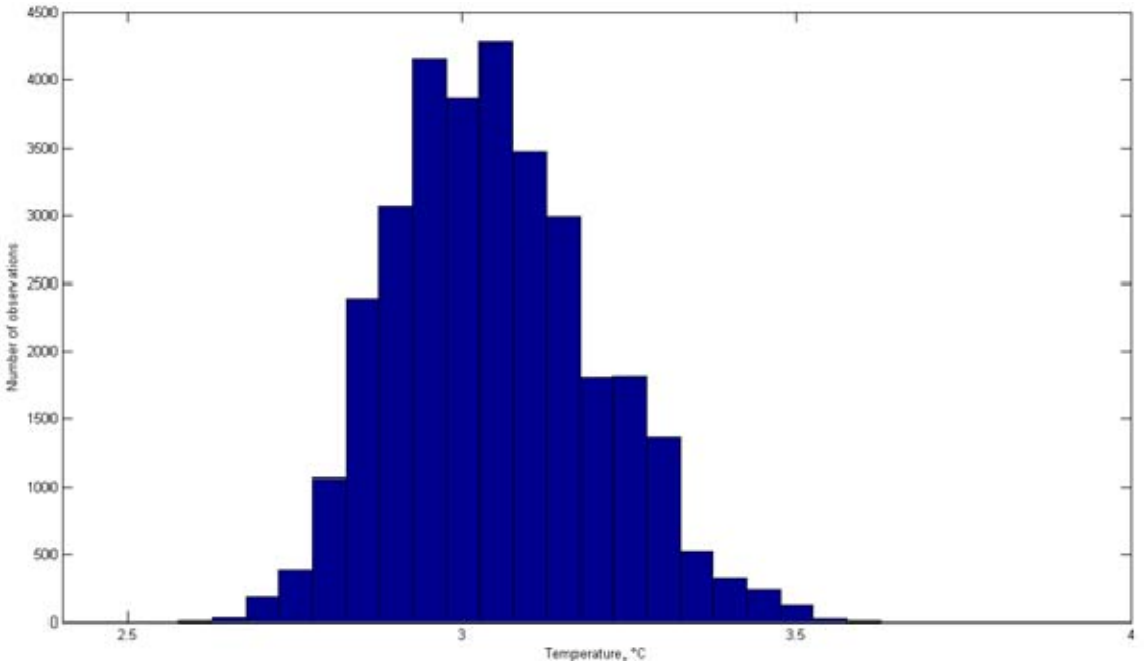

Figure I8. Temperature histogram of currents at Pt. Sur SOSUS (1-4) using a bin size of 0.05°C.

Figure I9. Temperature time series of currents at Pt. Sur SOSUS deployments 1-4. Temperatures were smoothed using a Butterworth filter that cut off periods less than one week.

Deployment Name	Date of Deployment	Latitude	Longitude	Instrument Depth (m)	Bottom Depth (m)	Compass Correction (E)	Timing Error
1	03 October 2006 – 24 January 2007	36° 17.946'N	122° 23.628'W	1378	1402	0’	2’38”
2	24 January 2007 – 17 July 2007	36° 17.924'N	122° 23.583'W	1376	1400	0’	2’15”
3	18 July 2007 – 24 January 2008	36° 17.918'N	122° 23.595'W	1372	1396	0’	1’30”
4	24 January 2008 – 02 August 2008	36° 18.876'N	122° 23.465'W	1345	1386	1’	4’40”

Table I1. Pt. Sur SOSUS mooring deployment data. The sampling rate for the RCM 8 device for all deployments was 30 minutes.

APPENDIX J DAVIDSON SEAMOUNT

This appendix describes data from the mooring deployed at Davidson Seamount (Fig. J1) from 30 July 1998 to 06 February 2000. The mooring utilized the RCM 8 and SEACAT 16 for oceanographic measurements with respective instrument depths of 1235 m and 1236 m (Fig. J2). The respective instrument height above the bottom was 55 m and 54 m. Table J1 contains specific information about these instruments and the mooring. The sampling rate for the RCM 8 current meter was twenty minutes and for the SBE SEACAT 16 was a half hour.

Southward flow dominated the currents at the Davidson Seamount. The mean speed was 8.2 cm/s. The direction and speed of the vector mean flow was 196.4°T and 2.0 cm/s, respectively (Fig. J3). The variance ellipse displays the standard deviation along the principal axis of variation. The semi-major (minor) axis magnitude was 8.2 cm/s (5.4 cm/s) and the eccentricity of the variance ellipse was 0.58. The semi-major axis was directed along 323°T to 143°T.

The velocity histogram (Fig. J4) showed the principal mode contained 105 observations per bin at an approximate heading of 180°T and a median speed of 10.0 cm/s. There was a secondary mode on a median heading of 160°T at a speed of 4.0 cm/s with 113 observations per bin.

The PVD (Fig. J5) confirmed the persistence of southward flow in all seasons except winter. Seasonal southward displacements were largest for fall. Net winter flow was westward in 1999 and northeastward in 2000. From deployment in 1998 through January 1999, the southward flow had a westward component; in summer and fall 1999 the southward flow had an eastward component.

For 1998, the stick plot showed a trend of acceleration of the southwestward currents from 2 cm/s after deployment to 5 cm/s in December (Fig. J6). In 1999, flow reversals occurred at 2- to 10-week intervals; the strength of the northward (southward) flows decreased (increased) through the year, with largest magnitude, about 12 cm/s, in December. The maximum speed observed was 30.79 cm/s on 17 May 1999 (not shown).

Semi-diurnal tidal energy (0.082 cph) completely dominated the kinetic energy spectrum (Fig. J7). Smaller but statistically significant spectral peaks occurred at the diurnal frequency (0.041 cph), the local inertial frequency (0.0498 cph with a period of 20 hours), and over tides at 0.123, 0.1611, and 0.2432 cph. The rotary spectra and coefficient (Fig. J8) indicated that clockwise motion dominated motions from frequencies 0.035 to 0.33 cph. The largest rotary coefficient, 0.89, occurred at the local inertial frequency, but was almost as large at the semi-diurnal frequency.

Since this mooring also included a SEACAT 16, both temperature and salinity data were available. The temperature histogram (Fig. J9) and time series (Fig. J10) were taken from RCM 8 measurements. The temperature histogram used bin sizes of 0.023°C, and the median and mean temperature were 3.21°C and 3.22°C, respectively. The temperature time series shows a number of about 0.05°C oscillations superimposed upon a seasonal warming pattern; the latter had winter minimums and warmest temperatures in October. The warmest temperature, 3.32°C, was observed on 05 October 1999, while the minimum, 3.12°C, occurred on 07 January 1999.

The mean salinity was 34.51, with a maximum salinity occurring on 25 December 1999 at 34.52 and minimum occurring on 26 October 1999 at 34.5 (Fig. J11 and J12). Figure J13 displays the bi-variate histogram of temperature vs. salinity and displays the density contour lines. The density contour lines show the *in situ* value of density, or what is normally referred to as $\sigma_{s,t,p}$. What is interesting to note is the trend of decreasing salinity and a small decrease in density with an increasing temperature. A good number of observations show that the density fluctuated more with increasing temperature than with any changes in salinity.

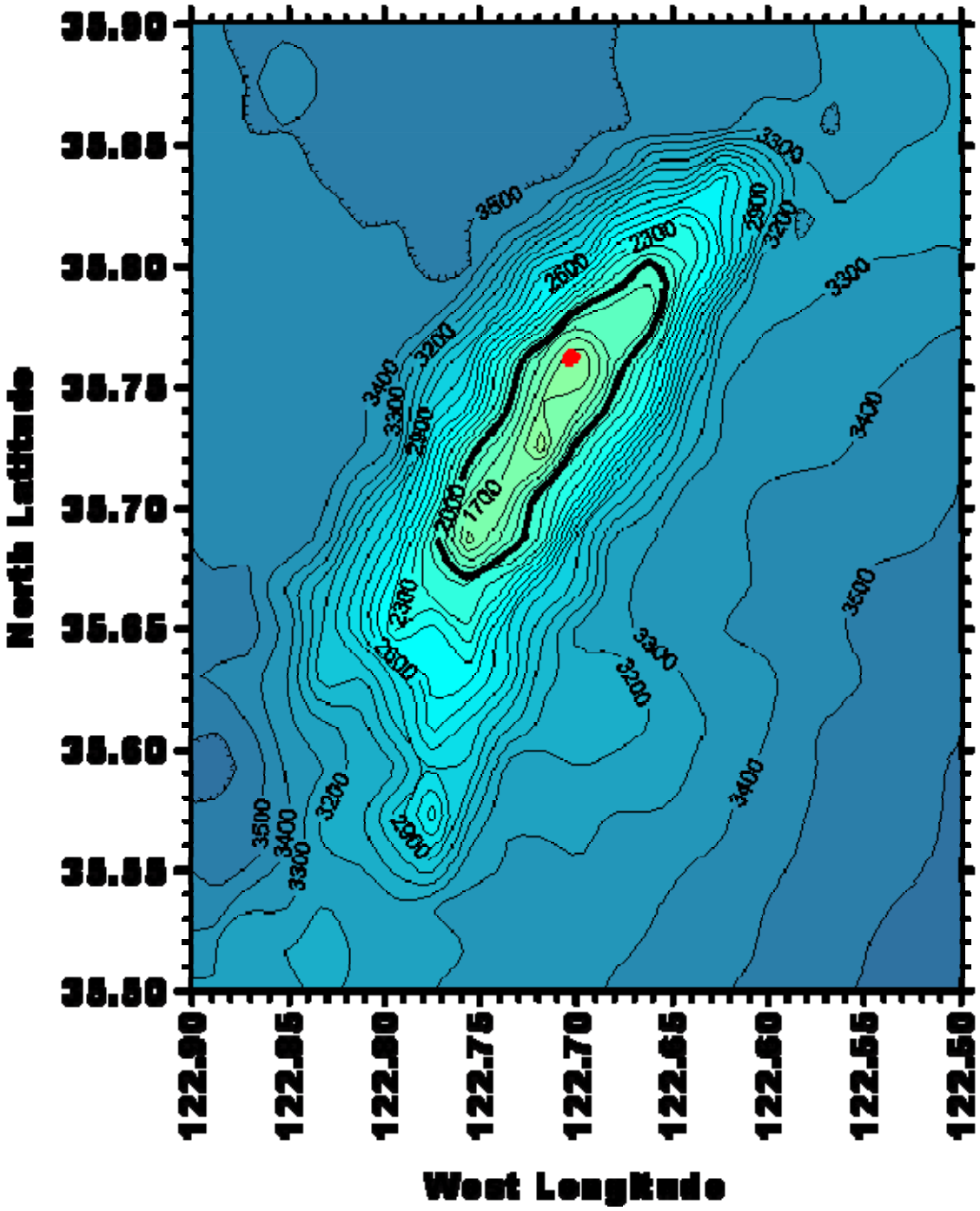

Figure J1. Davidson Seamount mooring location. Soundings are in meters and the contour interval is 100 m.

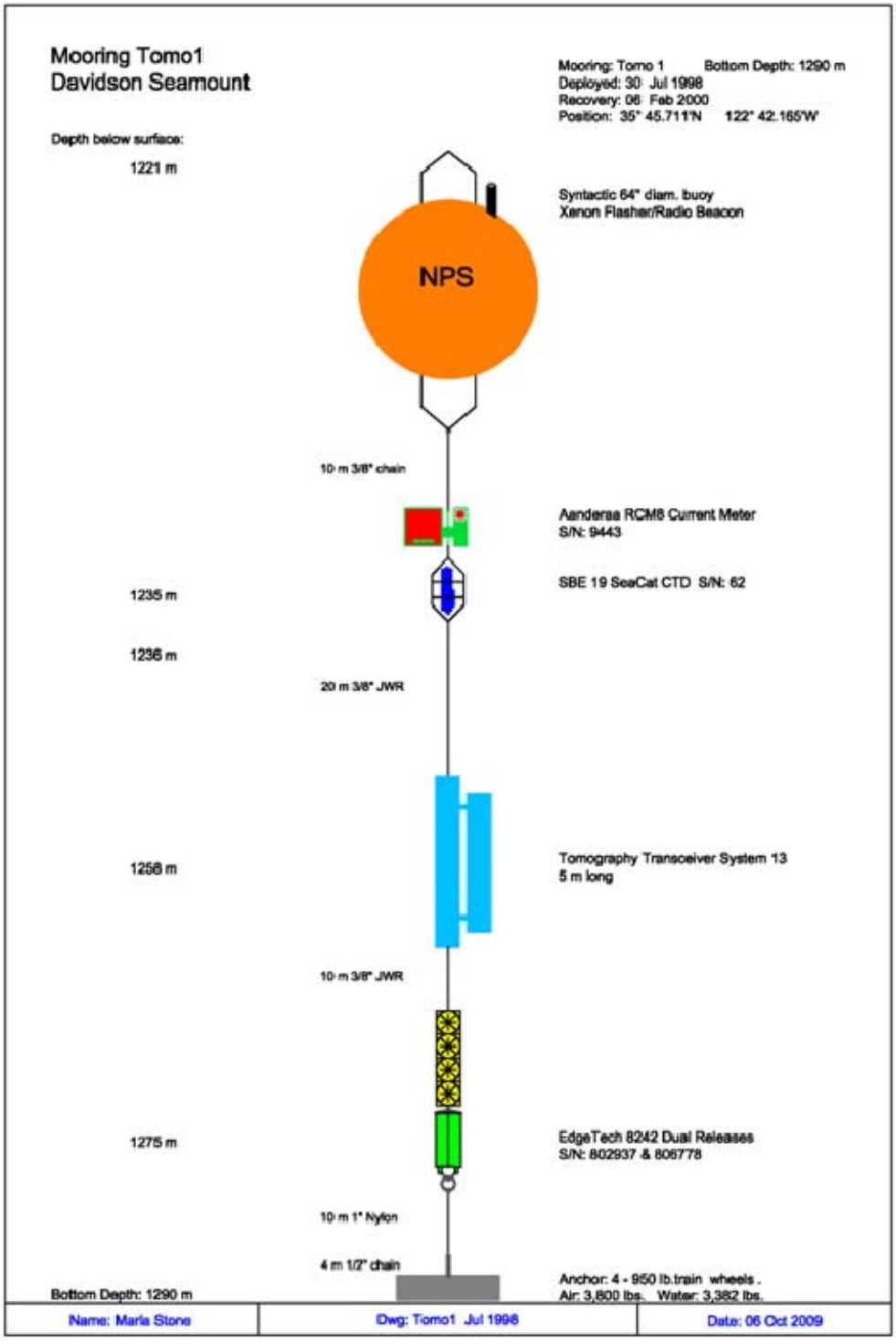

Figure J2. Schematic diagram of the intermediate mooring used at Davidson Seamount.

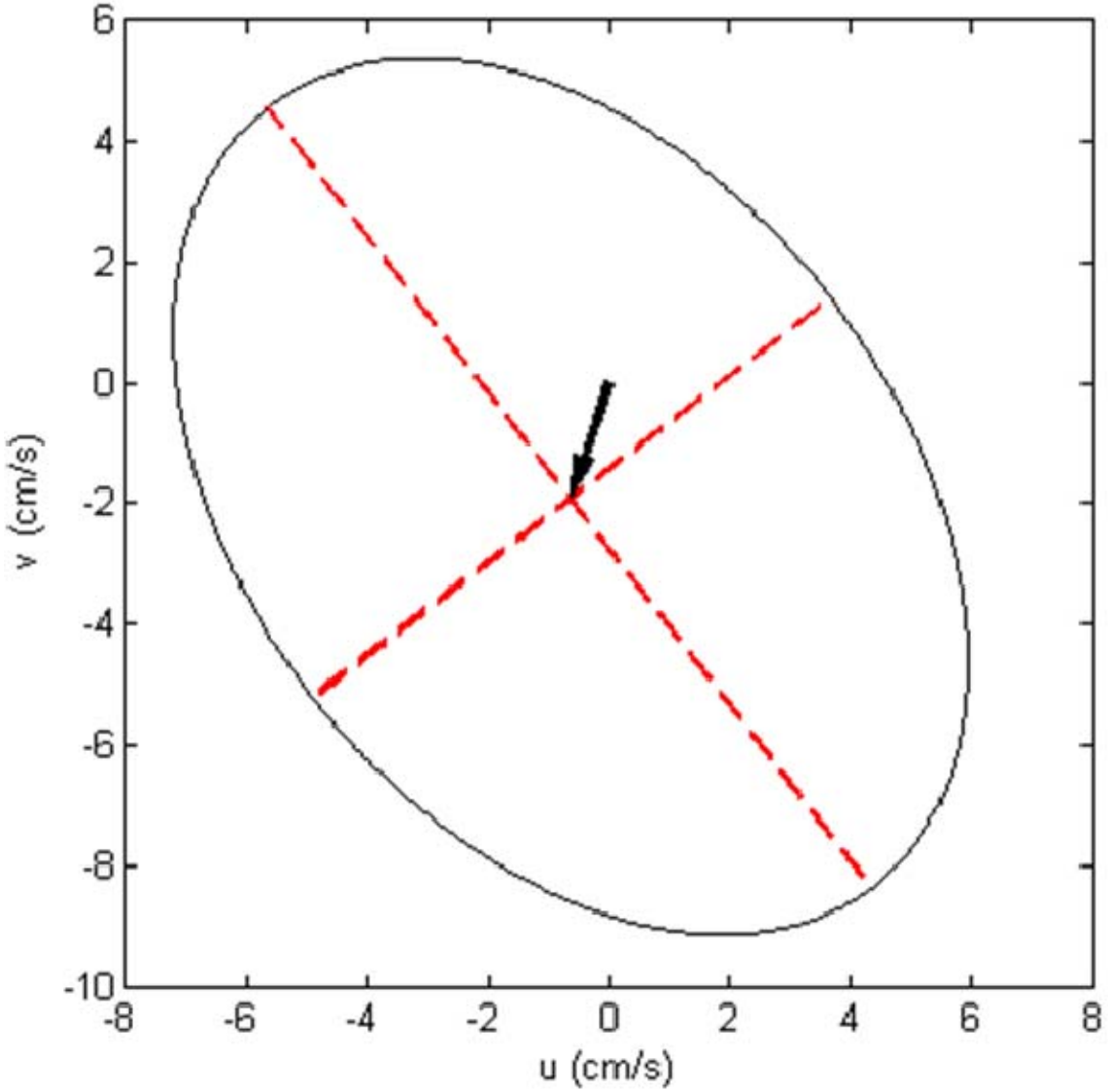

Figure J3. Mean and standard deviation of currents measured at 1235 m over Davidson Seamount. Mean speed (direction) of the mean vector flow was 2 cm/s (196.4°T). The semi-major (semi-minor) axis was 8.2 cm/s (5.4 cm/s) and was oriented along 322.7°-142.7°T.

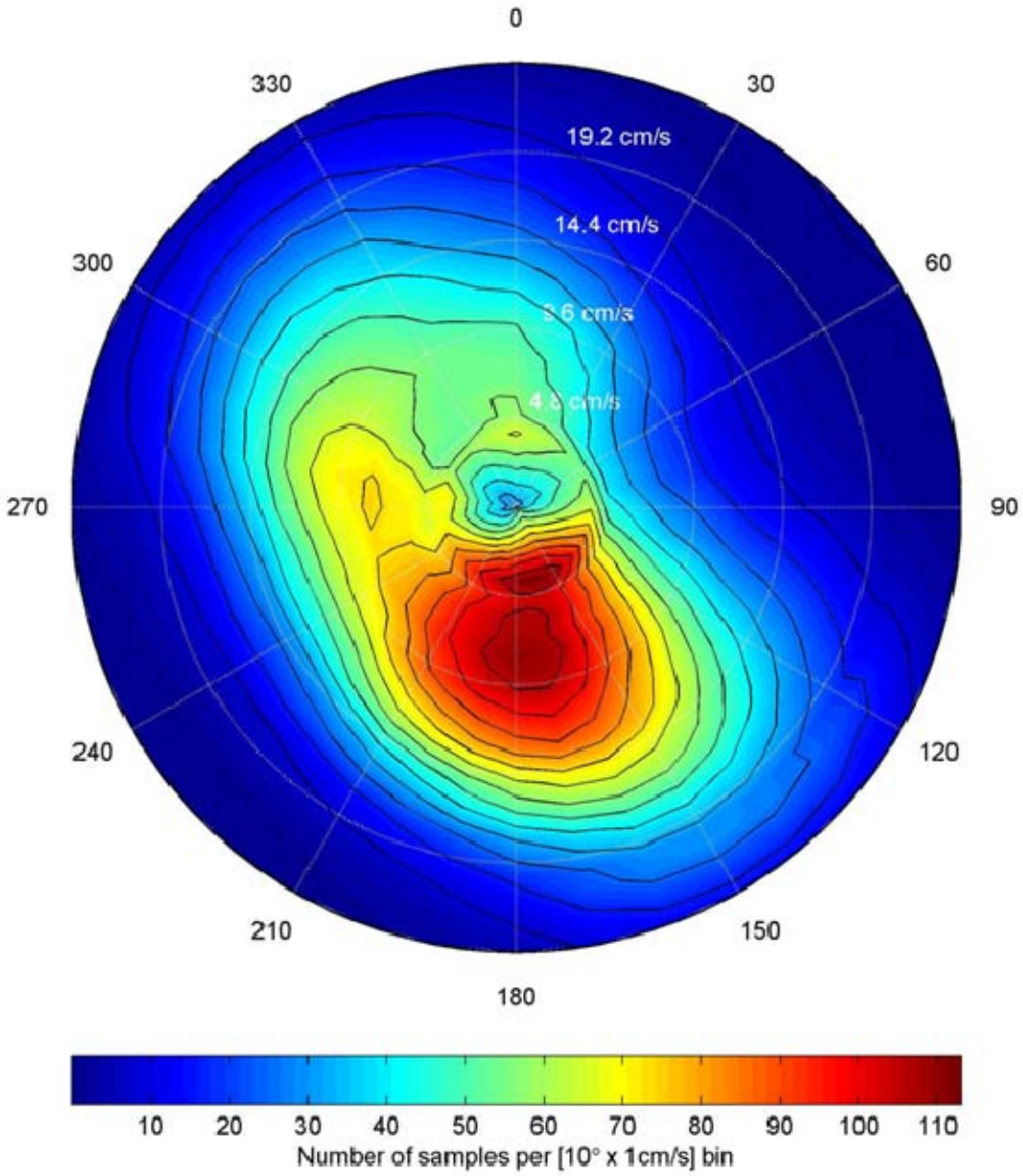

Figure J4. Histogram of velocity observations at 1235 m depth over Davidson Seamount. The total number of 20 minute observations was 40,043 but 3324 observations with a speed less than 1 cm/s were omitted. The total number of bins is 925.

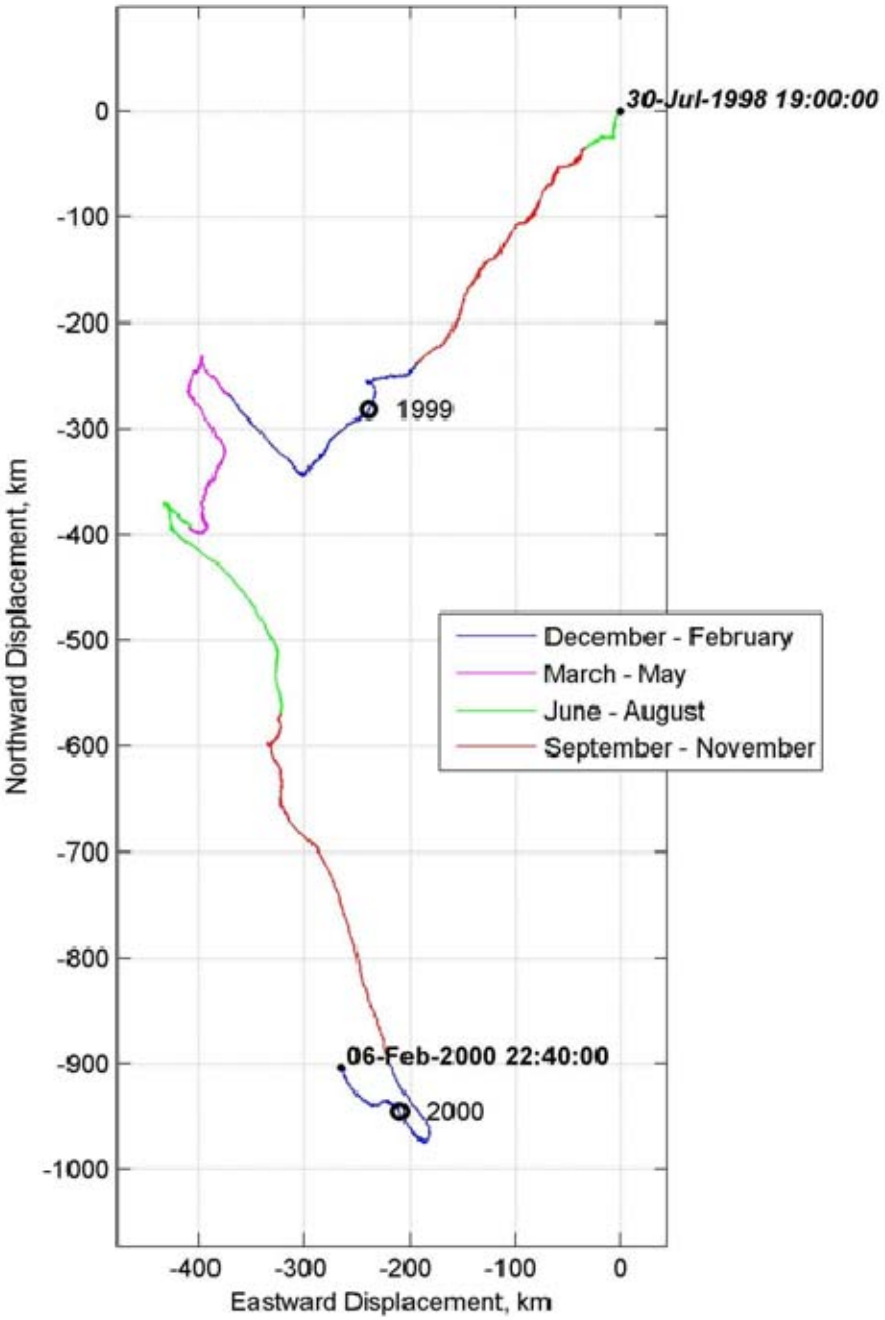

Figure J5. Progressive vector diagram for currents at 1235 m over Davidson Seamount.

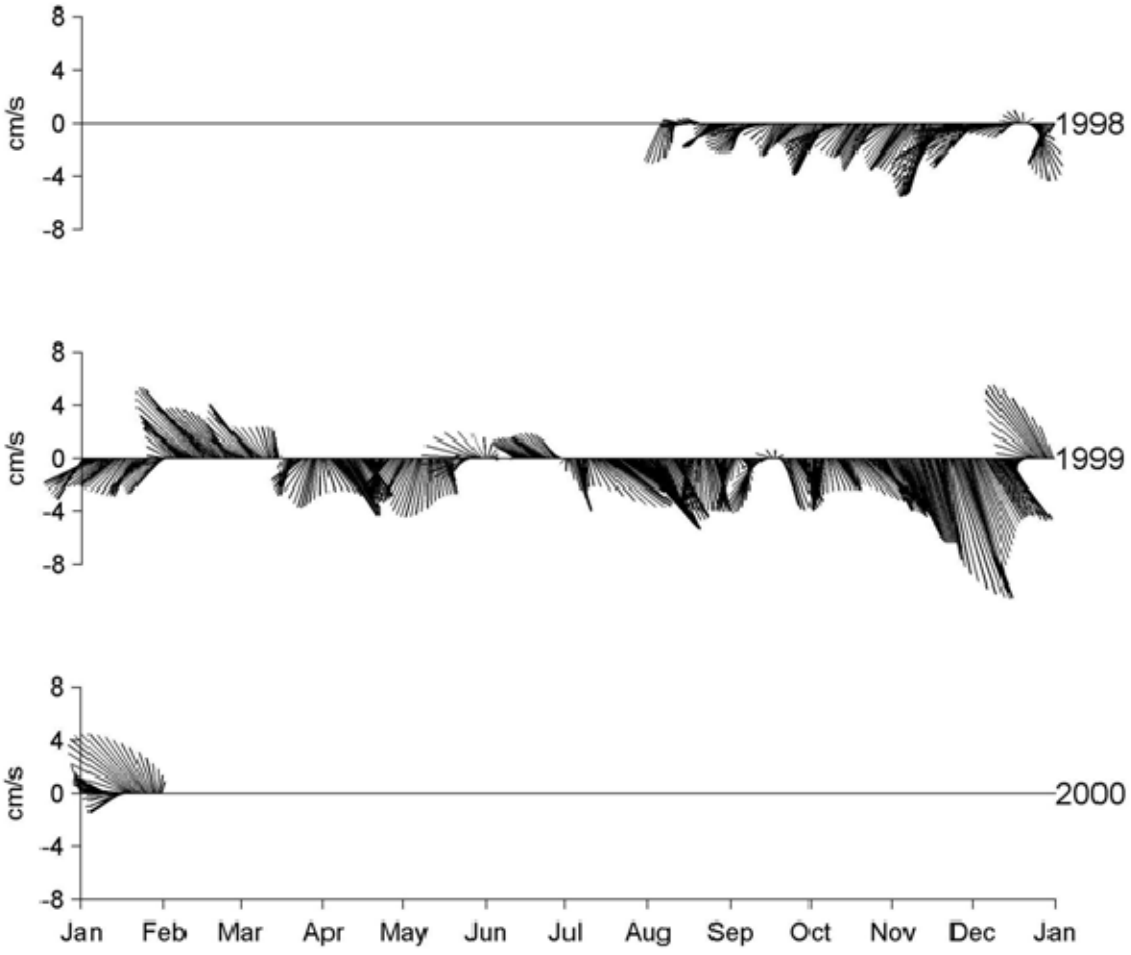

Figure J6. Current velocity at a depth of 1235 m over Davidson Seamount as a function of time. Currents were smoothed using a Butterworth filter with a cutoff period of one week.

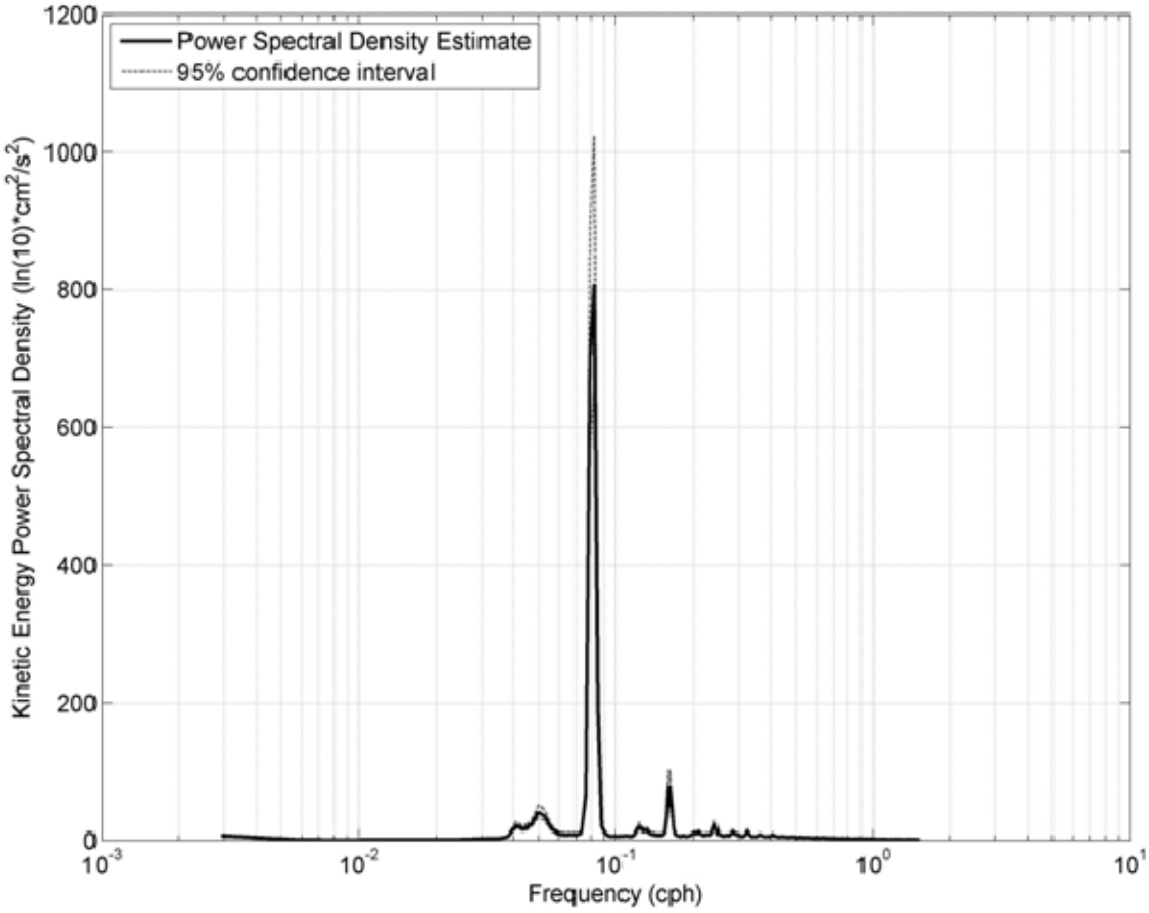

Figure J7. Kinetic energy spectrum for currents at 1235 m over Davidson Seamount. Inertial peak at 0.0498 cph, semi-diurnal peak at 0.082 cph, with smaller peaks at 0.123, 0.161, and 0.2432 cph.

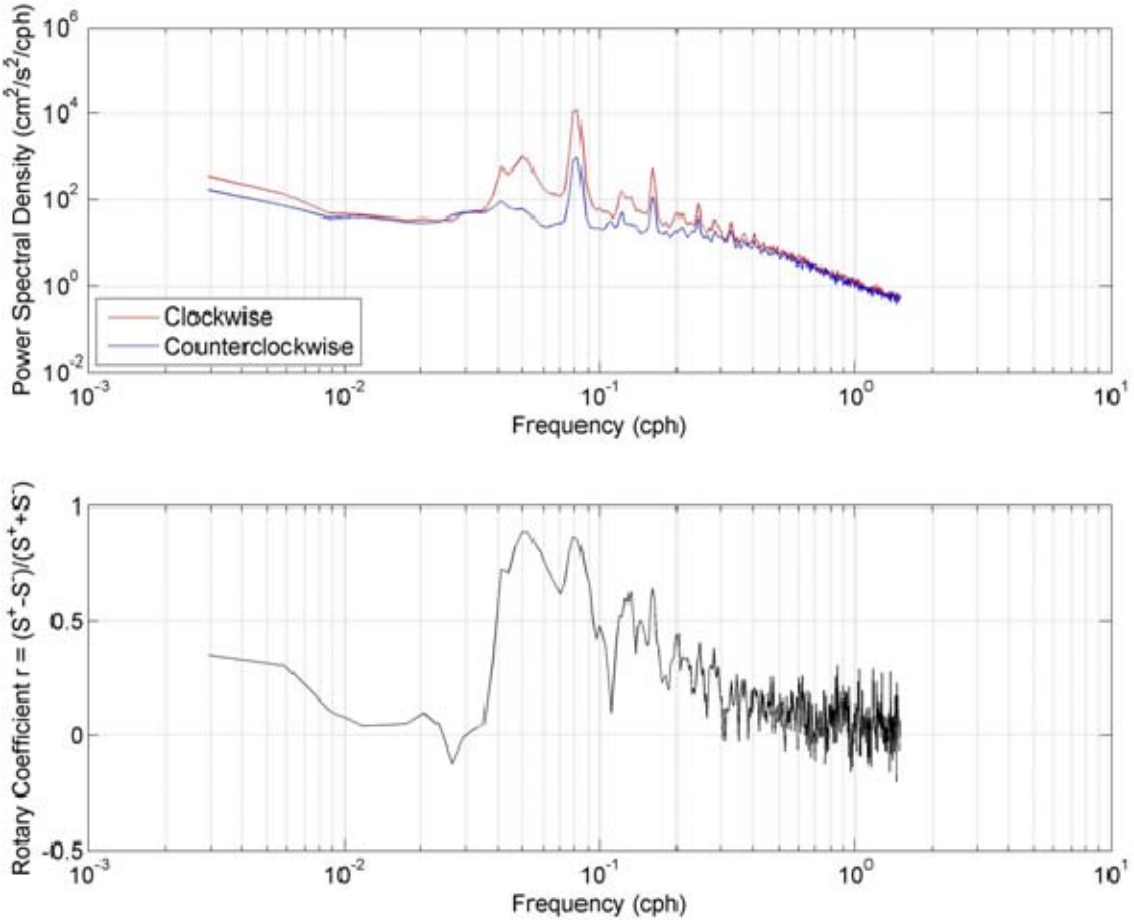

Figure J8. (upper) Rotary spectra for Davidson Seamount currents at 1235 m. (lower) Rotary coefficient for Davidson Seamount currents.

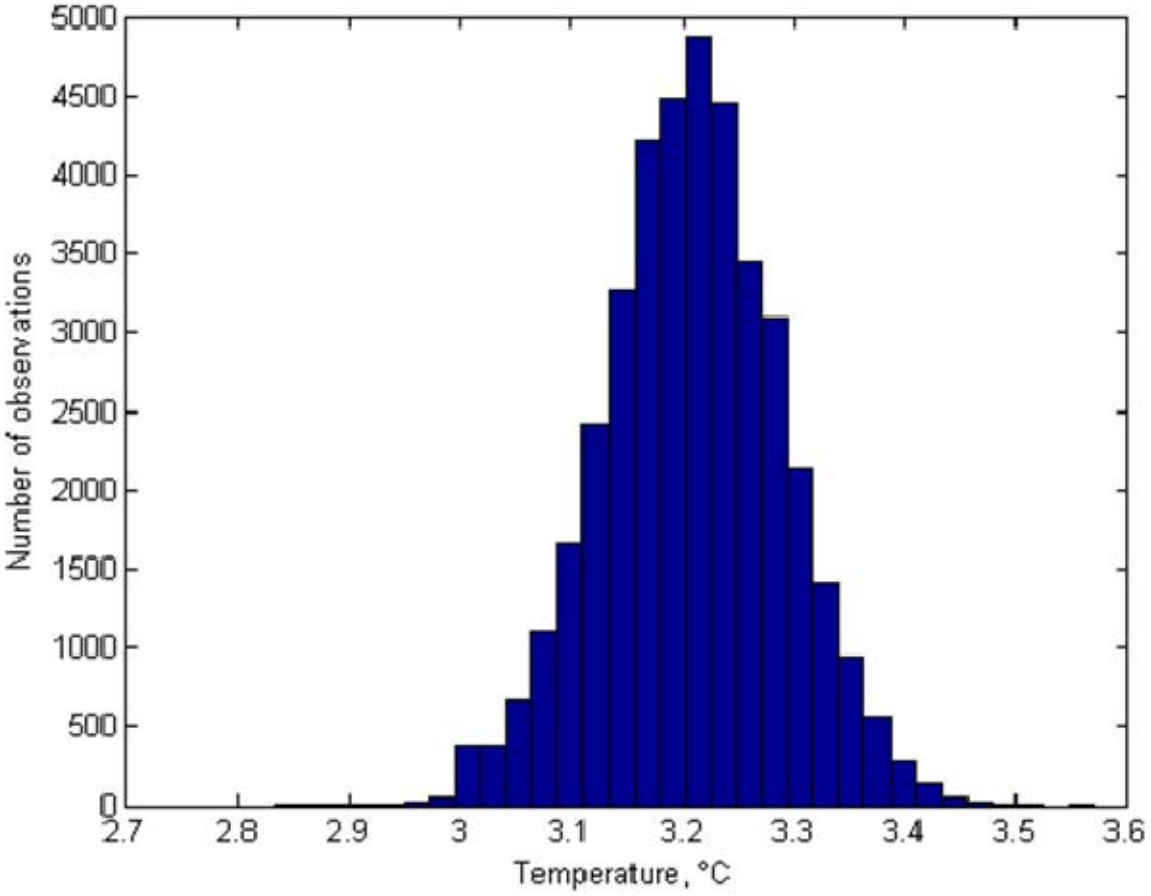

Figure J9. Temperature histogram at 1235 m over Davidson Seamount using a bin size of 0.023°C.

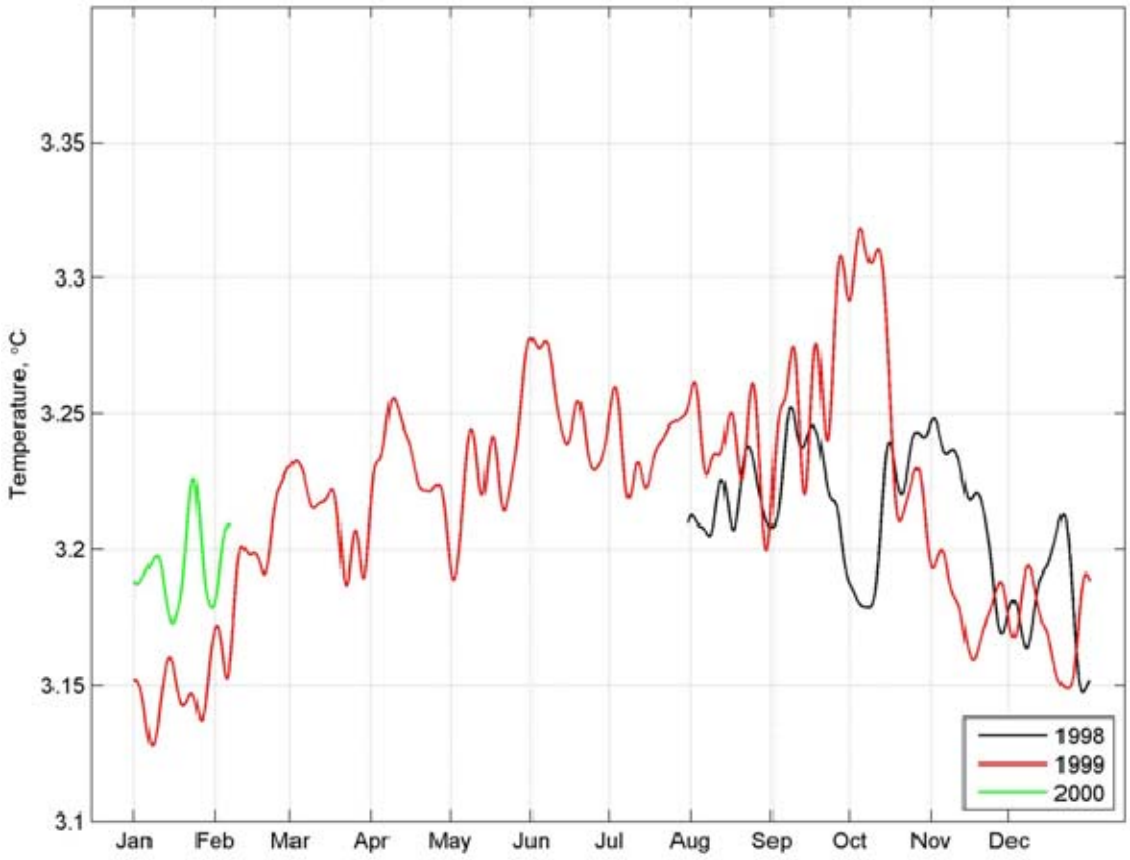

Figure J10. Temperature time series at 1235 m over Davidson Seamount. Temperatures were smoothed using a Butterworth filter that cut off periods less than one week.

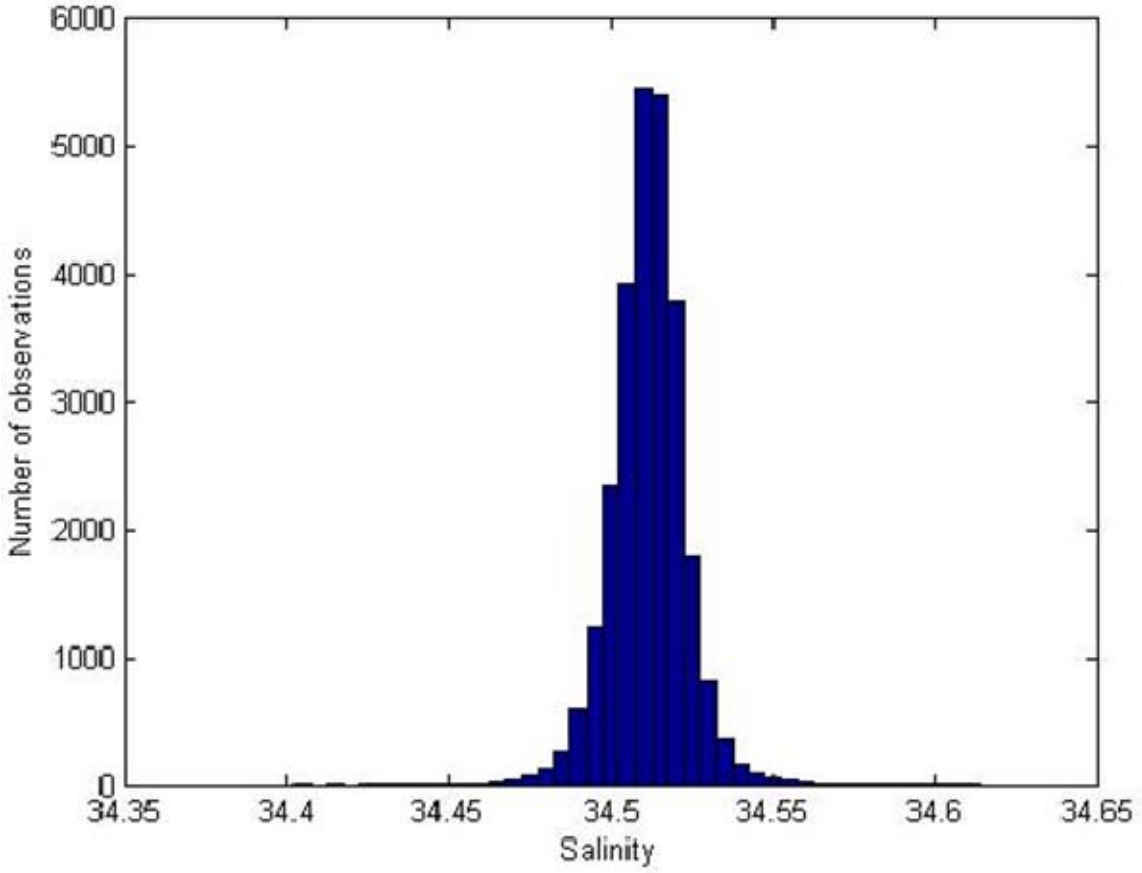

Figure J11. Salinity histogram at 1235 m depth over Davidson Seamount using a bin size of 0.005°C.

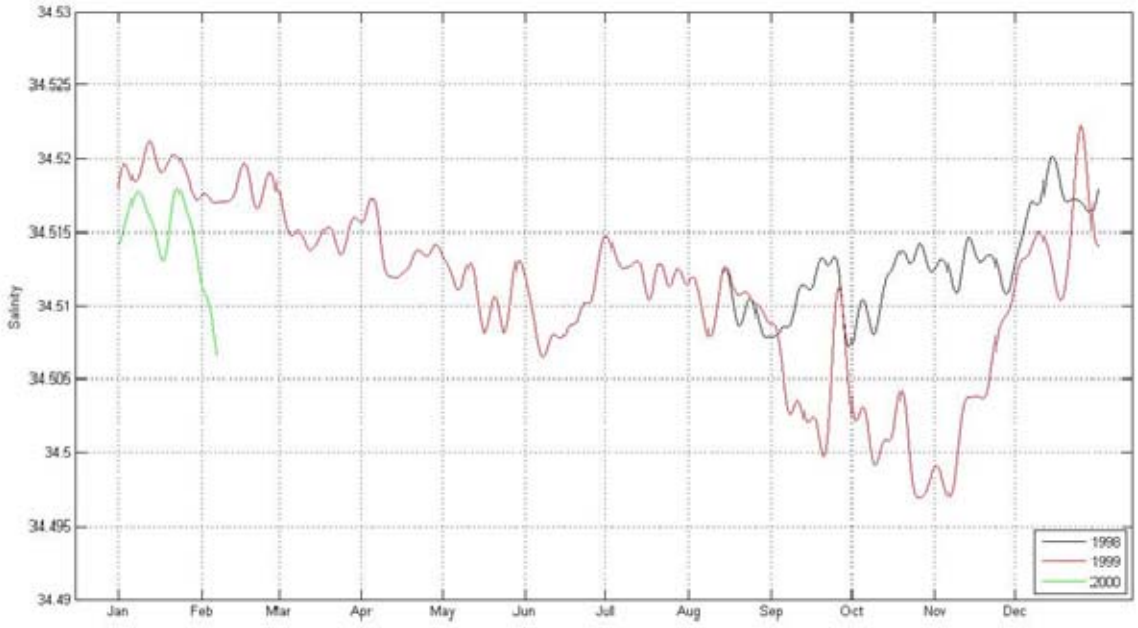

Figure J12. Salinity time series at 1236 m over Davidson Seamount. Salinities were smoothed using a Butterworth filter that cut off periods less than one week.

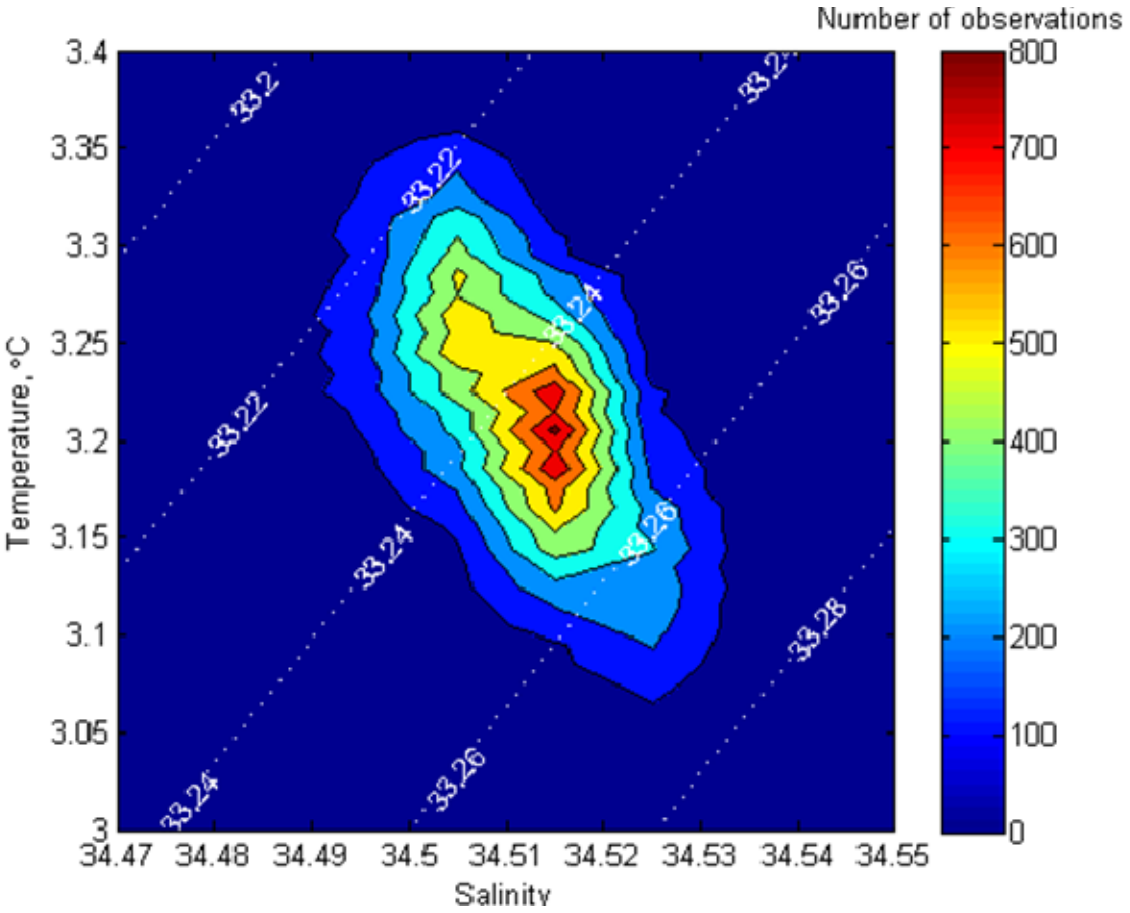

Figure J13. Temperature vs Salinity bi-variate histogram at 1235 m depth over Davidson Seamount. The density contour lines represent the *in situ* value of density.

Deployment Name	Date of Deployment	Latitude	Longitude	Instrument Depth RCM8/SEACAT 16 (m)	Bottom Depth (m)	Compass Correction (E)	Timing Error RCM8/SEACAT 16
Davidson Seamount	30 July 98-06 Feb 00	35° 45.711'N	122° 42.165'W	1235/1236	1290	8'	2' 10"/11' 25"

Table J1. Davidson Seamount Deployment Data. An RCM 8 device and SBE SEACAT 16 device were utilized for measurements in this deployment. The sampling rate was twenty and thirty minutes for the RCM 8 and SBE SEACAT 16 device, respectively.

THIS PAGE INTENTIONALLY LEFT BLANK

APPENDIX K SANTA ROSA GAP

This appendix describes measurements from a current meter mooring deployed from 10 August 2004 to 3 October 2004 near the sill of a gap at the northern end of Santa Rosa Cortez Ridge (Fig. K1). The intermediate mooring at Santa Rosa Gap was moored with a bottom depth of 359 m with the current meter at a depth of 337 m, about 22 meters above the bottom. Figure K2 shows the specifications of this mooring. Table K1 includes details regarding this deployment. Since this was meant to be a short term mooring, the sampling rate for the RCM 8 current meter was 10 minutes.

The mean speed was 24.9 cm/s. Direction and speed of vector mean flow was 250.4°T and 16.9 cm/s, respectively (Fig. K3). The semi-major (minor) axis magnitude was 20.9 cm/s (6.1 cm/s) and the eccentricity of the variance ellipse was 0.84. The semi-major axis was directed along 250.1°T to 070.1°T.

The velocity histogram (Fig. K4) showed the principle mode in a direction of 260°T and speed of 11 cm/s; this bin contained 93 observations. In nearly the opposite direction (070°T), a smaller mode occurred with a few (21) observations for a speed of 21 cm/s. The principle mode and mean indicated the predominance of strong outflow from Santa Rosa Basin into the Pacific Ocean at the bottom of the gap in the ridge.

The PVD (Figure K5) confirms that west-southwestward flow dominated during the deployment period. At the very end of the record, the currents reversed direction and flowed into Santa Rosa Basin. The stick plot (Figure K6) confirmed the fast moving west-southwestward currents observed from the PVD and histogram in August and September. The maximum speed, 54.8 cm/s, occurred on 12 September 2004, and the minimum speed was 0.17 cm/s observed on 8 September 2004.

Diurnal and semi-diurnal tides dominated the kinetic energy spectrum (Figure K7). The calculated local inertial frequency is 0.046 cph with a period of 21.7 hours, but there was no discernible inertial energy. There was also a strong diurnal tidal peak at 0.04 cph. Several smaller peaks at higher frequencies corresponded to overtides at 0.123, 0.164, 0.2, 0.25, and 0.29 cph.

The gap constrained the ability of the tides to freely rotate, so cyclonic and anticyclonic rotary spectra (Figure K8) were nearly not significantly different from one another and the rotary coefficient was close to zero. An exception to this occurred at the semidiurnal frequency, where cyclonic motion was largest and the rotary coefficient was -0.5.

The temperature histogram (Fig. K9) used a bin size of 0.05°C and the median temperature was 7.76°C with a mean temperature of 7.73°C. The shape of the histogram was unusual in that the lower temperature tail (from 6.5°C to 7.0°C) was extensive with a secondary mode while the high temperature tail at 8.5°C consisted of three bins. The smoothed temperature time series (Fig. K10) showed that temperature increased from 13 August 2004 (when it was coldest, 7.43°) to 17 September 2004 (when temperature was warmest, 8.05°C).

The unfiltered data showed that temperatures typically exceeded the limits of the smoothed time series (Fig. K10) during a typical daily tidal cycle. Figure K11 shows the relationship between the observed flow along the gap (along the principal axis shown in Fig. K3) with temperature. The currents were strongly diurnal.

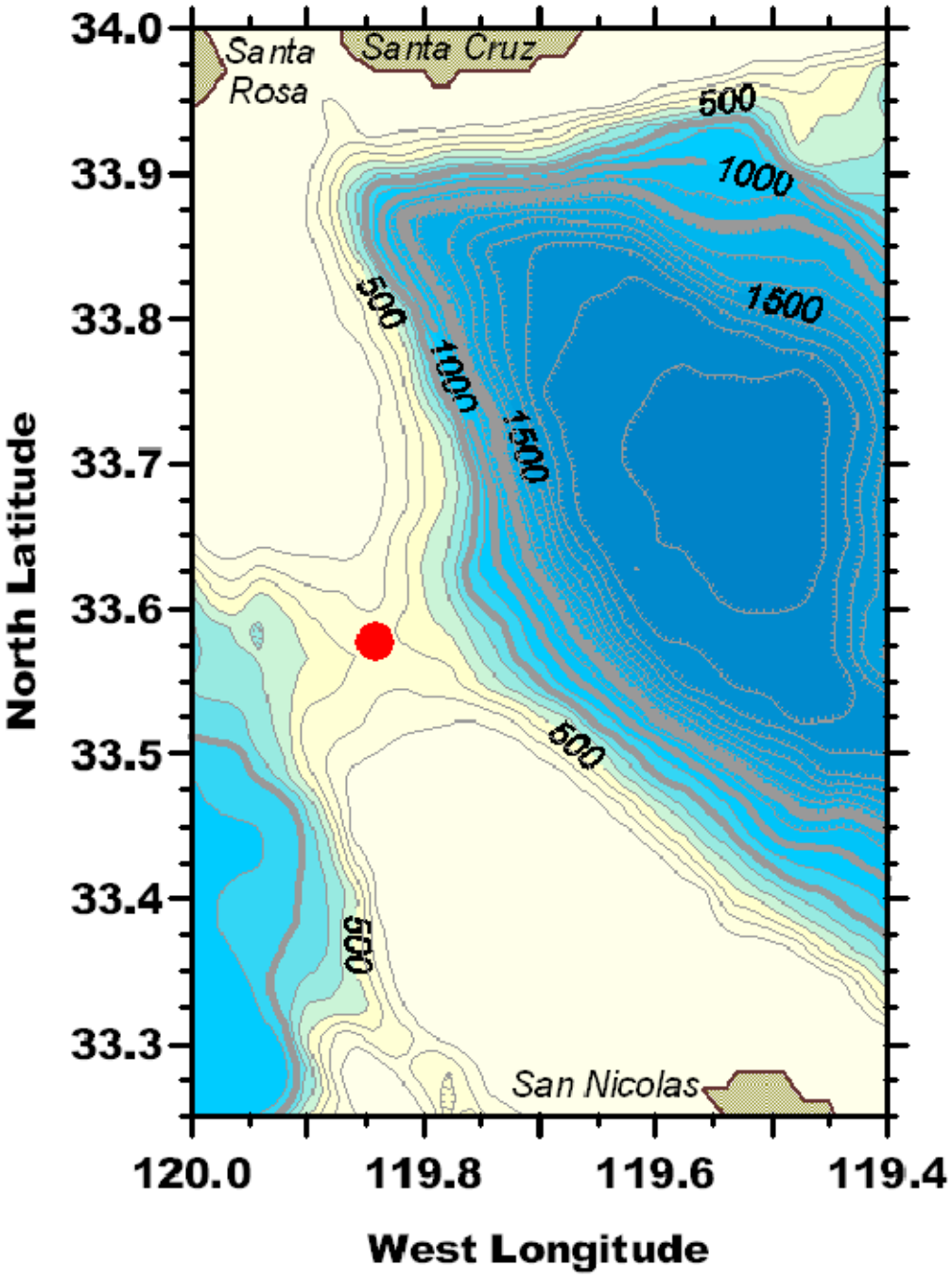

Figure K1. Mooring location for Santa Rosa Gap. Soundings are in meters and the contour interval is 100 m.

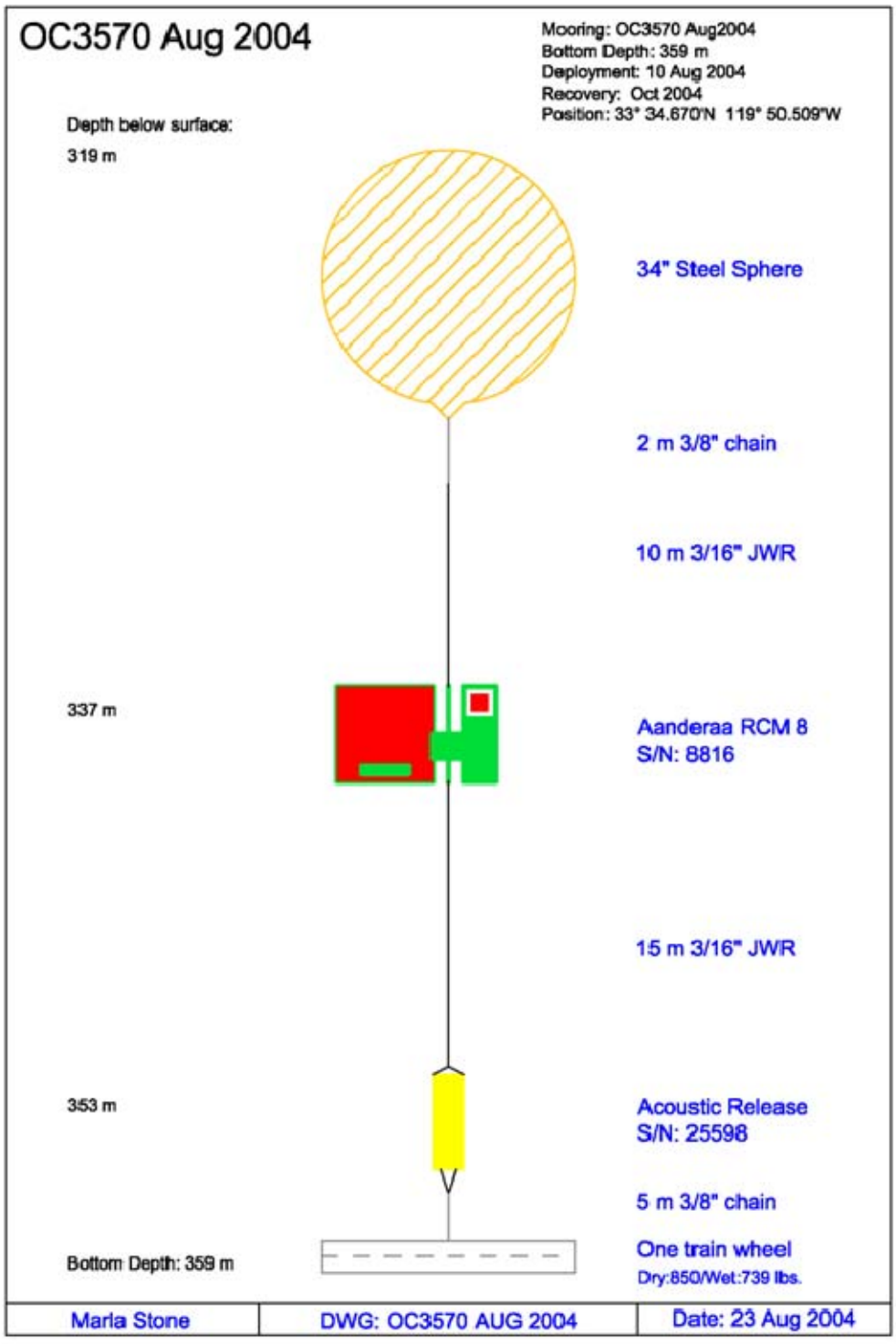

Figure K2. Intermediate mooring design for Santa Rosa Gap.

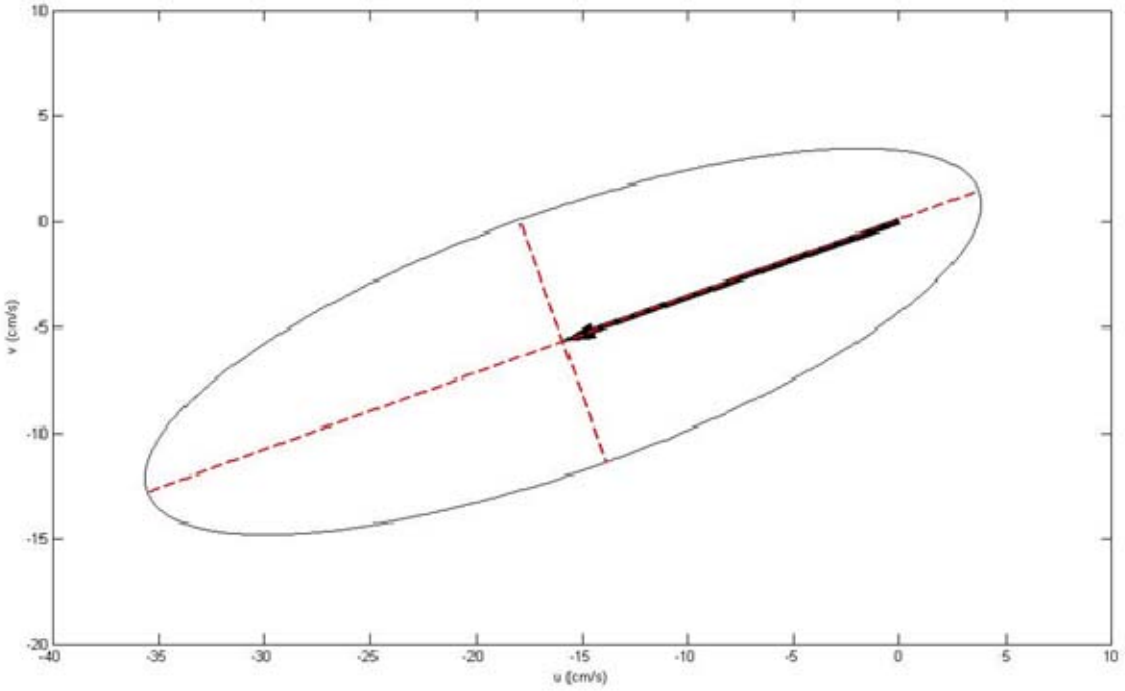

Figure K3. Mean and standard deviation of currents measured at a depth of 337 m near the sill in the northern gap of Santa Rosa Cortez ridge. Mean speed (direction) of the mean vector flow was 16.9 cm/s (250.4°T). The semi-major (semi-minor) axis was 20.9 cm/s (6.1 cm/s) and was oriented along 250.1°-070.1°T.

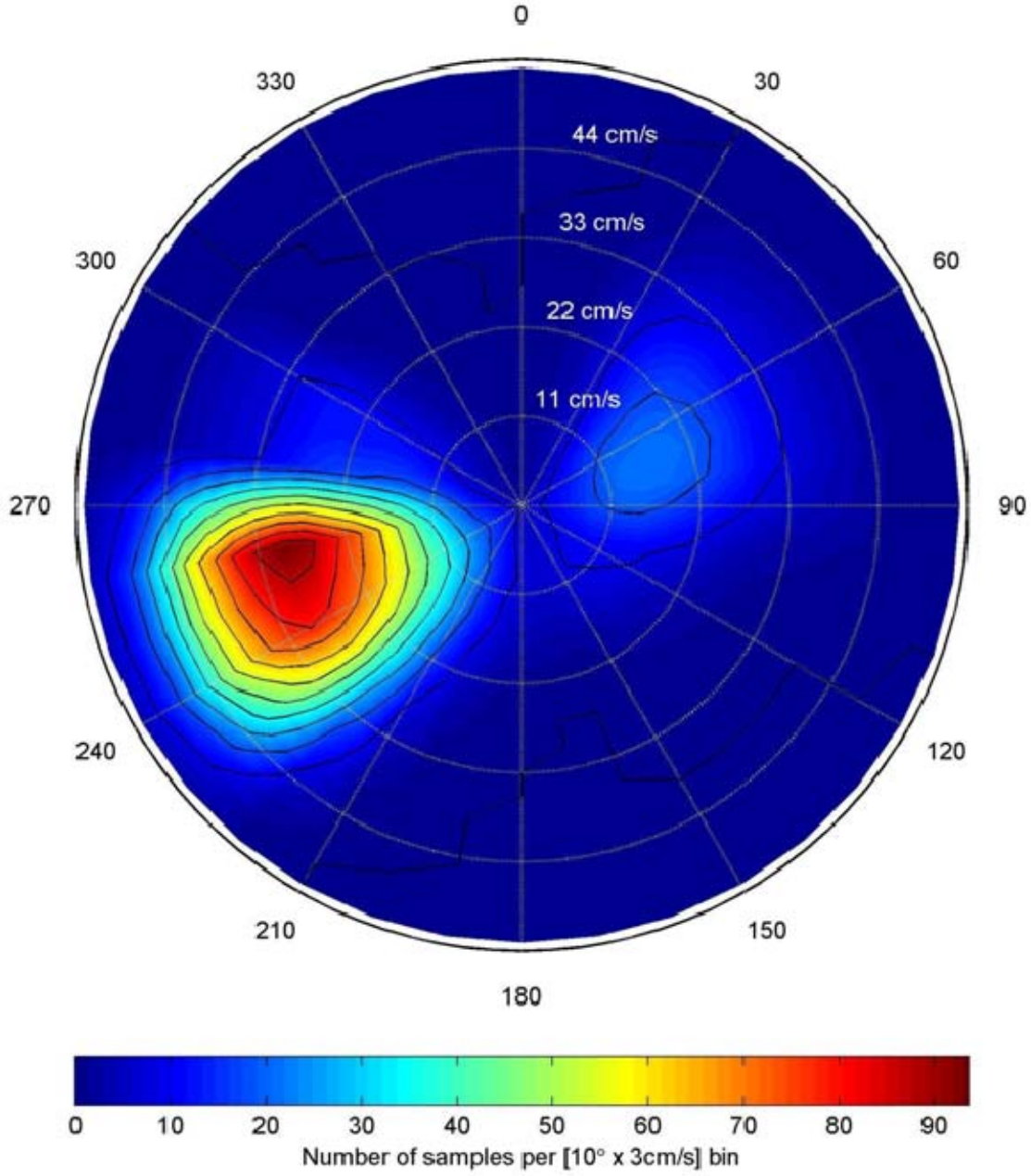

Figure K4. Histogram of velocity observations of currents measured at a depth of 337 m near the sill in the northern gap of Santa Rosa Cortez ridge. The total number of observations is 7,762. 33 observations with a speed less than 1 cm/s were omitted. Total number of bins is 703.

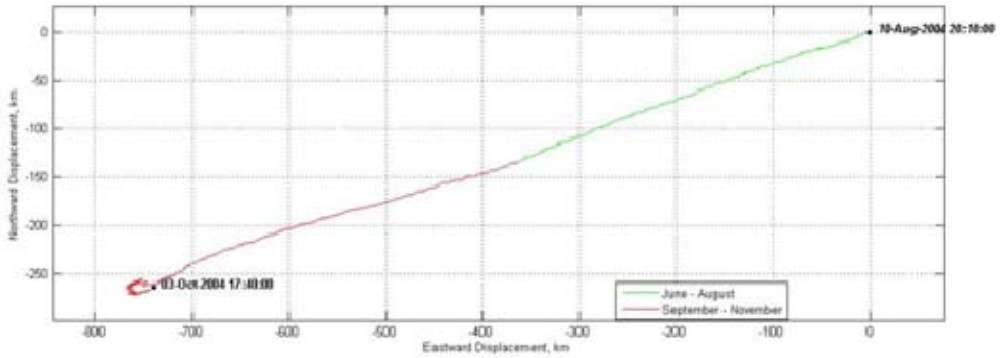

Figure K5. Progressive vector diagram of currents measured at a depth of 337 m near the sill in the northern gap of Santa Rosa Cortez ridge.

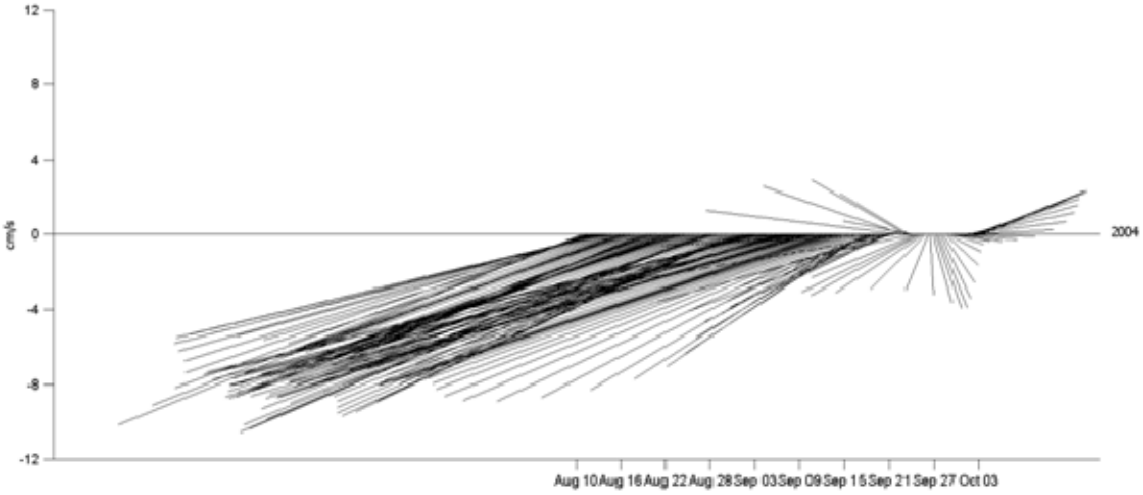

Figure K6. Currents measured at a depth of 337 m near the sill in the northern gap of Santa Rosa Cortez ridge as a function of time. Currents were smoothed using a Butterworth filter with a cutoff period of 72 hours.

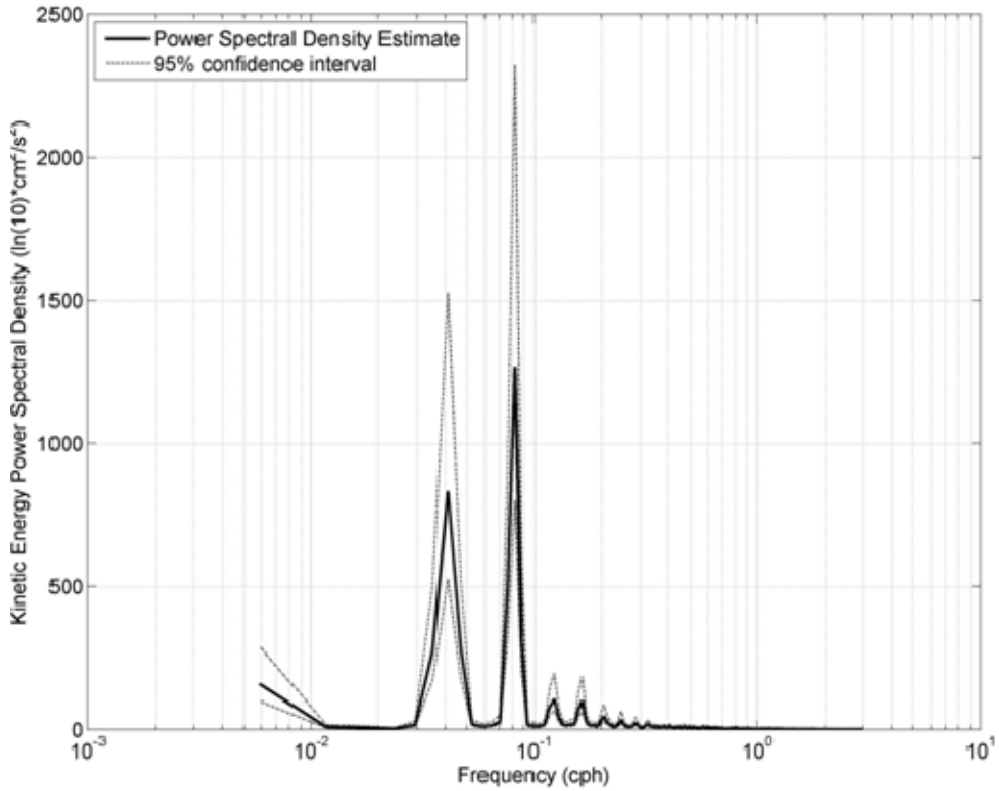

Figure K7. Kinetic energy spectrum for currents measured at a depth of 337 m near the sill in the northern gap of Santa Rosa Cortez ridge. Semi-diurnal peak at 0.08 cph with diurnal peak at 0.041 cph and local inertial frequency at 0.046 cph.

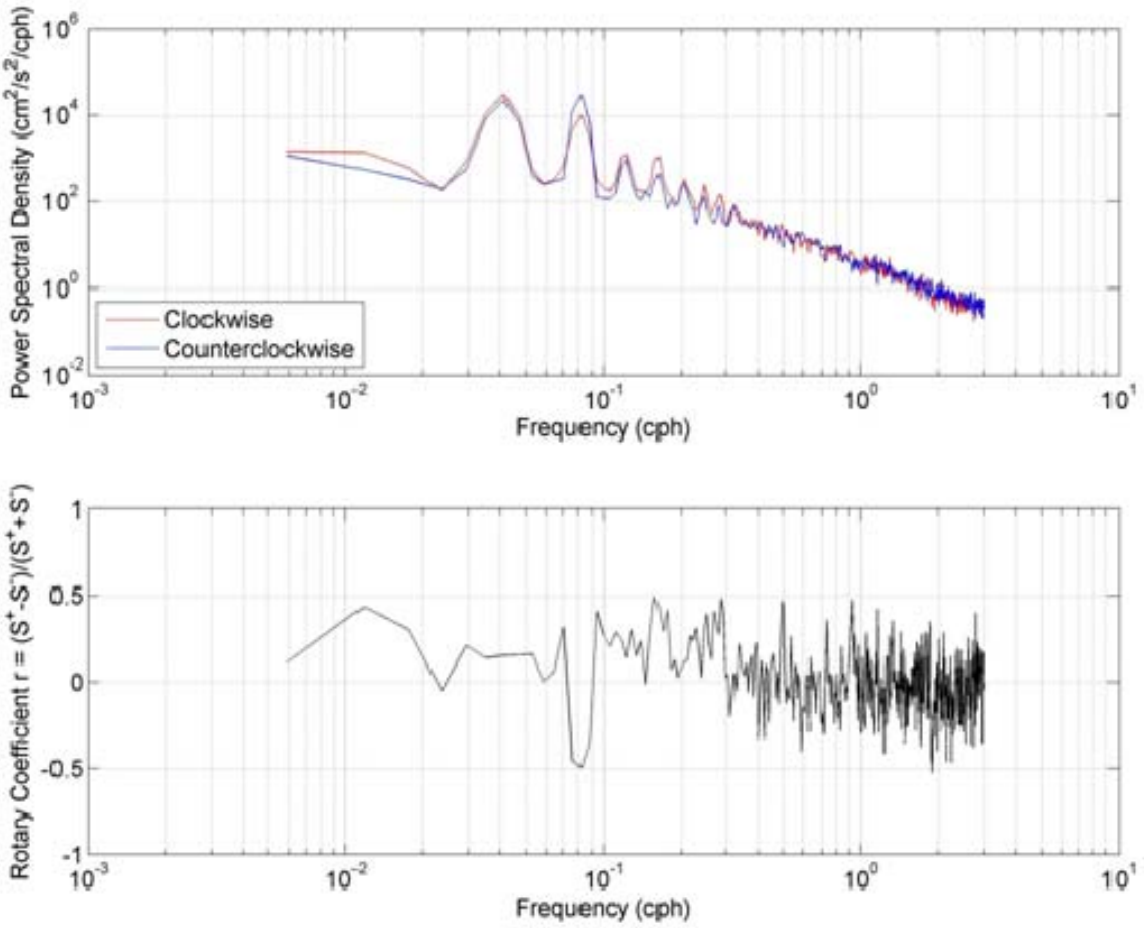

Figure K8. (upper) Rotary spectra of currents measured at a depth of 337 m near the sill in the northern gap of Santa Rosa Cortez ridge. (lower) Rotary coefficient.

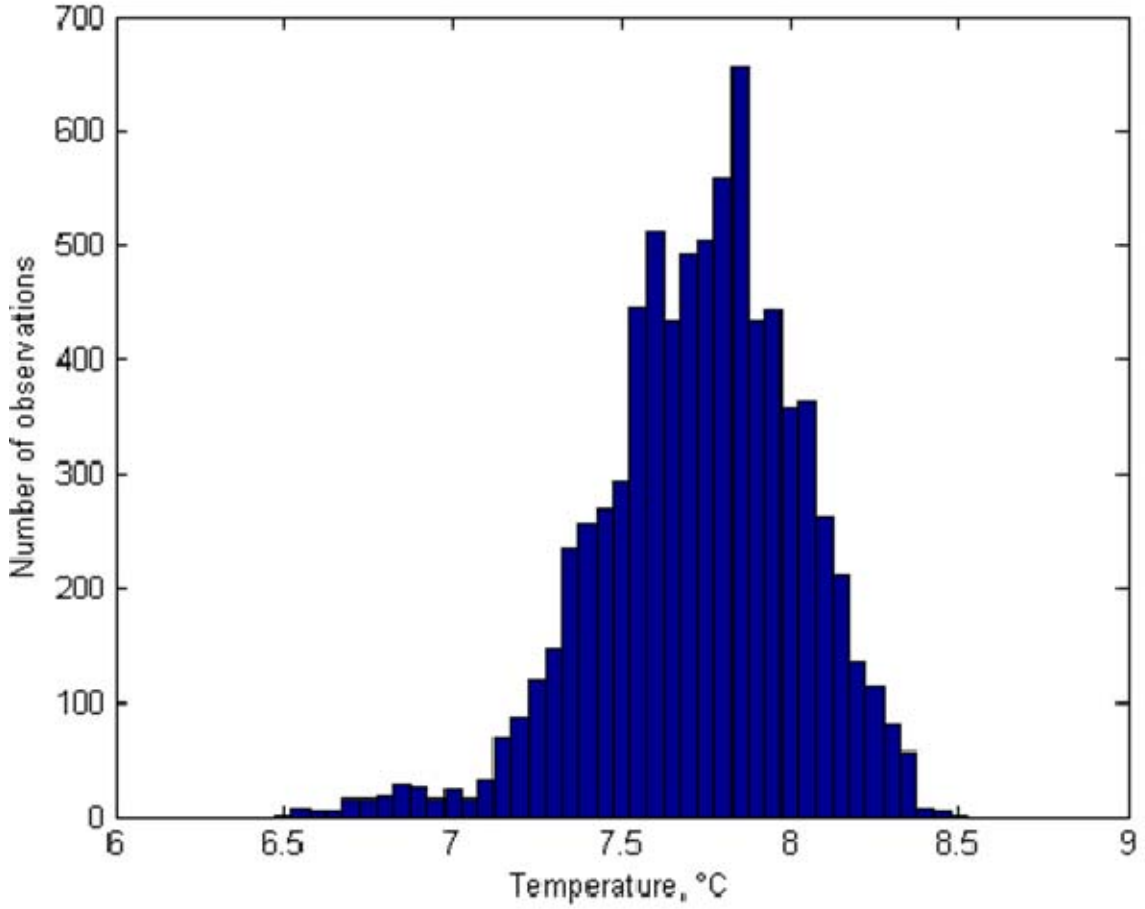

Figure K9. Temperature histogram at a depth of 337 m near the sill in the northern gap of Santa Rosa Cortez ridge using a bin size of 0.05°C.

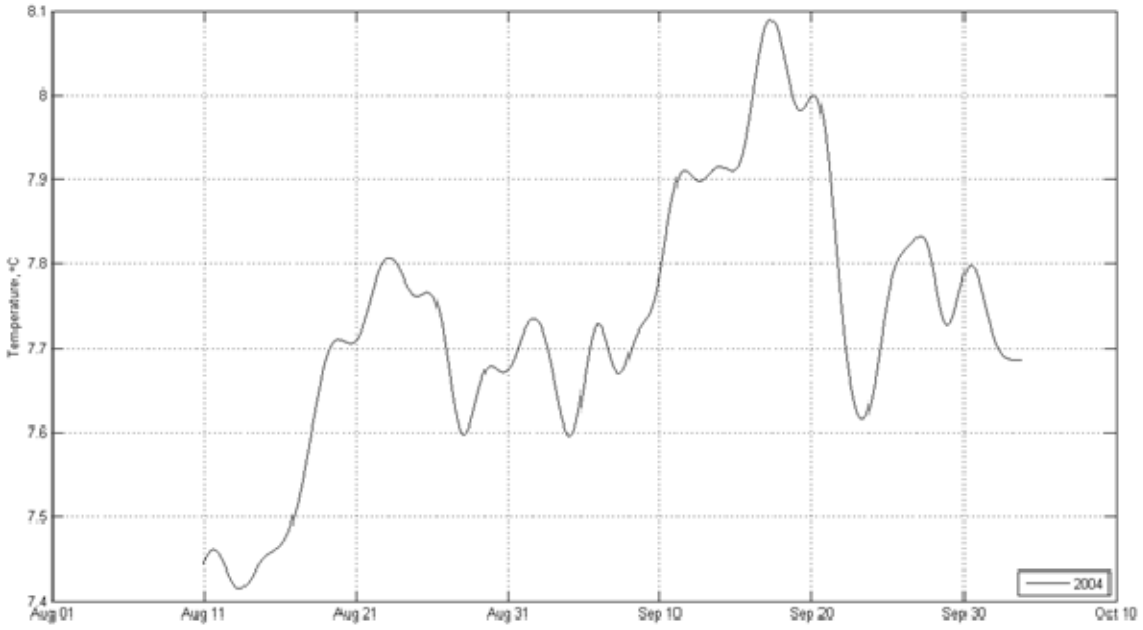

Figure K10. Temperature time series measured at a depth of 337 m near the sill in the northern gap of Santa Rosa Cortez ridge currents. Temperatures were smoothed using a Butterworth filter that cut off periods less than one week.

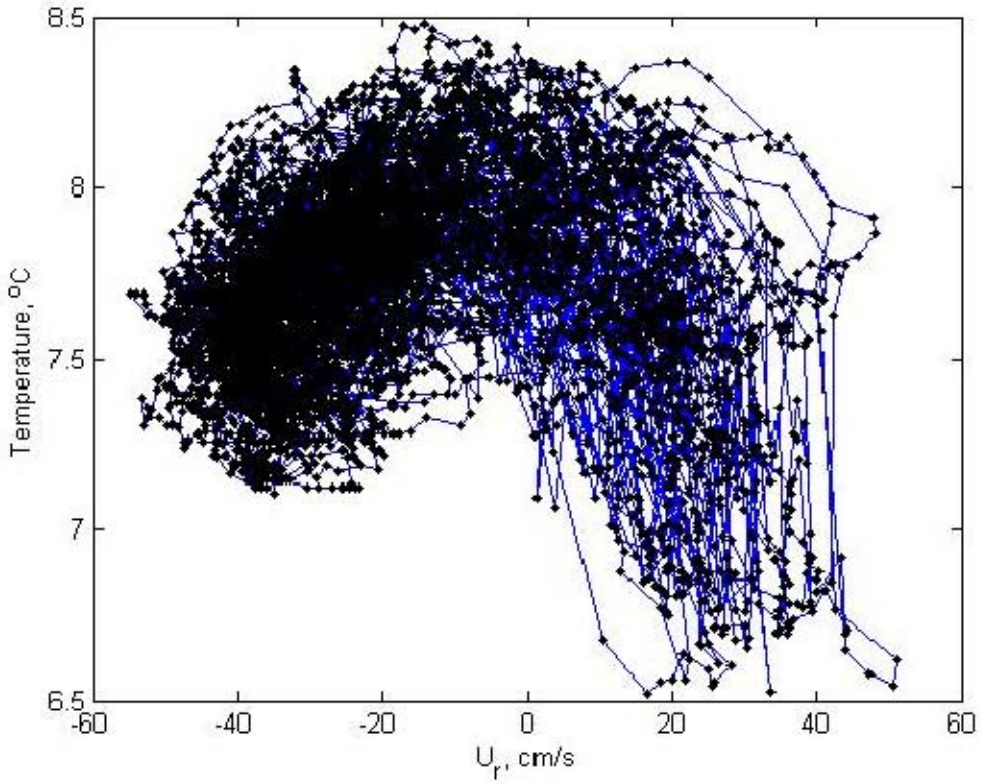

Figure K11. Temperature vs. along gap (u_r) flow. The blue line connects sequential 10 minute measurements, which are indicated as black dots.

Deployment Name	Date of Deployment	Latitude	Longitude	Instrument Depth (m)	Bottom Depth (m)	Compass Correction (E)	Timing Error
Santa Rosa Gap	10 August 2004 – 03 October 2004	33° 34.670'N	119° 50.509'W	337	359	1° 5’	0’ 13”

Table K1. Deployment information for a mooring near the sill in the northern gap of Santa Rosa Cortez ridge. The sampling rate for the RCM 8 current meter was 10 minutes.

APPENDIX L HOKE SEAMOUNT

This appendix covers a series of moorings on the summit of Hoke Seamount over a ten year period from May 1999 through June 2009 (mooring locations are shown in Fig. L1). Hoke Seamount is the most eastward seamount in the Fieberling Seamount group and is located about 600 km west of San Diego. Hoke was chosen as a measurement location because its summit is located at about 770 m, close to the axis of the deep sound channel. Table L1 contains information on current measurements, while Table L2 contains information on self-contained conductivity-temperature-pressure instruments. The first five deployments were intermediate moorings that extended 73 to 233 meters above the summit. An example of one of these moorings is shown in Fig. L2. The last deployment was a bottom mounted acoustic listening station.

Seasonal and annual flows at Hoke Seamount varied greatly from one year to the next, which resulted in a small eastward (073.7°T) vector mean flow, 0.2 cm/s (Fig. L3). The mean speed was 5.19 cm/s. The semi-major (minor) axis magnitude was 4.6 cm/s (4.1 cm/s) and the eccentricity of the variance ellipse was 0.33. The semi-major axis was directed along 337.3°T to 157.3°T (Fig L3).

The velocity histogram (Fig. L4) showed the most frequently observed speeds greater than 1 cm/s as an " Ə "-shaped ridge along the 5 cm/s isotach. The principal mode contained 456 observations in the bin corresponding to a speed of 5 cm/s and a direction of 180°T.

Currents measured from May through October 1999 resulted in an eastward displacement of 250 km (not shown). The progressive vector diagram for the RCM 8 deployments began in May 2000 (Fig. L5). Flow was initially northward, but reversed in winter 2002, meandered eastward beginning in winter 2003, and then northward in winter 2005. Winter flow had a northward component, but the largest seasonal northward displacement occurred in summer 2005.

Stick plots are shown in Figs. L6a and L6b. Currents appeared to be strongest in 2002 and 2005. It should be noted that the maximum speed observed in the raw data was on 21 January 2002 at 26.33 cm/s, corresponding to the period of strong northward flow

shown in Fig. L6a (although reduced in magnitude due to smoothing). With the reversal of this northward flow in late February 2002, relatively strong southward flow persisted through November. Subsequent bursts of southward flow were noted in August-September 2003, October 2004 and 2005, and September 2006. Strong northward flow was observed in summer 2005-6, but not in other years.

The semi-diurnal tides dominated the variance of the kinetic energy spectrum (Fig. L7). A broad peak was centered at the local inertial frequency (0.0449 cph), with higher frequencies corresponding to tidal harmonic frequencies (0.125, 0.1621, 0.2422, and 0.3242 cph). The rotary spectra (Fig. L8) showed that the clockwise (anticyclonic) component was larger through the tidal/inertial range. The counterclockwise (cyclonic) component also had peaks at tidal frequencies; but at the local inertial frequency the energy was at the level of "noise". As a consequence of these variations in the relative strengths of the clockwise and counterclockwise rotary components through the tidal band, the rotary coefficient approached 1 at the local inertial frequency but was much less, about 0.2, for the semidiurnal tide.

The histogram of the observed temperature data (Fig. L9) used 0.05°C bins and half-hour observations. This histogram includes the temperature data from all deployments. There are two modes. One, which corresponds to temperatures from deployment #2, has a median temperature of 5.42°C, the mean temperature (standard deviation) was 5.43°C (0.1244°C) and the maximum (minimum) temperature was 5.94°C (4.97°C). The median temperature for the lower temperature mode was 4.62°C, the mean temperature (standard deviation) was 4.624°C (0.164°C), and the maximum (minimum) temperature was 5.47°C (4.08°C). The temperature difference between the two modes is attributable to the shallower depth of deployment #2.

The smoothed temperature time series is shown in Figure L10. The maximum (minimum) temperature (not including Hoke 2, due to its higher depth) occurred on 8 February 2002 (20 June 2006). The temperature in 2002 from January to mid-March reaches a maximum which, compared to other years, was unusually high. The temperature for the other years was normally from 4.9°C to 4.5°C, though there was a slight spike in 2005 from August to early September.

The R/V Atlantis was used to recover an acoustic receiver at Hoke Seamount in June 2009. The sea-beam mapping system was used on this cruise to image the bathymetry of the seamount. These bathymetry data were reprocessed by the Monterey Bay Aquarium Research Institute (J. Paduan), and the resulting chart is shown in Figure L11.

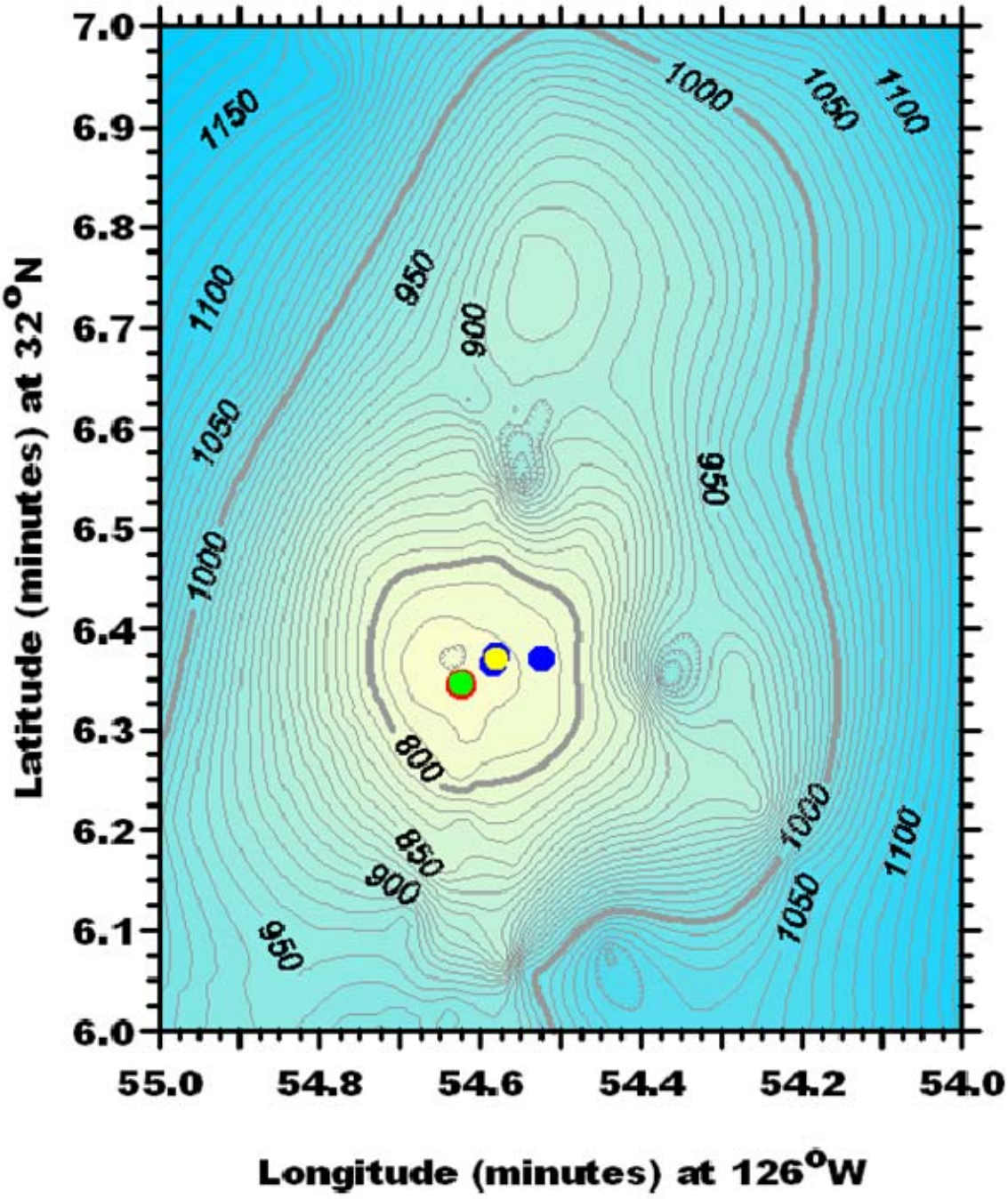

Figure L1. Hoke Seamount mooring locations. Soundings are in meters and the contour interval is 50 m.

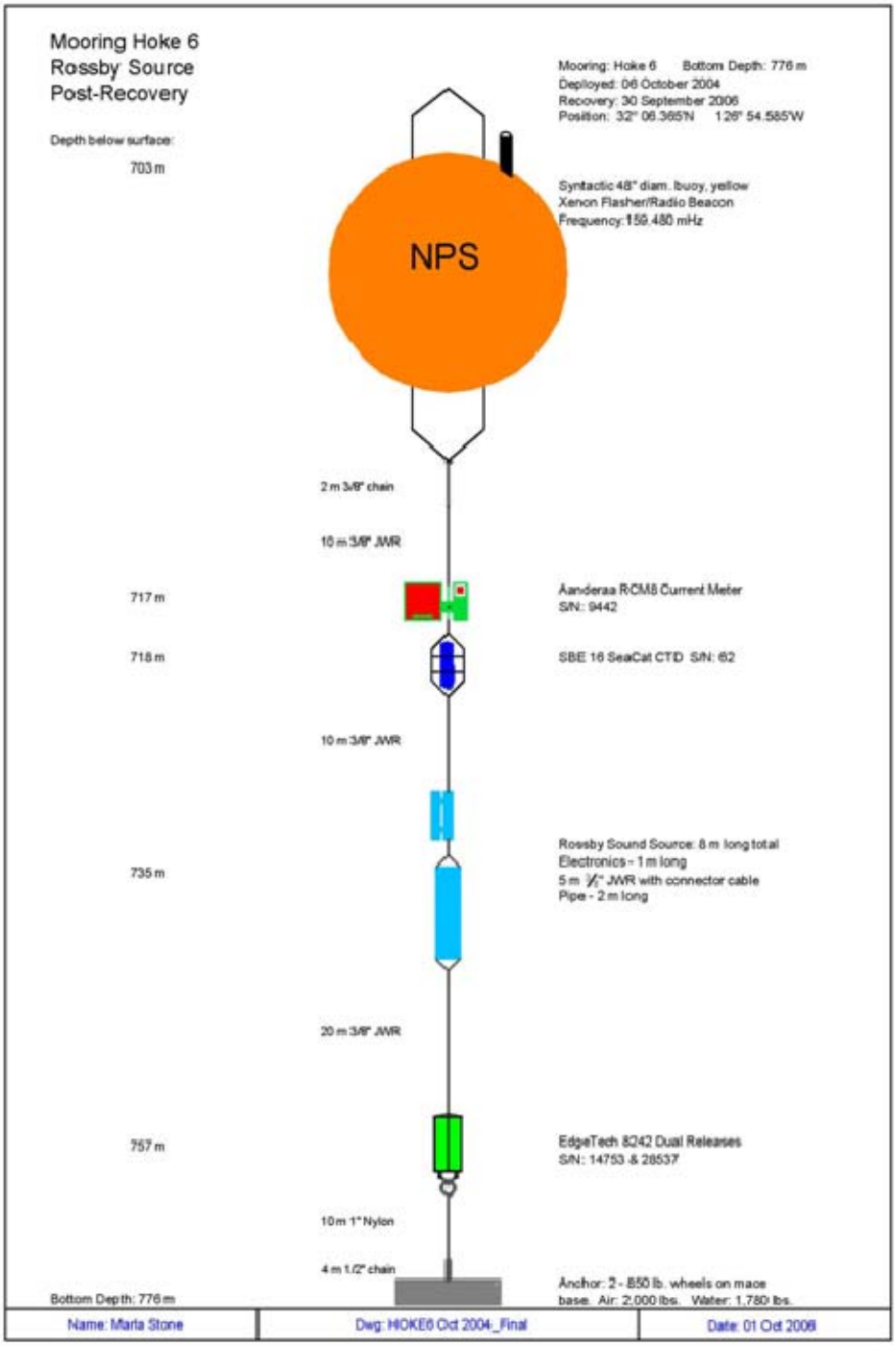

Figure L2. Schematic diagram for an intermediate mooring deployed on the top of Hoke Seamount. Mooring contains a RAFOS sound source, RCM8 current meter, SeaCat, and dual acoustic releases. Jacketed wire rope (JWR) was used to connect mooring components. The acoustic releases were connected to the anchor by 10 m of 1" nylon line and 4 m of ½" chain.

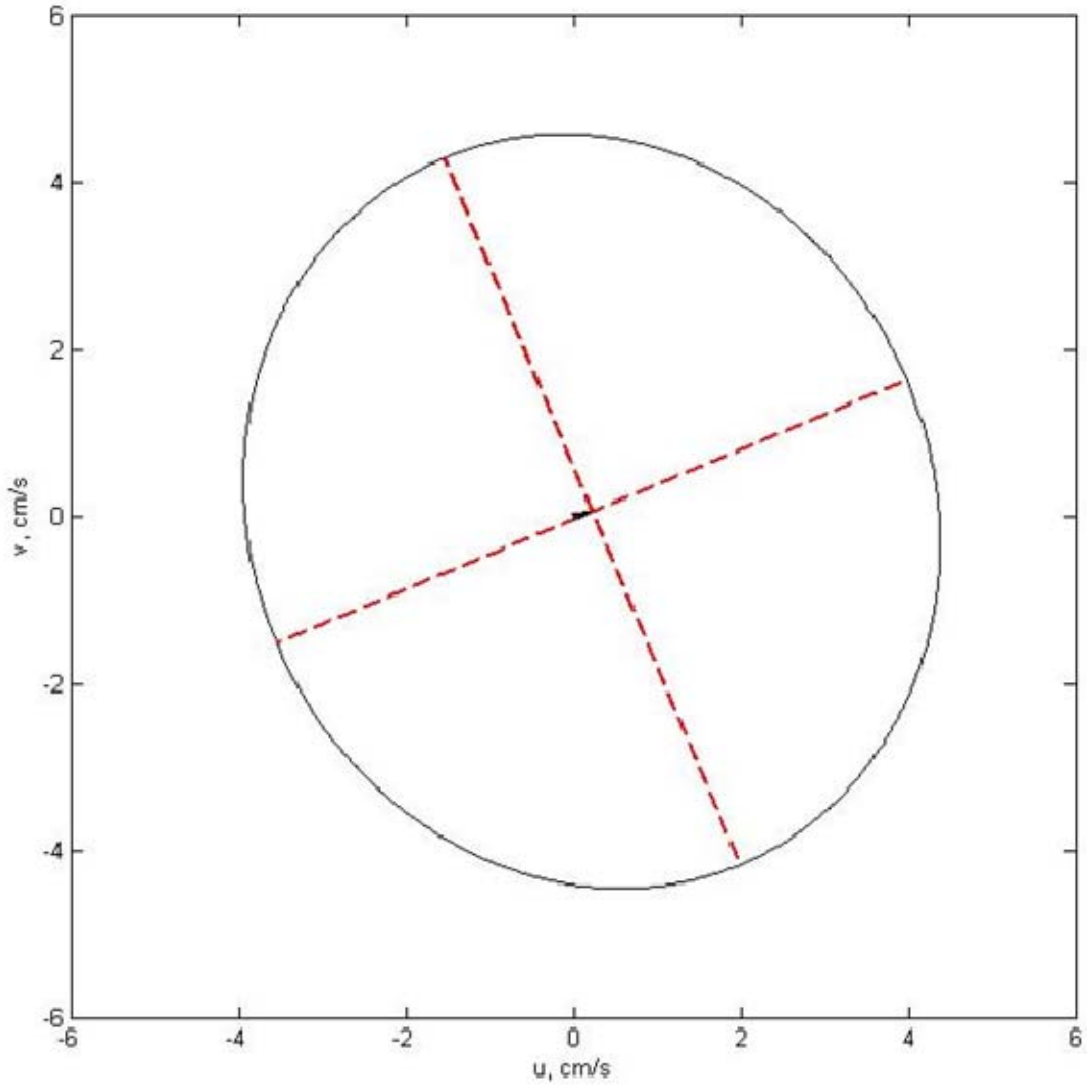

Figure L3. Mean and standard deviation of currents observed at Hoke Seamount. Mean speed (direction) of the mean vector flow was 0.2 cm/s (073.7°T). Mean speed (direction) of the mean vector flow was 0.2 cm/s (073.7°T). The semi-major (semi-minor) axis was 4.6 cm/s (4.1 cm/s) and was oriented along 337.3°-157.3°T.

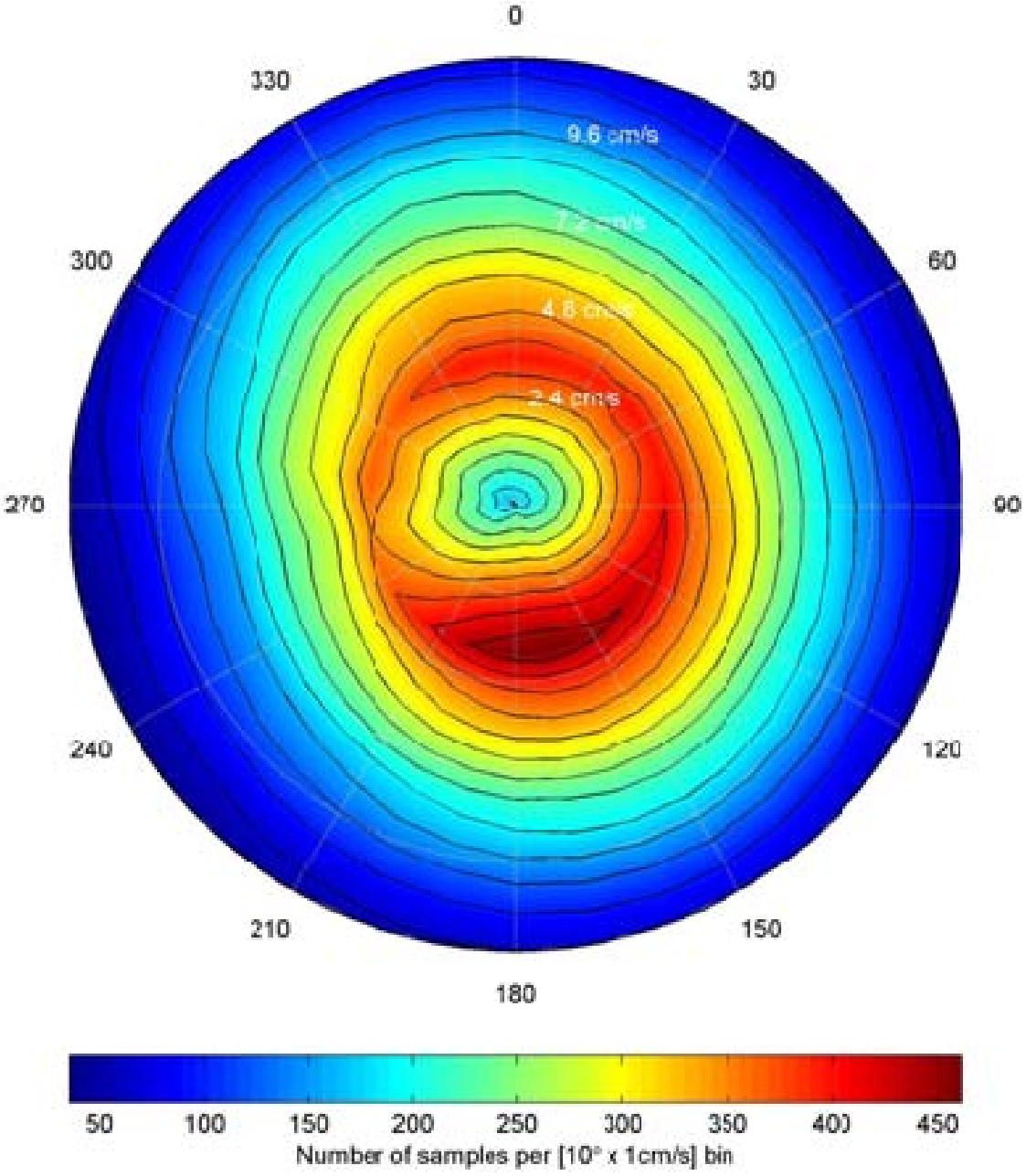

Figure L4. Histogram of Hoke Seamount current observations. The total number of observations was 121,168, with 6591 observations omitted because the speed was less than 1 cm/s.

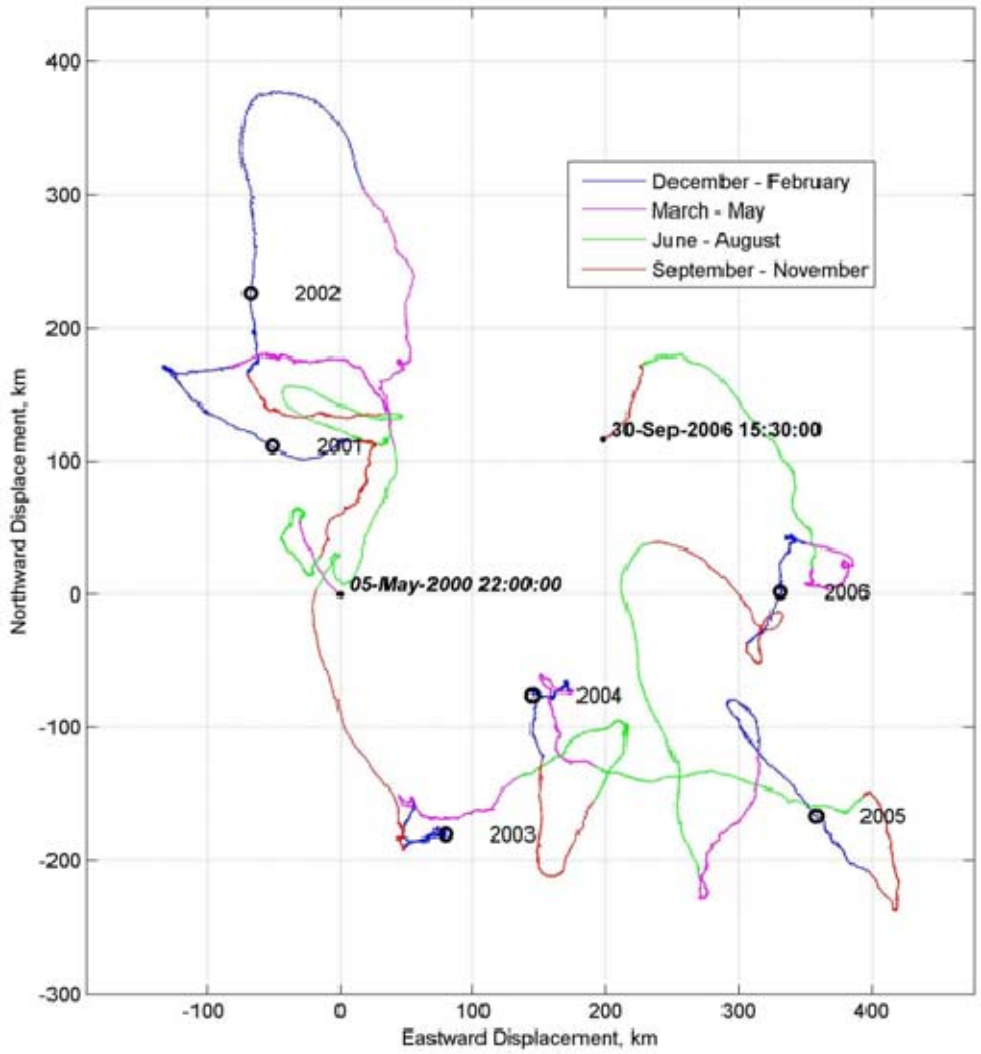

Figure L5. Progressive vector diagram for Hoke Seamount deployments # 2, 3, 4, and 5.

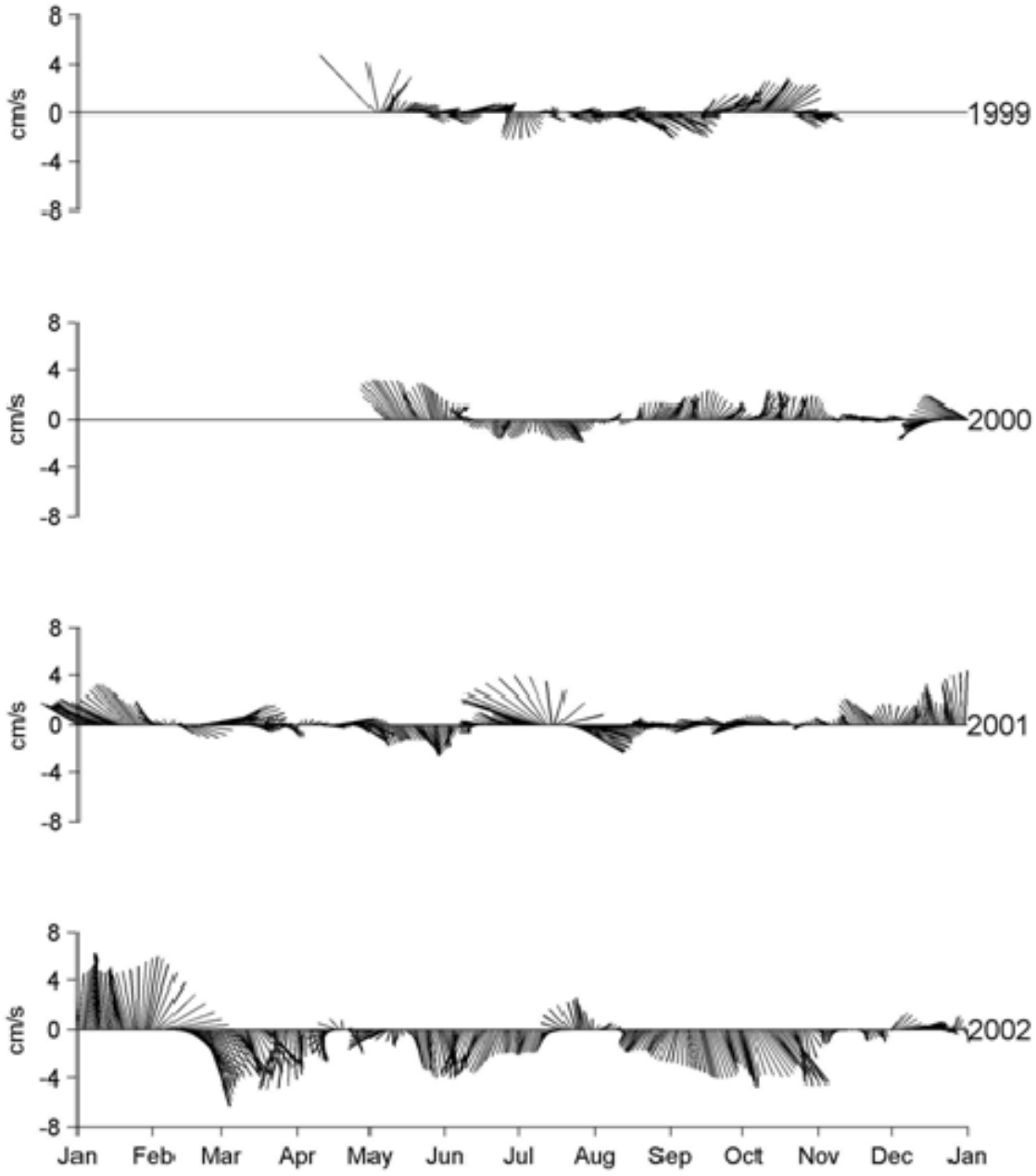

Figure L6. Hoke Seamount currents as a function of time. Tides were removed by filtering using a Butterworth filter and convolution of the filter with the data. (a) 1999-2002.

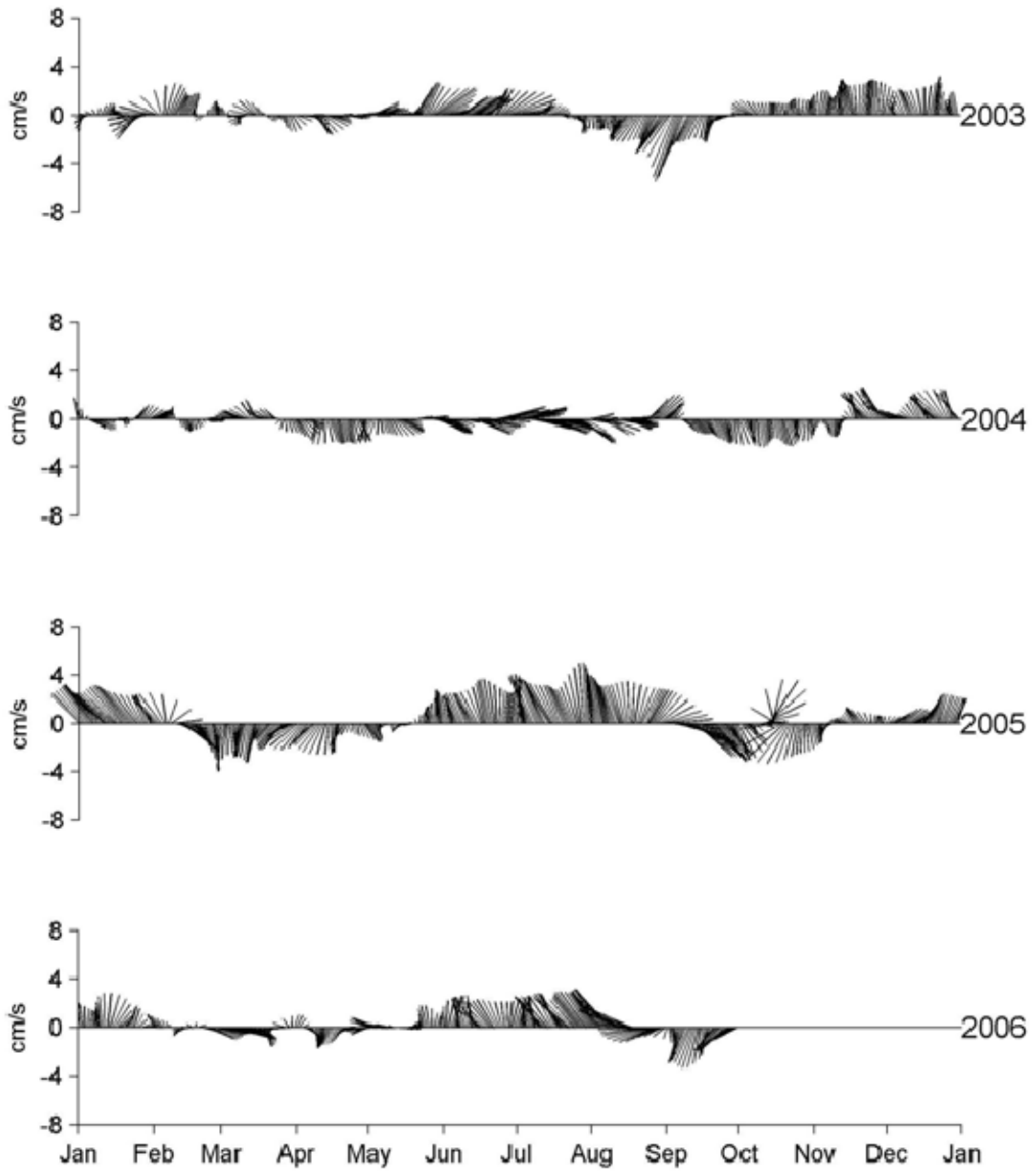

Figure L6b. Hoke Seamount currents as a function of time. Tides were removed by filtering using a Butterworth filter and convolution of the filter with the data. (b) 2003-2006.

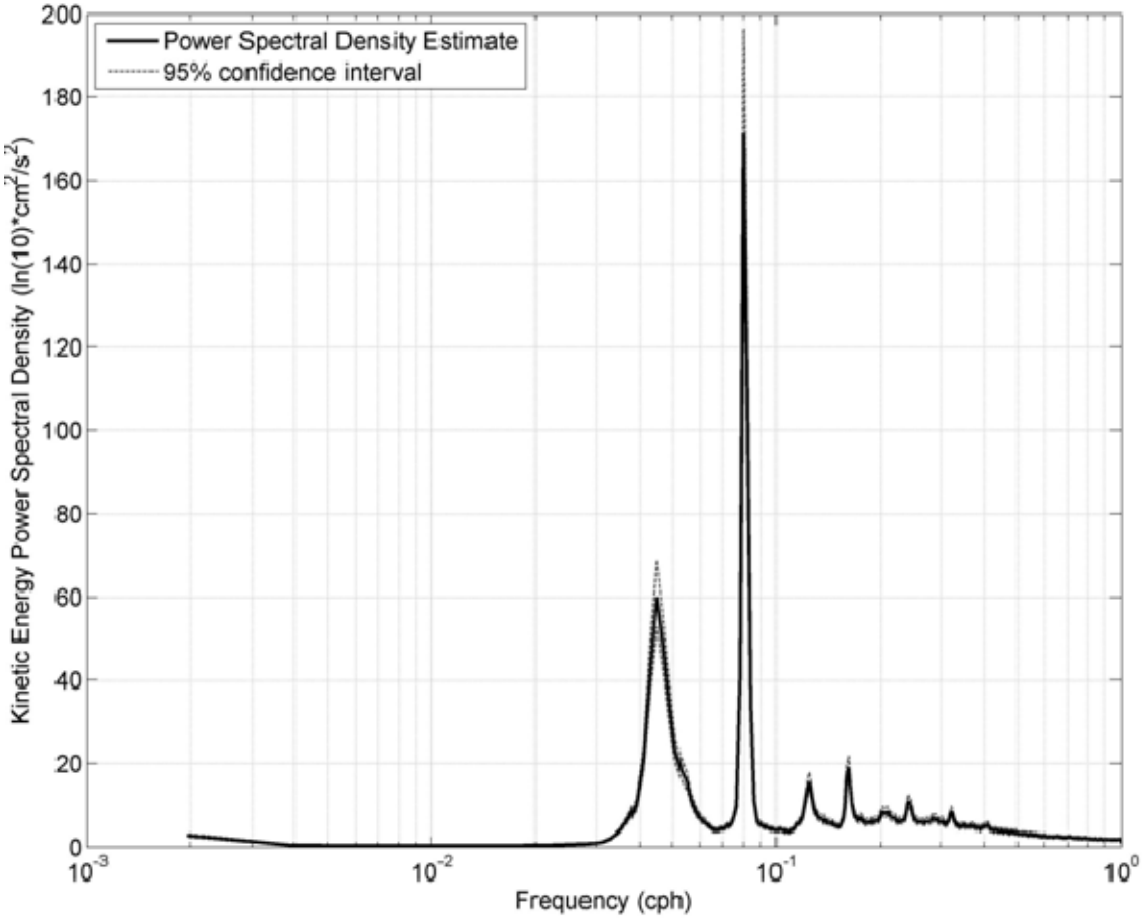

Figure L7. Kinetic energy spectrum for Hoke Seamount deployments # 2-4. Peaks correspond to inertial-period motion at 0.045 cph and semi-diurnal tides at 0.08 cph, with smaller tidal peaks at 0.125, 0.162, 0.21, 0.24, 0.29, and 0.32 cph.

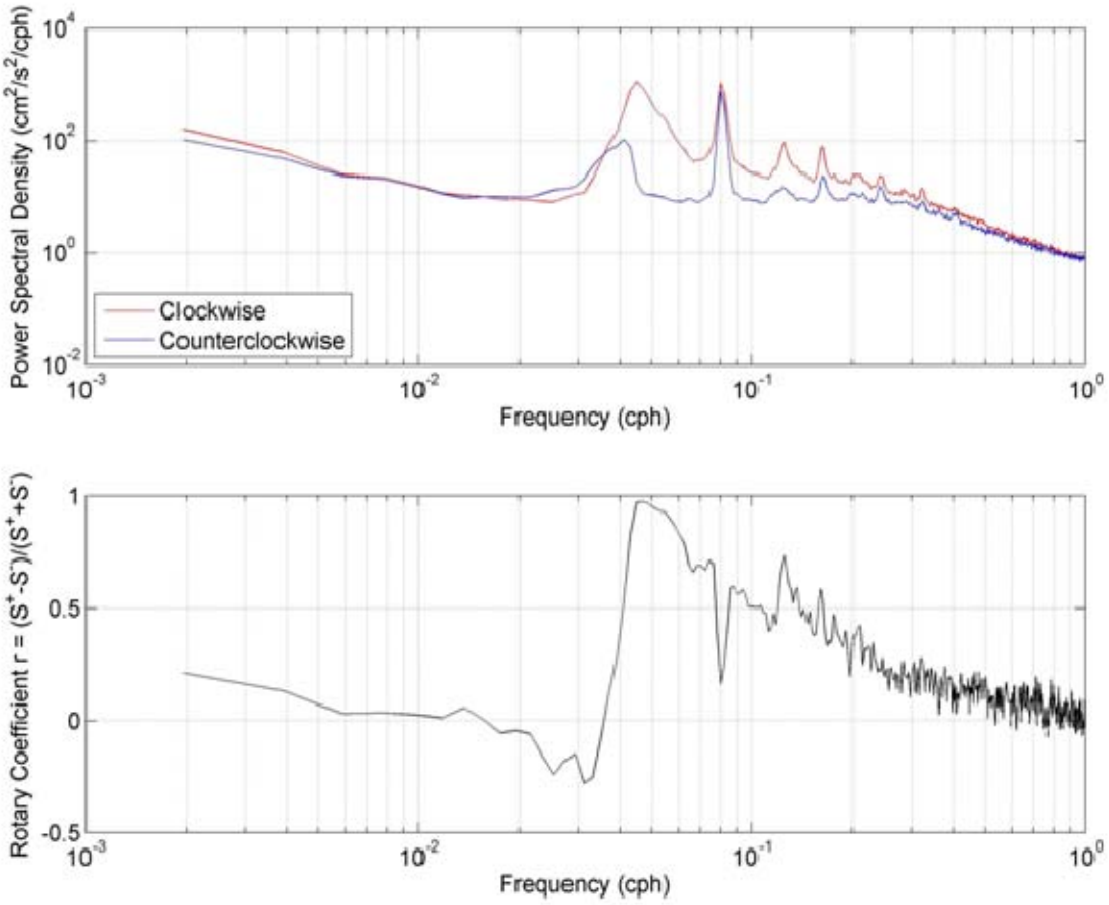

Figure L8. (upper) Rotary spectra for Hoke Seamount deployments # 2-4. (lower) Rotary coefficient.

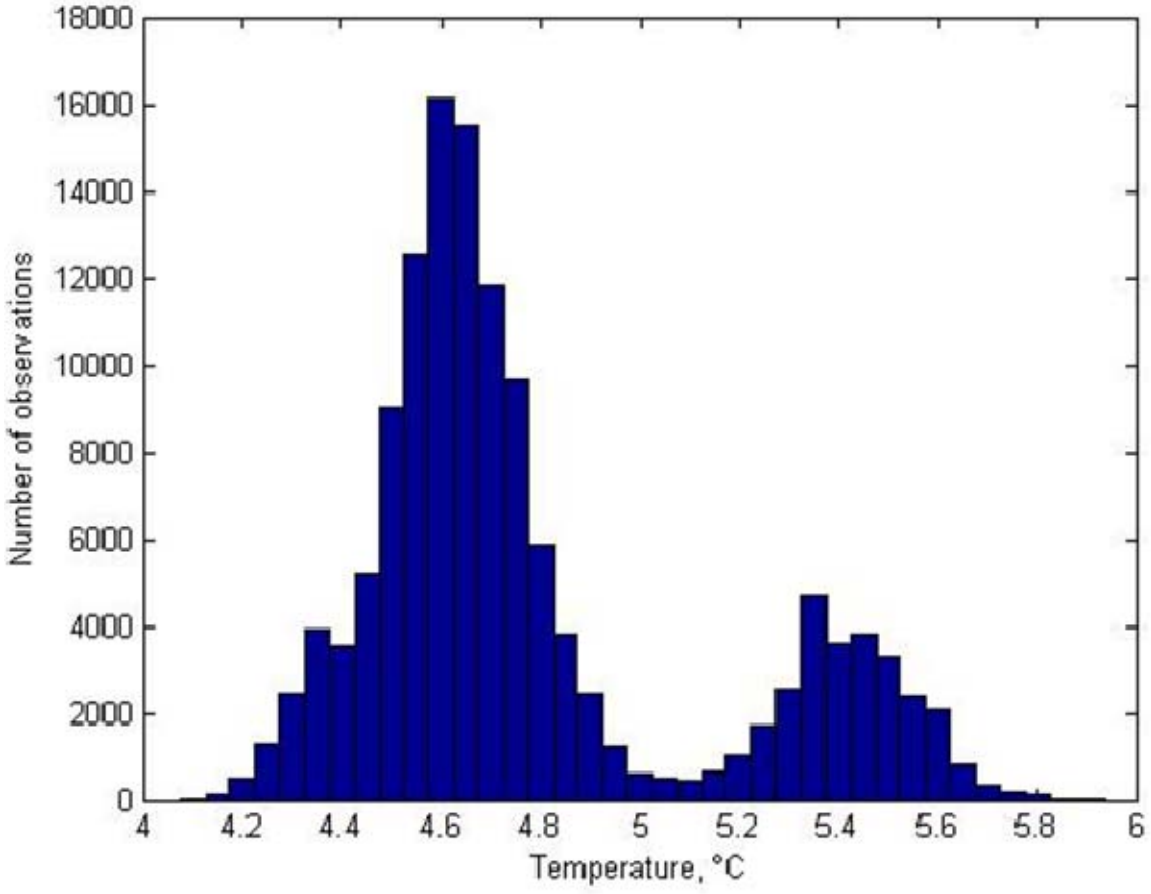

Figure L9. Histogram of temperature measurements at Hoke Seamount using a bin size of 0.05°C. Note: all data were analyzed at a sampling rate of half an hour. All deployment data were utilized for this histogram.

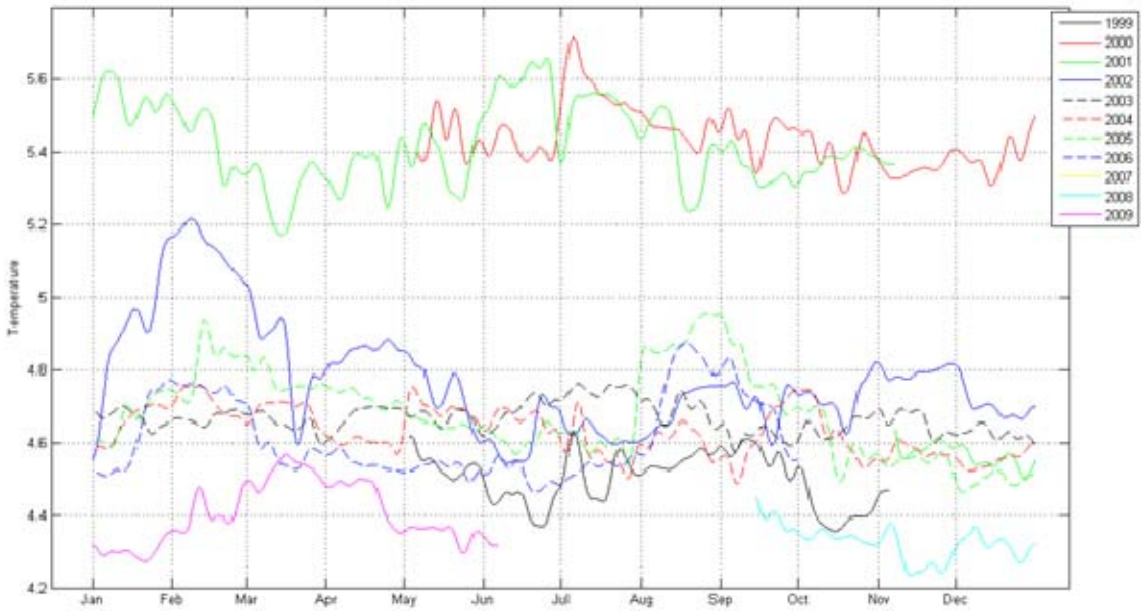

Figure L10. Temperature time series of Hoke Seamount deployments # 1-6. Temperature was smoothed using a Butterworth filter that cut off periods less than one week.

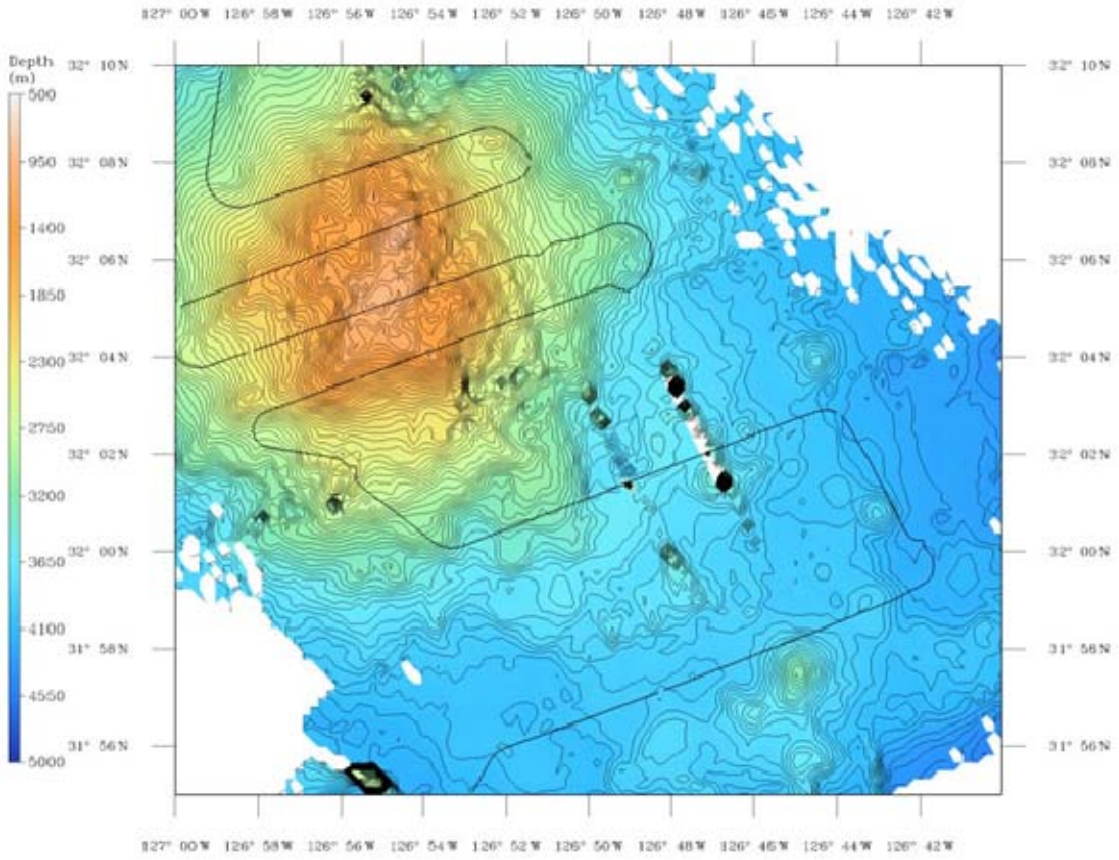

Figure L11. High resolution bathymetry for Hoke Seamount. Data were collected by *R/V Atlantis* using a SeaBeam 2100/12 system, which generated 121 bathymetric points and 2000 co-located sidescan pixels for every ping cycle. Data were processed and the chart generated by Jenny Paduan, Monterey Bay Aquarium Research Institute.

Deployment Number	Date of Deployment (start-end)	Latitude	Longitude	Instrument Depth (m)	Bottom Depth (m)	Compass Correction (E)	Timing Error	Instrument Type
1	02 May 1999 - 05 May 2000	32° 6.344'N	126° 54.624'W	718	765	unknown	unknown timing error.	FSI Acoustic Current Meter
2	05 May 2000 - 07 Nov. 2001	32° 6.347'N	126° 54.625'W	552	785	46'	7' 35"	RCM 8
3	07 Nov. 2001 - 25 Oct. 2002	32° 6.371'N	126° 54.524'W	727	770	44'	9' 15"	RCM 8
4	25 Oct. 2002 - 6 Oct. 2004	32° 6.374'N	126° 54.581'W	726	768	43'	9' 54"	RCM 8
5	6 Oct. 2004 - 30 Sep. 2006	32° 6.365'N	126° 54.585'W	719	776	40'	6' 52"	RCM 8

Table L1. Hoke Seamount current observations. An FSI acoustic current meter was used for deployment 1 and Aanderaa RCM8 current meter for deployments 2-5. The sampling rate for Hoke deployments#2-5 was 30 minutes. Note: The deployment 3 pressure sensor failed, so the depth of the instrument was determined by position in relation to the SEACAT device on the mooring.

Deployment Number	Dates of Deployment	Latitude	Longitude	Instrument Depth (m)	Bottom Depth (m)	Sampling Interval (minutes)	Instrument Name	Timing Error
3	07 Nov. 2001 - 25 Oct. 2002	32° 6.371'N	126° 54.524'W	728	770	30	SBE Seacat 16 CTD	5'31"
4	25 Oct. 2002 - 6 Oct. 2004	32° 6.374'N	126° 54.581'W	728	768	60	SBE Seacat 19 CTD	Unknown
5	6 Oct. 2004 - 30 Sep. 2006	32° 6.365'N	126° 54.585'W	719	776	60	SBE Seacat 16 CTD	Unknown
6	13 Sept. 2008 – 6 June 2009	32° 6.37'N	126° 54.58'W	780	781	6	SBE 37-SM Microcat	1'36"

Table L2. Hoke Seamount measurements of conductivity, temperature and pressure. The sampling rate for Hoke deployment 3 was 30 minutes, and 60 minutes for deployments 4 and 5. The sampling rate for deployment 6 was 6 minutes, but was collated to 30 minutes for data analysis purposes.

APPENDIX M RAFOS FLOAT 15

RAFOS 15 was launched on 21 August 1994 and surfaced on 22 February 1996 at a water depth of 4320m approximately 390 km northwest of Point Sur. Details of this mission are given in Table M1. The mission was planned for 925 days but ended after only 538 days because the float sank too deep and reached its bailout point. Figure M1 displays the pressure and temperature recorded by RAFOS 15. The float behaved normally (pressure was inversely related to temperature) until late October to early November 1995 at which point the float began to sink; after December 1995 the rate of sinking was about 100 m per month. The maximum (last) recorded pressure was 1804 dbar. The reason for sinking is likely leakage of seawater associated with failure of the seal between the end plate and the glass hull. The mean pressure from launch to late October and early November 1995 (when the float began to sink) was 1586 dbar.

Figure M2 shows the entire trajectory of the RAFOS 15 float. A portion of the float trajectory has been included in Brink *et al.* (2000). The mean speed of the RAFOS float for the length of its deployment was 3.5 cm/s and the vector mean flow was 1.2 cm/s with a mean direction of 002°T. After launch 270 km to the west of Pt. Reyes in August 1994 (where the bottom is 4320 m deep), the float moved northward during the remainder of 1994 to a point 60 km to the west of Cape Mendocino (40.4°N) where water depth is 1590 m. The float subsequently moved offshore along the northern side of the Mendocino escarpment from January through March 1995 through one mesoscale anticyclonic loop at 125° 45'W. On 1 May 1995 it had returned eastward to the point where it had started the year; but this time as it moved to the northwest it followed the 2000 m isobath to the east and thence northward into Gorda Basin. In August 1995 it moved to the northwest across Gorda Basin and thence executed a figure eight, initially an anticyclonic loop and then cyclonic back to the eastern side of the basin. It then continued to move northward, and, as it sank beginning in early winter 1994, looped cyclonically across northern Gorda Basin off Cape Blanco (42.8°N).

Upon initial inspection of Figures M1 and M2 it appeared that the float might have grounded at several points along its trajectory. Figure M3 compares the bathymetry

along the float trajectory with the depth of the float. Although at several points the float appeared to be deeper than the water, the variability of the bottom depth and the accuracy of the float navigation were such that grounding was uncertain. The speed of the RAFOS float was examined and seemed unaffected at those points where bathymetry shoaled. Apparently the float managed to avoid the bottom throughout its mission.

The along- and cross-shore diffusivity estimates for the first four months of the RAFOS 15 mission are shown in Figure M4, and estimates for this as well as the four subsequent periods are tabulated in Table M2. Alongshore (cross-shore) diffusivity estimates varied by a factor of about 30 from 0.02 to 0.54 (0.07 to 2.22) cm^2/s. The cross-shore diffusivity exceeded the alongshore diffusivity in each reference period, so that the ratio of the alongshore to cross-shore diffusivity was never greater than 0.5.

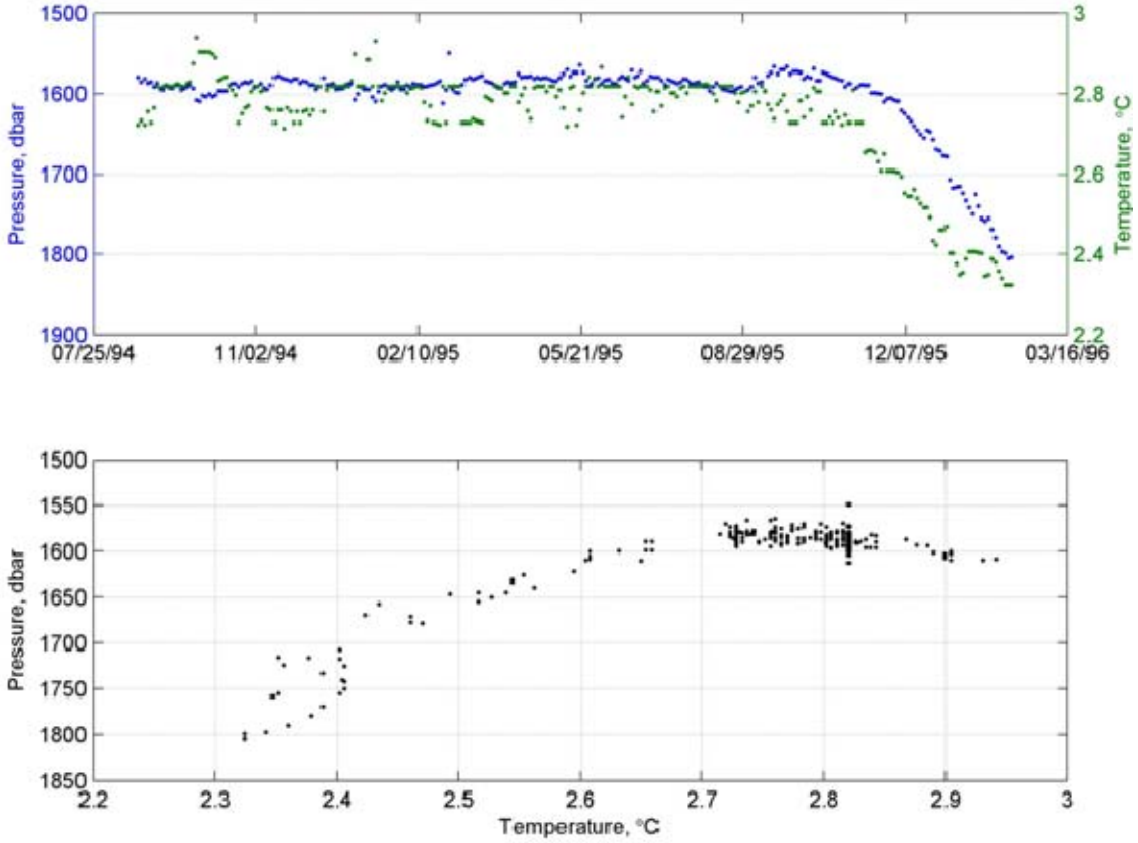

Figure M1. Temperature and Pressure data for RAFOS 15. (upper) Time series. (lower) Temperature vs. pressure.

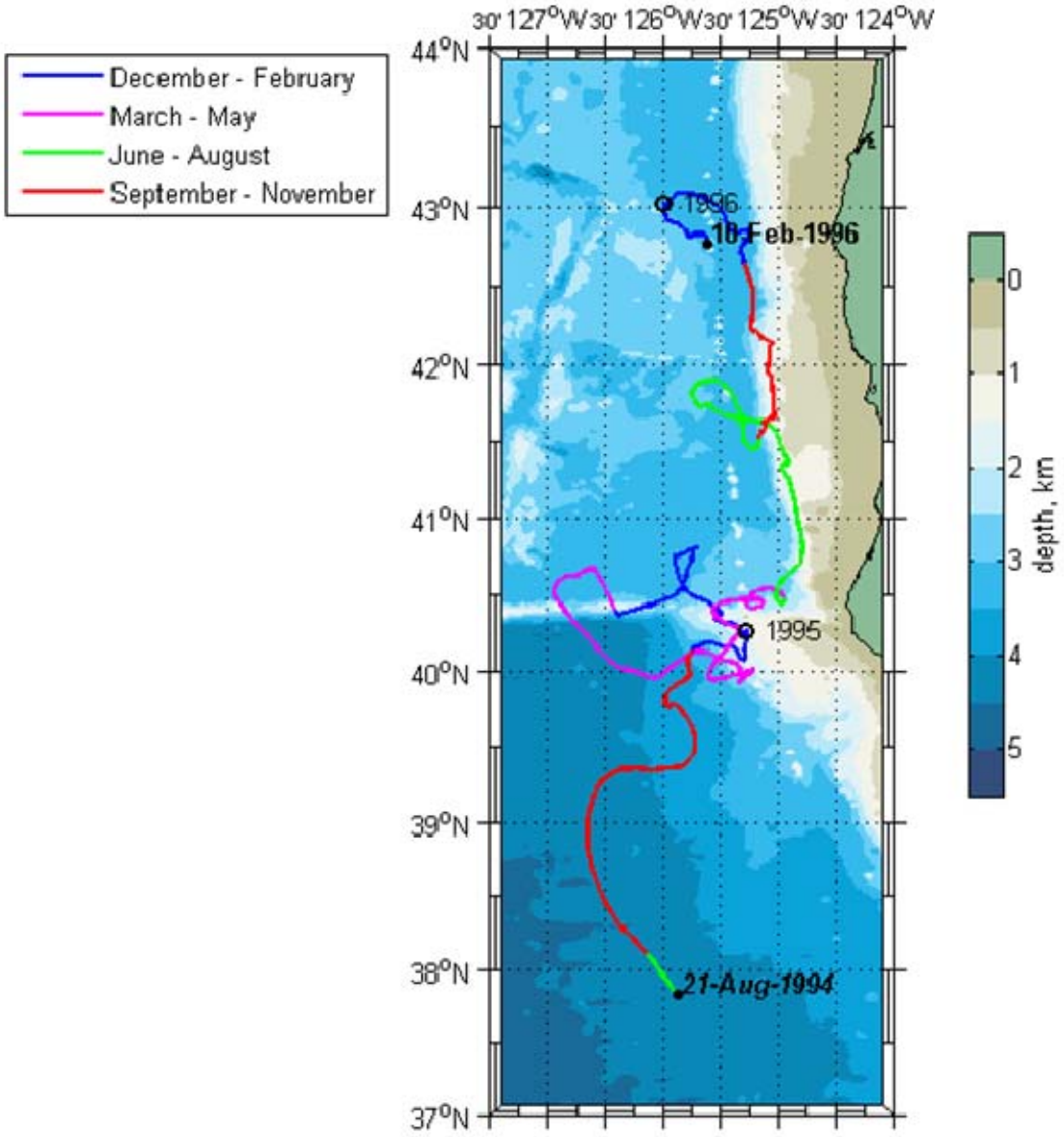

Figure M2. The trajectory for RAFOS 15. Trajectory color indicates season (upper left legend).

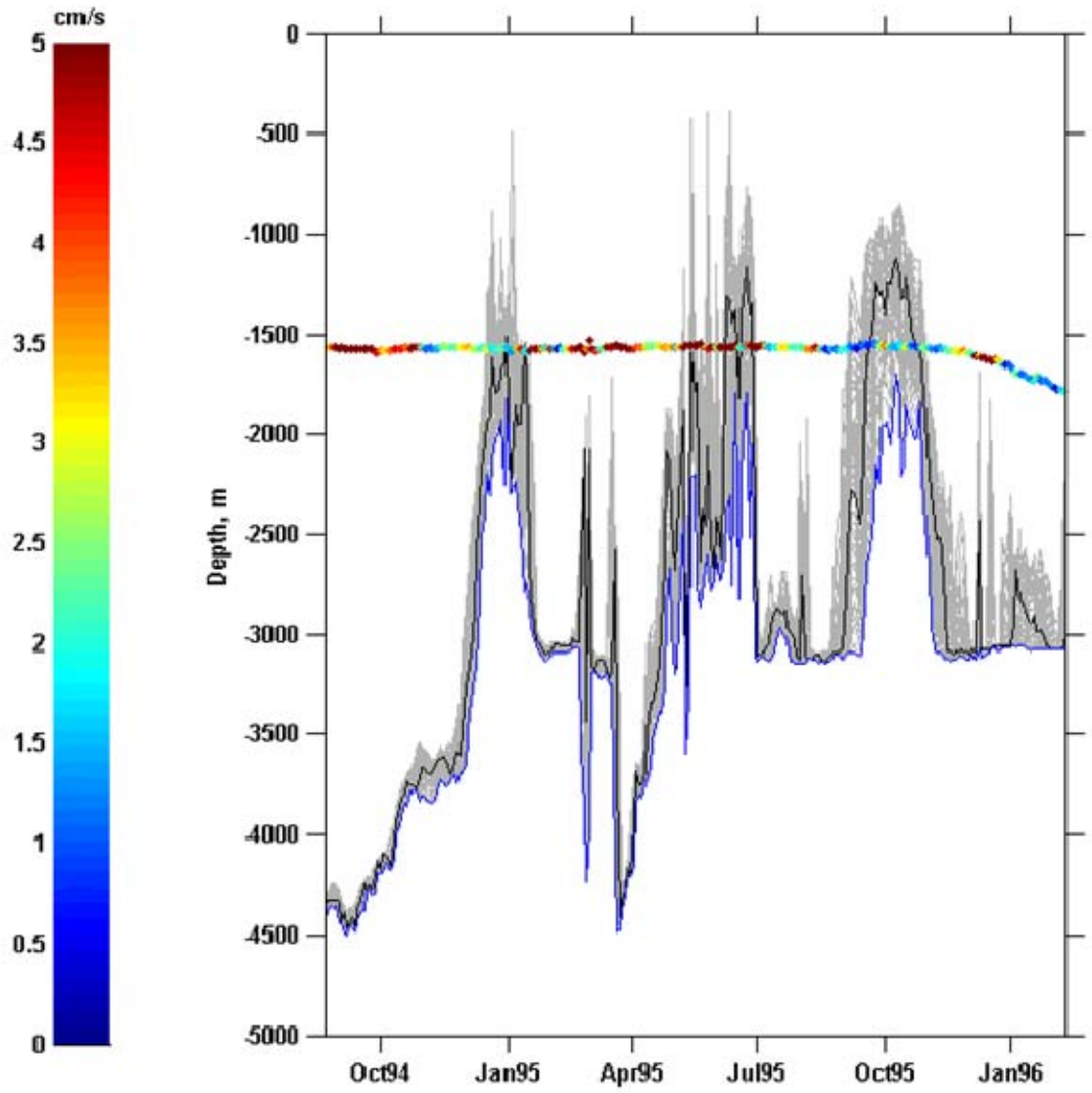

Figure M3. Bathymetry during the RAFOS 15 float mission. The solid black line indicates the ocean depth using the float position and the Sandwell 2' bathymetry (Smith and Sandwell, 1997). The grey indicates the range of possible depths within 10 km; the blue line indicates the maximum depth in this range. The multicolored line indicates the measured RAFOS depth, where the colors correspond to the RAFOS float speed given in cm/s by the bar on the left; speeds greater than 5 cm/s are dark red.

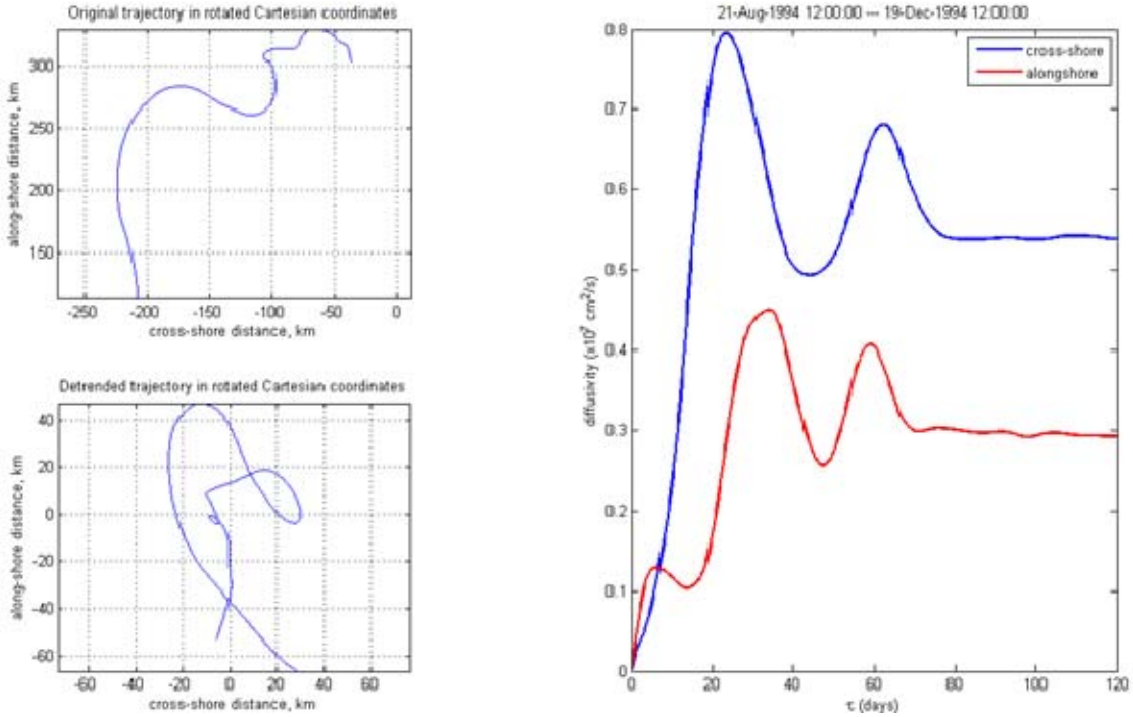

Figure M4. Diffusivity estimate for the first 120 days of RAFOS 15 drift. (upper left) Original trajectory in Cartesian coordinates. (lower left) Detrended trajectory in a coordinate system rotated by 030°. (right) Diffusivity, cm^2/s.

Launch				Surface		Sampling rate	RAFOS performance		Mission, days	
Date	$\frac{\varphi^o\text{N}}{\lambda^o\text{W}}$	T, ºC	Pressure, dbar	Date	$\frac{\varphi^o\text{N}}{\lambda^o\text{W}}$		Planned pressure, dbar	Actual pressure and temperature	Planned	Actual
21 August 1994	37.83ºN 125.87 ºW	2.72	1579	Feb. 22 1996	42.76 ºN 125.636 ºW	1 every two days	1500	1586.1 ± 8.72 2.8 ± 0.04	925	538

Table M1. RAFOS 15 deployment data. The pressure and temperature in this table were calculated from the data prior to the float's sinking in the last 100 days of its deployment.

Cross-shore diffusivity (σ_{UU} ,cm^2/s)	Alongshore diffusivity (σ_{VV} ,cm^2/s)	Diffusivity ratio ($\frac{\sigma_{VV}}{\sigma_{UU}}$)	Period of estimates
0.54	0.3	0.162	21 Aug. 1994 – 19 Dec. 1994
1.07	0.54	0.5	19 Dec. 1994 – 18 April 1995
2.22	0.24	0.11	18 April 1995 – 16 Aug. 1995
0.07	0.02	0.29	16 Aug. 1995 – 14 Dec. 1995
0.47	0.12	0.26	14 Dec. 1995 – 10 Feb. 1996

Table M2. RAFOS 15 Diffusivity Estimates.

THIS PAGE INTENTIONALLY LEFT BLANK

APPENDIX N RAFOS FLOAT 16

RAFOS 16 was paired with RAFOS 15. RAFOS 16 was launched 188.5 km to the west of San Francisco on 22 August 1994 at a water depth of 4050m, a day later than RAFOS 15 and a distance (bearing) of 125 km (102°T) from RAFOS 15. The mission was planned and executed for 925 days, so RAFOS 16 surfaced about one year after RAFOS 15 on 4 March 1997.

Figure N1 displays the pressure and temperature recorded by RAFOS 16. There appear to be problems with both sensors. Temperatures of 2.595°C and 2.665°C appeared too frequently. Pressure tended to increase gradually with time, except for large decreases on about 15 May 1996 (50 dbar) and on 28 October 1996 (20 dbar). Following the latter decrease, the rate of pressure increase was 40 m per month, which is indicative of leaking, albeit at a little less than half the rate of RAFOS 15. Temperature vs. pressure curves were compared with those from deep CTD casts in the area; the lower (deeper, colder) RAFOS 16 data were within the range of the CTD data, but temperatures at shallower RAFOS pressures (1600 to 1650 dbar) corresponded to CTD temperature at lower pressure (1500 to 1550 dbar). The last recorded pressure was 1802 dbar. The mean pressure (temperature) for the entire deployment was 1657 dbar (2.61°C) with a standard deviation of 35.3 dbar (0.09°C).

Figure N2 shows the trajectory of RAFOS 16. Unlike the northward drift of RAFOS 15, the track of RAFOS 16 remained within an approximately 2.5° latitude by 3.25° longitude region off Central California, and the float surfaced just 31 km southwest of its launch position. The track is complex, with closed loops ranging from 10 to 80 km in diameter, both cyclonic and anticyclonic movement, and multiple flow reversals. After launch the float moved in the opposite direction of NPS 15. But during fall 1994 it followed an anticyclonic loop to the west, moving northward then onshore, where, instead of returning to the launch point, it continued to drift northward. In December 1994, the flow reversed and meandered to the southeast, reaching the track's most southern position on 9 May 1995. RAFOS 16 then moved inshore cyclonically, and thence northward to its most northern point, arriving on 24 July 1995, while moving

anticyclonically toward the coast. It continued moving anticyclonically around an 80 km diameter feature and then repeated a second 80 km anticyclonic loop somewhat to the south. In early October 1995, it left the anticyclonic feature and moved cyclonically through another 80 km loop, completing a figure "8" and turning toward the coast in mid November 1995. On 17 December 1995 the eastward motion ceased, and the track subsequently followed a smaller figure "8" with loops of 30 km diameter, first anticyclonically around the northern loop and then cyclonically around a southern loop. (A second 10 km diameter loop was circumscribed in the southern loop.)

On 16 March 1996 the northward flow reversed, and then reversed again on 7 May 1996, moving northward again along the portion of the RAFOS 16 track that was closest to shore. On 16 June 1996 the float began to move southward, away from the coast and thence anticyclonically around another 80 km loop, and then to the south-southeast, looping cyclonically (eastward) to flow northward again for two weeks beginning on 9 November 1996. After a period of south-southeastward motion, the track turned back upon itself on 10 January 1997 and RAFOS 16 moved north-northeastward until it surfaced on 4 March 1997.

Figure N3 shows the bathymetry RAFOS 16 traversed. Around April to May 1995 the RAFOS trajectory flows in shallow depths, and Figure N3 displays a mountainous peak where the float could have run aground. But analyzing the speed bar indicates this was not the case, because the speed of the float remained above 5 cm/s. The next instance the float could have run aground was around the May 1996 timeframe. Although the float would appear to be above the bathymetry, the speed bar indicates the float slowed to below 0.5 cm/s and that it 'jumped' in depth, indicating that the float could have hit a seamount.

The along- and cross-shore diffusivity estimates for the first 120 days of the RAFOS 16 mission are shown in Figure N4, and estimates for this as well as the subsequent periods are tabulated in Table N2. Given the complex character of the flow during the mission, alongshore (cross-shore) diffusivity estimates varied greatly by about two (three) orders of magnitude. For two estimates (22 August 1994 to 20 December 1994 and 11 August 1996 to 9 December 1996), the cross-shore diffusivity was greater

than the alongshore diffusivity. The mean alongshore (cross-shore) diffusivity for RAFOS 16 was 1.29 (0.6) cm^2/s and the mean diffusivity ratio was 6.36.

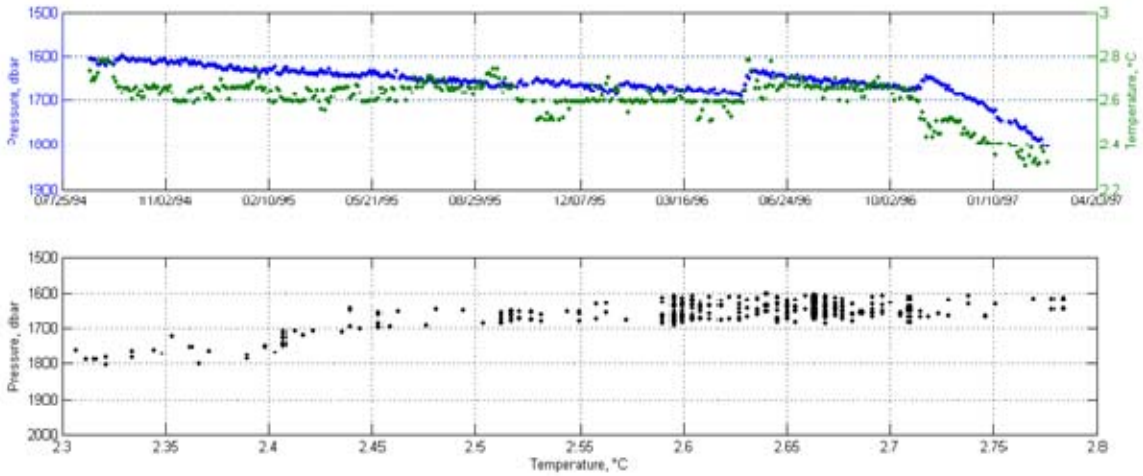

Figure N1. Temperature and Pressure data for RAFOS 16. (upper) Time series. (lower) Temperature versus pressure.

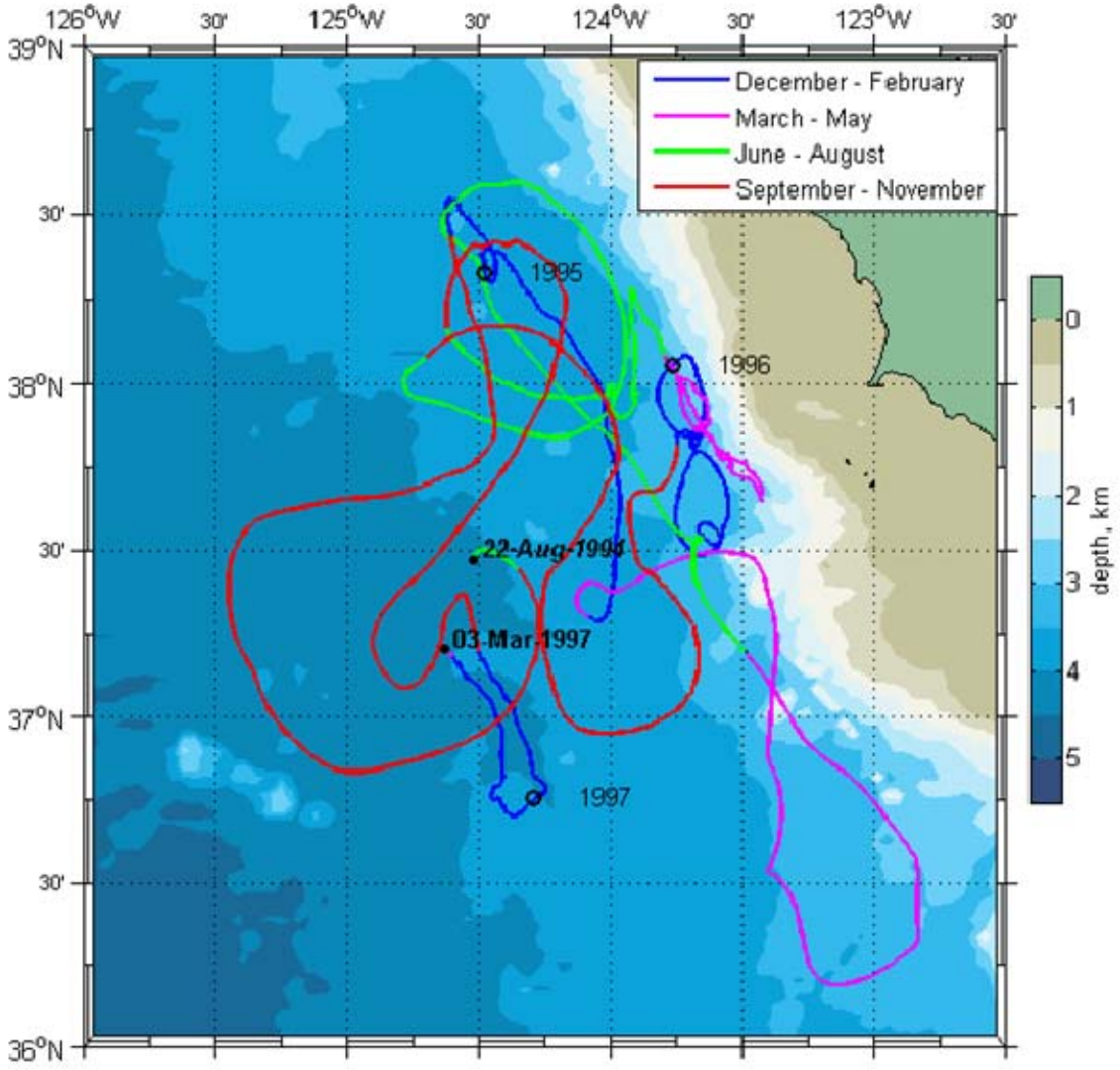

Figure N2. The trajectory for RAFOS 16. Trajectory color indicates season (upper right legend).

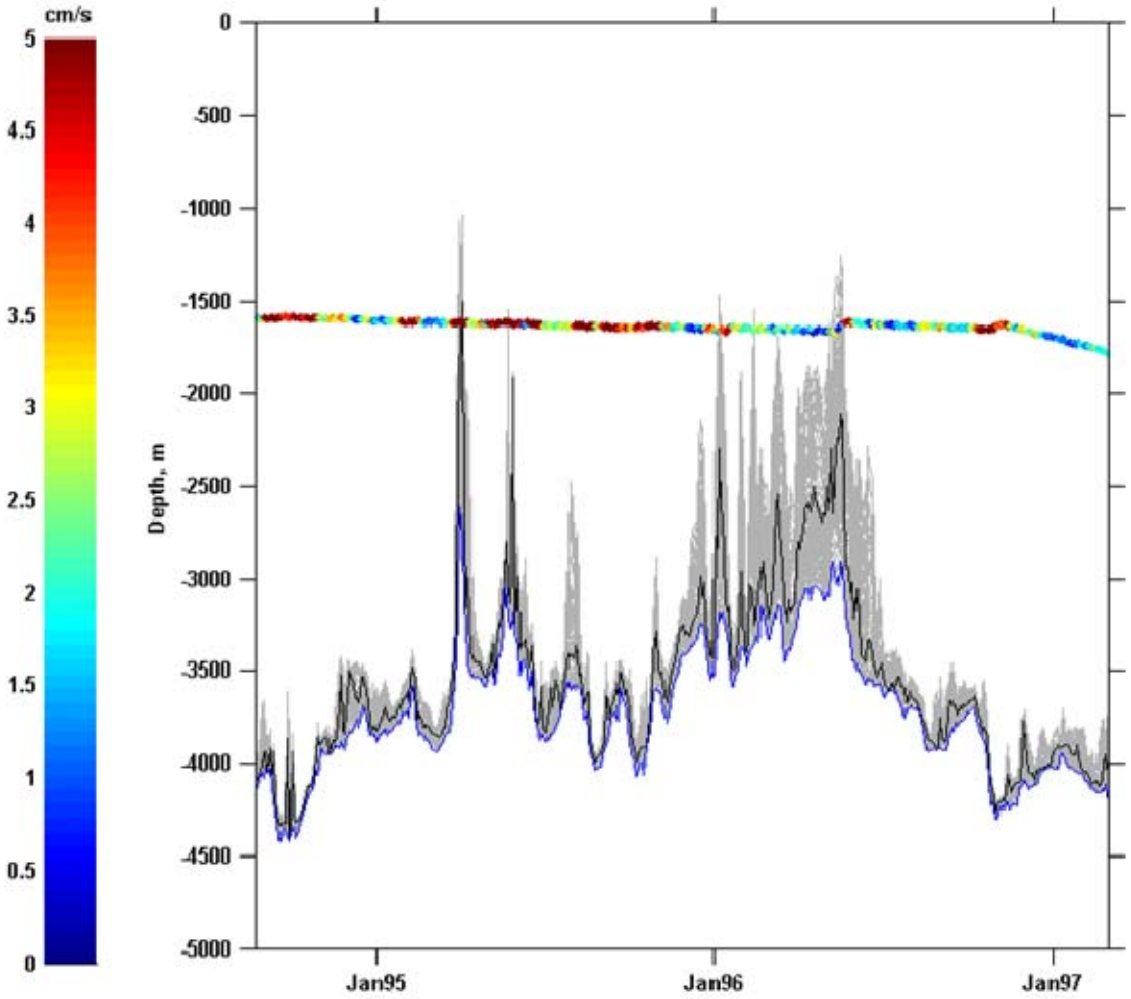

Figure N3. Bathymetry during the RAFOS 16 float mission. The solid black line indicates the ocean depth using the float position and the Sandwell 2' bathymetry (Smith and Sandwell, 1997). The grey indicates the range of possible depths within 10 km; the blue line indicates the maximum depth in this range. The multicolored line indicates the measured RAFOS depth, where the colors correspond to the RAFOS float speed given in cm/s by the bar on the left; speeds greater than 5 cm/s are dark red.

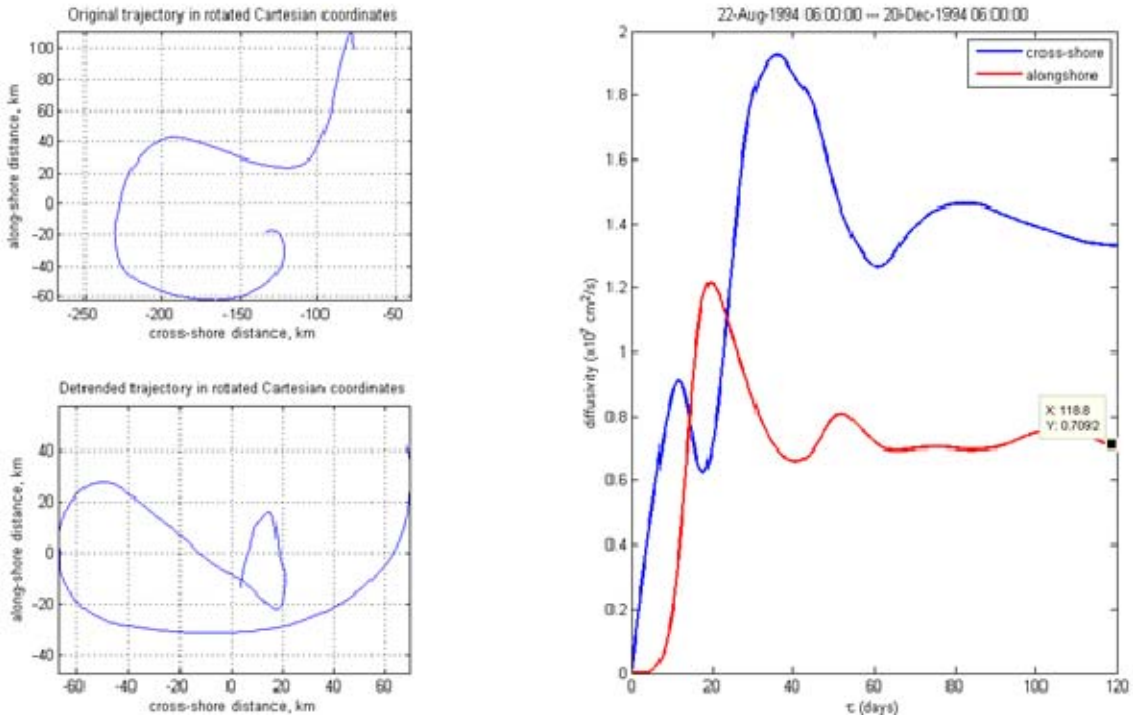

Figure N4. Diffusivity estimate for the first 120 days of RAFOS 16 drift. (upper left) Original trajectory in Cartesian coordinates. (lower left) Detrended trajectory in a coordinate system rotated by 030°. (right) Diffusivity, cm^2/s.

Launch				Surface		Sampling rate	RAFOS performance		Mission, days	
Date	$\frac{\varphi^o\text{N}}{\lambda^o\text{W}}$	T, ºC	Pressure, dbar	Date	$\frac{\varphi^o\text{N}}{\lambda^o\text{W}}$		Planned pressure, dbar	Actual pressure and temperature	Planned	Actual
22 August 1994	37.47ºN 124.52 ºW	2.74	1606	March 4 1997	37.208 ºN 124.632 ºW	once every two days	1500	1656.9 ± 35.3 2.61 ± 0.09	925	925

Table N1. RAFOS 16 deployment data.

Cross-shore diffusivity (σ_{UU} ,cm^2/s)	Alongshore diffusivity (σ_{VV} ,cm^2/s)	Diffusivity ratio ($\frac{\sigma_{VV}}{\sigma_{UU}}$)	Period of estimates
1.34	0.71	0.53	22 Aug. 1994 – 20 Dec. 1994
0.06	0.24	4	20 Dec. 1994 – 19 April 1995
0.39	5.2	13.3	19 April 1995 – 17 Aug. 1995
2.11	3.45	1.64	17 Aug. 1995 – 15 Dec 1995
0.06	0.21	3.5	15 Dec. 1995 – 13 April 1996
0.008	0.185	23.13	13 April 1996 – 11 Aug. 1996
0.49	0.25	0.51	11 Aug. 1996 – 09 Dec. 1996
0.016	0.068	4.25	09 Dec. 1996 – 03 March 1997

Table N2. RAFOS 16 Diffusivity Estimates.

APPENDIX O RAFOS FLOAT 37

RAFOS 37 was launched on 16 April 1996 in a hydrothermal plume over Gorda Ridge. RAFOS 37 surfaced on 10 June 1996. Results of this 56-day mission have been described by Lupton *et al* (1998). Details of this mission are given in Table O1. Figure O1 shows the pressure and temperature data for RAFOS 37 (see also *Ibid.,* Fig. 5). The inverse relationship between temperature and pressure indicate that the float did not leak. The mean pressure (temperature) for the entire deployment was 2204.9 dbar (2.1°C) with a standard deviation of 4.6 dbar (0.2°C).

Figure O2 shows the trajectory of RAFOS 37. The interpretation of the trajectory given below is from Lupton *et al* (1998):

"The float track described several large anticyclonic circles with mean diameter of 6.6 km. This is precisely the sense and approximate diameter of rotation expected for a float entrained into a circulating event plume in the Northern Hemisphere. The mean rotational period of the float was 8.5 days, the net velocity was ~0.5 cm/s, and its particle velocity averaged 2.4 cm/s. Although the float traveled a net distance of only 8.8 km, the total track length was 127 km.

The float motion was both rapid and periodic at the beginning and end of the mission; but during days 18 to 38, the average float speed dropped to ~1.2 cm/s as compared to the average of 2.4 cm/s for the entire float track. The anticyclonic motion seemed to disappear during this 20-day period. The core of each event plume should be in solid body rotation. Thus, this interval of low float speed may be due to migration of the float into the center of the event plume, where the float speed would be lower and the circular motion less pronounced."

The relative vorticity, ζ, was 8.45×10^{-6} rad/s (*Ibid*.).

The along- and cross-shore diffusivity estimates for the entire length of the RAFOS 37 mission are shown in Figure O3. The cross-shore diffusivity is greater than the alongshore diffusivity with a ratio of 0.375.

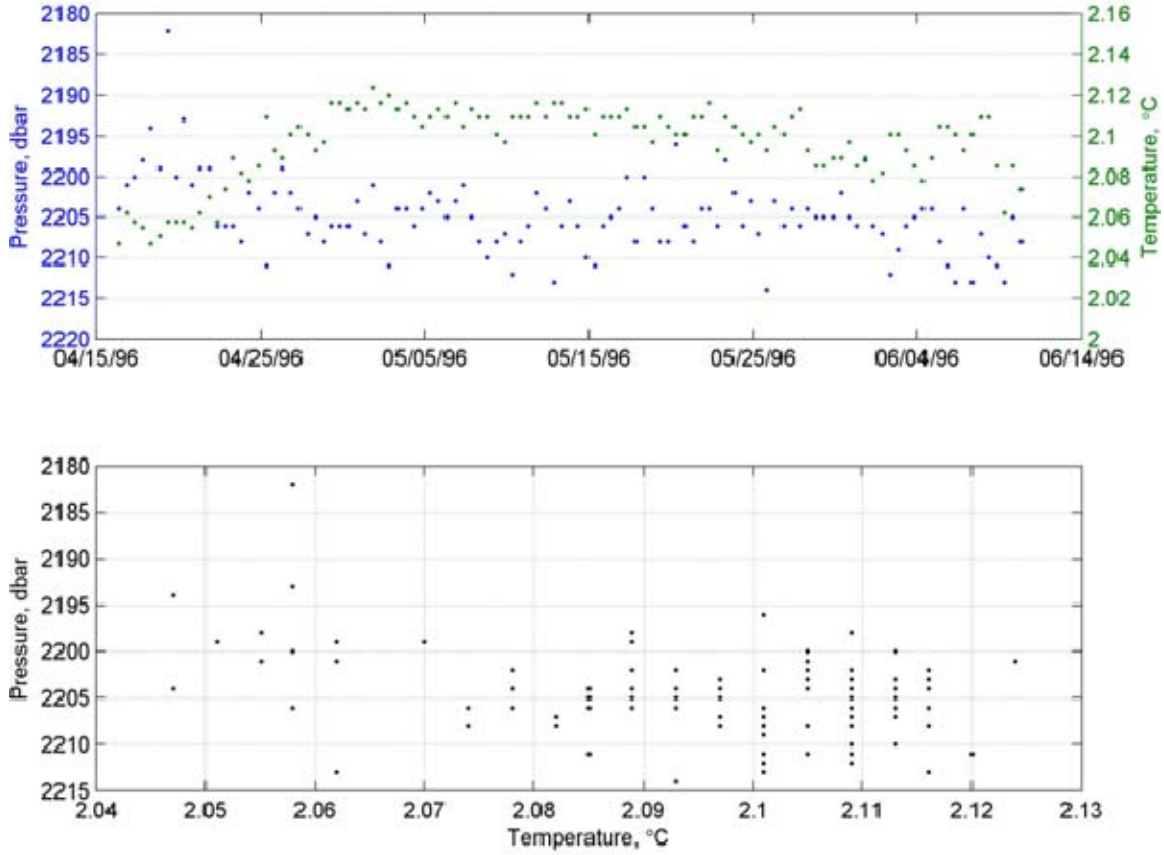

Figure O1. Temperature and Pressure data for RAFOS 37. (upper) Time series. (lower) Temperature vs. pressure.

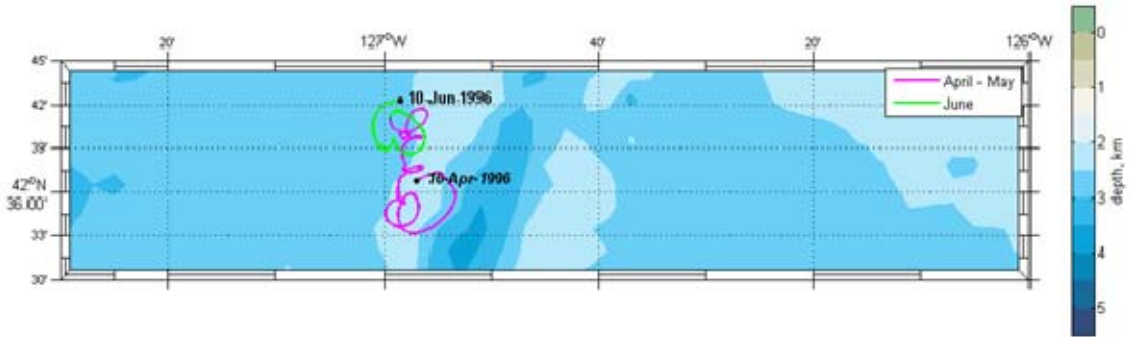

Figure O2. The trajectory for RAFOS 37. Trajectory color indicates season (upper right legend).

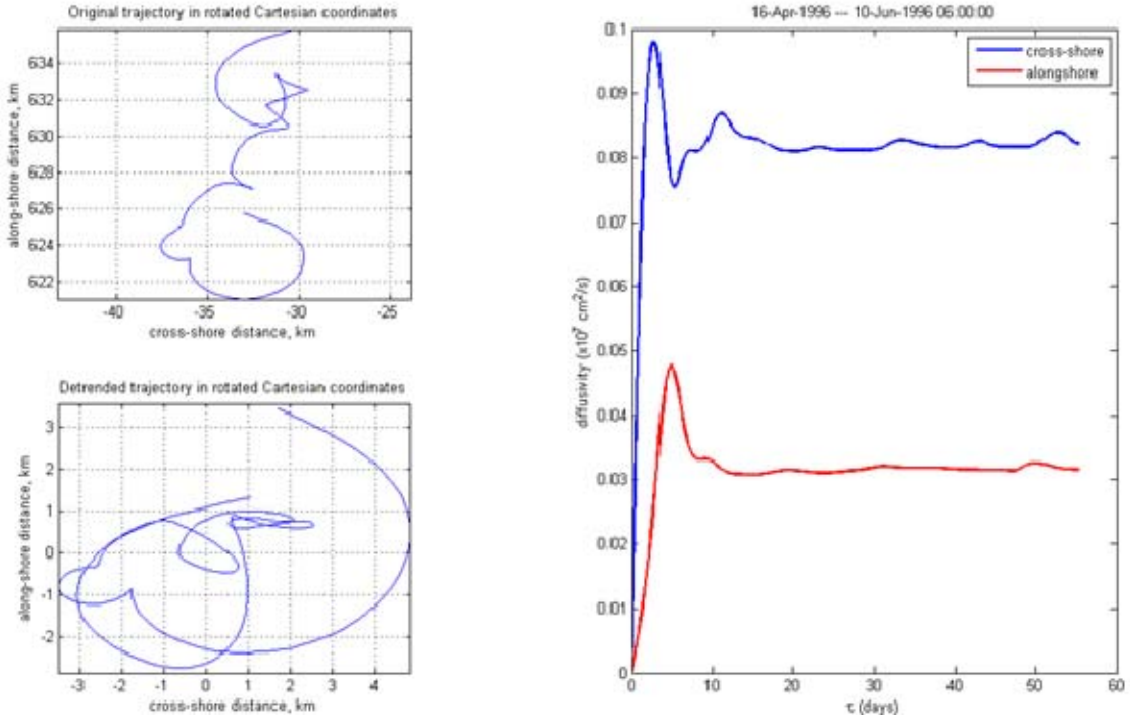

Figure O3. Diffusivity estimate for RAFOS 37. (upper left) Original trajectory in Cartesian coordinates. (lower left) Detrended trajectory in a coordinate system rotated by 030°. (right) Diffusivity, cm^2/s.

Launch				Surface		Sampling rate	RAFOS performance		Mission, days	
Date	$\frac{\varphi^o \mathrm{N}}{\lambda^o \mathrm{W}}$	T, ºC	Pressure, dbar	Date	$\frac{\varphi^o \mathrm{N}}{\lambda^o \mathrm{W}}$		Planned pressure, dbar	Actual pressure and temperature	Planned	Actual
16 April 1996	42.62ºN 126.92ºW	2.05	2204	10 June 1996	42.696 ºN 126.962 ºW	2 per day	1998	2204.9 ± 4.56 2.1 ± 0.02	64	64

Table O1. RAFOS 37 deployment data.

Cross-shore diffusivity (σ_{UU})	Alongshore diffusivity (σ_{VV})	Diffusivity ratio ($\frac{\sigma_{VV}}{\sigma_{UU}}$)	Period of diffusivities
0.08	0.03	0.375	16 April 1996 – 10 June 1996

Table O2. RAFOS 37 Diffusivity Estimate.

THIS PAGE INTENTIONALLY LEFT BLANK

APPENDIX P RAFOS FLOAT 38

RAFOS 38 was launched on 17 June 1996 (one week after RAFOS 37 surfaced) over Gorda Ridge at the position where RAFOS 37 surfaced. Details of this mission are given in Table P1. The mission was part of the NOAA Vents program. The mission was planned for 434 days, but the float surfaced early after 126 days. Figure P1 displays the pressure and temperature recorded by RAFOS 38. The initial pressure (temperature) was 2146 dbar (2.079°C), and during the first ten days the pressure (temperature) increased (decreased) by about 40 m (0.13°C). After 30 days, the pressure seemed to stabilize for about a month, and then commenced to sink steadily at about 10 m per month. Two days before the mission ended, the pressure (temperature) increased (decreased) suddenly from 2225 dbar (2.011°C) to 2658 dbar (1.935°C), the RAFOS float exceeded its bailout depth, dropped its ballast and surfaced. The cause of this behavior was most likely a seawater leak.

Figure P2 shows a smoothed trajectory of the RAFOS 38 float. The float initially continued the northward movement previously observed by RAFOS 37. On 13 July, as the float moved eastward away from Gorda Ridge, it continued to turn anticyclonically, subsequently moving southward along the eastern flank of Gorda Ridge. On 22 August, the float reached its most southern point while continuing to move anticyclonically, reversing course again to nearly retrace its path back to the north before surfacing over the western flank of Gorda Ridge on 20 October 1996.

The float trajectory included a number of shorter period movements at periods from ten to twenty days. No attempt is made here to resolve these features or to relate them to possible hydrothermal plumes. Although both hyperbolic and circular navigation were used for navigation of RAFOS 38, both navigation results yielded noisy positions, in part because the hyperbolae of position diverge at long distance from the sound sources. Better navigation could result from improved understanding of the sound speed.

The along- and cross-shore diffusivity estimate for the RAFOS 38 mission is shown in Figure P3. The cross-shore diffusivity, 0.04, was lesser than the alongshore diffusivity, 0.042, with a ratio of 1.05.

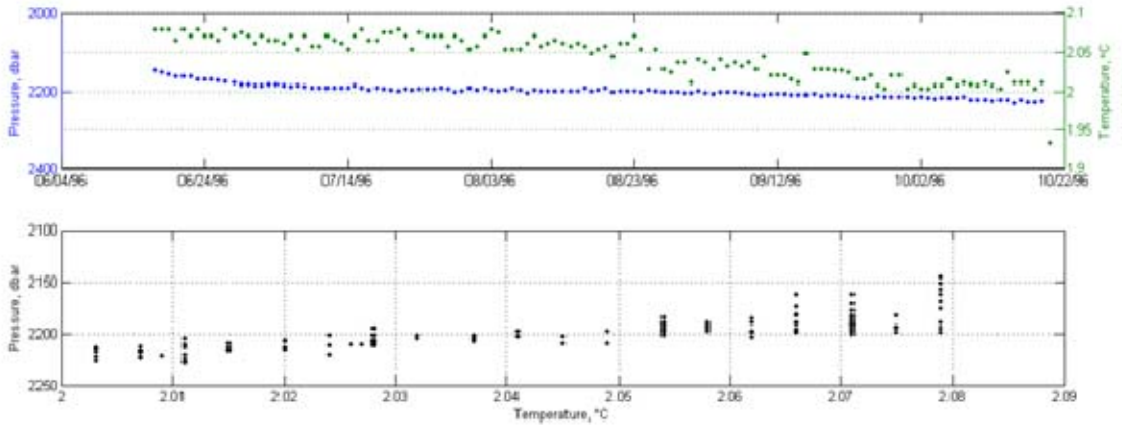

Figure P1. Temperature and Pressure data for RAFOS 38. (upper) Time series. (lower) Temperature versus pressure.

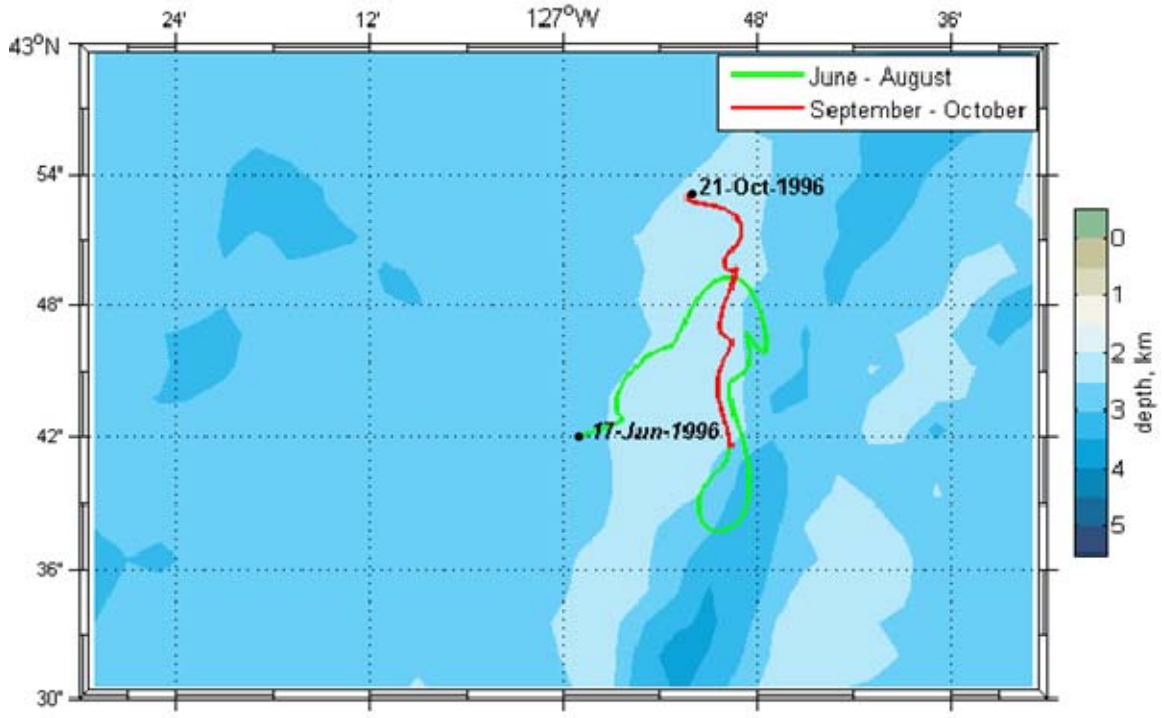

Figure P2. The trajectory for RAFOS 38. Trajectory color indicates season (upper right legend).

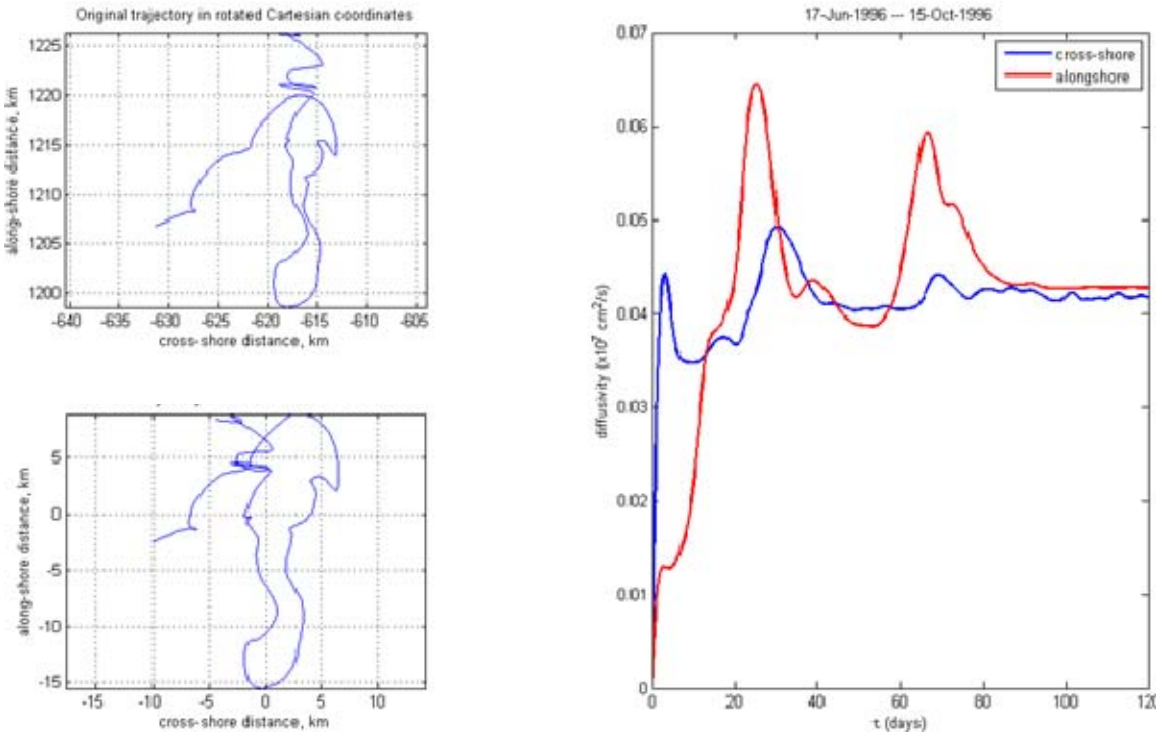

Figure P3. Diffusivity estimate for the RAFOS 38 drift. (upper left) Original trajectory in Cartesian coordinates. (lower left) Detrended trajectory. (right) Diffusivity.

Launch				Surface		Sampling rate	RAFOS performance		Mission, days	
Date	$\frac{\varphi^o \text{N}}{\lambda^o \text{W}}$	T, ºC	Pressure, dbar	Date	$\frac{\varphi^o \text{N}}{\lambda^o \text{W}}$		Planned pressure, dbar	Actual pressure and temperature	Planned	Actual
17 June 1996	42.7ºN 126.98ºW	2.08	2146	20 October 1996	42.874 ºN 126.913 ºW	1 per day	1998	2202.5 ± 43.88 2.04 ± 0.03	434	126

Table P1. RAFOS 38 deployment data.

Cross-shore diffusivity (σ_{UU} ,cm^2/s)	Alongshore diffusivity (σ_{VV} cm^2/s)	Diffusivity ratio ($\frac{\sigma_{VV}}{\sigma_{UU}}$)	Period of estimates
0.04	0.042	1.05	17 June 1996 – 15 Oct. 1996

Table P2. RAFOS 38 Diffusivity Estimate.

THIS PAGE INTENTIONALLY LEFT BLANK

APPENDIX Q RAFOS FLOAT 44

RAFOS 44 was launched on 28 August 1996 and surfaced on 23 October 1996. Details of this mission are given in Table Q1. The mission was planned for 925 days but the float surfaced early at 57 days due to leakage. Figure Q1 displays the pressure and temperature recorded by RAFOS 44. The pressure measurements show an increasing pressure throughout the float's short mission, indicating that the float started to leak shortly after its launch. The initial pressure was 1701 dbar and the last recorded pressure was 2004 dbar, this pressure increase occurring over a 57 day period and indicating the instability of the float. When the float reached this final pressure, its bailout point had been exceeded and the float surfaced and transmitted its data. The temperature decreased as pressure increased, indicating a normal inverse relationship between temperature and pressure.

Figure Q2 shows the trajectory of the RAFOS 44 float. The float moved in a southwesterly direction after launch then shifted to a northwesterly direction, the heading on which it would remain until near the end of its deployment, where the float moved in a northeasterly heading then shifted to a northwesterly heading.

The along- and cross-shore diffusivity estimates for the length of the RAFOS 44 mission are shown in Figure Q3. The cross-shore diffusivity is greater than the alongshore diffusivity with a ratio of 0.421.

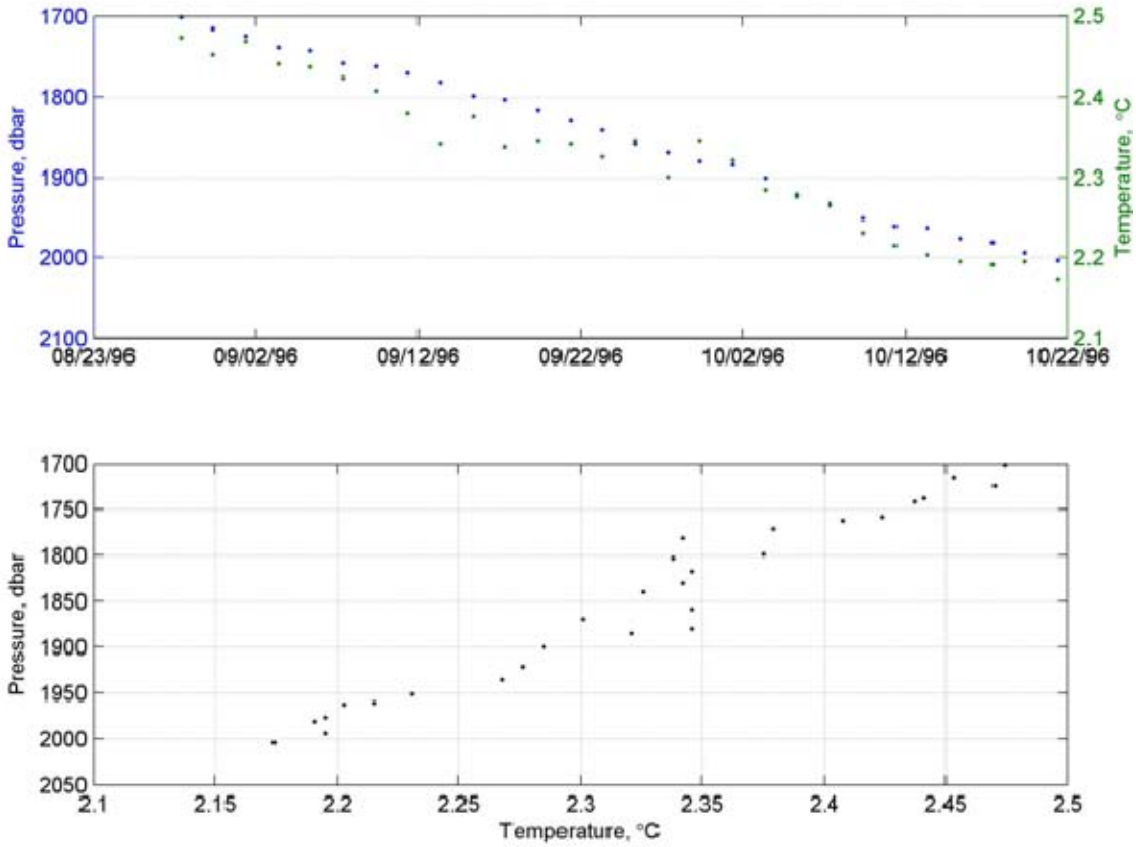

Figure Q1. Temperature and Pressure data for RAFOS 44. (upper) Time series. (lower) Temperature versus pressure.

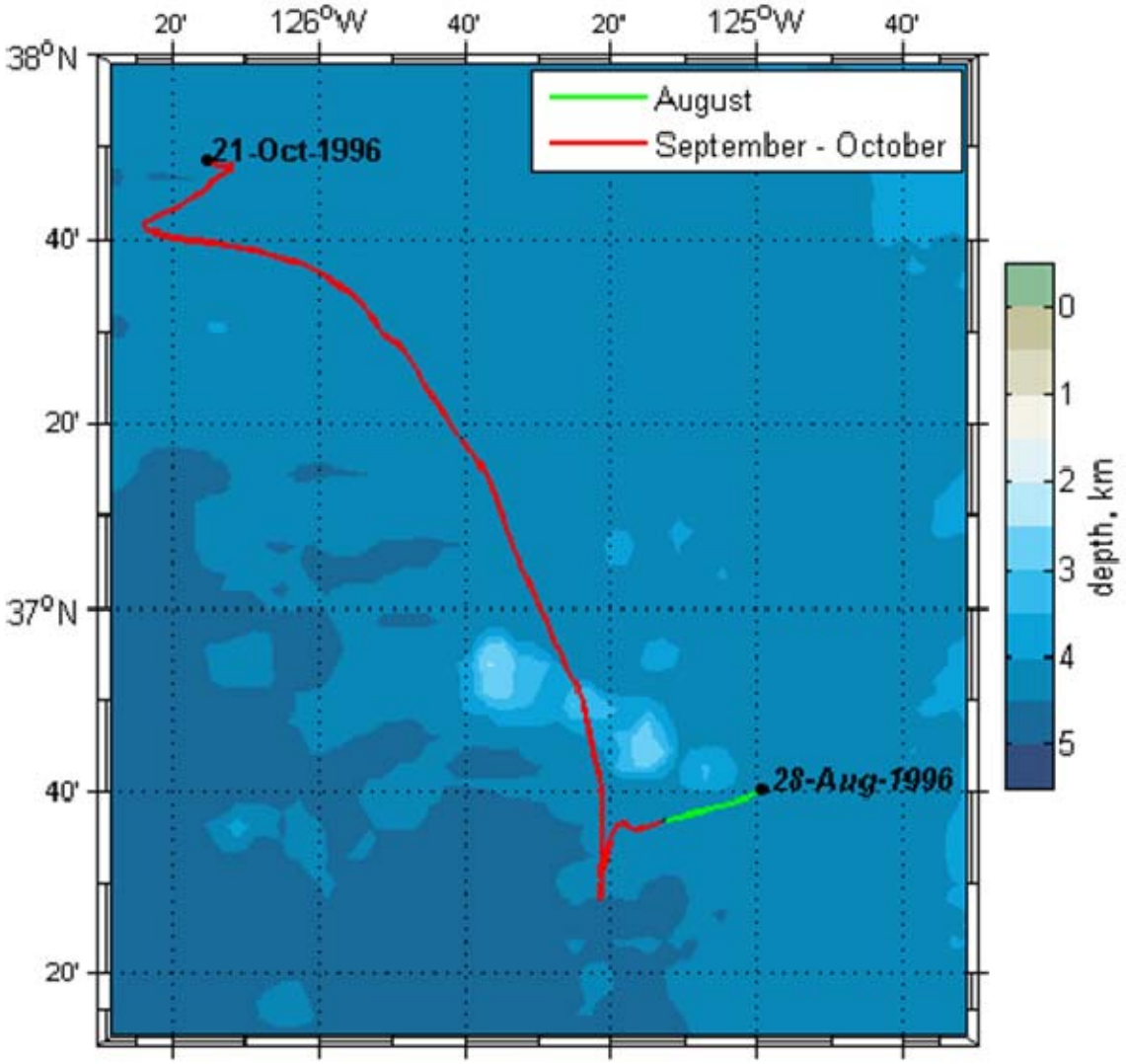

Figure Q2. The trajectory for RAFOS 44. Trajectory color indicates season (upper right legend).

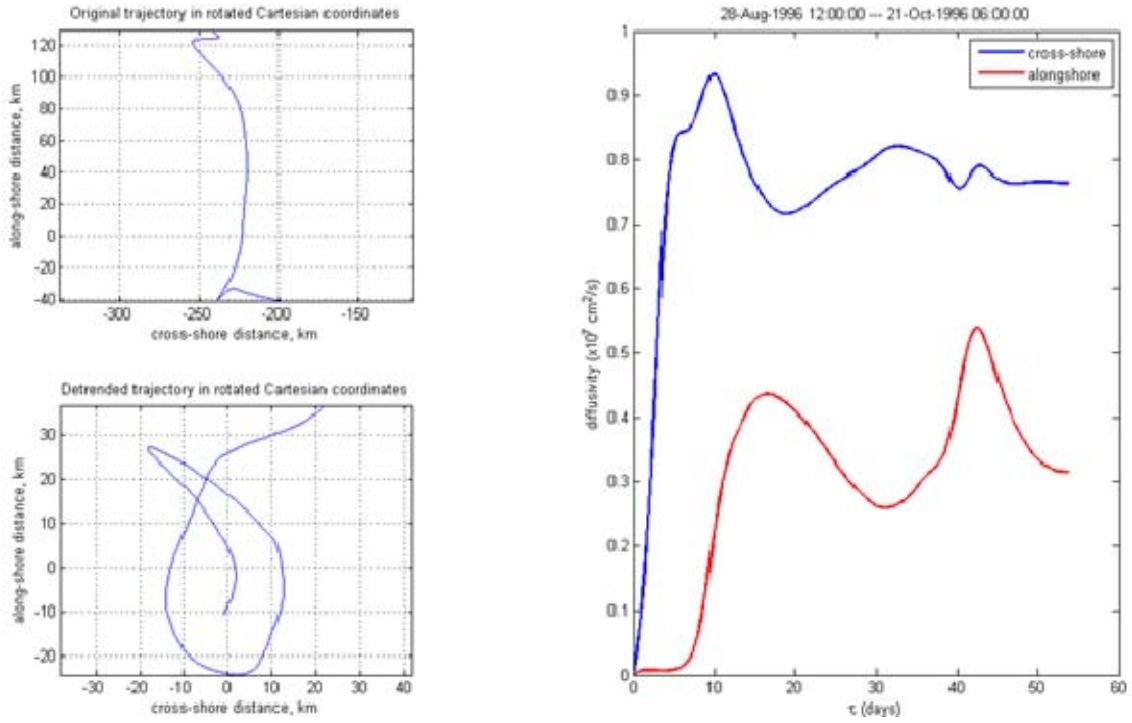

Figure Q3. Diffusivity estimate for the RAFOS 44 drift. (upper left) Original trajectory in Cartesian coordinates. (lower left) Detrended trajectory in a coordinate system rotated by 030°. (right) Diffusivity, cm^2/s.

Launch				Surface		Sampling rate	RAFOS performance		Mission, days	
Date	$\frac{\varphi^o \text{N}}{\lambda^o \text{W}}$	T, ºC	Pressure, dbar	Date	$\frac{\varphi^o \text{N}}{\lambda^o \text{W}}$		Planned pressure, dbar	Actual pressure and temperature	Planned	Actual
28 August 1996	36.7ºN 125ºW	2.47	1701	23 October 1996	37.814 ºN 126.287 ºW	1 every other day	1500	1852 ± 95 2.33 ± 0.09	925	56

Table Q1. RAFOS 44 deployment data.

Cross-shore diffusivity (σ_{UU} ,cm^2/s)	Alongshore diffusivity (σ_{VV} ,cm^2/s)	Diffusivity ratio ($\frac{\sigma_{VV}}{\sigma_{UU}}$)	Period of estimates
0.76	0.32	0.421	28 Aug. 1996 – 21 Oct. 1996

Table Q2. RAFOS 44 Diffusivity Estimate.

THIS PAGE INTENTIONALLY LEFT BLANK

APPENDIX R RAFOS FLOAT 58

RAFOS 58 was the last NOAA Vents RAFOS mission. It was launched on 29 September 1997 over the axis of Juan de Fuca Ridge. The float surfaced early on 06 May 1998, but did not broadcast until its scheduled mission end on 14 September 1998. Due to this discrepancy there was not an exact surface position recorded, so it was difficult to estimate the actual float clock drift. The float clock drift was estimated from the time difference between the Argos satellites and the internal clock of the RAFOS float. For the source clock drifts, the results from Pt. Sur SOSUS monitoring were used directly for source 2 and indirectly for source 5 (i.e., source drifts for sources 1 through 3 were averaged and then assumed to be the source 5 drift, since source 5 cannot be received at Pt. Sur). The pressure and temperature time series for RAFOS 58 are shown in Fig. R1 (upper). The maximum (minimum) temperature was 25.56°C (1.93°C) measured on 18 October 1997 (07 December 1997). It should be noted that neither the maximum nor minimum temperature is displayed on Fig. R1. The mean temperature is 2°C, which includes this unusual spike of 25.56°C. This temperature spike can be explained by either a volcanic plume or bad instrument measurement; it is difficult to determine which the case is. The maximum (minimum) pressure was 2033 dbar (2010) measured on 08 February 1998 (03 October 1997). The shape of the pressure/temperature graph shows the float gradually moving to a greater depth and lower temperature until the ballast weights unexpectedly release where after the float recorded decreased pressure. For the last 22 days of the mission before weight release, pressure decreased from 2024 dbar to 2015 dbar. Temperature did not appear to depend upon pressure (Fig. R1, lower). These results suggest that the float surfaced early due to loss of ballast weights.

Figure R2 shows the trajectory of RAFOS 58. The mean speed for the length of the deployment was 3.64 cm/s with a vector mean flow (direction) of 0.9 cm/s (259.2°T). The float track consisted of a series of six anticyclonic perturbations, five to the north and one to the south, spaced about equally along the mean track. Dates associated with the latitude extremes of each of these loops were: 27 October 1997, 23 November 1997, 25

December 1997, 20 January 1998 (southward excursion), 19 February 1998, and 05 April 1998.

For the first period measured, the cross-shore diffusivity (0.15) is considerably larger than the alongshore diffusivity (0.05) with a ratio of 0.33. During the second period, the diffusivities reversed and the alongshore diffusivity (0.12) was considerably larger than the cross-shore diffusivity (0.075) with a ratio of 1.6. Overall, the diffusivity mean ratio was 0.97, meaning that the dispersion was almost equal in the alongshore and cross-shore directions.

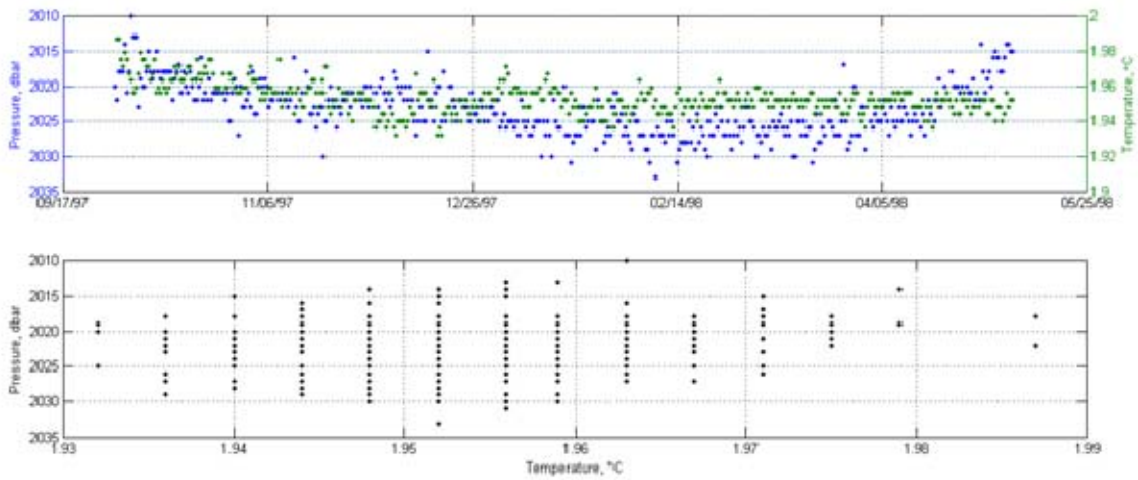

Figure R1. Temperature and Pressure data for RAFOS 58. (upper) Time series. (lower) Temperature versus pressure.

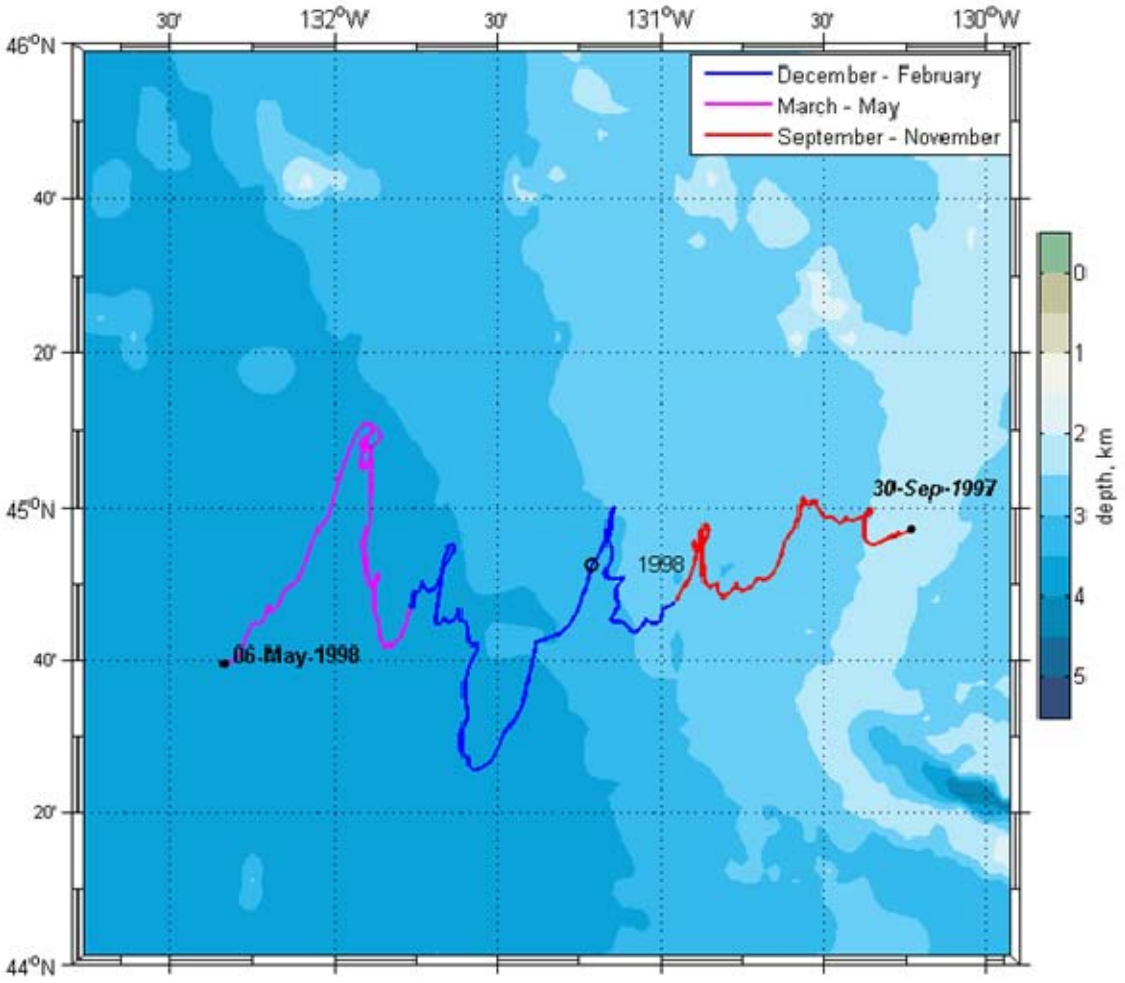

Figure R2. The trajectory for RAFOS 58. Trajectory color indicates season (upper right legend).

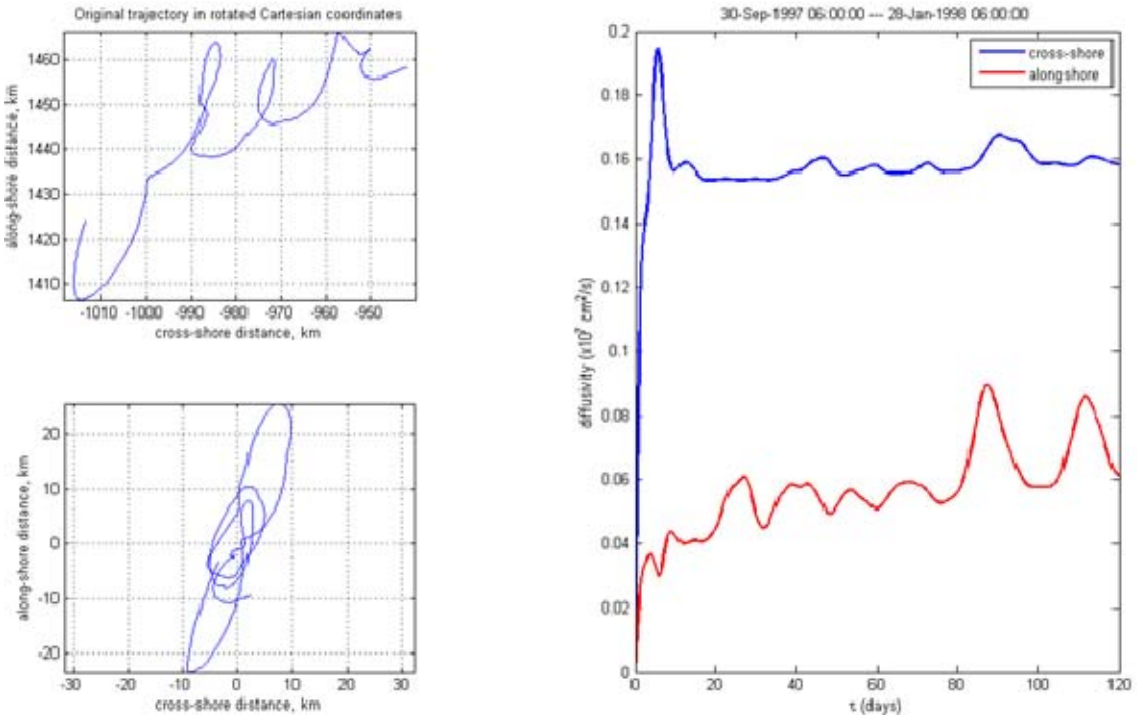

Figure R3. Diffusivity estimate for the RAFOS 58 drift. (upper left) Original trajectory in Cartesian coordinates. (lower left) Detrended trajectory. (right) Diffusivity, cm^2/s.

Launch				Surface		Sampling rate	RAFOS performance		Mission, days	
Date	$\frac{\varphi^o \text{N}}{\lambda^o \text{W}}$	T, ºC	Pressure, dbar	Date	$\frac{\varphi^o \text{N}}{\lambda^o \text{W}}$		Planned pressure, dbar	Actual pressure and temperature	Planned	Actual
29 September 1997	44.97ºN 130.2ºW	1.99	2022	14 Sept. 1998	36.795 ºN 132.329 ºW	2 per day	2000	2023 ± 3.58 2 ± 1.14	350	220

Table R1. RAFOS 58 deployment data. Note: Surface time and position reflect data transmission from, not actual surfacing of, float.

Cross-shore diffusivity (σ_{UU} ,cm^2/s)	Alongshore diffusivity (σ_{VV} ,cm^2/s)	Diffusivity ratio ($\frac{\sigma_{VV}}{\sigma_{UU}}$)	Period of estimates
0.15	0.05	0.33	30 Sept. 1997 – 28 Jan. 1998
0.075	0.12	1.6	28 Jan. 1998 – 07 May 1998

Table R2. RAFOS 58 Diffusivity Estimates.

APPENDIX S RAFOS FLOAT 74

RAFOS 74 was launched adjacent to the continental slope (64 km southwest of Point Sur) in 3105 m of water on 21 November 1999. Table S1 contains specific information on the RAFOS 74 mission. The 450-day mission was successfully completed. RAFOS 74 was an improved float design and included an o-ring seal for the end plate, better temperature and pressure measurement, and increased microprocessor capacity.

The pressure and temperature time series are shown in Fig. S1 (upper). The initial pressure (temperature) was 1520 dbar (2.65°C), but over the next eight days pressure (temperature) increased to 1545 dbar (2.68°C). Pressure generally remained between 1545 and 1555 dbar until 5 November 2000, when pressure increased to 1525 dbar on 30 January 2001. The temperature time series through September 2000 was marked by a series of 8- to 10-day fluctuations which were correlated with an anticyclonic looping motion described below. After 9 March the temperature steadily increased to 2.83°C on 13 October and then decreased to 2.54°C on 1 February 2001. Note that temperature and pressure fluctuations corresponded to circulation features described below. Temperature increased with pressure (Fig. S1, upper), indicating proper isobaric functioning of the float (i.e. it did not leak).

Figure S2 shows the trajectory of RAFOS 74. The mean speed for the entire trajectory is 7.53 cm/s and the vector mean speed (direction) was 0.77 cm/s (294.6°T). For the first ten days after launch, the float moved about 100 km to the north-northwest along the continental slope. It then became entrained in an anticyclonic eddy 80 km west of Monterey. The float spent the winter, spring, summer and the first twenty days of September 2000 trapped in this eddy, for a total of 34 loops of eight to ten days' duration each. These loops varied in size from 5 to 40 km. The eddy initially moved quickly to 37°N, 123°W, then slowly due south. At the end of January 2000, when it had returned to the latitude where it had first captured RAFOS 74, it proceeded to the west-northwest. In April 2000, the eddy was caught in a larger anticyclonic feature, about 45 km in diameter and centered near 37°N, 124.5°W. As RAFOS 74 began a second anticyclonic

transit around this loop, the larger loop appeared to move to the west (centered at 37°N, 125°W) and increase in diameter to 75 km, while the smaller loops shrank in size, finally disappearing on 17 September 2000. RAFOS 74 reached its most northern point on 24 September 2000, and continued anticyclonic movement around the larger loop (centered at 37°N, 125°W) until 13 October 2000, when it was immediately to the north of the easternmost of the Taney Seamounts. At this point, it reversed direction and began a final anticyclonic transit which took it to the east of these seamounts, reaching its westernmost point of 36.7°N, 127.1°W on 14 December 2000. In mid-January 2001, RAFOS 74 began to move cyclonically and crossed just to the east of the westernmost Taney Seamount before surfacing on 12 February 2001.

The cross-shore diffusivity decreased from the first period to the second, then increased from the second to the third, and finally decreased from the third to the fourth. The alongshore diffusivity decreased as the float moved offshore. The diffusivity ratio decreased from 6.85 to 1.6 to 0.18 and 0.202. While the float was closest to the coast, the cross-shore (alongshore) diffusivity was 0.66 cm^2/s (4.52 cm^2/s). When the float was offshore, typical cross-shore (alongshore) diffusivity was 1.53 cm^2/s (0.29 cm^2/s).

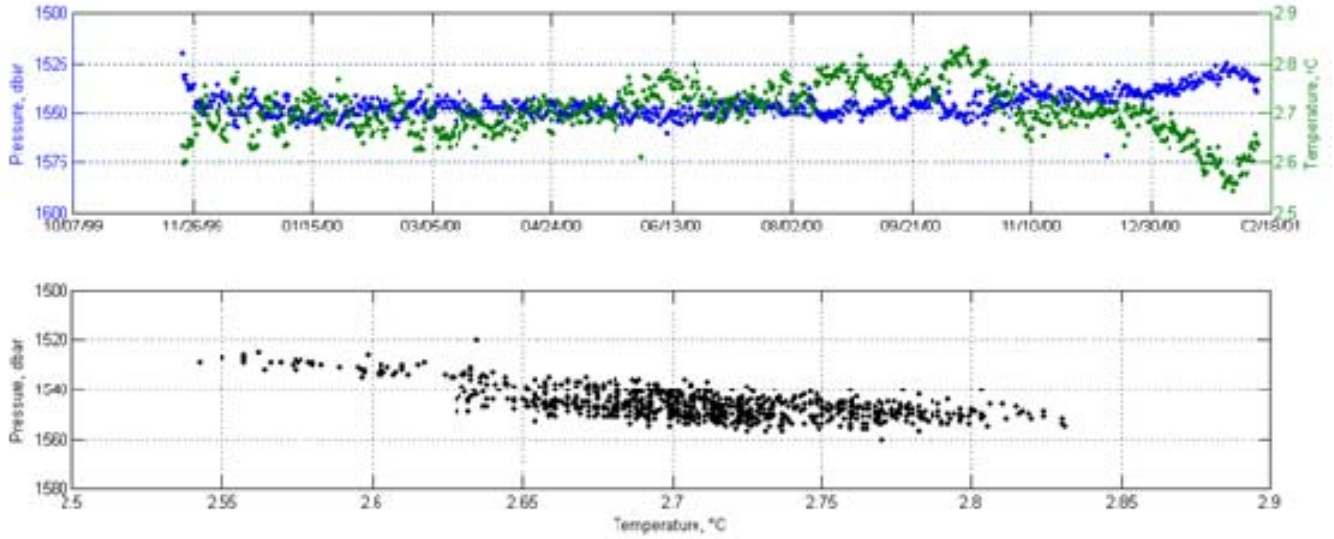

Figure S1. Temperature and Pressure data for RAFOS 74. (upper) Time series. (lower) Temperature versus pressure.

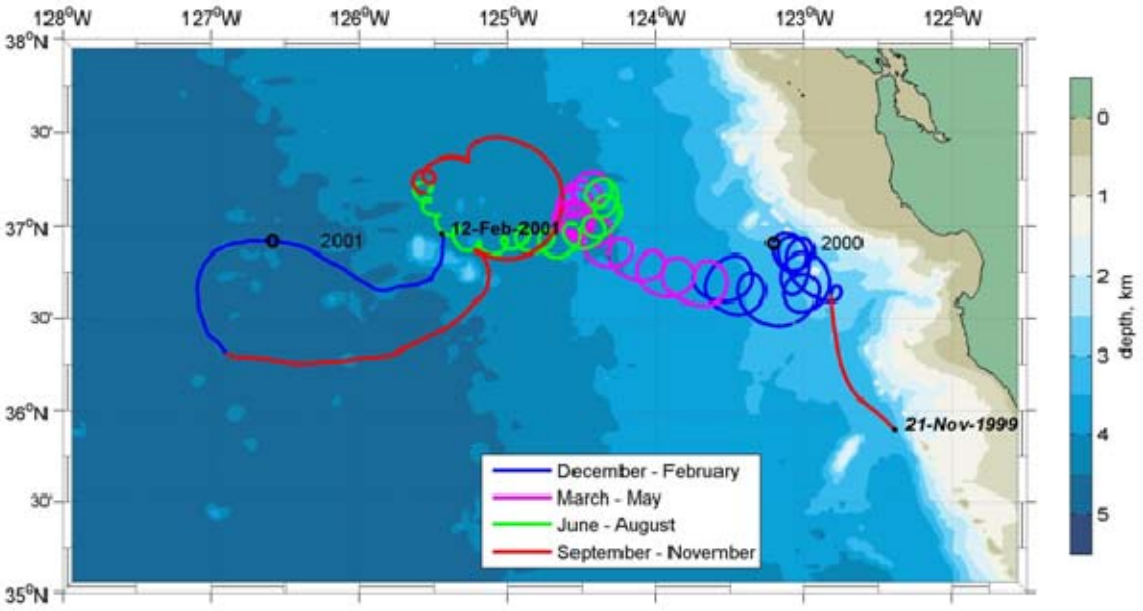

Figure S2. The trajectory for RAFOS 74. Trajectory color indicates season (lower center legend).

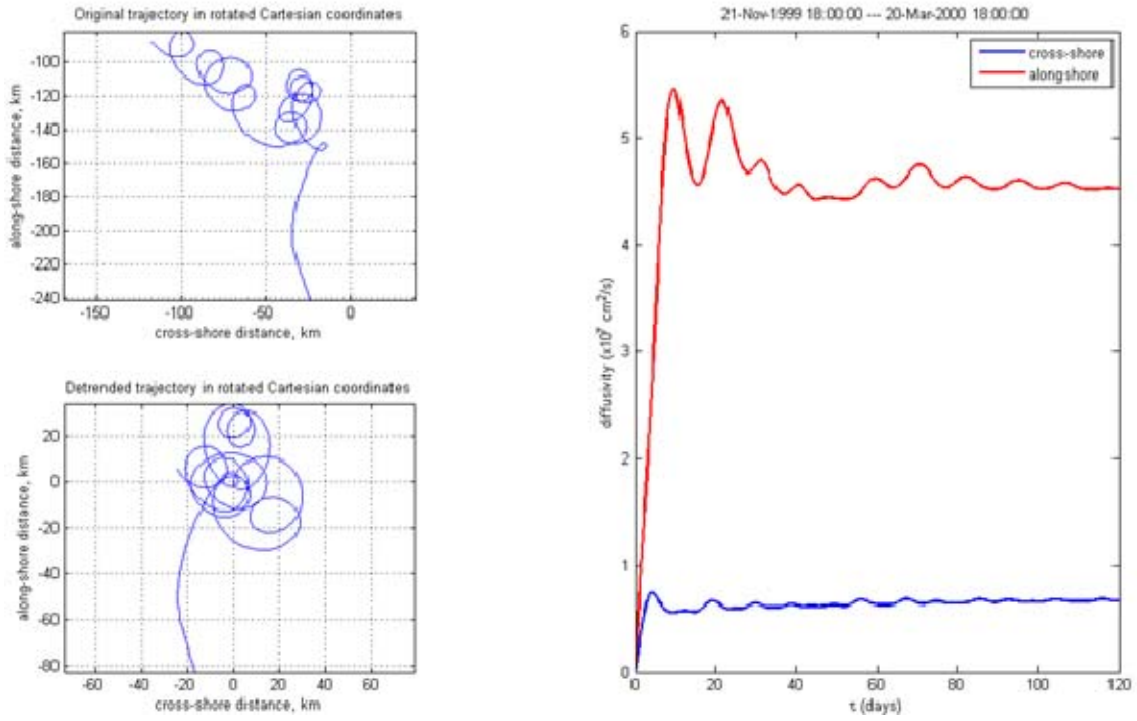

Figure S3. Diffusivity estimate for the RAFOS 74 drift. (upper left) Original trajectory in Cartesian coordinates. (lower left) Detrended trajectory in a coordinate system rotated by 030°. (right) Diffusivity, cm^2/s.

Launch				Surface		Sampling rate	RAFOS performance		Mission, days	
Date	$\frac{\varphi^o \text{N}}{\lambda^o \text{W}}$	T, ºC	Pressure, dbar	Date	$\frac{\varphi^o \text{N}}{\lambda^o \text{W}}$		Planned pressure, dbar	Actual pressure and temperature	Planned	Actual
21 November 1999	35.88ºN 122.38ºW	2.64	1520	12 Feb. 2001	36.965 ºN 125.447 ºW	2 per day	1500	1541.6 ± 37.08 2.7 ± 0.07	450	450

Table S1. RAFOS 74 deployment data.

Cross-shore diffusivity (σ_{UU})	Alongshore diffusivity (σ_{VV})	Diffusivity ratio ($\frac{\sigma_{VV}}{\sigma_{UU}}$)	Period of diffusivities
0.66	4.52	6.85	21 Nov. 1999 – 20 March 2000
0.5	0.8	1.6	20 March 2000 – 18 July 2000
1.83	0.33	0.18	18 July 2000 – 15 Nov. 2000
1.24	0.25	0.202	15 Nov. 2000 – 12 Feb. 2001

Table S2. RAFOS 74 Diffusivity Estimates.

APPENDIX T RAFOS FLOAT 79

RAFOS 79 was launched on 26 July 2000 (about eight months after RAFOS 74) 98.16 km to the west of Moss Landing in water of 3031 m depth. The mission was 666 days, as planned, and the float surfaced on 22 May 2002. Table T1 contains specific information on RAFOS 79.

The planned pressure for RAFOS 79 was 1500 dbar, but the mean observed pressure was considerably less, 1162.5 dbar. Figure T1 upper shows the time series of pressure and temperature for RAFOS 79. The initial pressure (temperature) was 1115 dbar (3.71°C). After launch, the pressure remained less than 1125 dbar until February 2001, when pressure began to increase, reaching 1225 dbar in April 2001. The pressure subsequently remained less than 1225 dbar until 20 June 2001, when pressure began to rapidly increase to 1447 dbar on 26 July 2001. The temperatures for the time period corresponding to this 1447 dbar pressure spike were about 3.5°C, too warm for this depth (Fig T1 lower and upper). Hence pressure data from 20 June through 28 July 2001, are regarded as unreliable, suggesting that all pressure data for RAFOS 79 should be used with caution. Two days after the pressure maximum, the pressures returned to 1125 dbar and remained near this value until RAFOS 79 surfaced.

The mean temperature was 3.48°C. The highest temperature, 3.75°C, occurred four days after launch and subsequently decreased steadily, reaching 3.21°C twenty days before the float surfaced (Fig T1 upper). Two periods of warming, April to May 2001 and June to mid-August 2001, were superimposed on the decreasing temperatures. At times, temperature oscillated at periods of about ten days when RAFOS 79 was looping within a mesoscale eddy (see below).

Given the uncertainty of pressure measurement, the temperature vs. pressure data for RAFOS 79 were compared with deep CTD casts (Fig. T2). Generally, the temperature vs. pressure relationship indicated isobaric behavior and fell within the range of values observed by CTD. As noted above, pressure data from June and July 2001 were outside this range and therefore unreliable.

Figure T3 shows the trajectory of the RAFOS 79 float. The vector mean flow (direction) was 0.75 cm/s (284.5°T) with a mean speed of 5.37 cm/s. For the first 5 months of the mission, RAFOS 79 remained over the continental slope between offshore northern Monterey Bay and the southern portion of the Gulf of the Farallones. The float began by executing a figure "8", first moving in an anticyclonic loop to the north and then a cyclonic loop to the south (west of Monterey Bay). The float returned to the north during January 2001. It reversed direction on 6 February, and appeared to stall on 18 February 2001. On 1 March the direction reversed again and RAFOS 79 moved northwestward along its previous track, turning onshore and stalling again on 1 April near 37.4°N, 123.2°W. After a short period of southward flow, RAFOS 79 moved offshore in mid-April 2001, and on April 21 began looping cyclonically. RAFOS 79 moved steadily to the west, executing a total of 12 of these cyclonic loops with diameters ranging from 10 to 40 km with a period of 10 to 25 hours. On 4 November 2001, near 36.7N, 126.3W, RAFOS 79 entered an east-west elongated loop around the Taney Seamounts, continuing in a cyclonic manner. As it moved to the west, it traced out three half circles along the top of this loop. On 21 March 2002 near 36.8N, 126.4W, the half circle pattern ended, and RAFOS 79 moved to the northwest, reaching its western extreme on 24 April 2001, and its northern extreme on 7 May 2001. It continued this anticyclonic movement with a 100-km diameter, completing about one loop when it surfaced on 20 May 2002.

Figure T4 displays the bathymetry during the RAFOS float mission. Between November and December 2000 the RAFOS float trajectory appears to slow down dramatically as the trajectory crosses the local peak, indicating the float may have collided with a seamount, thus accounting for its slower speed. The float did manage to move past the seamount and continue its journey. Later the float appears to sink to a lower depth; but this correlates with the questionable pressure measurements mentioned earlier in the appendix.

Cross-shore (alongshore) diffusivities ranged from 0.2 to 1.68 cm^2/s (0.1 to 4.1 cm^2/s). For all but the 18 November 2001 to 18 March 2002 estimate, the cross-shore diffusivity exceeded the alongshore diffusivity. This period corresponded to the period when the RAFOS 79 trajectory was expelled from the cyclonic eddy and began its long

wide arc during the winter of 2002. The mean ratio of the alongshore to cross-shore diffusivity was 1.71 for RAFOS 79.

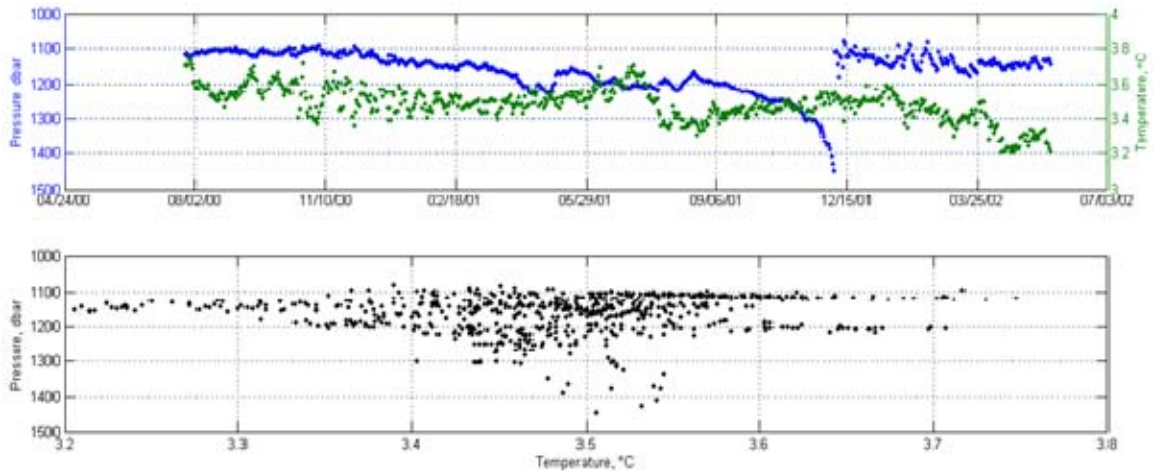

Figure T1. Temperature and Pressure data for RAFOS 79. (upper) Time series. (lower) Temperature versus pressure.

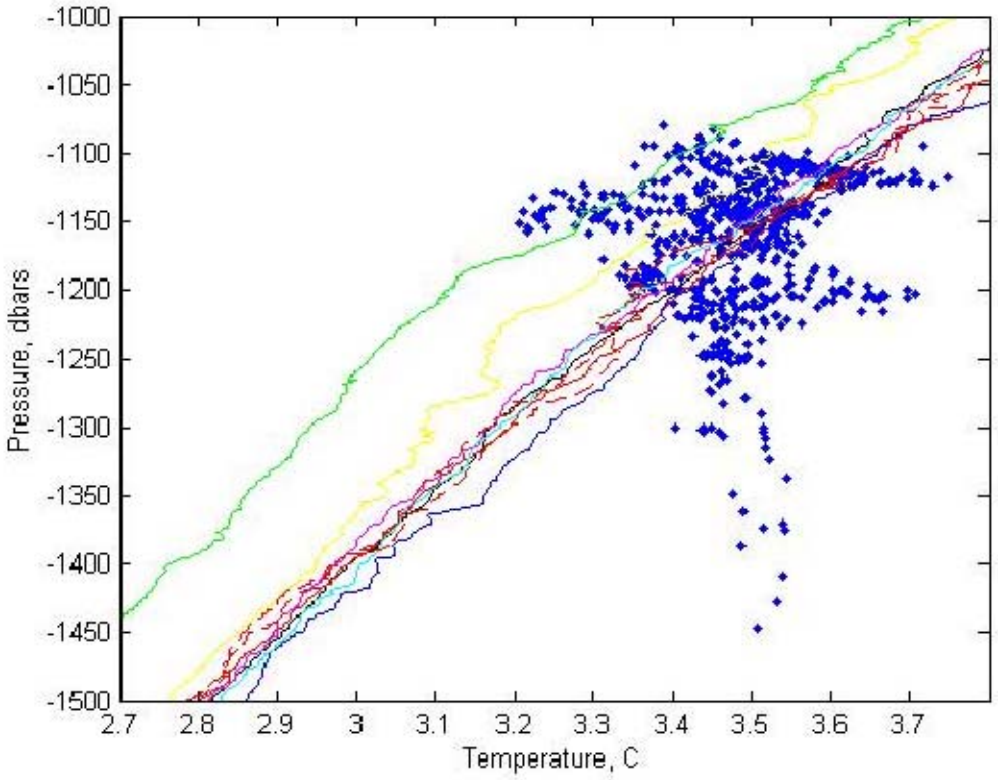

Figure T2. Distribution of temperature and pressure (blue dots). Lines are from regional CTD casts.

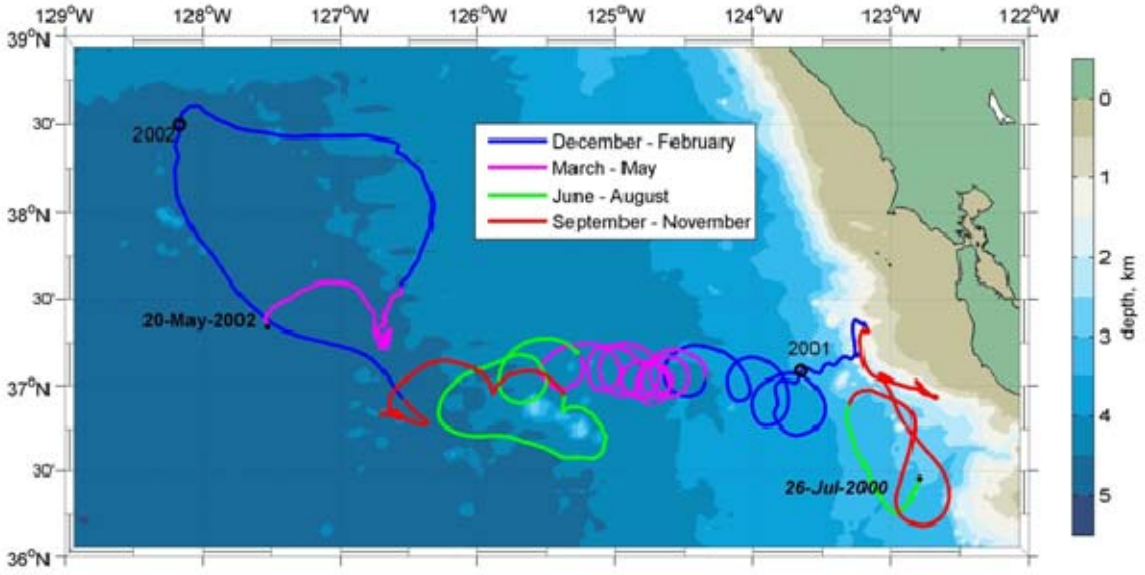

Figure T3. The trajectory for RAFOS 79. Trajectory color indicates season (upper center legend).

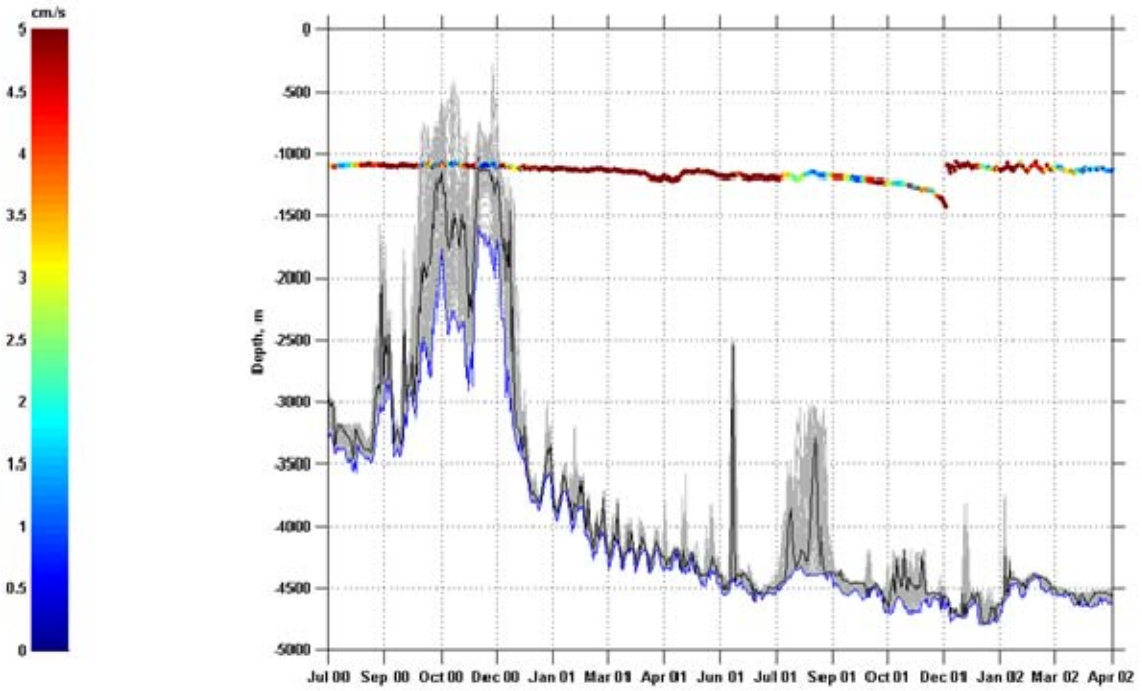

Figure T4. Bathymetry during the RAFOS 79 float mission. The solid black line indicates the ocean depth using the float position and the Sandwell 2' bathymetry (Smith and Sandwell, 1997). The grey indicates the range of possible depths within 10 km; the blue line indicates the maximum depth in this range. The multicolored line indicates the measured RAFOS depth, where the colors correspond to the RAFOS float speed given in cm/s by the bar on the left; speeds greater than 5 cm/s are dark red.

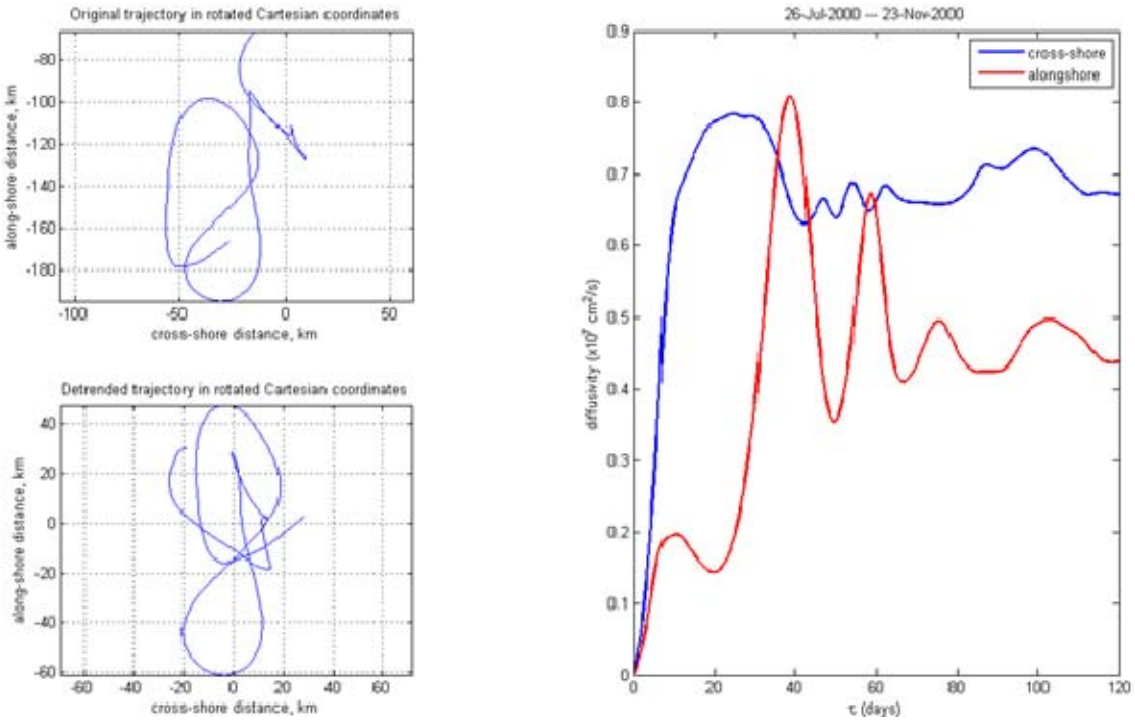

Figure T5. Diffusivity estimate for the RAFOS 79 drift. (upper left) Original trajectory in Cartesian coordinates. (lower left) Detrended trajectory in a coordinate system rotated by 030°. (right) Diffusivity, cm^2/s.

Launch				Surface		Sampling rate	RAFOS performance		Mission, days	
Date	$\frac{\varphi^o \text{N}}{\lambda^o \text{W}}$	T, ºC	Pressure, dbar	Date	$\frac{\varphi^o \text{N}}{\lambda^o \text{W}}$		Planned pressure, dbar	Actual pressure and temperature	Planned	Actual
26 July 2000	36.46ºN 122.8ºW	3.71	1115	22 May 2002	37.34 ºN 127.52 ºW	1 per day	1500	1162.5 ± 0.08 3.48 ± 0.09	666	666

Table T1. RAFOS 79 deployment data.

Cross-shore diffusivity (σ_{UU} cm^2/s)	Alongshore diffusivity (σ_{VV} cm^2/s)	Diffusivity ratio ($\frac{\sigma_{VV}}{\sigma_{UU}}$)	Period of diffusivities
0.66	0.44	0.67	26 July 2000 – 23 Nov. 2000
0.45	0.1	0.22	23 Nov 2000 – 23 March 2001
0.68	0.42	0.62	23 March 2001 – 21 July 2001
1.68	1.26	0.75	21 July 2001 – 18 Nov. 2001
1.35	4.1	3.04	18 Nov. 2001 – 18 March 2002
0.2	0.1	0.5	18 March 2002 – 20 May 2002

Table T2. RAFOS 79 Diffusivity Estimates.

APPENDIX U RAFOS FLOAT 86

RAFOS 86 was launched on 4 August 2001 163 km west of Pt. Conception in water 3991 m deep. The 1146 day mission was successfully executed and RAFOS 86 surfaced on 23 September 2004 just 80 km to the east-southeast of the launch point. Table U1 contains specific information on RAFOS 86.

The mean pressure for RAFOS 86 was 1568 dbar, which was somewhat deeper than its planned pressure of 1500 dbar. The initial pressure (temperature) was 1560 dbar (2.82°C). Although a number of oscillations of ±5 to ±10 dbar occurred, pressure increased steadily, reaching maximum pressure, 1597 dbar, four days before RAFOS 86 surfaced (Fig. U1, upper). Temperature was 2.73°C with oscillations about ±0.03°C until 25 May 2003, when temperature first decreased to near minimum , 2.60°C, on 12 July 2003, then increased to near maximum, 2.82°C, on 2 September 2003, then returned to 2.60°C on 20 October 2003. Subsequently, temperature remained near 2.67°C, although it decreased to a minimum on 25 August 2004 during a large oscillation near the end of the record. The mean temperature was 2.71°C.

RAFOS 86 behaved in an isobaric manner during this mission. Temperature and pressure oscillations were out of phase (Fig. U1, upper). Fig. U1 (lower) also shows that temperature and pressure were inversely related, although a shift in the relationship occurred during the mission, possibly due to a change in the temperature-salinity relationship.

Figure U2 shows the trajectory of RAFOS 86. The mean speed of the entire RAFOS trajectory was 3.01 cm/s. The mean vector flow (direction) was 0.076 cm/s (114.85°T). Upon deployment, RAFOS 86 moved southward for the remainder of 2001 and then southwestward in winter of 2002, reaching its most southern latitude, 32.21°N, on 1 March 2002 as part of a cyclonic reversal of course to a northward heading. In May 2002, RAFOS 86 changed course to west-northwestward. On 29 June 2002, RAFOS 86 reached its most western point at 124.27°W, and, turning anticyclonically, reversed course to east-southeastward and then gradually turned cyclonically, returning to a point close to the launch position on 7 October 2002. At this point, it abruptly reversed course

and completed a 30-km cyclonic loop on 6 December 2002. RAFOS 86 thence meandered southward until 22 March 2003, meandered to the northwest until 2 September 2003, and returned southwestward again to a position near launch on 16 October 2003, and thence turned northward, reaching the most northern point of the trajectory, 35.54°N, on 7 December 2003. RAFOS 86 continued to move cyclonically about 100 km to the west, then 150 km southeast, and finally northeastward, arriving near the launch point once again on 8 June 2004. RAFOS 86 continued along this northward course, changing direction to southeastward on 12 July 2004, and moved along a portion of the track closest shore, reaching the most eastern point, 120.90°W, on 15 August 2004. From this eastern extreme, RAFOS 86 moved anticyclonically with about a 100 km radius to the position where it surfaced.

Cross-shore (alongshore) diffusivities ranged from 0.03 to 0.86 cm^2/s (0.05 to 2.58 cm^2/s) (Table U2). Only three diffusivity ratios were less than one and the mean diffusivity ratio was 0.519. Thus so alongshore diffusivity was typically greater than the cross-shore diffusivity.

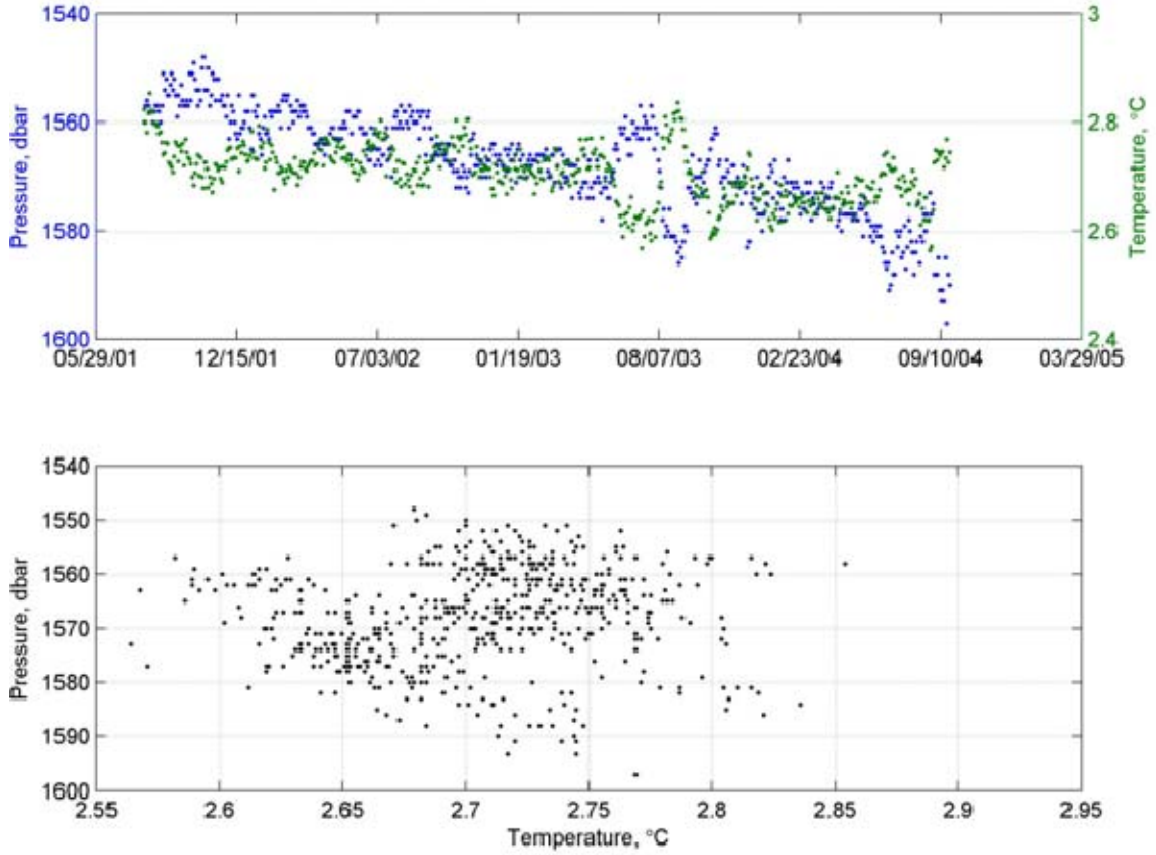

Figure U1. Temperature and Pressure data for RAFOS 86. (upper) Time series. (lower) Temperature versus pressure.

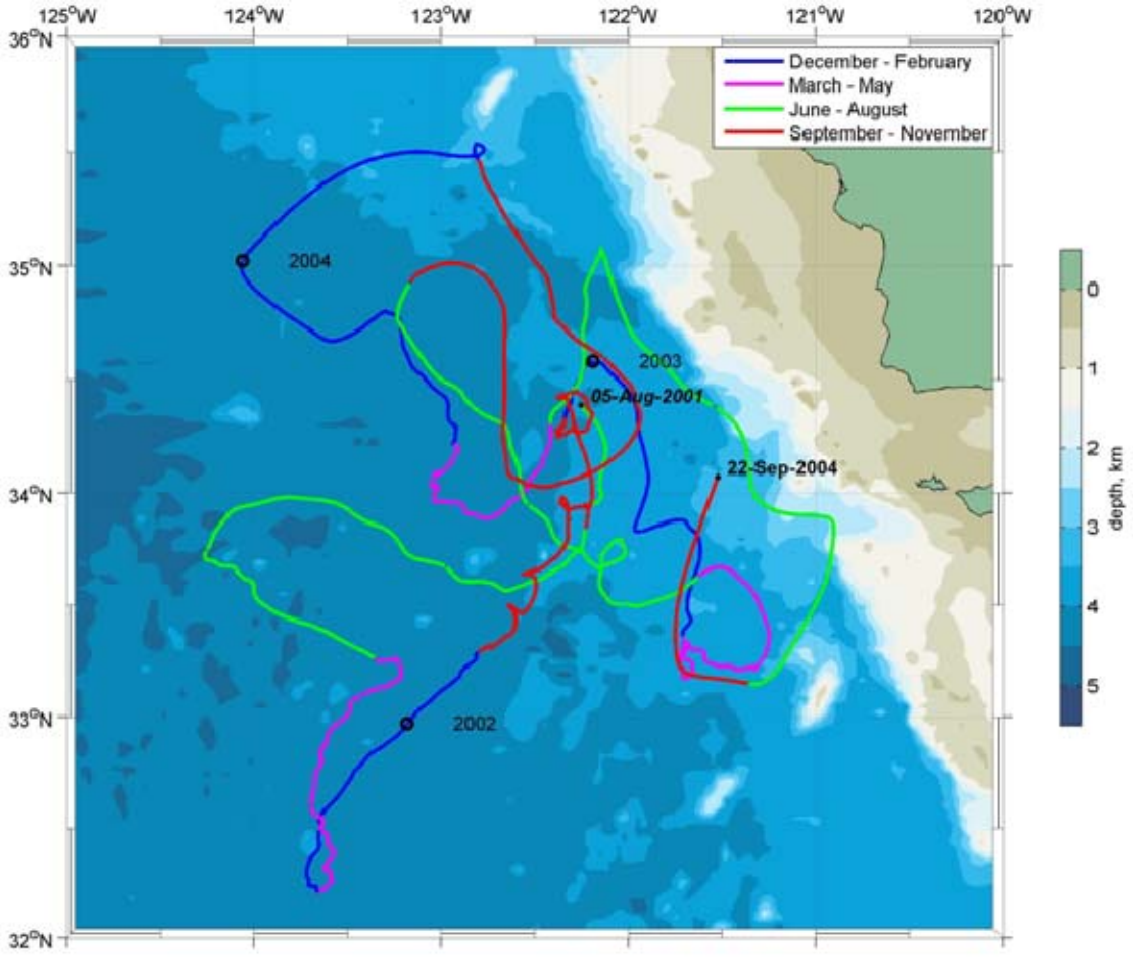

Figure U2. The trajectory for RAFOS 86. Trajectory color indicates season (upper right legend).

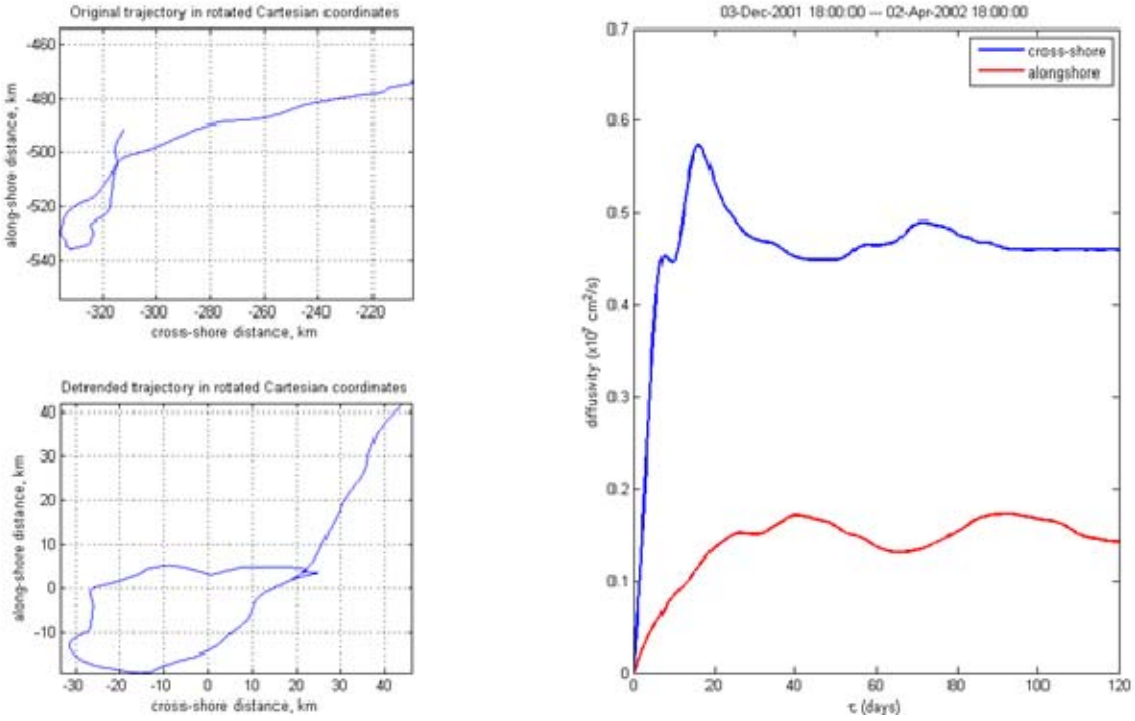

Figure U3. Diffusivity estimate for the RAFOS 86 drift. (upper left) Original trajectory in Cartesian coordinates. (lower left) Detrended trajectory in a coordinate system rotated by 030°. (right) Diffusivity, cm^2/s.

Launch				Surface		Sampling rate	RAFOS performance		Mission, days	
Date	$\frac{\varphi^o \text{N}}{\lambda^o \text{W}}$	T, ºC	Pressure, dbar	Date	$\frac{\varphi^o \text{N}}{\lambda^o \text{W}}$		Planned pressure, dbar	Actual pressure and temperature	Planned	Actual
4 August 2001	34.39ºN 122.25ºW	2.82	1560	23 Sept. 2004	34.104 ºN 121.51 ºW	1 every other day	1500	1567.7 ± 8.96 2.71 ± 0.05	1146	1146

Table U1. RAFOS 86 deployment data.

Cross-shore diffusivity (σ_{UU} cm^2/s)	Alongshore diffusivity (σ_{VV} cm^2/s)	Diffusivity ratio ($\frac{\sigma_{VV}}{\sigma_{UU}}$)	Period of diffusivities
0.09	0.19	2.11	5 Aug. 2001 – 3 Dec. 2001
0.46	0.14	0.3	3 Dec. 2001 – 2 April 2002
0.56	0.34	0.61	2 April 2002 – 31 July 2002
0.06	1	16.67	31 July 2002 – 28 Nov. 2002
0.03	0.53	17.67	28 Nov. 2002 – 28 Mar. 2003
0.09	0.19	2.11	28 March 2003 – 26 July 2003
0.21	2.58	12.29	26 July 2003 – 23 Nov. 2003
0.86	0.98	1.14	23 Nov. 2003 – 22 Mar. 2004
0.2	0.05	0.25	22 Mar. 2004 – 20 July 2004
0.86	0.96	1.12	20 July 2004 – 22 Sept. 2004

Table U2. RAFOS 86 Diffusivity Estimates.

LIST OF REFERENCES

Brink, K.H., R.C. Beardsley, J. Paduan, R. Limeburner, M. Caruso, and J.G. Sires. 2000. *A view of the 1993-1994 California Current based on surface drifters, floats, and remotely sensed data.* Journal of Geophysical Research, Vol. 105, No. C4, pp. 8575-8604, April 15, 2000.

Collins, C. A., L. M. Ivanov, O.V. Melnichenko, and N. Garfield. 2004. *California Undercurrent variability and eddy transport estimated from RAFOS float observations*. Journal of Geophysical Research, Vol. 109, 19 pp.

Davis, R.E. 1991. *Observing the general circulation with floats.* Deep Sea. Res. 38, Suppl. 1, S531-S571.

Emery, W.J., and R.E. Thomson. 1997. *Data Analysis Methods in Physical Oceanography*. Pergamon, New York, 638 pp.

Fofonoff, N. 1965. *A Technique for analyzing Buoy System Motion.* Geo-Marine Technology, V, 222-225.

Fofonoff, N. 1966. *Oscillation modes of a Deep-Sea mooring.* Geo-Marine Technology, V, 327-331.

Foreman, M. G. G. 1977. *Manual for tidal heights analysis and prediction*. Pacific Marine Science Report 77-10, Institute of Ocean Sciences, Patricia Bay, Sidney, BC, 97 pp.

Foreman, M.G.G. 1978. Manual for tidal currents analysis and prediction. Pacific Marine Science Report 78-6, Institute of Ocean Sciences, Patricia Bay, Sidney, BC, 57 pp.

Freeland, H.J., P.B. Rhines, and T. Rossby. 1975. *Statistical observations of the trajectories of neutrally buoyant floats in the North Atlantic.* J. of Marine Res. 3 33, 383-404.

Garfield, N., C. A. Collins, R.G. Paquette, and E. Carter. 1999. *Lagrangian Exploration of the California Undercurrent, 1992-1995.* Journal of Physical Oceanography, Vol. 29, pp. 560-583.

Godin, G. 1972. *The Analysis of Tides.* University of Toronto Press, Toronto, 264 pp.

Gonella, J. 1972. *A rotary-component method for analyzing meteorological and oceanographic vector time series.* Deep-Sea Research, 1972, Vol. 19, pp. 833-846.

Goodman, L., E. R. Levine. 1990. *Vertical Motion of Neutrally Buoyant Floats.* Journal of Atmospheric and Oceanic Technology, Volume 7, pp. 38-49.

Hamilton, J.M., G.A. Fowler, D.J. Belliveau. 1997. *Mooring Vibration as a Source of Current Meter Error and Its Correction.* Journal of Atmospheric and Oceanic Technology, Volume 14, pp. 644-655.

Irish, J., W. Munk, and F. Snodgrass, 1971. *M_2 amphidrome in the northeast Pacific*. Geophysical Fluid Dynamics 2: pp. 355-360.

Isaacs, J. D., J. L. Reid, Jr., G.B. Schick, and R.A. Schwartzlose. 1966. *Near-Bottom Currents Measured in 4 kilometers Depth off the Baja California Coast.* Journal of Geophysical Research, Vol. 71, No. 18, pp. 4297-4303.

Lupton, J. E., E. T. Baker, N. Garfield, G. J. Massoth, R. A. Feely, J. P. Cowen, R. R. Greene, T. A. Rago. 1998. *Tracking the Evolution of a Hydrothermal Event Plume with a RAFOS Neutrally Buoyant Drifter. Science,* New Series, Vol. 280, No. 5366, pp. 1052-1055.

Mantyla, A. W. 1970. *Characteristics of the Deep Water Below the California Current.* A thesis submitted in partial satisfaction of the requirements for the degree Master of Science in Oceanography. 76 pp.

Margolina, T., C. A. Collins, T.A. Rago, and R. G. Paquette. 2006. *Intermediate Level Lagrangian Subsurface Measurements in the Northeast Pacific: Isobaric RAFOS Float Data.* Geochem. Geophys. Geosyst., 7, Q09002, doi: 10.1029/2006GC001295. 37 pp.

Mooers, C.N.K. 1973. *Instruments and Methods: A technique for the cross spectrum analysis of pairs of complex-valued time series, with emphasis on properties of polarized components and rotational invariants.* Deep-Sea Research, 1973, Vol. 20, pp. 1129-1141.

Morales, J.A. 2003. *Subtidal Circulation Over the Upper Slope to the west of Monterey Bay, California.* M.S. Thesis Naval Postgraduate School. 110 pp.

Munk, W., F. Snodgrass, and M. Wimbush, 1970. *Tides offshore: transition from California coastal to deep-sea waters*, Geophysical Fluid Dynamics 1:161-235.

Nowroozi, A. A., M. Ewing, J.E. Nafe, and M. Fleigel. 1968. *Deep Ocean Current and Its Correlation with the Ocean Tide off the Coast of Northern California.* Journal of Geophysical Research, Vol. 73, No. 6, March 15, 1968. pp. 1921-1932.

Operating Manual, RCM 7&8 Recording Current Meter Models 7&8. Technical Description No. 159, May 1995. 80 pp.

Pawlowicz, R., B. Beardsley, S. Lentz. 2002. *Classical tidal harmonic analysis including error estimates in MATLAB using T_TIDE*. Computers & Geosciences 28 (2002), 929-937.

Reid, J. L. and A. W. Mantyla. 1978. *On the Mid-Depth Circulation of the North Pacific Ocean.* Journal of Physical Oceanography, Volume 8. pp. 946-951.

Reid, J.L. and A.W. Mantyla. 1976. *The Effect of the Geostrophic Flow Upon Coastal Sea Elevations in the Northern North Pacific Ocean.* Journal of Geophysical Research, Volume 81, No. 18. pp. 3100-3109.

Rossby, T., D. Dorsen, and J. Fontaine. 1986. *The RAFOS System.* Journal of Atmospheric and Oceanic Technology, Vol. 3. pp. 672-679.

SBE 37-SM MicroCAT. Conductivity and Temperature Recorder with RS-232 Interface. Configuration and Calibration Manual. 13 May 2004. Sea-Bird Electronics, Inc. 109 pp.

Schmitz, Niiler & Koblinsky. 1987. *Two-Year Moored Instrument Results Along 152ºE.* Journal Geophysical Research, 92 (c10), 10826-10834.

SEACAT SBE 16/Dual Mode. Conductivity, Temperature, Depth Recorder Operating and Repair Manual Serial number 161463-62. 19 August 1987. Sea-Bird Electronics, Inc. 34 pp.

SEACAT SBE 19-01. Conductivity and Temperature Recorder with RS-232 Interface. Configuration and Calibration Manual. 13 May 2004. Sea-Bird Electronics, Inc. 43 pp.

Smith, W.H.F., D.T. Sandwell. 1997. *Global Sea Floor Topography from Satellite Altimetry and Ship Depth Soundings.* Science, Vol. 277, 26 September 1997, pp. 1956-1962.

Stabeno, P. J. and Robert L. Smith. 1987. *Deep Sea Currents off Northern California.* Journal of Geophysical Research, Vol. 93, No. C1, pp. 755-771, January 15, 1987.

INITIAL DISTRIBUTION LIST

1. Defense Technical Information Center
   Ft. Belvoir, Virginia

2. Dudley Knox Library
   Naval Postgraduate School
   Monterey, California

3. Maury Library, Navy Oceanographic Office
   Belch Boulevard
   Stennis Space Center

4. Library
   Moss Landing Marine Laboratories
   California State Colleges
   Moss Landing, CA

5. Curtis A. Collins
   Naval Postgraduate School
   Monterey, CA

6. Tetyana Margolina
   Naval Postgraduate School
   Monterey, CA

7. Thomas R. Rago
   Naval Postgraduate School
   Monterey, CA

8. Marla Stone
   Naval Postgraduate School
   Monterey, CA

9. CDR Rebecca Stone
   Naval Postgraduate School
   Monterey, CA

10. Jeffrey Paduan
    Naval Postgraduate School
    Monterey, CA

11. Scripps Institution of Oceanography Library
University of California
La Jolla, CA

12. Estanislao Zamora Jr.
10432 Toledo St. NW
Albuquerque, NM 87114